University of Alberta

Protochelin and the Catecholate Siderophores of *Azotobacter vinelandii*: Characterization of their Function in Iron Acquisition, Interaction with Molybdate, and Role in Oxygen Stress Management.

by

Anthony Sean Cornish

A thesis submitted to the Faculty of Graduate Studies and Research in partial fulfillment of the requirements for the degree of Doctor of Philosophy

in

Microbiology and Biotechnology
Department of Biological Sciences

Edmonton, Alberta
Spring, 1999

National Library of Canada
Acquisitions and Bibliographic Services
395 Wellington Street
Ottawa ON K1A 0N4
Canada

Bibliothèque nationale du Canada
Acquisitions et services bibliographiques
395, rue Wellington
Ottawa ON K1A 0N4
Canada

Your file Votre référence

Our file Notre référence

The author has granted a non-exclusive licence allowing the National Library of Canada to reproduce, loan, distribute or sell copies of this thesis in microform, paper or electronic formats.

L'auteur a accordé une licence non exclusive permettant à la Bibliothèque nationale du Canada de reproduire, prêter, distribuer ou vendre des copies de cette thèse sous la forme de microfiche/film, de reproduction sur papier ou sur format électronique.

The author retains ownership of the copyright in this thesis. Neither the thesis nor substantial extracts from it may be printed or otherwise reproduced without the author's permission.

L'auteur conserve la propriété du droit d'auteur qui protège cette thèse. Ni la thèse ni des extraits substantiels de celle-ci ne doivent être imprimés ou autrement reproduits sans son autorisation.

0-612-39518-9

Canada

University of Alberta

Library Release Form

Name of Author: Anthony S. Cornish

Title of Thesis: Protochelin and the Catecholate Siderophores of *Azotobacter vinelandii*: Characterization of their Function in Iron Acquisition, Interaction with Molybdate, and Role in Oxygen Stress Management.

Degree: Doctor of Philosophy

Year this Degree Granted: 1999

Permission is hereby granted to the University of Alberta Library to reproduce single copies of this thesis and to lend or sell such copies for private, scholarly, or scientific research purposes only.

The author reserves all other publication and other rights in association with the copyright in the thesis, and except as hereinbefore provided, neither the thesis nor any substantial portion thereof may be printed or otherwise reproduced in any material form whatever without the author's prior written permission.

17947-78 Ave
Edmonton, AB.
T5T-3A1
Canada

Date: April 13/99

"If I have been able to see farther than others, it is because I have stood on the shoulders of giants" -Sir Isaac Newton-

University of Alberta

Faculty of Graduate Studies and Research

The undersigned certify that they have read, and recommend to the Faculty of Graduate Studies and Research for acceptance, a thesis entitled "**Protochelin and the Catecholate Siderophores of *Azotobacter vinelandii*: Characterization of their Function in Iron Acquisition, Interaction with Molybdate, and Role in Oxygen Stress Management**" submitted by **Anthony S. Cornish** in partial fulfillment of the requirements for the degree of **Doctor of Philosophy** in **Microbiology and Biotechnology**.

Dr. W. J. Page, Supervisor

Dr. P. M. Fedorak

Dr. B. K. Leskiw

Dr. M. Peppler

Dr. P. A. Sokol, External Examiner

Date: March 31, 1999

This work is dedicated to:

My Father who watches over me, My Wife who stands next to me, and My Son who looks up to me.

ABSTRACT

In the course of studying the response of the obligately aerobic, nitrogen fixing, gram negative soil bacterium *Azotobacter vinelandii* to high concentrations of molybdate under iron-limited conditions, it was observed that the number of catecholate compounds that accumulated in culture fluid changed. The catecholate siderophores azotochelin and aminochelin disappeared and were replaced with a single, new catecholate compound. This compound also accumulated when high concentrations of vanadate, tungstate, zinc, or manganese were present in iron-limited conditions. Chemical characterization of this compound by acid hydrolysis and fast atom bombardment mass spectrometry indicated that it was formed from one molecule of azotochelin and one molecule of aminochelin suggesting it was the tricatecholate protochelin. Comparison of the unknown compound to authentic protochelin confirmed its identity. Protochelin was found to be a superior iron chelator with a proton-independent formation constant of 10^{44}. Biological analysis of the ability of protochelin to deferrate the chromogenic iron-Chrome Azurol-S complex, to promote the growth of a siderophore deficient strain of *A. vinelandii* under iron-limited conditions, and to be taken up by *A. vinelandii* in ^{55}Fe-uptake assays confirmed it as a siderophore. The role of the metals that promoted protochelin accumulation was investigated and each was found to inhibit the uptake of ^{55}Fe-siderophore complexes. In competition assays between iron, molybdate, and protochelin, molybdate was found to initially associate with the siderophore, but it was ultimately displaced forming a ferric-siderophore complex. As well, each metal was found to inhibit ferric reductase activity, thereby decreasing iron-uptake. In addition, the

overproduction of protochelin by the *A. vinelandii* ferredoxin I (*fdxA*)-negative mutant LM100, which is unable to properly respond to oxidative stress, was investigated. This work demonstrated that protochelin and azotochelin could prevent the formation of the hydroxyl radical in the Fenton reaction by sequestering iron indicating a role for protochelin in the management of oxidative stress. Finally, a hypothetical mechanism for the synthesis of protochelin from 2,3-DHBA, ornithine, and lysine is described, consistent with data that suggest that protochelin is the primary siderophore of *A. vinelandii* and azotochelin and aminochelin are breakdown products released during the cleavage and deferration of protochelin.

ACKNOWLEDGEMENTS

A project that takes six and half years to complete is never done alone and I would like to acknowledge and thank those who helped make this work possible.

I must thank my supervisor Dr. W. J. Page for his support and guidance during my time in his lab. He gave me the freedom to pursue this project down avenues that I thought would be interesting, even though this often meant doing work that had not been done in his lab before. When I ran into obstacles Dr. Page always had suggestions for alternative approaches, or he knew of someone who could help solve my problem. Finally, in the last year and a half of my PhD, Dr. Page was generous enough to support me financially when the five year departmentally imposed time limit on my GTA funding expired. For this and much more I am truly grateful.

I must thank the people who worked in Dr. Page's lab with me. When I first joined the lab Brent Rudy and Jan Manchak taught me a lot about working in a lab setting. Brent in particular taught me a lot about organizing my data, and designing experiments that would be meaningful in a scientific sense. Most recently Anne Sharpe has been a wonderful lab companion, overall, these people made the Page lab a great place to work.

I must also thank Tom Hantos, Richard Mah, Elsa Bruno, and Anna Szenthe for their help over the years. If I ever needed to borrow something, or needed help with a piece of equipment, one of these four would help me out, which made my life much easier.

Finally, I must recognize the contribution made to this work by my wife Karen Gwozd-Cornish. If it were not for her support and encouragement this work would not have been completed. She has listened to hours of practice seminars, endured endless conversations about my work, and recently she has spent many late nights looking after our son Brendan while I completed this thesis. Thank you very much dear, I couldn't have done it without you.

Table of Contents

	Page Number
CHAPTER 1 - Review of the Literature	1
1.1 Introduction	2
1.2 *Azotobacter vinelandii*	3
1.2.1 Introduction to the organism	3
1.2.2 Responses of *A. vinelandii* to its environment	4
1.2.3 Nitrogen fixation	6
1.2.4 Introduction to siderophore mediated iron-uptake	10
1.2.5 Negative regulation of siderophore synthesis by ferric uptake regulator (Fur)	12
1.2.6 Introduction to topic of thesis	15
1.3 Molybdenum	15
1.3.1 Basic chemistry of molybdenum	15
1.3.2 Role of molybdenum in the cell	18
1.3.3 Uptake and storage of molybdenum.	19
1.3.4 Similarity of vanadium, tungsten, and molybdenum	22
1.4 Iron	23
1.4.1 Basic chemistry of iron	23
1.4.2 Biological role of iron	25
1.4.3 Chemistry of iron binding by catecholate siderophores	28
1.4.4 Determination of the affinity of a siderophore for iron	28
1.5. Catecholate siderophore mediated iron uptake, the *E. coli*-enterobactin model	32
1.5.1 Enterobactin synthesis	32
1.5.2 Siderophore export	39
1.5.3 Ferric-enterobactin uptake	40
1.5.4 Iron release by ferric reductase	47
1.6 Oxygen stress	48
1.6.1 Enzymatic sources of ROIs.	49
1.6.2 Non-enzymatic sources of ROIs	50

1.6.3 OxyR: hydrogen peroxide sensing and response in *E. coli* 51
1.6.4 SoxRS: superoxide sensing and response in *E. coli* 53
1.6.5 SoxRS-like system in *A. vinelandii* 57
1.7 Scope of thesis 57

CHAPTER 2 - Materials and Methods 59
2.1 Analysis of cells and cell culture fluids 60
2.1.1 Growth conditions and bacterial strains 60
2.1.2 Spectrophotometric and colorimetric analyses 61
2.1.3 Extraction and identification of catecholate siderophores 62
2.1.4 Cell free extract preparation and membrane differentiation 63
2.2 Characterization of protochelin 64
2.2.1 Purification of protochelin by silicic acid chromatography 64
2.2.2 Production and purification of catecholate siderophores 64
2.2.3 Total and partial hydrolysis of protochelin 66
2.2.4 Fast atom bombardment (FAB) spectrometry 67
2.2.5 Chrome Azurol-S (CAS) siderophore assay 67
2.2.6 Siderophore bioassay using strain P100 68
2.2.7 ^{55}Fe-uptake assay 68
2.2.8 Molar iron and molybdenum siderophore binding ratios 70
2.2.9 Iron and molybdate siderophore affinity determination 71
2.3 Interaction of metals and protochelin 72
2.3.1 Molybdate-iron siderophore complex competition 72
2.3.2 Effect of metals on protochelin accumulation 74
2.3.3 Effect of metals on $^{55}Fe^{3+}$-siderophore uptake 74
2.3.4 SDS-PAGE examination of IROMPs 75
2.3.5 Ferric reductase assay 77
2.3.6 Effect of high molybdate concentrations on *A. vinelandii* P100 growth 78
2.4 Determination of the role of protochelin in O_2 stress management 79
2.4.1 Non-denaturing PAGE of CFX proteins 79

2.4.2 Catalase assay 80
2.4.3 Superoxide dismutase assay 81
2.4.4 Oxygen radical mediated iron (II) release 83
2.4.5 Inhibitory role of siderophores in •OH generation 84

CHAPTER 3 - Results and Discussion 86
3.1 Characterization of protochelin 87
3.1.1 Production of an unknown catecholate compound by *A. vinelandii* 87
3.1.2 Purification of unknown catecholate by silicic acid chromatography 91
3.1.3 Acid hydrolysis of unknown catecholate 91
3.1.4 Molecular mass of unknown catecholate 91
3.1.5 Purification of *A. vinelandii* catecholate siderophores 93
3.1.6 Molar binding ratios of iron-siderophore complexes 100
3.1.7 Affinity of catecholate siderophores for Fe^{3+} and Fe^{2+}. 106
3.1.8 Iron repressibility of protochelin production 108
3.1.9 Protochelin reaction in the CAS assay 110
3.1.10 Protochelin promotes iron-restricted growth of *A. vinelandii* 114
3.1.11 Uptake of ^{55}Fe-siderophore complexes 115
3.2 Role of molybdate and other metals in the accumulation of protochelin 119
3.2.1 Effect of molybdate on protochelin stability and production 119
3.2.2 Molar binding ratio of molybdo-siderophore complexes 121
3.2.3 Affinity of siderophores for molybdate 126
3.2.4 Molybdate-iron siderophore complex competition 130
3.2.5 Effect of metals on protochelin accumulation 134
3.2.6 Effect of metals on ^{55}Fe-siderophore uptake 134
3.2.7. Effect of molybdate on IROMP profiles of *A. vinelandii* 139
3.2.8 Ferric reductase assay 143

3.2.9 Effect of high molybdate concentrations *A. vinelandii* P100 growth in iron-restricted medium 143
3.3 Role of protochelin in O_2 stress management 145
3.3.1 Strain LM100 and protochelin accumulation 145
3.3.2 Oxidative stress and catecholate siderophore production 145
3.3.2.1 Increased aeration effects 145
3.3.2.2 Effect of paraquat on the growth of *A. vinelandii* strains LM100 and UW 149
3.3.3 Activity of enzymes in oxygen stress management 152
3.3.4 Oxygen radical mediated iron (II) release 154
3.3.5 Inhibitory role of siderophores in •OH generation 156

CHAPTER 4 – General Discussion 157
4.1 Characterization of unknown compound as protochelin, a tricatecholate siderophore 158
4.2 Interaction of molybdate and protochelin 161
4.3 Effect of metals on ferric reductase activity 165
4.4 Alternative explanation of role of MoO_4^{2-} in protochelin accumulation 167
4.5 Effect of oxygen stress on iron-limited *A. vinelandii* 169
4.6 Model for the synthesis of protochelin 174
4.7 Overview of study and perspective on results 178

REFERENCES 182

APPENDIX 1 - Sample Calculations 202

APPENDIX 2 Additional $^{55}Fe^{3+}$ Uptake Assays 209

List of Tables

CHAPTER 3 Page Number

3.1	Catecholate siderophore formation constants with Fe^{3+} and Fe^{2+}.	107
3.2	Free iron concentrations in ferric-siderophore systems.	109
3.3	Activity of siderophore preparations in the CAS assay.	113
3.4	$Log_{10} K_{Form}$ of molybdo-siderophore complexes in 100 mM MOPS buffer (pH 7.0)	127
3.5	The effects of various molybdate treatments on the uptake of ^{55}Fe by *A. vinelandii*.	137
3.6	The effect of metals that promote protochelin accumulation on the uptake of ferric-protochelin and ferric-azotochelin.	141
3.7	Effect of metals that promote protochelin accumulation on ferric reductase activity.	144
3.8	Effect of paraquat on the growth of nitrogen-sufficient and -limited and iron-sufficient and -limited cultures of *A. vinelandii* strains UW and LM100 after 24 hr	151
3.9	Enzyme activities and electromorph relative mobilities from cells grown under iron-sufficient and iron-limited conditions.	153

List of Figures

CHAPTER 1

		Page Number
1.1	Examples of the three classes of siderophore.	11
1.2	The siderophores of *A. vinelandii*.	13
1.3	Three-dimensional coordination chemistry models.	17
1.4	Molybdate uptake operon and model system.	20
1.5	Formation of 2,3-dihydroxybenzoic acid from chorismate.	34
1.6	Formation of the precursors of enterobactin synthesis.	36
1.7	Enterobactin synthesis from precursors by EntF.	37
1.8	Model of ferric-enterobactin uptake in *E. coli*.	42
1.9	Cyclic oxidation and reduction of paraquat and its interaction with iron.	52
1.10	Model of SoxRS oxidative stress sensing system.	55

CHAPTER 3

3.1	TLC analysis of the catecholates extracted from strain UA1 culture supernatant grown in molybdate-containing medium.	88
3.2	TLC analysis of the catecholates extracted from strain UW culture supernatant grown in 1 μM molybdate-containing medium.	89
3.3	Effect of molybdate concentration on the accumulation of unknown catecholate.	90
3.4	Acid hydrolysis of unknown catecholate.	92
3.5	FAB mass spectrum of unknown catecholate.	94
3.6	Structures of the siderophores of *A. vinelandii*.	95
3.7	FAB mass spectrum of protochelin standard.	96
3.8	TLC analysis of unknown catecholate compound extracted from strain UA1 grown in 1 mM molybdate culture supernatant and protochelin standard.	97
3.9	Elution profile of aminochelin from CM Sephadex column.	99

3.10 TLC analysis of catecholate siderophores present in ethyl acetate and sodium phosphate buffer pool fractions. 101

3.11 Elution profile of azotochelin from Sephadex LH-20 column. 102

3.12 Spectrophotometric characteristics of ferric-protochelin. 103

3.13 Spectrophotometric characteristics of ferric-azotochelin. 104

3.14 Spectrophotometric characteristics of ferric-aminochelin. 105

3.15 TLC of catechol siderophores under increasing iron (III) concentrations in Burk's medium containing 1 mM molybdate. 111

3.16 Effect of increasing iron (III) on catecholates produced by *A. vinelandii* strain UA1. 112

3.17 Iron uptake of ferric-siderophore complexes and mixtures of ferric-siderophore complexes. 116

3.18 Iron uptake of individual ferric-siderophore complexes. 118

3.19 Stability of protochelin and formation in 1 mM molybdate. 120

3.20 Spectrophotometric characteristics of molybdo-azotochelin complex. 122

3.21 Spectrophotometric characteristics of molybdo-aminochelin complex. 123

3.22 Spectrophotometric characteristics of molybdo-protochelin in MES buffer pH 6.0. 124

3.23 Spectrophotometric characteristics of molybdo-protochelin in MOPS buffer pH 7.0. 125

3.24 Effect of molybdate competition on the formation of a ferric-protochelin complex. 131

3.25 Effect of molybdate competition on the formation of a ferric-azotochelin complex. 132

3.26 Effect of molybdate competition on the formation of a ferric-aminochelin complex. 133

3.27 The effect of metals other than molybdate on protochelin accumulation. 135

3.28 The effect of metals on the uptake of the $^{55}Fe^{3+}$-protochelin complex. 138

3.29 The effect of metals on the uptake of the $^{55}Fe^{3+}$-azotochelin complex. 140

3.30 SDS-PAGE of IROMPs from strains UW and UA1 grown in Burk's medium with 1 mM or 1 μM molybdate. 142

3.31 TLC analysis of the time course for the production of siderophores by *A. vinelandii* strain LM100. 146

3.32 Effect of increasing aeration on *A. vinelandii* strains UW and LM100 after 22 hr growth. 148

3.33 The effects of increasing aeration on the siderophores produced by *A. vinelandii* strains UW and LM100. 150

3.34 Non-denaturing PAGE gel of catalase activity gel of *A. vinelandii* strains UW and LM100 under high and low iron (III) concentrations. 155

CHAPTER 4

4.1 Proposed protochelin synthesis by EntF homolog. 175

4.2 Small siderophores produced by different microorganisms. 180

APPENDIX 2

A2.1 The effect of 70 µM molybdate on the uptake of $^{55}Fe^{3+}$-protochelin by *A. vinelandii* UW. 211

A2.2 The effect of 70 µM molybdate on the uptake of $^{55}Fe^{3+}$-azotochelin by *A. vinelandii* UW. 212

List of Abbreviations

A	absorbance at given wavelength
ABC	ATP binding cassette
Abs	absorbance
ATP	adenosine 5'-triphosphate
AMP	adenosine 5'-monophosphate
cAMP	cyclic adenosine 5'-monophosphate
CAP	catabolite-activator protein
CAS	chrome azurol S
CFX	cell free extract
Ci	Curie
2,3-DHBA	2,3-dihydroxybenzoic acid
2,3-DHBS	2,3-dihydroxybenzoylserine
Da	daltons
DFMO	diflurormethylornithine
dH_2O	distilled water
DMB	3,3'-diaminobenzidine
DMSO	dimethylsulfoxide
DNA	deoxyribonucleic acid
DNAse	deoxyribonuclease
DTPA	diethylenetriaminepentaacetic acid
EDDHA	ethylenediamine di-(o-hydroxyphenylacetic acid)
EDTA	ethylenediaminetetraacetic acid
FAB	fast atom bombardment
FMN	flavin mononucleotide
Form	formation
HDTMA	hexadecyltrimethylammonium bromide
HPLC	high pressure liquid chromotography
hr	hour(s)
IROMPS	iron repressible outer membrane protein(s)
kb	kilobase pairs
kDa	kilodaltons
M	molar
mA	milliamperes
MES	2-(N-morpholino)ethanesulfonic acid
min	minute(s)
MOPS	3-(N-morpholino)propanesulfonic acid
mRNA	messenger ribonucleic acid
MQ-dH_2O	deionized distilled water
NADH	ß-nicotinamide adenine dinucleotide reduced form
NADPH	ß-nicotinamide adenine dinucleotide phosphate reduced form
NBT	nitroblue tetrazolium
OD	optical density
PAGE	poly acrylamide gel electrophoresis

PCP	peptidyl carrier protein
R_F	relative mobility
ROIs	reactive oxygen intermediate(s)
RNA	ribonucleic acid
RNAse	ribonuclease
ROI	reactive oxygen intermediate
rpm	revolutions per minute
rRNA	ribosomal ribonucleic acid
SDS	sodium dodecylsulfate
Ser	serine
SOD	superoxide dismutase
TE	transesterase
TEMED	N,N,N',N'-tetramethylethylenediamine
TLC	thin layer chromotography
Tris	tris(hydroxymethyl)aminomethane
U	units
UV	ultraviolet
v/v	volume per volume
w/v	weight per volume
w/w	weight per weight

CHAPTER 1 - Review of the Literature

1.1 Introduction

The ability of microorganisms to respond to stress in their environment is key to their survival. In general terms, any condition that prevents an organism from growing at its optimal rate may be considered a form of environmental stress. Whether it is the absence of a nutrient, extremes in temperature, pH or oxidative state, or the presence of toxic compounds, for an organism to survive it must respond to the environmental conditions imposed upon it (Silva & Wong, 1995; Gauthier & Clement, 1994; Heipieper *et al.*, 1996). Bacterial responses to inhibitory environmental conditions are varied and can include the expression of new proteins, the loss of plasmids, changes in membrane fatty acid content, changes in DNA supercoiling and, in some cases, cross-tolerances to yet unencountered forms of environmental stress (Yamashita *et al.*, 1993; Pannekoek *et al.*, 1992; Heipieper *et al.*, 1996; Wrigley-Jones *et al.*, 1993; Flahaut *et al.*, 1996). It is the ability of bacteria to adapt to, and survive, detrimental growth conditions that enables them to inhabit many diverse environments.

One of the most diverse and complex environments bacteria inhabit is soil. Soil environments are characterized by the presence of a wide variety of organic substrates, physio-chemical gradients, variability in nutrient concentration and complex interactions among microorganisms. In terms of bacterial diversity, it has been estimated that one gram of soil may contain up to 10^{10} bacterial cells representing as many as 10^{4} different bacterial species, based on DNA analysis (Torsvik *et al.*, 1996). The lack of homogeneity and varied make up of soil dictates that organisms living in it must be able to adapt to survive. It was the purpose of this study to examine the interplay of nutrient limitation, specifically that of iron, and the presence of a very high concentration of molybdate on the ability of the soil bacterium *Azotobacter vinelandii* to adapt to its environment. To understand the role these metals play in the survival of *A. vinelandii,* an overview of the organism is first required.

1.2 *Azotobacter vinelandii*

1.2.1 Introduction to the organism

Azotobacter vinelandii is a gram negative, obligately aerobic rod that is commonly found in soil or aquatic environments. Its genus name is derived from two words "azote" which is French for nitrogen and "bacter" which is from the Greek for rod. Taken together the genus name, nitrogen rod, refers to one of the most intensely studied characteristics of *Azotobacter*, its ability to fix gaseous nitrogen into an organic form. The species name for the organism comes from Vineland, New Jersey, the location where *A. vinelandii* was first isolated and described in 1903 (Tchan, 1984).

Even though it is a gram negative rod, *A. vinelandii* possesses a number of interesting characteristics, not all of which are commonly seen in prokaryotes. Its cell is coated with an extracellular, protein surface layer and it can resist long periods of nutrient limitation by forming cysts. Stationary phase cells and cysts contain a lipid, poly-β-hydroxbutyric acid (PHB), which has potential for exploitation as a bio-plastic. In addition, at various stages in the cell cycle, it can contain up to 100 copies of its chromosome per cell and can be induced to natural competence by nutrient limitation. Finally, it is one of only a few genera of free-living organisms that can fix nitrogen aerobically (Bingle *et al.*, 1984; Stevenson & Socolofsky, 1966; Moreno *et al.*, 1986; Maldonado *et al.*, 1994; Tchan & New, 1984). Although *Azotobacter* has its own unique features, it shares many common characteristics with *Pseudomonas aeruginosa* and *Escherichia coli*, (de Vos *et al.*, 1989) which are by far two of the best studied prokaryotes. As a result, many systems discussed in the context of *A. vinelandii* will be based on models elucidated for *E. coli* or *P. aeruginosa*. To fully appreciate how *A. vinelandii* has evolved to survive in its environment an examination of some of its adaptation mechanisms is required.

1.2.2 Responses of *A. vinelandii* to its environment

Surface layers are two dimensional, paracrystalline protein arrays which associate with and cover the entire surface of the cell envelope. These structures have been found to be present on an ever increasing number of prokaryotic cells, including *A. vinelandii* (Koval, 1988; Bingle *et al.*, 1984). Although these layers are thought to be present on many microorganisms isolated from the environment, normal laboratory strains often lose the ability to produce them. Surface layers are thought to play a number of roles in different microorganisms including shape determination, molecular sieving, ion trapping, antigenic variability, cell adhesion, and surface recognition (Sleyr & Messner, 1988).

In *A. vinelandii,* one of the functions associated with the S-layer appears to be competence. This is based on the fact that growth of the organism in Ca^{2+}-deficient medium dramatically reduces its ability to be transformed with plasmid or chromosomal DNA, while at the same time a lack of Ca^{2+} prevents normal S-layer assembly (Page & Doran, 1981; Doran *et al.*, 1987). In addition, because of its overall negative charge, the S-layer also has the ability to complex iron, thus serving to trap it from the environment for retrieval by the cell (Page & Huyer, 1984). Other functions of the S-layer of *A. vinelandii* have yet to be determined.

In addition to the requirement of Ca^{2+} and an S-layer for competence, *A. vinelandii* can become competent by nutrient limitation (Page, 1985). This nutrient-limited induction of competence is likely an attempt by the organism to survive by acquiring new genetic material which might encode novel nutrient acquisition proteins. The easy induction of this natural competence has proven to be a key factor in laboratory studies for the understanding *A. vinelandii* at the genetic level.

Another survival strategy that has evolved in *A. vinelandii* is the ability to survive periods of extreme nutrient limitation by forming cysts. These cysts have been shown to be viable after storage in dry soils for up to 24 years and are a stable, metabolically dormant form of the cell which is not only resistant to desiccation, but also UV radiation (Moreno *et al.*, 1986). Although similar in function to bacterial spores, cysts are less resistant to harsh environments and are very different structurally as they are formed from alginate and cell outer membranes (Sadoff, 1975). It should be noted that the laboratory strain *A. vinelandii* UW used in these studies does not produce alginate and as a result does not under go wild type encystment (Page, 1983).

Another adaptation strategy related to encystment is demonstrated when the organism grows under conditions of excess carbon but lacks a single nutrient such as phosphate, fixed-nitrogen or oxygen. Under these conditions it will synthesize and accumulate PHB. This compound is used by *A. vinelandii* as a carbon source to undergo encystment as nutrient limitation increases in the environment (Page & Knosp, 1989; Page, 1992). In addition to its use as a reserve carbon source, PHB is a natural polyester with physical properties that are similar to those of polypropylene (Page, 1992). Although PHB is formed by many other bacteria, *A. vinelandii* is one of the few to produce PHB at concentrations high enough to be of interest on an industrial scale. The attraction of this compound as a replacement for petrochemical based plastic lies in the fact that it can be degraded by a number of organisms (Lee, 1995; Budwill *et al.*, 1996). Ultimately, the accumulation of PHB represents not only an novel approach evolved by *A. vinelandii* to overcome nutrient limitation, but also one that potentially has great socio-economic value.

The chromosome of *A. vinelandii* is approximately 4500 kb long, which is similar in size to that of *E. coli* (Manna & Das, 1993). However, measurements of the amount of DNA

in individual *A. vinelandii* cells indicate that it possesses up to 40 times the amount of DNA found in *E. coli*. In practical terms, this implies that *A. vinelandii,* in early stationary phase, may contain in excess of 40 copies of its chromosome (Sadoff *et al.*, 1979). Although initially perplexing, this large number of chromosomes does seem to explain why stable *A. vinelandii* amino acid auxotrophs were difficult to isolate, even though mutations in *A. vinelandii* could be easily generated with UV radiation (Terzaghi, 1980).

Maldonado *et al.* (1994) suggested that the polyploidy observed in *A. vinelandii* was growth phase and medium-type dependent. They determined that during early exponential phase *A. vinelandii* had approximately four copies of its chromosome. This increased through exponential phase to as high as 100 copies for cells in late stationary phase. However, once cells in stationary phase began the process of encystment the number of chromosomes dropped back to low levels. Although an impressive mechanism to preserve genetic integrity, this polyploidy was not observed when the organism was grown in soil extract medium and as a result may be a laboratory artifact not found in nature (Maldonado *et al.*, 1994).

1.2.3 Nitrogen fixation

By far the most unique characteristic of *A. vinelandii* is its ability to reduce atmospheric nitrogen to ammonia (Bishop, 1993). It is one of only two genera of free living, aerobic bacteria capable of doing this, the other being *Azomonas*, and is the defining characteristic of the family *Azotobacteraceae.* At one time. the genera *Derxia* and *Beijerinckia* were also considered members of the family *Azotobacteraceae*, but comparison of these organisms to *Azotobacter* and *Azomonas* at the level of rRNA has lead to their removal (Tchan, 1984). The ability to fix nitrogen allows *A. vinelandii* to reduce the stress of NH_3-limitation by synthesizing the NH_3 it needs from the atmosphere.

This unique reaction uses 8 H^+ and 8 e^-, plus 18-24 ATP, to reduce N_2 into 2 NH_3 plus H_2. This may seem "expensive" in terms of biological energy, but it is essential for the organism to survive under NH_3-limited conditions. The reaction is carried out by the nitrogenase enzyme which is made up of a complex with two functional components. These are the dinitrogenase reductase, which donates electrons to the second component of the complex, the dinitrogenase which converts N_2 to NH_3 To date, three different nitrogenase complexes have been characterized in *A. vinelandii* and are differentiated by the metal co-factors found at the reactive center of each dinitrogenase. Although these three enzymes are functionally equivalent, they differ greatly at the amino acid and genetic level (Bishop, 1993).

Nitrogenase I is made up of a dinitrogenase reductase which is a dimer (60-kDa) and a dinitrogenase that contains an iron-molybdate center and is a tetramer of two non-identical pairs of proteins (220-kDa). Nitrogenase I is expressed under NH_3-limiting conditions in the presence of molybdate (Hausinger & Howard, 1983). Nitrogenase II is composed of a dinitrogenase reductase dimer (62-kDa) and a dinitrogenase (240-kDa) that is thought to be a hexamer with an iron-vanadium (FeV) cofactor. Nitrogenase II is synthesized in the absence of NH_3 and molybdenum and in the presence of vanadium (Bishop, 1993). Finally, the nitrogenase III complex is made up of a dinitrogenase reductase dimer (62-kDa) and a dinitrogenase which is a tetramer (216-kDa). The unique feature of nitrogenase III is that it contains only iron as a metallic cofactor and it is expressed under ammonium-, molybdenum-, and vanadium-limited conditions (Pau *et al.*, 1989; Bishop, 1993).

The dinitrogenase reductase dimers of nitrogenase I and II are very similar and are interchangeable with each other (Page & Collinson, 1982). This complementation does not extend to nitrogenase III, which shares little homology to nitrogenase I or II. The

rationale behind the ability to form three functionally interchangeable, but very different nitrogenase enzyme complexes has been elusive. The use of different metals as co-factors suggests that this redundancy may be a way to adapt to different soil types. In addition, recent evidence has indicated that nitrogenase II is more effective than nitrogenase I at forming NH_3 at low temperatures (Walmsley & Kennedy, 1991). However, the iron-vanadium and pure iron nitrogenases are less effective in nitrogen fixation as they generate more hydrogen (da Silva & Williams, 1991). Inevitably, the ability to produce three nitrogenase complexes has the effect of broadening the range of environments *A. vinelandii* can occupy.

Although different, all three nitrogenase complexes generate hydrogen as a waste product. Unfortunately, hydrogen appears to be a competitive inhibitor of nitrogen for binding at the active site of the dinitrogenase (Robson & Postgate, 1980) As a result of this, organisms that fix nitrogen, also produce hydrogenases to deal with this waste product. In *A. vinelandii,* a unidirectional uptake hydrogenase is formed that is a heterodimer with a total molecular weight of 98-kDa and contains a nickel-iron active center (Menon & Robson, 1994). Hydrogenases have been shown to convert the hydrogen formed by nitrogen fixation into reductant (NAD(P)H) and ATP. In addition, they aid in respiratory protection by taking electrons from hydrogen and using them to "waste" or remove oxygen (Kow & Burris, 1984). Finally, in some *Anabena* spp., hydrogenase enzymes have been shown to directly couple to nitrogenase under anaerobic conditions (Robson & Postgate, 1980). In these ways, the hydrogen formed during nitrogen fixation is used productively by the cell, increasing the overall efficiency of nitrogen fixation.

Another problematic characteristic of the nitrogenase enzyme is its extreme sensitivity to oxygen. To deal with this, a number of approaches have evolved in nitrogen-fixing

bacteria. These include the formation of a physical barrier between the nitrogenase and O_2, the rapid conversion of O_2 to water through rapid respiration (respiratory protection), and the formation of a stable complex between the nitrogenase and an auxiliary protein in the presence of O_2, known as conformational protection.

To protect its nitrogenase, *A. vinelandii* uses both respiratory and conformational protection depending on the environmental conditions present (Moshiri *et al.*, 1994; Robson & Postgate, 1980). The use of respiratory protection by *A. vinelandii* is evident by the fact that it has the highest respiration rate of any known microorganism (Jurtshuk & Yang, 1980). Being an obligate aerobe, *A. vinelandii* uses O_2 as a terminal electron acceptor in respiration, but when the organism is exposed to high O_2 concentrations under NH_3-limited conditions, oxygen is converted to water without the formation of ATP. This "wasting" of O_2 is possible because *A. vinelandii* has a branched electron transport chain and can change the terminal oxidase used in response to oxidative conditions (Liu *et al.*, 1995).

Under conditions of limiting carbon supply, when high respiratory turnover is not possible, a secondary method of nitrogenase protection is used. Conformational protection of the nitrogenase in *A. vinelandii* relies on the synthesis of the FeSII "Shethna" protein. This dimer contains two sub-units with 2Fe-2S centers and in the presence of O_2 binds to nitrogenase and inhibits nitrogen fixation. Inhibition is not permanent and when O_2 levels drop, the nitrogenase once again begins to fix nitrogen. Using these two systems, *A. vinelandii* has the ability to survive and protect its nitrogenase(s) under a variety of conditions (Moshiri *et al.*, 1994).

1.2.4 Introduction to siderophore mediated iron-uptake

In order to use enzymatic systems like nitrogenase, which may contain iron, bacteria must develop a strategy to overcome iron-limited environments. Under aerobic conditions of neutral pH free iron concentrations are on the order of 10^{-17} M, far below that needed for growth (10^{-8} to 10^{-7} M) (Guerinot, 1994). Some bacteria, specifically *Lactobacillus* spp. have solved this problem by evolving such that they do not require iron. Organisms such as, *Neisseria* spp., *Hemophilus influenzae, Helicobacter pylori*, and members of the genera *Vibrio* and *Yersina* are able to acquire iron by direct interaction with the eukaryotic iron-binding proteins transferrin, lactoferrin, and ferritin (Guerinot, 1994). The final strategy seen for the acquisition of iron is the use of small, low molecular weight (usually under 1000 Da) iron chelators called siderophores that have a higher affinity for iron (III) than any other metal ions, including iron (II). This is the strategy that has evolved in aerobes and most facultative aerobes. Siderophores that have been characterized to date can be classified into three groups based on structural differences. These are the catecholates, hydroxamates and the pyoverdins (Fig. 1.1).

Catecholate siderophores are so named because of the catechol moieties present in the siderophore. Iron is chelated by the hydroxyl oxygen groups in these residues and as such each catecholate group can form two coordinate bonds with iron. Up to three catechol residues have been found in a single siderophore and this allows the compound to form the maximum six coordinate bonds with iron. An example of this is enterobactin, produced by *E. coli* (Fig. 1.1-A), which is a trimer of 2,3-dihydroxylbenzoylserine residues arranged as a cyclic triester (Hider, 1984). Hydroxamate siderophores chelate iron via a characteristic nitrogenous group that contains a hydroxyl group and a carbonyl oxygen (Fig. 1.1-B box). Aerobactin (Fig. 1.1-B) is an example of this type of siderophore, originally isolated from *Aerobacter aerogenes* and is able to form four coordinate bonds with iron (Neilands, 1992). Finally, pyoverdin siderophores

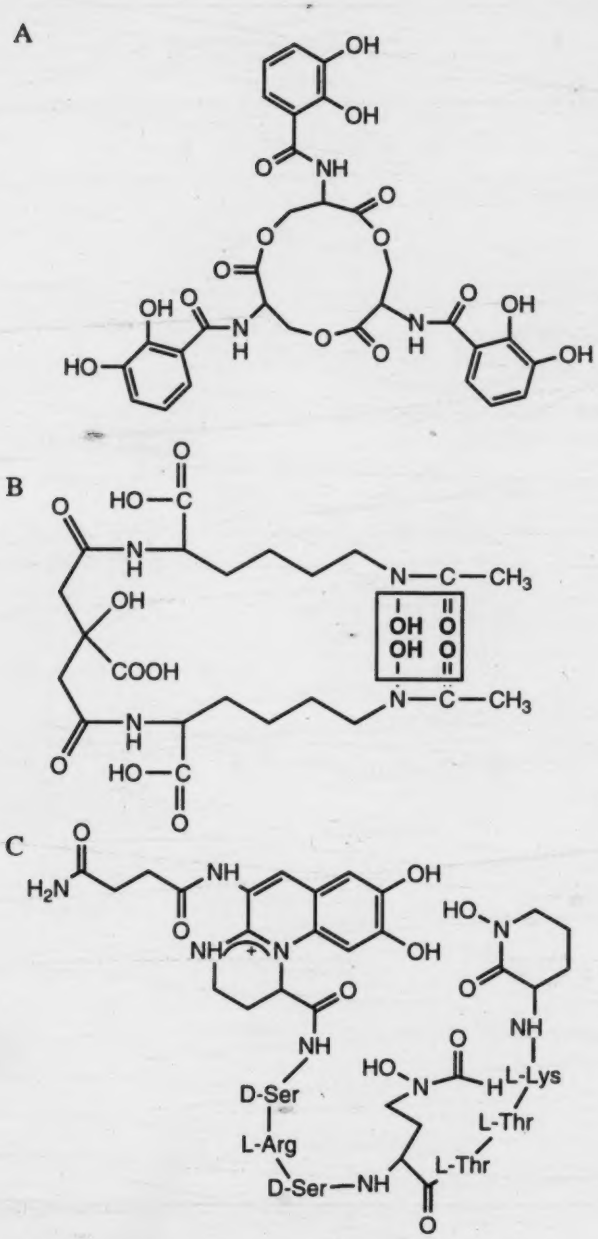

Figure 1.1 Examples of the three classes of siderophore.

(A) Catecholate: Enterobactin. (B) Hydroxamate: Aerobactin. (C) Pyoverdin.

(Fig. 1.1-C), which are commonly produced by *P. aeruginosa* use both catecholate-like and hydroxamate-like groups to chelate iron. A major difference between pyoverdins and the catecholate or hydroxamate siderophores is that pyoverdins have an unusual peptide component and a large heterocyclic chromophore which gives them an intense color (Coffman *et al.*, 1990).

A. vinelandii produces both catecholate and pyoverdin-like siderophores dependent on the iron concentration of the growth medium. These siderophores are the catecholates azotochelin (Corbin & Bulen, 1969) and aminochelin (Page & von Tigerstrom, 1988) (Fig 1.2-A & B). The third *A. vinelandii* siderophore is azotobactin (Page *et al.*, 1991) (Fig 1.2-C) which has been recognized as a member of a separate class of "pyoverdin-like" molecules, each of which has a unique peptide chain, iron coordinating groups, as well as chromophores that lack the substitution found in true pyoverdins (Abdallah, 1991; Briskot *et al.*, 1989). The siderophores of *A. vinelandii* are unique in that their production shows sequential regulation by iron availability. The catecholates are produced only at iron concentrations between 0 and 7 μM, while the formation of azotobactin begins at iron concentrations below 2 μM (Page *et al.*, 1991).

It should be noted, that although one of the key points of this study is high affinity iron-uptake, there is also evidence for a low affinity system used by most microorganisms when iron is plentiful or in a soluble state which does not require specific iron carriers (Guerinot, 1994).

1.2.5 Negative regulation of siderophore synthesis by ferric uptake regulator (Fur)

Fur is a 17-kDa protein that is rich in histidine residues and has the ability to bind to DNA when the protein is associated with iron (II) (Escolar *et al.*, 1998). Fur

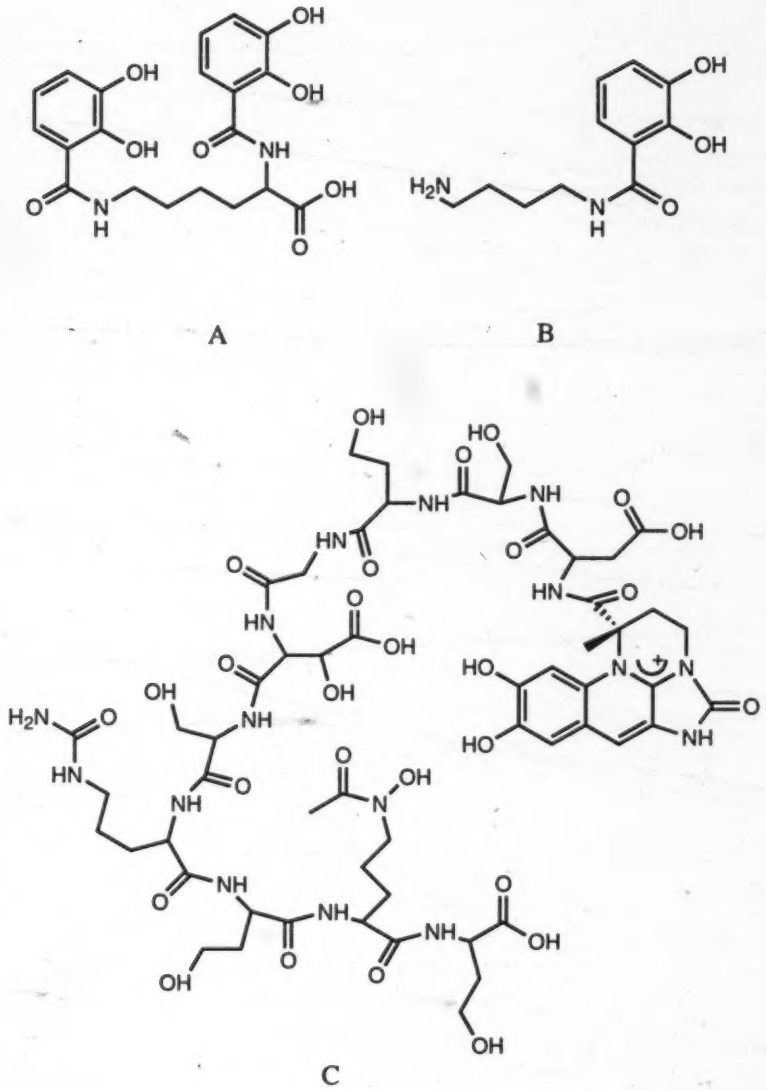

Figure 1.2 The siderophores of *A. vinelandii*.

(A) Azotochelin. (B) Aminochelin. (C) Azotobactin.

homologues have been found in many organisms besides *E. coli,* including *Pseudomonas* spp., *Neisseria* spp., *Synechococcus* spp. (cyanobacterium), *Klebsiella pneumoniae, Campylobacter jejuni, Salmonella typhimurium* (O'Sullivan *et al.*, 1990; Tomas & Sparling, 1996; Ghassemain & Straus, 1996; Achenbach & Yang, 1997; Woolridge *et al.*, 1994; Foster & Hall, 1992). The finding of a Fur-type protein in *A. vinelandii* by Western analysis (Mehrotra, 1997) indicates that there is a genetic control system in *A. vinelandii* that uses elements common to the well characterized system in *E. coli*. This, in addition to similarities in siderophore structure suggests that the use of the catecholate iron-uptake system of *E. coli* as a model for a similar system in *A. vinelandii* is valid.

Fur has been shown to function by binding to operator sites near the promoters of genes which are regulated by iron availability. As a result, Fur is a negative regulator of gene expression in the presence of high cellular iron (II) concentrations. During iron-limitation, iron (II) no longer associates with Fur and Fur can no longer bind to DNA at the consensus sequence known as an "iron box", this consensus sequence for Fur binding is the palindrome: 5'-GATAATGATAATCATTATC-3' (Crosa, 1989). In *E. coli*, it has been shown that upstream of the *fur* gene is a binding site for the catabolite activator protein (CAP). Thus, in addition to cellular iron (II), the expression of *fur* is tied to the over all metabolic state of the cell (de Lorenzo *et al.*, 1988). Whether this control exists in *A. vinelandii* is debatable, because *A. vinelandii* does not exhibit glucose catabolite repression and many not have an equivalent cAMP/CAP transcription activator system (George *et al.*, 1985). Fur exerts control over the iron uptake genes of *E. coli* as iron boxes are positioned in front of each cluster of genes in the 22 kb enterobactin operon (Silver & Walderhaug, 1992). In addition to the genes involved in iron-uptake, Fur has also been shown to regulate the expression of other genes which encode proteins that require iron. This includes proteins such as fumarase, superoxide dismutase and catalase (Hasset *et al.*, 1996; Hasset *et al.*, 1997; Iuchi & Lin, 1991). In the case of iron-

superoxide dismutase, Fur appears to act as a positive regulator in the expression of the iron-superoxide dismutase gene *sodB* (Fee, 1991; Foster & Hall, 1992).

1.2.6 Introduction to topic of thesis

This study was undertaken when it was observed that high concentrations of molybdate caused the formation of a new catecholate compound by *A. vinelandii*. This was considered unique as most microorganisms respond to high metal concentrations by expressing efflux systems to remove the metal from the microorganism (Ji & Silver, 1995). In addition to this, *A. vinelandii* strain LM100, which is not able to properly respond to oxidative stress (Isas *et al.*, 1995), was also seen to accumulate large amounts of this compound. However, it did so under conditions of low molybdate concentration. It was the goal of this work to: (1) understand what new catecholate compound was being produced in the presence of high molybdate and if it was a siderophore, (2) determine how molybdate concentration caused this to occur and (3) understand the connection between this compound and oxygen stress seen in strain LM100.

In addition to an examination of the microorganism central to this study, it is necessary to look at the metals that were studied. The two metals used extensively in this study were molybdenum and iron. To understand how they are involved in this work and how they interact with the cell it is necessary to examine some of the chemistry of each.

1.3 Molybdenum

1.3.1 Basic chemistry of molybdenum

In sea water, molybdenum is one of the most common heavy metals, found at a concentration of approximately 0.1 μmol kg^{-1}, however in the earth's crust, it is present at an average concentration of 15 μmol kg^{-1} in various types of ores (Pope *et al.*, 1980). As an ore, molybdenum is chiefly found as molybdenite (MoS_2), wulfenite ($PbMoO_4$) and

other molybdates such as $MgMoO_4$. In terms of its industrial use, molybdenum is primarily used in the formation of hard, strong, "high speed" steel (Cotton & Wilkinson, 1980). Elemental molybdenum has a molecular weight of 95.9 Da and is the forty-second element on the periodic table. As a result of this, it is a member of the second series of transition elements; it has a large atomic radius, it is a Lewis acid (it is able to accept electrons from other polarizable atoms), and it is able to exist in a number of oxidation states. In addition to this, as molybdate it can change oxidation states without considerable change in its already low redox potential, thus allowing for electron transfer between oxidation states.

Molybdenum can exist in oxidation states ranging from II to VI in aqueous environments. In the 2^+ and 3^+ oxidation states, molybdenum behaves largely as a cation and its reaction with water is not significant. Thus, it does not stay in solution at concentrations above 10^{-8} M (Pope *et al.*, 1980). However, as molybdenum (VI), molybdenum undergoes significant reaction with water to form amphoteric compounds, whose overall charge is pH dependent. For example, in aqueous solution molybdenum (VI) can exist as either MoO_2^{2+} or MoO_4^{2-}, however at pH 7 the ratio of $[MoO_2^{2+}]:[MoO_4^{2-}]$ is $10^{-19.4}$ indicating that MoO_4^{2-} is the favored form. The stereochemistry of these compounds is also pH dependent. Thus, as the pH changes so does the way in which molybdenum oxo-ions bind ligands. As the pH is lowered from alkaline conditions the coordination number of molybdate changes from 4 to 6 (tetradentate to hexadentate) and as a result the manner in which it coordinates ligands changes from a tetrahedral form to an octahedral one (Fig. 1.3-A). This octahedral coordination gives the molybdenum at the center of the complex a small ionic radius and as a result molybdenum is always displaced from the center of the complex. This leads to the formation of two short molybdenum-oxygen bonds which are *cis* to each other and, as a result of this, one side of the complex is always open

A

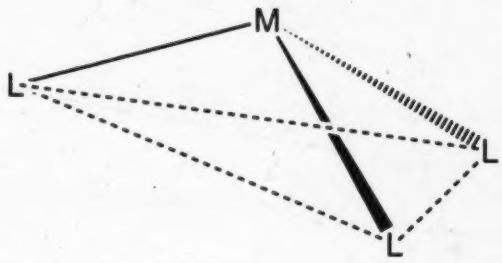

Coordination #3
Trigonal pyramid symmetry

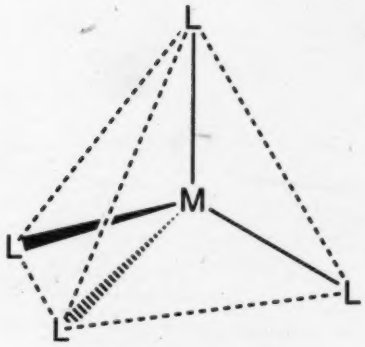

Coordination #4
Tetrahedral symmetry

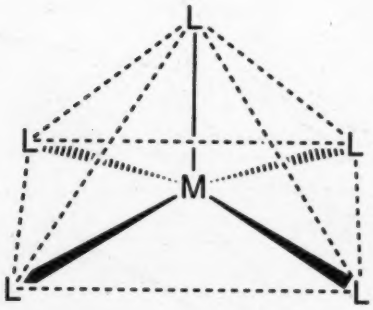

Coordination #5
Square pyramid symmetry

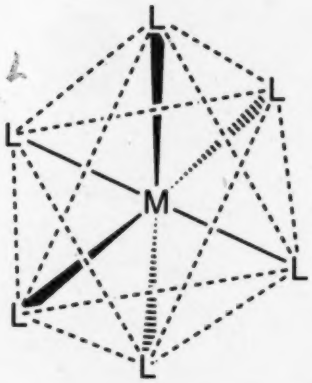

Coordination #6
Octahedral Symmetry

B

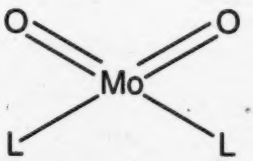

Cis configuration

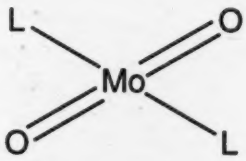

Trans configuration

Figure 1.3 Three-dimensional coordination chemistry models.

(A) Example of coordination conformation symmetry.
(B) Cis and Trans conformation of molybdenum binding to oxygen.
In all cases: L = ligand M = metal.

(Fig. 1.3-B) (Pope *et al.*, 1980). Under these aqueous conditions it is possible for molybdenum to react with itself to form polymolybdates or mixed polymolybdates such as phosphomolybdate, in addition to its reaction with water. This competition between water and molybdenum itself can be extended to include other ligands, such as proteins (da Silva & Williams, 1991).

1.3.2 Role of molybdenum in the cell

As seen in Section 1.2.3, molybdenum plays an important role in the nitrogenase I enzyme of *A. vinelandii*. Molybdenum interacts with iron to form an iron-molybdenum cofactor which serves as a catalyst for N_2 reduction. As nitrogen is converted to ammonia, electrons are added to molybdo-ammonia intermediates held at the active site of the nitrogenase, changing the way in which molybdenum interacts with nitrogen. This necessitates the use of a cofactor, such as molybdenum, that can change oxidation states and remain stable with only a small change in redox state (da Silva & Williams, 1991).

In addition to the nitrogenase I enzyme, molybdenum centers are also found in another class of about 20 enzymes found in many microorganisms. These mononuclear molybdenum enzymes catalyze oxygen atom or two-electron transfer as seen in xanthine oxidase, nitrate reductase, sulfite reductase or formate dehydrogenase (Hille, 1996). The reason molybdenum is found in this type of enzyme is due to the fact that molybdenum can easily undergo metal-oxygen bond cleavage to convert M=O to M + O (where M = metal). The presence of molybdenum in nitrogenase is not thought to be due to the formation of an analogous Mo-N_2 complex, which does occur, but rather due to the ability of molybdenum to change its oxidation states rapidly and easily (da Silva & Williams, 1991). In all cases, these molybdenum containing enzymes are large, multimeric complexes with other metal cofactors such as iron or iron-sulfur groups. In addition, in all of these molybdenum enzymes the molybdenum is coordinated by an

sulfur containing organic cofactor called a pterin (Hille, 1996). As in the case of nitrogenase, all of these enzymes allow the producing cell to respond to its environment and in some way to increase its chance for survival.

1.3.3 Uptake and storage of molybdenum

As stated in Section 1.3.1, molybdate availability in the environment is quite variable, and even in sea water, molybdate is not found at high concentrations. To overcome the lack of molybdate in the environment microorganisms that require it for growth have evolved low and high affinity uptake systems for its acquisition. In *A. vinelandii*, the low affinity uptake system has been shown to be active when molybdate concentrations are above 10 μM. Although this system has not yet been characterized, it is thought that it may involve either a passive, non-enzymatic process or the induction of specific, low affinity uptake proteins. However, it has been demonstrated that in mutants lacking the control elements of the high affinity system, the low affinity system can be repressed. This suggests that even the low affinity system is controlled by some type of "molybdate sensing" mechanism (Mouncey *et al.*, 1995). In *E. coli,* low affinity molybdate uptake is thought to occur via sulfate transporters and it may also occur through a nonspecific anion transport system that has been shown to transport sulfate, selenate, and selenite (Rosentel *et al.*, 1995).

The high affinity uptake system on the other hand is active at molybdate concentrations below 10 μM and had been well characterized in four microorganisms; *A. vinelandii, E. coli, Haemophilus influenzae,* and *Rhodobacter capsulatus*. In all four cases, the proteins used for high affinity molybdate acquisition are encoded for by the *mod* genes (Fig. 1.4-A) (Grunden *et al.*, 1996). As the *E. coli* and *A. vinelandii* systems are the best characterized, they will be discussed in detail. Within the *mod* operon, the *modABC*

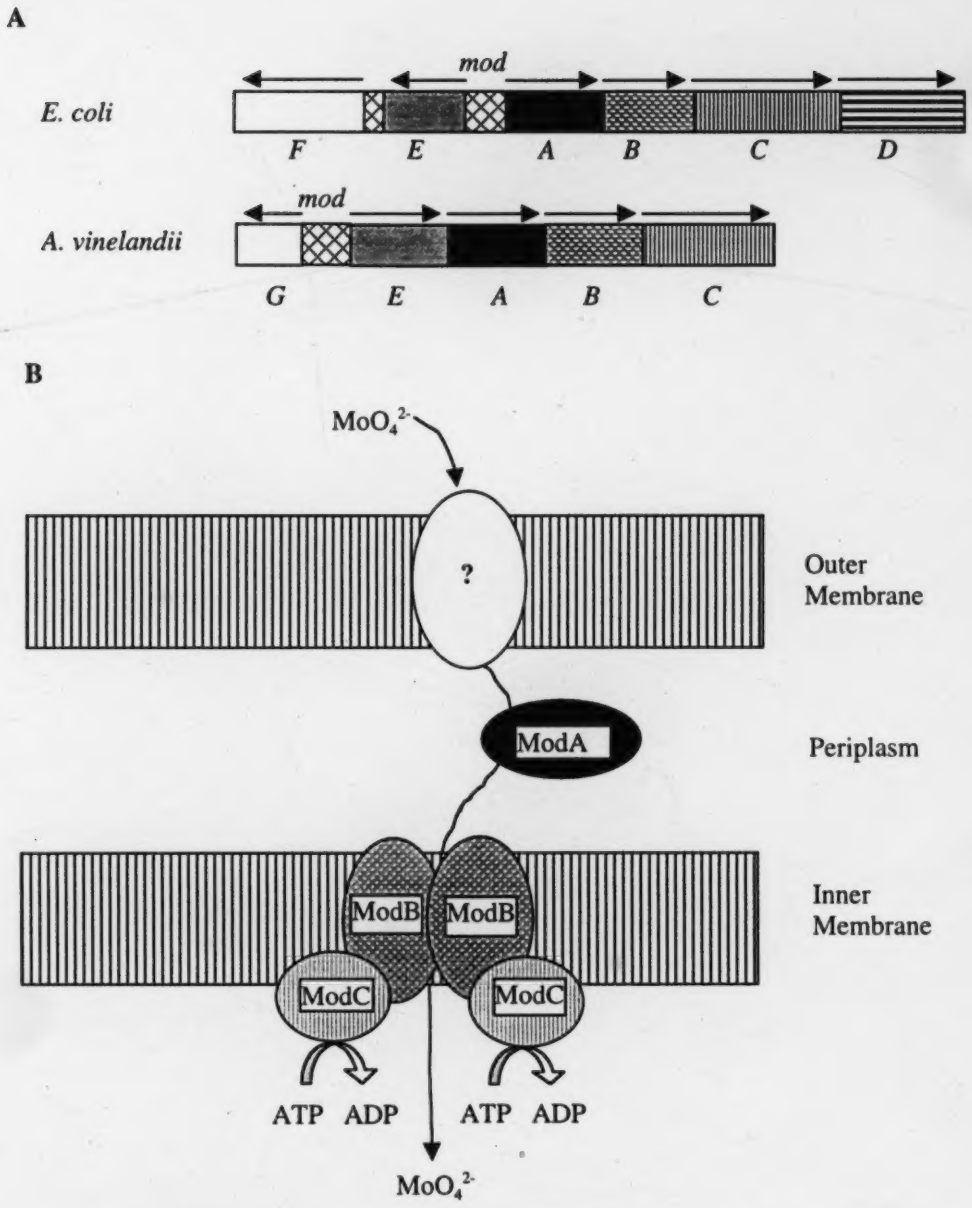

Figure 1.4 Molybdate uptake operon and model system.

(A) Molybdate uptake operon in *E. coli* and *A. vinelandii.*
(B) Model of molybdate uptake system taken from Grunden *et al.* (1996). Details in text

genes are responsible for the synthesis of the molybdate transport apparatus. The *modA* gene encodes a periplasmic protein that is specific for molybdate binding while the *modB* gene encodes an internal membrane transport protein which presumably transports molybdate into the cell. Finally, *modC* encodes a protein which energizes the system by hydrolyzing ATP and contains an ATP-binding cassette (ABC). Based on the model of the ABC super family of transporters that use a periplasmic permease, it would be expected that there should be two ModB and two ModC proteins acting to transport molybdate across the inner membrane (Fath & Kolter, 1993) (Fig. 1.4-B). In the *E. coli* operon there is a fourth gene, *modD*, whose product has not yet been characterized (Mouncey *et al.*, 1995).

In both *E. coli* and *A. vinelandii*, the molybdate uptake operon is regulated by the product of the *modE* gene which is thought to bind to molybdate and repress the synthesis of the high affinity uptake system. In *E. coli, modE* is located in a separate operon with *modF* and is located upstream from *modABC*. These genes are transcribed from a promoter divergent from *modABC* and are thought to act together to repress the *modABC* operon, although the role for *modF* has yet to be determined (Grunden *et al.*, 1996). In *A. vinelandii, modE* is the first gene transcribed in the *modEABC* operon and has also been shown to repress *modABC* expression. *A. vinelandii* also has a gene designated *modG* located upstream of *modEABC* and is expressed through a divergent promoter. Its function is unknown, but it shares some homology with *modE* and is also thought to bind molybdate (Mouncey *et al.*, 1995). Although the manner in which molybdate is transported from the periplasm across the inner membrane has been well studied, the manner in which molybdate crosses the outer membrane has yet to be established. There is evidence that suggests a carrier molecule is used to bind extracellular molybdate and transport it into the cell.

Molybdate coordinating compounds have been identified in *Azospirillum lipoferum*, *Bacillus thuringiensis*, and in cowpea *Rhizobium* (Saxena *et al.*, 1989; Ketchum & Owens, 1975; Patel *et al.*, 1988). All of the compounds studied appear to be produced at higher concentrations when cultures are grown under molybdate-limited conditions. These molybdate transport compounds also appear to be similar to siderophores. Whether, in fact, these compounds are the true mediators of high affinity molybdate transport or just misidentified members of a high affinity iron uptake system remains to be seen. It is, however, a well established fact that catecholate siderophores are capable of binding molybdate (Hider, 1984).

Once molybdenum is taken up by the cell there is evidence from both *A. vinelandii* and *K. pneumoniae* that excess molybdate is stored until needed. In the case of *A. vinelandii*, the excess molybdate is bound to a 100-kDa storage protein made up of 21-kDa and 25-kDa sub-units (Pienkos & Brill, 1981). This protein is able to bind up to 15 atoms of molybdenum per molecule and in doing so, keeps stored molybdenum separate from the pool of free molybdate in the cell. Evidence indicates that molybdenum is not bound to this protein as molybdate, as it is not possible to exchange radio-labeled molybdenum bound to the protein with unlabeled molybdate. Molybdenum has been found to be stored by this protein even in cells grown under nitrogen-sufficient conditions, allowing the cells to accumulate molybdate for future nitrogen-limited growth conditions (Shah *et al.*, 1984).

1.3.4 Similarity of vanadium, tungsten, and molybdenum

With respect to other heavy metals found in biology, molybdenum shares a number of common characteristics with vanadium and tungsten. Both of the latter elements are transition elements, vanadium from the first series and tungsten from the third series. Each has a large molecular weight, they are both Lewis acids, and they can exist in a

number of oxidation states. In addition, tungsten (VI) and vanadium (V), like molybdenum (VI), readily interact with water at neutral pH to stay in solution by forming the oxo-cations vanadate (VO_4^{3-}) and tungstate (WO_4^{2-}) (Pope *et al.*, 1980) and both vanadium and tungsten have been found to have roles in biological systems.

The best studied role for vanadium is in the nitrogenase II enzyme where it forms an iron-vanadium cofactor with iron. The fact that vanadium can exist in a number of oxidation states is taken advantage of to reduce nitrogen in the absence of molybdenum (Bishop, 1993). Tungsten, on the other hand, has been characterized in a number of enzymes found in anaerobic bacteria, specifically the NADP-dependent formate dehydrogenase of some *Clostridium* spp. and a carboxylic-acid reductase/aldehyde dehydrogenase found in *Clostridium thermoaceticum* (da Silva & Williams, 1991). In addition, because of its similarity to molybdate and the fact that molybdate and tungstate appear to share a common uptake system, tungstate has been used as an inhibitor of molybdate transport for the isolation of nitrogenase III mutants (Premakumar *et al.*, 1996).

1.4 Iron

1.4.1 Basic chemistry of iron

Iron is ubiquitous to the planet earth, it is present in sea water at a concentration of approximately 7.5×10^{-2} µmol kg^{-1} and is the second most abundant metal in the earth's crust (Cotton & Wilkinson, 1980). As an ore, iron is found predominantly as hematite (Fe_2O_3), magnetite (Fe_3O_4), limonite (FeO(OH)), and siderite ($FeCO_3$). Its importance as an industrial metal cannot be understated as the production of steel is one of its primary uses in industrialized nations. Elemental iron has an atomic weight of 55.8 Da and is the twenty-sixth element in the periodic table. As a result of this, it is a member of the first series of transition metals along with vanadium, manganese and zinc. As such, iron is a powerful Lewis acid due to its high charge density and readily forms stable bonds with

easily polarizable atoms such as oxygen (Hider, 1984). This is demonstrated by the reaction of metallic iron with oxygen to rapidly form oxides (rust) in the presence of humid air. Iron can also exist in a number of oxidation states ranging from II to VI, although the existence of iron in its higher oxidation states is rare and it is only iron (II) and iron (III) that are common under biological conditions. Both iron (II) and iron (III) can form six coordination bonds with various ligands and this results in complexes with octahedral symmetry. Iron (III) can also form tetrahedral and square pyramidal (Fig. 1.3-A) complexes whereas iron (II) cannot (Cotton & Wilkinson, 1980).

Iron (II) easily forms salts with almost any anion, and these salts readily go into solution in water where the iron (II) reacts with water to form $[Fe(H_2O)_6]^{2+}$. If however, dissolved oxygen is present in the water at neutral pH, iron(II) is rapidly converted to iron (III) as the redox potential of the Fe^{3+}-Fe^{2+} couple is +0.771V. This effect is lessened under acidic conditions, but eventually iron (II) is oxidized to iron (III) and precipitates out of solution as $Fe_2O_3 \cdot nH_2O$. If iron (III) is present in aqueous solutions, it can react with water to form $[Fe(H_2O)_6]^{3+}$ or it can react with itself to form large, multimeric iron complexes, even when pH is on the order of 2 or 3. To avoid the formation of these complexes, the pH of an iron (III) solution must be near zero. As the iron (III) continues to react with itself and water it forms a highly condensed species, ultimately leading to the formation of a colloidal iron (III)-water gel. With time, this hydrous-ferric oxide gel precipitates out of solution as an insoluble red brown mass (Cotton & Wilkinson, 1980). The oxidation of iron (II) to iron (III) can also occur in aqueous solution by the action of hydrogen peroxide. Hydrogen peroxide reacts with iron (II) to form iron (III), OH^- and the hydroxyl radical $\cdot OH$, the biological impact of this reaction will be discussed in Section 1.6.2.

So, even though iron (II) and iron (III) salts dissolve readily in water, they do not remain soluble, although they may not appear to immediately precipitate out of solution. Therefore, the inherently insoluble nature of iron, $Fe(OH)_3$ has a solubility constant of $2x10^{-39}$, must be considered when working with iron-containing solutions in chemical and biological systems (Tufano & Raymond, 1981). Biologically, this insolubility of iron is overcome in some cases by the use of solublizing agents such as siderophores.

1.4.2 Biological role of iron

As can be seen, iron has the ability to be converted back and forth between the 2^+ and 3^+ oxidation states. It is this ability to exist in one of two oxidation states that makes iron so biologically valuable that it functions in many key processes essential to life. The form of iron found in cellular systems can be divided into two groups, heme and non-heme iron. All proteins which have heme-iron as a cofactor contain a porphyrin moiety which provides a rigid structure for elemental iron binding; conversely, non-heme iron proteins lack this structure. Iron is present at the center of the porphyrin as a result of its specific incorporation during the synthesis of the porphyrin ring moiety (da Silva & Williams, 1991).

Proteins which contain heme iron generally have one of three functions. The first is the simple enzymatic transfer of electrons by iron-sulfur proteins and cytochromes which can have redox potentials ranging from –0.32 V (NADH-ubiquinone reductase) to +0.30 V (*a* type cytochrome). From the range of these redox potentials it can be seen that the electron transfer ability of iron is greatly modified by the protein environment in which it is held (Guerinot, 1994). These enzymes are found in the electron transport systems of cells and are responsible for the sequential transfer of an electron from a high redox state to a low one. This sequential passage of electrons allows the difference in redox potential between oxygen, the aerobic terminal electron acceptor, and the first iron-sulfur protein

in the transport chain to be converted into a proton gradient. As the electron is passed from one cytochrome to the next, protons are displaced across the cytoplasmic membrane (in prokaryotic systems) and this results in the formation of a potential difference (Cotton & Wilkinson, 1980). Ultimately, this stepwise transfer of electrons results in the reduction of dioxygen to water and the formation of ATP as protons pass back into the cytoplasm through ATP synthetase (ATPase) enzymes.

The second major function of heme iron proteins is the transport of oxygen. These functions are typified by the proteins hemoglobin and myoglobin; however, as these proteins are not found in bacterial sources, they will not be examined further. Finally, the third major function of heme-containing proteins is the transfer of oxygen molecules. Examples of this class of protein are oxidases, which often carry out the first step in the oxidation of complex organic molecules, and catalase which degrades hydrogen peroxide into water and oxygen. Cytochrome oxidase also functions in the transfer of oxygen and provides a link between oxidation of organic compounds and the transfer of electrons (da Silva & Williams, 1991).

The second form of iron found in proteins, non-heme iron, also plays an important role in the cell and once again depends on the ability of iron to exist in one of two redox states. Non-heme iron, when present as a protein cofactor, is often found in association with sulfur. This class of non-heme, low molecular weight protein is common and includes mononuclear rubredoxins, which contains one iron atom, and ferredoxins which may contain two or four atoms of iron. Rubredoxins are able to transfer one electron from a substrate, where as ferredoxins are able to transfer more than one electron and as a result their redox chemistry is much more complex (Cotton & Wilkinson, 1980). Iron-sulfur proteins have redox potentials that cover a range from –0.5 V to 0 V. For example, ferredoxin I from *A. vinelandii* has a midpoint potential of –0.424 V. Although the

majority of iron-sulfur proteins are involved in the transfer of electrons, other enzymes with different functions have also been characterized. Two of these which are of particular importance to *A. vinelandii* are nitrogenase I and hydrogenase (da Silva & Williams, 1991)and have already been discussed (Section 1.2.3).

In summary, it can be seen that iron plays a key role, in not only the energetics of microorganisms, but also in a vast number of strategies used by microorganisms to adapt to their environment. Key to the role iron plays in these systems is its ability exist in two redox states at physiological pH and its incorporation into proteins which results in the wide range of activities and redox potentials seen.

In addition to cases where iron plays a catalytic role in enzyme activity, there are two other iron proteins that are of importance to the cell. The first is the iron storage protein known as ferritin. As opposed to defining a specific protein, "ferritin" refers to a group of proteins, all of which are involved in the storage of excess iron for later use by the cell (Swenson *et al.*, 1991). It is important to limit the availability of free iron in the cell since free iron can generate damaging hydroxyl radicals. This sequestering of iron is accomplished, in part, by storing it as an insoluble oxide in ferritin. In addition, as a strategy to reduce the ability of bacterial pathogens to grow within in a eukaryotic host, concentrations of free iron are kept to a minimum. This is done by binding the iron in an inaccessible form in the proteins lactoferrin and transferrin. From these proteins iron can then be transferred into ferritin proteins for storage within eukaryotic cells (Cornelissen & Sparling, 1994). A second example of a protein that binds iron in a manner unlike those described is the ferric uptake regulator (Fur), which, as discussed in Section 1.2.5, has the ability to control gene expression based on cellular iron (II) concentration (Silver & Waldenhaug, 1992).

1.4.3 Chemistry of iron binding by catecholate siderophores

With respect to the chemical process of forming coordination bonds with iron, catecholates are ideal ligands for interaction with iron because of the presence of the hydroxyl groups within the catechol moieties of the siderophores. These hydroxyl groups contain two protons that have high pKa values of 9.2 and 10.2. This indicates that the oxygen atoms present have a high electron density, and thus represent ligands with a high affinity for protons when deprotonated at pH values above 6.5. In addition, because iron (III) is a strong Lewis acid it readily donates protons to other atoms such as the polarizable oxygen atoms of the catechol moiety. This electrostatic interaction gives catecholate siderophores a greater affinity for iron (III) compared to their hydroxamate counterparts. In addition, because iron (III) has a small atomic radius of 0.65 Å, it is favored over other biologically important metal ions such as copper and nickel for chelation by catecholates. It should be also pointed out that the charge density of iron (II) is only about one third of iron (III), and it is for this reason that siderophores have a higher affinity for iron (III) compared to iron (II) (Hider, 1984).

1.4.4 Determination of the affinity of a siderophore for iron

To compare the affinity of different siderophores for iron, it is possible to look at the formation constant of a iron-siderophore complex and calculate a numerical representation of iron binding. When the equilibrium equation of the formation of an iron-siderophore complex is written as follows:

$$aFe^{3+} + bSiderophore \leftrightarrows Fe_a\text{-}Siderophore_b \qquad K_{Form} = \frac{[Fe_a\text{-}Siderophore_b]}{[Fe^{3+}]^a\,[Siderophore]^b}$$

where "a" and "b" are the coefficients of stoichometry used to balance the equation. The larger the value of K_{Form}, the more the chemical reaction is favored to the right, and the

greater the affinity the siderophore has for iron. Conversely, if the equation is written as the dissociation of the ferric-siderophore complex into iron (III) and siderophore, then the smaller the disassociation constant, the higher the affinity of the siderophore for iron (III).

The stoichometric binding ratio of iron with the siderophore of interest must be found before the formation constant for iron and the siderophore can be determined. This can be done using a spectrophotometric method known as "Job's method of continuous variation". This method can only be used when the iron-siderophore complex is colored and the iron and siderophore alone are essentially colorless. In practical terms, the method consists of a number of reactions in which different concentrations of siderophore and iron are present, but the molar sum of iron and siderophore remain constant. These reaction mixtures are then examined at a wavelength previously determined to be the wavelength of maximum absorbance for the iron-siderophore complex. The reaction mixture with the ideal or correct ratio of iron to siderophore will have the greatest absorbance. In any other mixtures, free iron or siderophore will decrease the amount of complex formed and the absorbance in that reaction will be lower (Chaberek & Martell, 1959).

Once the molar binding ratio of the siderophore and iron has been determined, the formation constant can then be found. This is, however, not a simple matter of mixing iron and siderophore and determining the concentration of each in a reaction mixture. The catecholate siderophores are difficult to study using the methods normally employed in formation constant determination because the catechol groups of free siderophores are prone to air oxidation and the ester linkages found in many catecholate siderophores, like enterobactin, are sensitive to base-catalyzed hydrolysis. In addition, because of the extremely high stability of ferric-siderophore complexes, the equilibrium concentrations

of free iron and free siderophore are small and difficult to determine. As a result, direct measurement of formation constants is impossible. Rather, a method using competition with another iron chelating ligand with known, well studied chemistry is used (Harris *et al.*, 1979). This other ligand is often ethylenediaminetetraceticacid (EDTA). In this type of study two equations are employed:

Fe-EDTA + Sid ⇆ Fe-Sid + EDTA	K_{Comp}= [Fe-Sid] [EDTA] / [Fe-EDTA] [Sid]	(1)
Fe + EDTA ⇆ Fe-EDTA	$K_{Fe\text{-}EDTA}$= [Fe-EDTA] / [EDTA] [Fe]	(2)
Fe + Sid ⇆ Fe-Sid	$K_{Fe\text{-}Sid}$= [Fe-Sid] / [Fe] [Sid]	(Net)

Reaction (1) defines the interaction of the siderophore and a ferric-EDTA complex and is the reaction actually set up at the lab bench. Reaction (2) defines the interaction of iron (III) and EDTA, this reaction has been well studied and the $K_{Fe\text{-}EDTA}$ value for it is available in the literature. Therefore, from the competition reaction (1) and the known formation constant of Fe-EDTA from reaction (2) it is possible to rearrange the relationships and calculate the formation constant of the ferric-siderophore complex.

$$K_{Fe\text{-}Sid} = K_{Fe\text{-}EDTA} * K_{Comp} \quad (3)$$

$$K_{Fe\text{-}Sid} = K_{Fe\text{-}EDTA} * ([Fe\text{-}Sid]\,[EDTA] / [\,Fe\text{-}EDTA]\,[Sid]) \quad (4)$$

All the needed variables can be calculated from equilibrium concentrations of ferric-siderophore and known stoichometric relationships or literature values. Using analogous relationships it is possible to determine the $K_{Fe\text{-}Sid}$ value using competition between Fe-Siderophore and EDTA.

Even with the knowledge of the formation constants for a number of siderophores it is impossible to compare siderophores to each other unless all of the siderophores bind iron

with the same ratio of ligand:iron. If this is not the case, the formation constants will have different units making direct comparison impossible. One solution to this problem was suggested by Harris *et al.* (1979) who determined the concentration of free iron in a hypothetical system involving the siderophores of interest. The determination of these free iron values relies on the iron-siderophore formation constant, but also takes into account the ratio in which the siderophore binds iron. Before this method can be employed, the pH-independent formation constant of the ferric-siderophore complex must be determined. The values determined in Equations 1 to 4 are dependent on the pH of the buffer system, since the concentration of protons is not considered in the equilibrium equations. The pH-independent values can be determined by following the method described by Reid *et al.* (1993). It is first necessary to calculate the proton-independent solubility coefficients (K^{PI}_{SidFe}) for a siderophore, as shown below.

$$K^{PI}_{SidFe} = K^{pH\ 7.0}_{SidFe} / \alpha^{j-}_{Sid} \quad (5)$$

$$\alpha^{j-}_{Sid} = K_1K_2K_j / \Sigma ([H^+]^j + K_1[H^+]^{j-1} + K_1K_2[H^+]^{j-2} \ldots\ldots K_1K_2K_j) \quad (6)$$

This is done by first determining the fraction of each siderophore that is present, at pH 7.0, in a fully deprotonated form (α^{j-}_{Sid}). The Ka values used in this calculation can be based on the model compound *N,N*-dimethyl-2,3-dihydroxybenzamide, since the values for most catecholate siderophores are not known. These values are $10^{-8.4}$ for the *o*-hydroxyl protonation sites and $10^{-12.1}$ for the meta protons of the catechol group (Loomis & Raymond, 1991). Once α^{j-}_{Sid} is determined, the formation constant of the ferric-siderophore complex can be calculated for any pH. This value is then used to determine the free iron in a hypothetical system containing 10^{-6} M iron and 10^{-5} M siderophore at pH 7.4. The amount of free iron in the system is expressed as pFe^{3+} where

pFe^{3+} = -log [free Fe^{3+}] (Harris *et al.*, 1979). In this manner, siderophores with different molar binding ratios can be compared based on the iron concentration that remains unbound in a standard mixture.

1.5. Catecholate siderophore mediated iron uptake, the *E. coli*-enterobactin model

The catechol mediated uptake system of *E. coli* utilizing enterobactin is one of the best studied model iron uptake systems and as a result is very well understood in terms of siderophore synthesis, iron solublization, ferric-siderophore uptake, and iron release. Since *A. vinelandii* also produces catecholate siderophores, this system may also serve as a model for catecholate-mediated iron uptake in *A. vinelandii*. As will be described, there are a number of shared components between the two microorganisms that strengthen the rationale for the use of the *E. coli* model in *A. vinelandii*.

1.5.1 Enterobactin synthesis

Enterobactin is a tri-ester of 2,3-dihydroxybenzoylserine (2,3-DHBS) residues that has the highest known affinity for iron of all siderophores, having a proton independent formation constant on the order of 10^{52} (Guerinot, 1994). The synthesis of the siderophore occurs in two stages, the first involves the *entC*, *entB*, and *entA* genes and results in the formation of 2,3-dihydroxybenzoic acid (2,3-DHBA) residues from chorismate, a precursor from the aromatic amino acids pathways. The second part of the pathway forms 2,3-DHBA and serine into enterobactin using the products of the *entD*, *entE*, *entF*, and *entB* genes (Ozenberger *et al.*, 1989). Of these genes, *entF* shares sequence homology with the peptide synthetases responsible for the non-ribosomal peptide synthesis of peptide antibiotics and the fatty acid synthase complex which forms fatty acids. As a result, it was once thought that the protein products of these genes associate together to form a polypeptide complex, referred to as the enterobactin synthetase, to form enterobactin from three 2,3-DHBS monomers (Hantash *et al.*, 1997).

Recent evidence however, suggests that this may not be the case as each Ent protein has been shown to function independently (Gehring *et al.*, 1998; Gehring *et al.*, 1997).

The first step in enterobactin synthesis is the reversible conversion of chorismate to isochorismate by isochorismate synthase, the product of the *entC* gene (Fig. 1.5). This 391 amino acid, Mg^{2+}-requiring protein functions as a monomer with a molecular weight of 42.9-kDa (Ozenberger *et al.*, 1989: Liu *et al.*, 1990). Homologues of this gene have been found in *Aeromonas hydrophila*, *Bacillus subtilis*, *Vibrio cholerae*, *Erwinia chrysanthemi*, and *A. vinelandii* (Barghouthi *et al.*, 1991; Rowland & Taber, 1996; Wyckoff *et al.*, 1997; Franz & Expert, 1991; Sharpe, 1999). The second protein involved in the formation of 2,3-DHBA is the 150-kDa product of the *entB* gene. (Rusnak e*t al.*, 1990) EntB is a bifunctional, pentameric protein that has isochorismatase activity at its N-terminal, which converts isochorismate into 2,3-dihydro-2,3-dihydroxybenzoic acid (2,3-DH-2,3-DHBA), and an aryl carrier protein (ArCP) domain in its C-terminus, which is involved in the final assembly of the enterobactin tri-ester (Gehring *et al.*, 1997). The final step in the formation of 2,3-DHBA is the NAD^+ dependent conversion of 2,3-DH-2,3-DHBA to 2,3-DHBA by a 2,3-DH-2,3-DHBA dehydrogenase. This protein is encoded by the *entA* gene and is an octamer with total molecular weight of 210-kDa (Liu *et al.*, 1990).

Considerable work has been done on the second portion of the enterobactin synthesis pathway in the last two years by Gehring and her co-workers. This has provided new insights into the mechanistic manner in which enterobactin is assembled by EntB, EntD, EntE, and EntF.

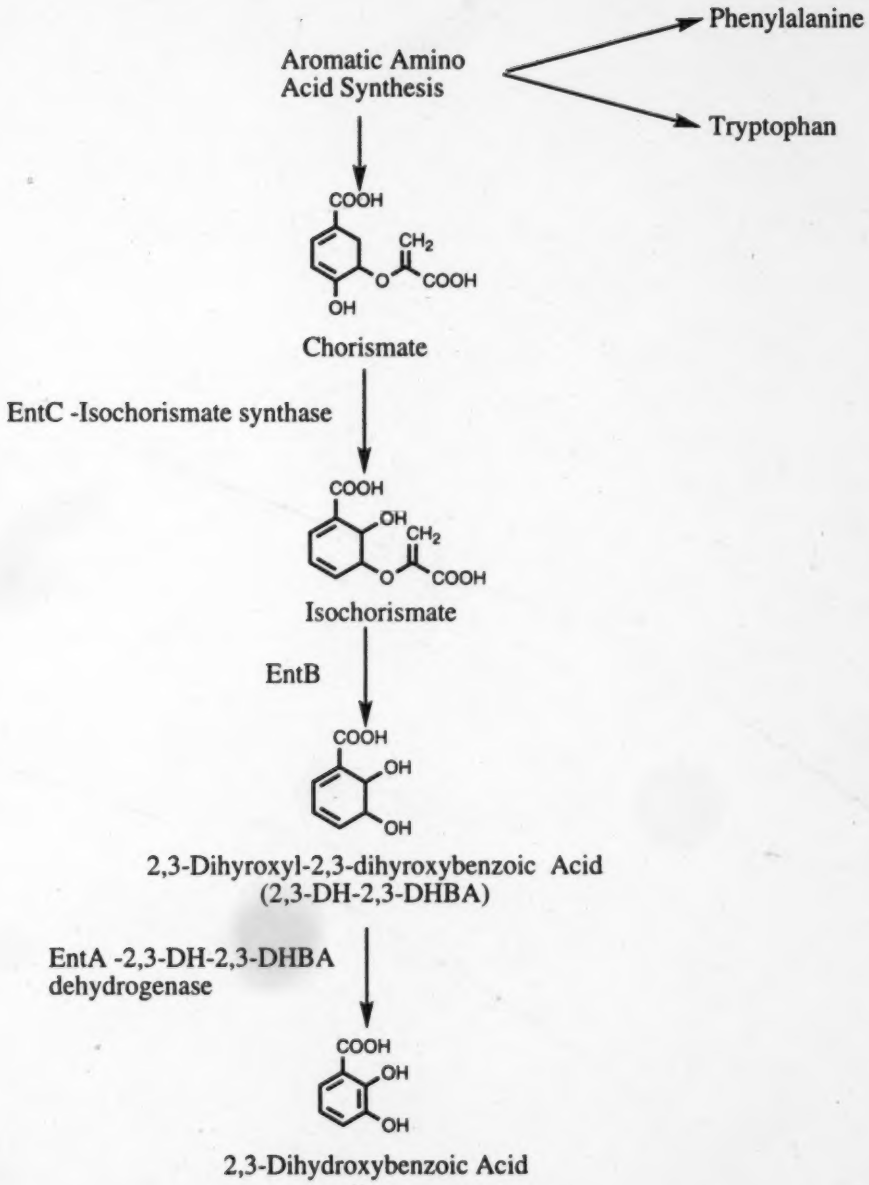

Figure 1.5 Formation of 2,3-dihydroxybenzoic acid from chorismate.

taken from Silver & Walderhaug (1992).

EntB contributes to enterobactin assembly through its C-terminus ArCP domain. This domain that receives a phosphopantetheinyl group from Co-enzymeA through the action of the 23-kDa EntD protein. In doing so, EntD forms phosphopantetheinyl holo-EntB which then participates in the transfer of 2,3-DHBA into enterobactin (Fig 1.6-A). The transfer of 2,3-DHBA into enterobactin had once been associated with the product of the *entG* gene, but extensive analysis by Staab & Earhart (1990) and work by Gehring *et al.* (1997) has confirmed that there is no *entG* gene in the enterobactin regulon and that in fact EntB is a bifunctional protein. EntD has also been shown to function in the transfer of a phosphopantetheinyl group into the peptidyl carrier protein (PCP) domain of the EntF protein forming holo-EntF and allowing EntF to interact with serine (Fig. 1.6-A) (Gehring *et al.*, 1998; Lambalot *et al.*, 1996). 2,3-DHBA enters into enterobactin assembly via the 118-kDa EntE protein. EntE is a 118-kDa dimer that functions as a ligase to specifically adenylate 2,3-DHBA into 2,3-DHBA-AMP and forms a covalent linkage between 2,3-DHB-AMP and EntE (Fig. 1.6-B) (Rusnak *et al.*, 1989). Once 2,3-DHB-AMP-EntE is formed, EntE then transfers 2,3-DHB-AMP onto holo-EntB forming holo-EntB-DHB (Fig. 1.6-C). In an similar manner, serine is adenylated (Fig. 1.6-D) and bound to EntF for assembly into enterobactin by the action of the 142-kDa holo-EntF protein itself (Fig. 1.6-E) (Rusnak *et al.*, 1991).

The protein that is ultimately responsible for the formation of enterobactin from its component parts is EntF, which serves as scaffolding for the assembly of enterobactin. EntF is a large, multifunctional protein (1293 amino acids) with four distinct functional domains. The N-terminal (residues 1 to 475) contains an elongation and condensation domain, an adenylation domain found at residues 476 to 960 forms serine-AMP, a peptidyl carrier protein (PCP) domain is located at residues 961 to 1049, and finally, a thioesterase (TE) domain is found at residues 1050 to 1293 (Fig 1.7) (Gehring *et al.*, 1998). EntF begins to assemble enterobactin by first adenylating serine then transferring

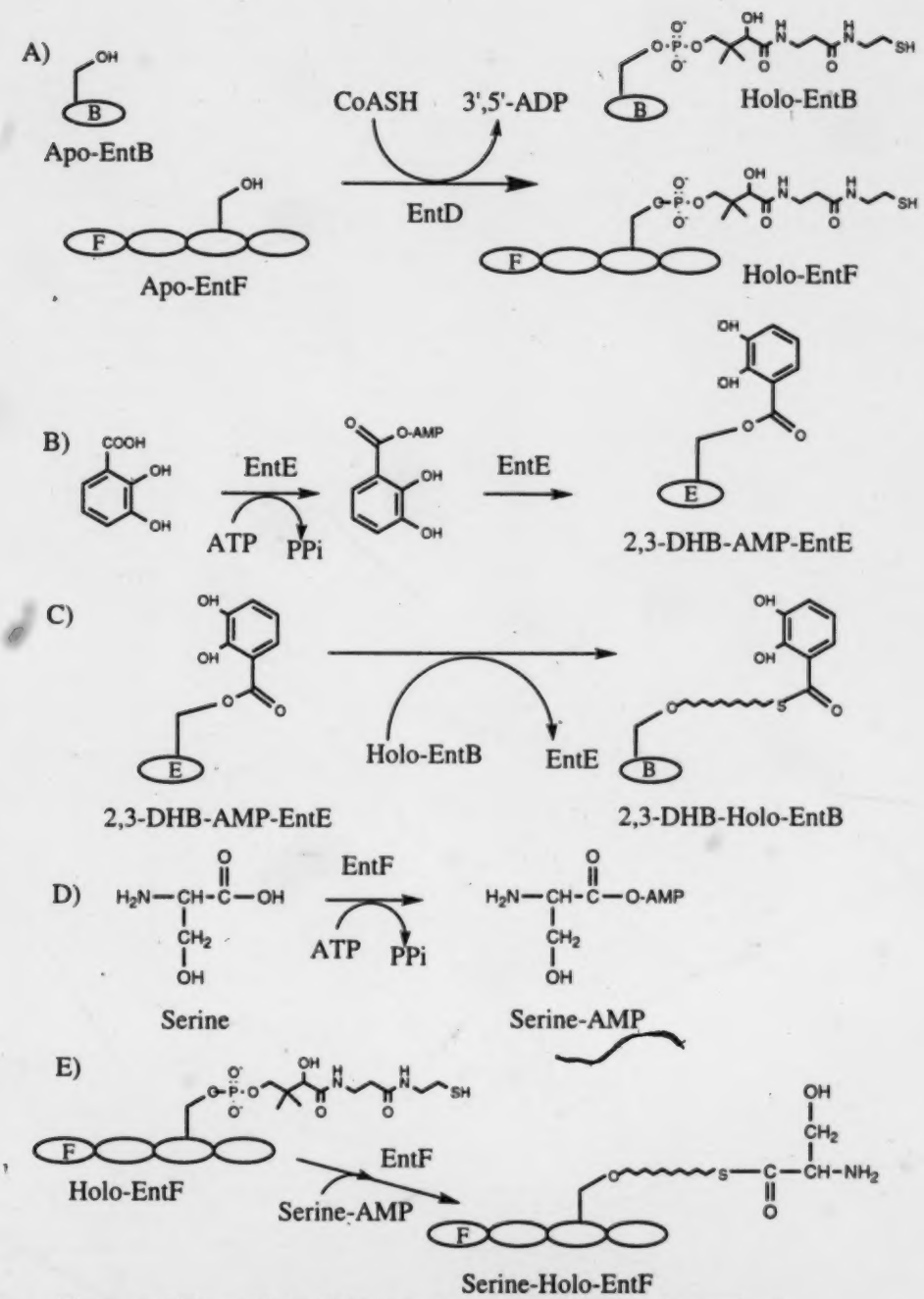

Figure 1.6 Formation of the precursors of enterobactin synthesis.
~~~SH = phosphopantetheine group ⬭ = Enterobactin protein as labeled.
CoASH = Coenzyme A (Gehring *et al.*, 1997; Gehring *et al.*, 1998).
~~~

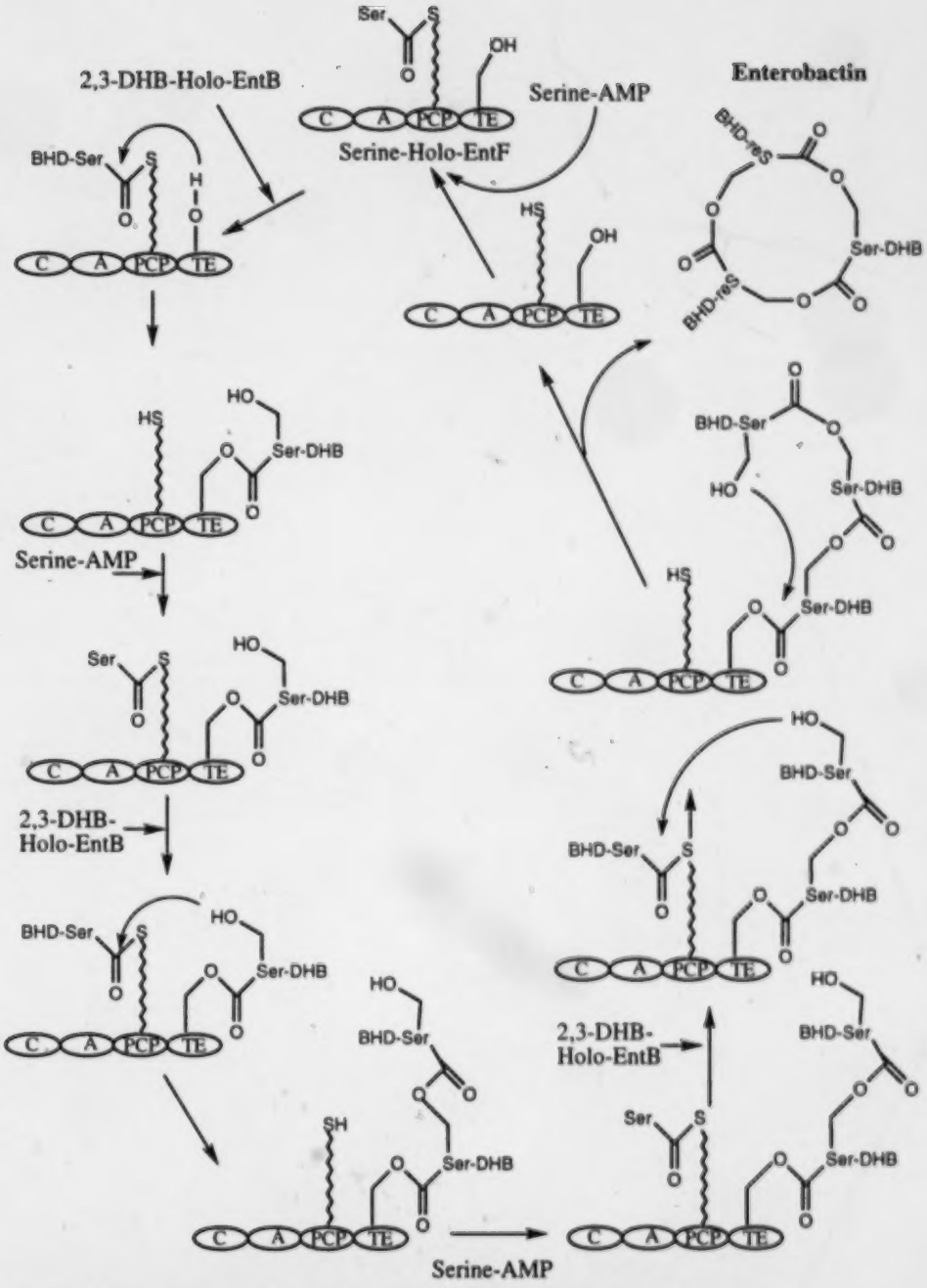

Figure 1.7 Enterobactin synthesis from precursors by EntF.
C=condensation domain, A=adenylation domain, PCP=peptidyl carrier protien domain TE=thioesterase domain of EntF. Ser=serine, DHB=2,3-dihydroxylbenzoic acid.
~~~~~SH= phosphopantetheine group (Gehring *et al.*, 1998).
~~~~~

serine-AMP to its PCP domain forming holo-EntF-serine through the phosphopantetheinyl group added by EntD. Once present as holo-EntF-serine, the amide linkage between 2,3-DHBA and serine is formed by the interaction of holo-EntF-serine and holo-EntB-DHB before the formation of any ester bonds linking serine residues. This occurs as the carbonyl oxygen on the DHB moiety of holo-EntB-DHB undergoes a nucleophilic attack by the terminal amine of the serine on holo-EntF-serine. This leads to the formation of holo-EntF-serine-DHB (Fig. 1.7). As there is only one PCP domain on EntF, and EntF has been shown to act as a monomer, the question arises as to how are three 2,3-DHBS groups esterified together on a protein that can only hold one 2,3-DHBS monomer?

Gehring *et al.* (1998) suggest that this limitation is over come by the TE domain of EntF. This portion of EntF is similar to non-ribosomal peptide synthetase and fatty acid synthetase enzyme complexes and the model Gehring *et al.* (1998) present is based on what is known about the formation of fatty acids and polyketide chains. Data have been collected that indicates that EntF has two sites to which a 2,3-DHBS monomer could be bound. The first is at ser-1006 in the PCP domain which is the site of phosphopantetheine attachment by EntD, and the second is at ser-1138 in the TE domain. Gehring *et al.* (1998) suggest that 2,3-DHBS is formed at ser-1006 and is then transferred to ser-1138 in the TE domain freeing ser-1006 for the formation of a second 2,3-DHBS monomer. In their model, as the second monomer is transferred into the TE domain, the ester bond between the two monomers is formed by a nucleophilic attack by the first monomer on the second, transferring the second monomer into the TE domain. This results in space being made available in the PCP domain for the formation of a third monomer which is then transferred into the TE domain by another nucleophilic attack. Finally, the formation of a third ester bond in this region could then occur with the subsequent release of enterobactin (Fig. 1.7) (Gehring *et al.*, 1998). To strengthen their

model, Gehring's group is currently looking for $(2,3\text{-DHBS})_n$ species that are covalently linked to EntF which should be present as intermediates in enterobactin assembly.

If in fact this model does represent the mechanism by which enterobactin is assembled, it indicates that EntF alone is the only enzyme required to assemble enterobactin. The other Ent proteins function only to provide EntF with the components required for enterobactin formation This is a departure from the long held hypothesis that the enterobactin synthetase was a multi-protein complex. To this end, Gehring *et al.* (1998) have demonstrated that when all activated precursors were present, only EntF was required to form enterobactin *in vitro*. If in fact EntD, EntE, EntF, and EntB do form a complex *in vivo*, these data would suggest that this complex is not essential for enterobactin formation.

With this information, the last real question to be answered involving the enterobactin system is how is the completed enterobactin transported out of the cytoplasm? Sequence homology data suggests that EntD may play a role in enterobactin export as EntD shares homology with proteins found in *B. subtilis* that are involved in peptide antibiotic secretion (Grossman *et al.*, 1993). This, in addition to the localization of EntD to the inner leaflet of the inner membrane, would suggest that it is involved in the secretion of the completed enterobactin molecule across the inner membrane into the periplasm (Armstrong *et al.*, 1989). Conformation of this second role for EntD and the manner in which enterobactin is released into the extracellular environment awaits further experimental evidence.

1.5.2 Siderophore export

Although the manner in which siderophores are exported out of *E. coli* remains something of a "black box", some evidence has been presented which suggests how

siderophores are exported out of *Pseudomonas* spp. This proposal comes from work by Poole *et al.* (1993a & 1993b) who have suggested that the Mex system (*mexA-mexB-oprK*), found to play a role in multiple antibiotic efflux in *P. aeruginosa*, may be involved in the export of the siderophore pyoverdin. The basis for this hypothesis is that the antibiotics effluxed out of the cell by the Mex system are structurally similar to pyoverdin and that these antibiotics can also bind metal ions. It has been previously shown that components of the iron-uptake system of *E. coli* (Fiu and Cir proteins involved in 2,3-DHBS uptake) have a broad substrate specificity and it is possible that this lack of specificity extends to those proteins involved in siderophore export. Poole *et al.* (1993a & 1993b) go on to suggest that, in a manner analogous to MexA-MexB-OprK, the AcrA and AcrB proteins involved in acriflavin dye efflux (Ma *et al.*, 1995) could play a role in siderophore export in *E. coli*. The rationale for this is that dye export is probably not the native function of these two proteins and that siderophore export could be. They suggest that the observed export of the dye is coincidental since the dye and the siderophore share a number of chemical characteristics. In addition to this, homology is seen between the proteins found in the Acr system and the Mex system of *Pseudomonas*, making the suggestion of siderophore export as a function of AcrA and AcrB tempting. Although this evidence does present some interesting possibilities in terms of future research, it is all quite speculative. For the time being, the elucidation of the manner in which siderophores are export out of *E. coli* has yet to be completed.

1.5.3 Ferric-enterobactin uptake

Once enterobactin has been released by the cell and bound iron, it must be taken up by the cell so that its cargo of iron can be used. The uptake and transport of ferric-enterobactin complexes is performed by 74-kDa to 84-kDa iron repressible outer membrane proteins (IROMPS) (Neilands, 1994) and in the case of enterobactin, these proteins are products of the *fep* genes. In this system, the ferric-enterobactin complex is

bound by an outer membrane protein, which is energized to do so by the membrane spanning TonB protein, and passed to a periplasmic intermediate before being shuttled across the inner membrane by proteins which hydrolyze ATP during transport (Guerinot, 1994).

As outlined in Fig. 1.8, the first step in the uptake of the ferric enterobactin complex by *E. coli* is the recognition and binding of the complex by the minor outer membrane protein FepA (Ozenberger *et al.*, 1987). FepA is different from other outer membrane proteins, such as OmpF, in that it exists as a monomer and based on predicted structural features is thought to have 29 membrane spanning domains. Once it has bound the ferric-enterobactin complex, FepA undergoes a conformational shift which allows the sequence of amino acids from 12 to 16, known as a "TonB box", to interact with TonB. Numerous outer membrane proteins which interact with TonB contain this "TonB box" consensus sequence and include proteins involved in the uptake of other classes of siderophores, colicins, and vitamin B12 (Schramm *et al.*, 1987). Further evidence for the interaction of TonB with FepA came when Skare *et al.* (1993) demonstrated that TonB could be chemically cross-linked to FepA.

TonB has been defined as a membrane-spanning protein that energizes the outer membrane protein receptors of microorganisms such as *P. aeruginosa, Xanthomonas campestris, E. coli* and many other members of the *Enterobacteriaceae* (Poole *et al.*, 1996; Wiggerich *et al.*, 1997; Larson *et al.*, 1996). From its deduced amino acid sequence, TonB is predicted to have a molecular weight of 26-kDa with hydrophobic amino and carboxyl termini and a hydrophilic central region (Postle, 1993). Analysis of this structure revealed that the amino terminus of the protein is anchored in the cytoplasmic membrane while the carboxyl terminus associates with the outer membrane

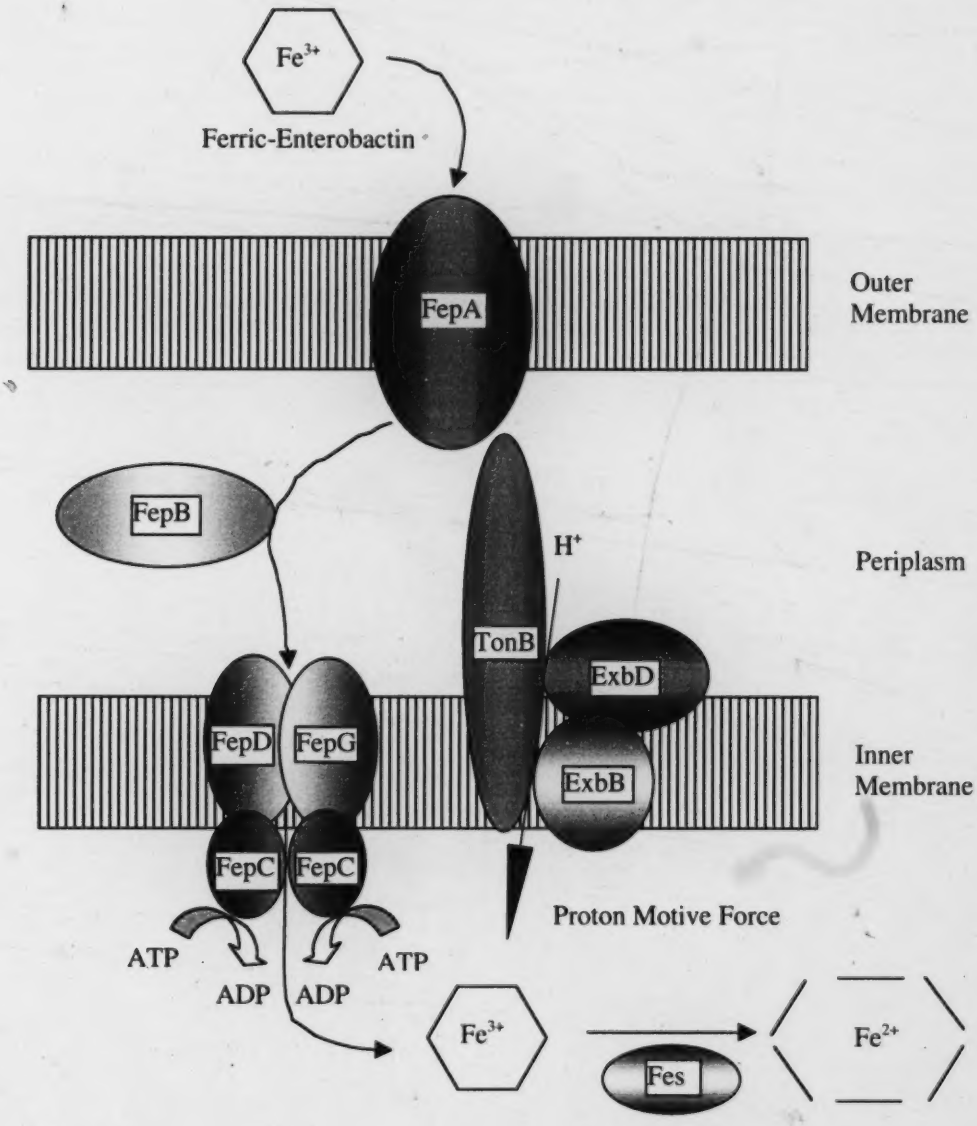

Figure 1.8 Model of ferric-enterobactin uptake in *E. coli*.

Modified from Silver & Walderhaug (1992). See text for details.

(Letain & Postle, 1997) and the rest of the protein is found in the periplasm (Silver & Waldenhaug, 1992).

For TonB to function in ferric-siderophore uptake, two accessory proteins must also be present. These are ExbB and ExbD, both of which are located in the inner membrane and serve to stabilize TonB. ExbB is a 26-kDa protein that resides predominately in the cytoplasm, with only the amino terminus of the protein extending into the periplasm (Kampfenkel & Braun, 1993). ExbD also plays a role in the functioning of TonB, since its absence abolishes all TonB related activities (Braun *et al.*, 1996). Topological analysis of ExbD indicates that, like TonB, a large portion of ExbD exists in the periplasm (Kampfenkel & Braun, 1992). The current hypothesis of ExbD and ExbB function is that the two proteins act to return TonB to its energized state within the cytoplasmic membrane after it has energized the outer membrane (Moeck & Coulton, 1998). Recent work by Higgs *et al.* (1998) has suggested that ExbB and ExbD do not interact as single proteins, but rather they are each present as trimers and in total form a heterohexamer. The authors suggest that this hexamer could form an ion transferring channel which could couple the proton motive force to changes in TonB conformation. Although interesting, Higgs *et al.* (1998) do not yet have direct biochemical evidence for the presence of such a heterohexamer.

Two different models for how TonB interacts with outer membrane proteins exist. In the first, TonB remains anchored in the inner membrane and changes conformation to interact with an outer membrane protein (Moeck & Coulton, 1998). In the second, suggested by Letain & Postle (1997), TonB disassociates from the inner membrane to fully associate with the outer membrane allowing the incorporation of receptor captured ligands. TonB then re-associates with the inner membrane via ExbB and ExbD for recycling to its active conformation. Both models account for TonB association with the

outer membrane, but the second model presents a number of problems in terms of the release and capture of TonB and the molecular mechanisms by which energy could be stored and "moved" to the outer membrane without connection to the inner membrane. It is the portion of the protein in the inner membrane is thought to allow for a connection to the cellular proton motive force, while the carboxyl terminus allows for interaction with outer membrane receptors. Removal of the periplasmic spanning portion of the protein has been shown to reduce, but not destroy TonB mediated uptake, as only the final 48 amino acids of TonB were determined to be essential for its function (Larsen *et al.*, 1997). So, in as much as the role of TonB has been well established in the transport of the ferric-enterobactin complex across the outer membrane via the FepA receptor, there are details of this system which remain to be described.

The next step in the transport of the ferric-enterobactin complex into the cell is the passage of the complex across the periplasm. This function was predicted by Pierce & Earhart (1986) to be carried out by the 34-kDa FepB protein (Fig. 1.8), this was confirmed by Stephens *et al.* (1995) who showed that FepB could bind to the ferric enterobactin complex. From FepB, the ferric-enterobactin complex then passes through the inner membrane by the action of the FepD, FepG and FepC proteins (Fig. 1.8). The hypothesis that FepD and FepG were involved in transport across the inner membrane was originally based on the fact that the ferric-enterobactin uptake system resembles a typical periplasmic permease, which is a subclass of the ABC transporter super-family (Chenault & Earhart, 1992).

Consistent with this model, hydrophobic protein(s) of about 30-kDa in size would be needed to span the inner membrane. FepD has a predicted molecular weight of 33.8-kDa and FepG has a predicted molecular weight of 35-kDa and both of these proteins are hydrophobic in nature (Shea & McIntosh, 1991). As well, the *fepD* and *fepG* genes share

significant sequence homology with genes for other inner membrane transport proteins such as FecD, FhuB and BtuC (Chenault & Earhart, 1991). This evidence suggests that FepD and FepG are in fact inner membrane transporters.

The final required transport component in this system is a protein which can drive transport of ferric-enterobactin across the cytoplasmic membrane via FepD and FepG through the use of ATP. FepC is predicted to have this function. FepC is a 31-kDa protein first located in the cytoplasmic membrane and was implicated in enterobactin mediated iron-uptake by Pierce and Earhart (1986). Analysis of the predicted amino acid sequence of FepC suggests that it has a hydrophobic, peripheral membrane location and that it also contains conserved ATP binding domains consistent with proteins in the ABC transporter super-family (Fath & Kolter, 1993; Shea & McIntosh, 1991). Based on the stoichometry suggested by this, it would be expected that in the FepD/G/C complex there would be two molecules of FepC, one for each molecule of FepD and G. This has not been confirmed however, as components of this type of system are typically difficult to detect and do not migrate in a typical fashion on SDS-PAGE gels; thus part of the problem in studying FepD, FepG, and FepC proteins has been a technical one (Chenault & Earhart, 1992).

Once the ferric-enterobactin complex enters the cytoplasm, iron must be released for use by the cell. The problem with this step is that the dissociation constant for the removal of iron from the ferric-enterobactin complex is 10^{-52} M. This is far too small for any amount of iron to be spontaneously released into the cell. This problem is overcome by the action of the 43-kDa ferric-enterobactin esterase (Fes), the product of the *fes* gene. Fes cleaves the enterobactin molecule back into 2,3-DHBS monomers (Fig. 1.8) such that the ferric-siderophore dissociation constant is lowered to 10^{-8} M, making the iron more accessible to the cell (Brickman & McIntosh, 1992).

Studies on the activity of the Fes protein have shown that it can cleave either the ferric-enterobactin complex, or enterobactin itself, but the enzyme hydrolyzes enterobactin four times faster than the ferric-enterobactin complex. Thus, the ability of Fes to cleave ester bonds is independent of the presence of iron (Brickman & McIntosh, 1992). Work done in the late 1970's and early 1980's suggested that the cleavage of the ester linkages of enterobactin was not necessarily an essential function in Fes-mediated iron release. Using enterobactin analogues that did not contain ester linkages Hollifield & Neilands (1978) and Heidinger *et al.* (1983) showed that these analogues could supply iron to cells with a functioning Fes protein, as long as a functioning FepB protein was also present. This would suggest that there is another function or protein either associated with Fes or acting at the same time as Fes that participates in making iron available to the cell. This protein or function of Fes has been suggested to be a ferric reductase that reduces iron (III) to iron (II) making iron available to the cell as catecholate siderophores have a low affinity for iron (II) (Section 1.4.3).

Brickman & McIntosh (1992), using purified Fes, addressed this controversy and their data confirmed that the hydrolysis of ferric-enterobactin was necessary for the release of iron (II). Their work also established that the reduction of iron from iron (III) to iron (II) was part of the process involved in the removal of iron from the ferric-enterobactin complex. Unfortunately, they did not establish whether an autonomous ferric reductase performed this function or whether Fes was bifunctional. It is possible that a ferric reductase may be encoded within the enterobactin operon as there are a number of open reading frames that have yet to be characterized.

Finally, once iron is released from the ferric-enterobactin complex it can be stored for later use in the ferritin protein or it can be incorporated into a heme or non-heme protein by ferrochetalase (Miyamoto *et al.*, 1994; Silver & Walderhaug, 1992).

1.5.4 Iron release by ferric reductase

As mentioned, there is a role to be played by ferric reductases in the release of iron from ferric-siderophore complexes. Examples of this have been demonstrated in *Bacillus* spp., *Agrobacterium tumefaciens, Mycobacterium smegmatis, Micrococcus denitrificans, Neurospora crassa, Ustilago sphaerogena, E. coli, P. aeruginosa, Rhodopseudomonas sphaeroides* and *A. vinelandii* (Lodge *et al.*, 1980; Lodge *et al.*, 1982; Halle & Meyer, 1992a; Huyer & Page, 1989). The ferric reductases that have been characterized share a number of common characteristics. They all use NAD(P)H as their source of electrons, they all appear to be sensitive to oxygen, and, for the most part FMN has a stimulatory effect on their activity (Halle & Meyer, 1992b).

With respect to the type of siderophore acted upon by a ferric reductase, the above list of microorganisms includes siderophores of all three types. The location of the ferric reductase enzyme is variable among the microorganisms examined. Many of the microorganisms examined, including *A. vinelandii*, have ferric reductase activity localized to the cytoplasm (Huyer & Page, 1989), whereas some are found in the periplasm, such as the ferric-pyochelin reductase of *P. aeruginosa* (Cox, 1980) and others are found to be membrane bound as in *B. subtilis* and *E. coli* (Gaines *et al.*, 1981; Fischer *et al.*, 1990).

The two ferric reductase enzymes of *A. vinelandii* are somewhat unique from the enzymes mentioned above in that they are both inhibited by the presence of Zn^{2+} and Mn^{2+}. Cells that were grown in the presence of Zn^{2+} showed lower intracellular iron

concentrations and produced siderophores at greater levels than cells grown in the absence of Zn^{2+}. Cells grown with Mn^{2+} also demonstrated increased siderophore production and contained less cellular iron. In both cases, the changes in cellular iron and siderophore production were attributed to the inhibition of ferric reductase activity by Zn^{2+} and Mn^{2+}. It is believed that the hyper-production of siderophore observed is a result of the cell "sensing" increased iron limitation due to lowered intracellular iron (II) concentrations (Huyer & Page, 1989; Page, 1995). In addition, it had been shown that Zn^{2+} increases the production of siderophores by *P. fluorescens* however, whether this is caused by the inhibition of a ferric reductase is not known (Hofte *et al.*, 1993).

1.6 Oxygen stress

In the last 10 years, another interesting role for siderophores, not demonstrated by *E. coli*, has come to light. This is the role that siderophores play in oxygen stress management either by the reduction of oxygen stress through the chelation of iron, or the promotion of oxygen stress by the solublization of iron. Both of which have been described in *P. aeruginosa* by Coffman *et al.* (1990) and shall be examined next in the context of oxygen stress.

One of the negative side effects of using oxygen as a terminal electron acceptor is the generation or presence of reactive oxygen compounds in the aerobic environment. These reactive oxygen species include superoxide ($\bullet O_2^-$), the hydroxyl radical ($\bullet OH$) and hydrogen peroxide (H_2O_2) and all are intermediates in the reduction of oxygen to water. These reactive oxygen intermediates (ROIs) can cause membrane peroxidation (Cohen, 1994), mutagenic events (Gutteridge, 1987), increased protein degradation (Davies & Lin, 1988), the disintegration of ribosomes, and in general lead to cellular damage collectively know as a oxidative stress (DiGuiseppi & Fridovich, 1984).

1.6.1 Enzymatic sources of ROIs

As electrons pass down the cytochrome chains it is possible for some electron "leakage" to occur and result in the formation of ROIs (Cohen, 1994). ROIs generated in this manner are of particular concern to *A. vinelandii* due to its high respiratory rate (Jurtshuk & Yang, 1980). This high rate of respiration is a result of the oxygen "wasting" approach the microorganism has evolved to protect the oxygen-labile nitrogenase (Section 1.2.3).

In addition to electron transport chains and the enzymes found within, other enzymes form different ROIs as the by-products of the reactions they catalyze. These enzymes include, but are not limited to, xanthine oxidase (a common source of $\bullet O_2^-$ under experimental conditions), aldehyde oxidase, monoamine oxidase, and nitric oxide synthase. In addition, whole eukaryotic cells such as granulocytes and macrophages have been shown to generate ROIs in a burst of respiration for the destruction of pathogenic microorganisms. A good portion of the toxicity associated with enzymatic sources of ROIs comes from the generation of hydrogen peroxide. Hydrogen peroxide is toxic to most cells and, along with the generation of superoxide, is part of the microbiocidal response of neutrophils (DiGuiseppi & Fridovich, 1984). Although the mentioned enzymes may contribute to the formation of ROIs, the greatest source of ROIs for aerobic or facultatively aerobic microorganisms will be the electron transport chains.

The formation of ROIs can also be induced by increasing the rate at which cultures of microorganisms are aerated. Increased aeration leads to higher growth rates and as a result more electron flow, and leakage, from electron transport chains. In addition, at increased aeration rates the spontaneous formation of hydrogen peroxide in aqueous environments is increased (Carlsson *et al.*, 1978).

1.6.2 Non-enzymatic sources of ROIs

The non-enzymatic generation of ROIs depends on the spontaneous auto-oxidation of compounds within the cell and the resulting reaction of a free electron with oxygen. Compounds that are known to auto-oxidize include thiols, catecholomines, leukoflavins, and reduced ferredoxins. These compounds are known as redox cycling compounds since once reduced, they can repeatedly auto-oxidize and become reduced again (DiGuiseppi & Fridovich, 1984).

As was briefly mentioned in Section 1.4.1, the oxidation of iron (II) to iron (III) can occur in solution as iron (II) interacts with hydrogen peroxide forming iron (III), OH^- and the hydroxyl radical (•OH). Since superoxide is also quite often present in low concentrations in solution, it is possible for the iron (III) to react with the superoxide and be reduced back to iron (II) with the generation of oxygen. This cyclic oxidation and reduction of iron, known as the Fenton reaction shown below, can continue until one of the components involved is exhausted (Coffman *et al.*, 1990).

Fe^{2+}	+	H_2O_2	⇆	Fe^{3+}	+	OH^-	+	•OH	(7)
Fe^{3+}	+	$•O_2^-$	⇆	Fe^{2+}	+	O_2			(8)
$•O_2^-$	+	H_2O_2	⇆	O_2	+	OH^-	+	•OH	(Net)

This can lead to the formation of large amounts of •OH, a very dangerous ROI in the cell as there is no enzymatic method to destroy it (Gutteridge, 1987). When ROIs are generated in this manner, siderophores can have both positive and negative effects. Coffman *et al.* (1990) demonstrated that the high affinity *Pseudomonas* siderophore pyoverdin could prevent the formation of ROIs *in vitro*. The affinity of pyoverdin for iron (III) is great enough to prevent its reduction to iron (II) and thus prevents the Fenton-mediated formation of •OH. On the other hand, Coffman *et al.* (1990) also showed that

the low affinity *Pseudomonas* siderophore pyochelin promoted the formation of •OH by the Fenton reaction. The authors suggested that the affinity of pyochelin for iron (III) was great enough to solublize iron (III), but not great enough to prevent its release as iron (II). Thus, they considered pyochelin to be a virulence factor, increasing oxidative stress in the host.

Paraquat (methyl viologen) is routinely used under laboratory conditions to generate $\bullet O_2^-$ as it can cycle between paraquat (II) and paraquat (I) by donating an electron to oxygen and then becoming reduced by NADPH (Korbashi *et al.*, 1986). If present together, paraquat and iron can interact such that the superoxide generated by paraquat (I) oxidation will drive the oxidation of iron (II) leading to the formation of •OH. In addition, paraquat (I) can be oxidized to paraquat (II) by the reduction of iron (III) to iron (II) which then interacts with hydrogen peroxide to form •OH. The situation is made worse when the microorganism reacts to the presence of oxygen stress by forming superoxide dismutase, converting superoxide into hydrogen peroxide. The hydrogen peroxide formed then serves as a substrate to be reduced as iron (II) is oxidized back to iron (III) while forming •OH (Gutteridge, 1987) (Equations 7 & 8 above and Fig. 1.9).

1.6.3 OxyR: hydrogen peroxide sensing and response in *E. coli*

When enteric bacteria such as *S. typhimurium* or *E. coli* are exposed to sub-lethal concentrations of hydrogen peroxide they become resistant to the lethal effects of higher hydrogen peroxide concentrations. This resistance is coincident with the transient induction of a distinct group of 30 proteins. Twelve of which are formed immediately after exposure to hydrogen peroxide while the other 18 are synthesized 10 to 30 min after exposure. Of these 30 proteins, 9 were shown to be under the positive control of OxyR, the product of the *oxyR* gene (Christman *et al.*, 1985). Proteins induced by under sub-

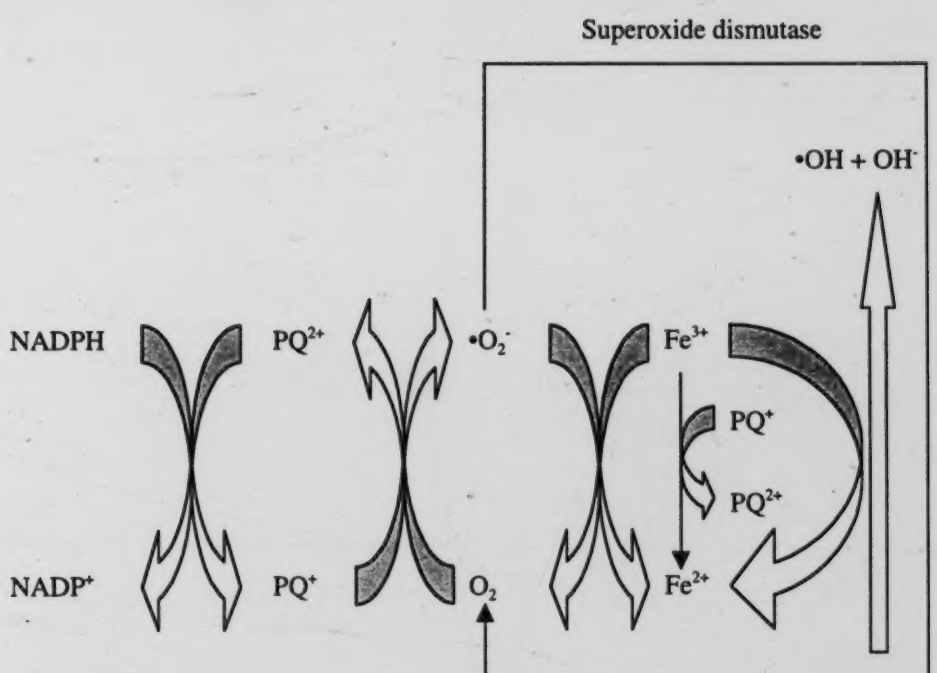

Figure 1.9 Cyclic oxidation and reduction of paraquat and its interaction with iron.

PQ=paraquat, $\bullet O_2^-$=superoxide. (Korbashi *et al.*, 1986).

lethal concentrations of hydrogen peroxide include catalase, an alkyl hydroperoxidase reductase, a glutathione reductase, and a non-specific DNA-binding protein with a yet undefined protective function. In addition to these proteins, OxyR also represses its own synthesis (Mukhopadhyay & Schellhorn, 1997). OxyR is a member of the LysR family of transcriptional regulators and as such has a DNA-binding, helix-turn-helix motif near its amino terminus. In addition, members of this family also share similarity in the way they are folded, a lack of relation to other regulatory proteins and a common ancestry (Henikoff *et al.*, 1988). The fact that, upon oxidation by H_2O_2, OxyR becomes a transcriptional activator indicates that it is both the sensor and transducer of the hydrogen peroxide stress signal (Altuvia *et al.*, 1994).

One of the best characterized and understood proteins induced by OxyR is catalase. It is found in all eukaryotic and prokaryotic cells that live in aerobic environments where it functions to convert hydrogen peroxide into water and oxygen (Deisseroth & Dounce, 1970). As described in Section 1.6.2, it is not only hydrogen peroxide that is dangerous to the cell, but also those ROIs generated by transformations of hydrogen peroxide, such as •OH. Thus catalase not only removes a potentially dangerous ROI from the cell, but can also act in the formation of ROIs.

1.6.4 SoxRS: superoxide sensing and response in *E. coli*

The SoxRS system for superoxide sensing is seen as the induction of up to 80 new proteins by *E. coli* after exposure to sub-lethal concentrations of superoxide. These proteins include, but are not limited to, superoxide dismutase, an endonuclease for DNA repair, glucose-6-phosphate dehydrogenase for NADPH formation, fumarase C, aconitase, ferredoxin reductase, and AcrA/B efflux pumps found in the inner membrane of the cell (Demple, 1996). From this response, it is evident that the action of SoxRS prepares the cell to survive a number of different types of environmental stress. The

system is composed of two proteins, SoxR and SoxS. SoxR is a 17-kDa protein that is a member of the MerR family of transcriptional regulators and promotes the expression of the *soxS* gene (Nunoshiba, 1996). The 13-kDa SoxS protein then acts as a transcriptional activator to promote the expression of the genes in the Sox regulon (Fig. 1.10-A). SoxS has been shown to share sequence homology with AraC (the positive regulator of arabinose uptake) family of regulatory proteins, which is consistent with the predicted function of SoxS in gene expression (Nunoshiba, 1996).

SoxR contains a [2Fe-2S] metal center and its function as a redox sensor occurs through this moiety. SoxR pre-exists in the cell at low concentrations (< 100 nM) in the absence of oxidative stress in its reduced, inactive form (Ding & Demple, 1997; Hidalgo & Demple, 1998). SoxR has been shown to bind to the *soxS* gene in its oxidized, reduced, and apo form. Thus, activation of *soxS* by SoxR is not a result of DNA binding, as only oxidized SoxR has the ability to promote *soxS* expression. This oxidation was once thought to be caused by the interaction of SoxR with superoxide. This assumption however, does not account for the fact that SoxR can be oxidized by molecular oxygen or by nitrous oxide in anaerobic environments, not just by superoxide (Gaudu *et al.*, 1997). Thus, the activation of SoxR does not appear to be by simple interaction with an oxygen radical. Rather, it has been suggested that SoxR is activated by the depletion of reducing equivalents which are required to maintain it in a reduced, inactive form (Fig. 1.10-B) (Liochev *et al.*, 1994). The depletion of NAD(P)H by interaction with superoxide, nitrous oxide, or the redox cycling compound paraquat leaves SoxR in an oxidized, active form, leading to the promotion of *soxS* expression (Gauda *et al.*, 1997).

Oxidized SoxR promotes *soxS* expression by compensating for the abnormally long spacing, 19 base pairs as opposed to the consensus 17±1, between the *soxS* –10 and –35 promoter elements. In doing so, SoxR stimulates open complex formation by RNA

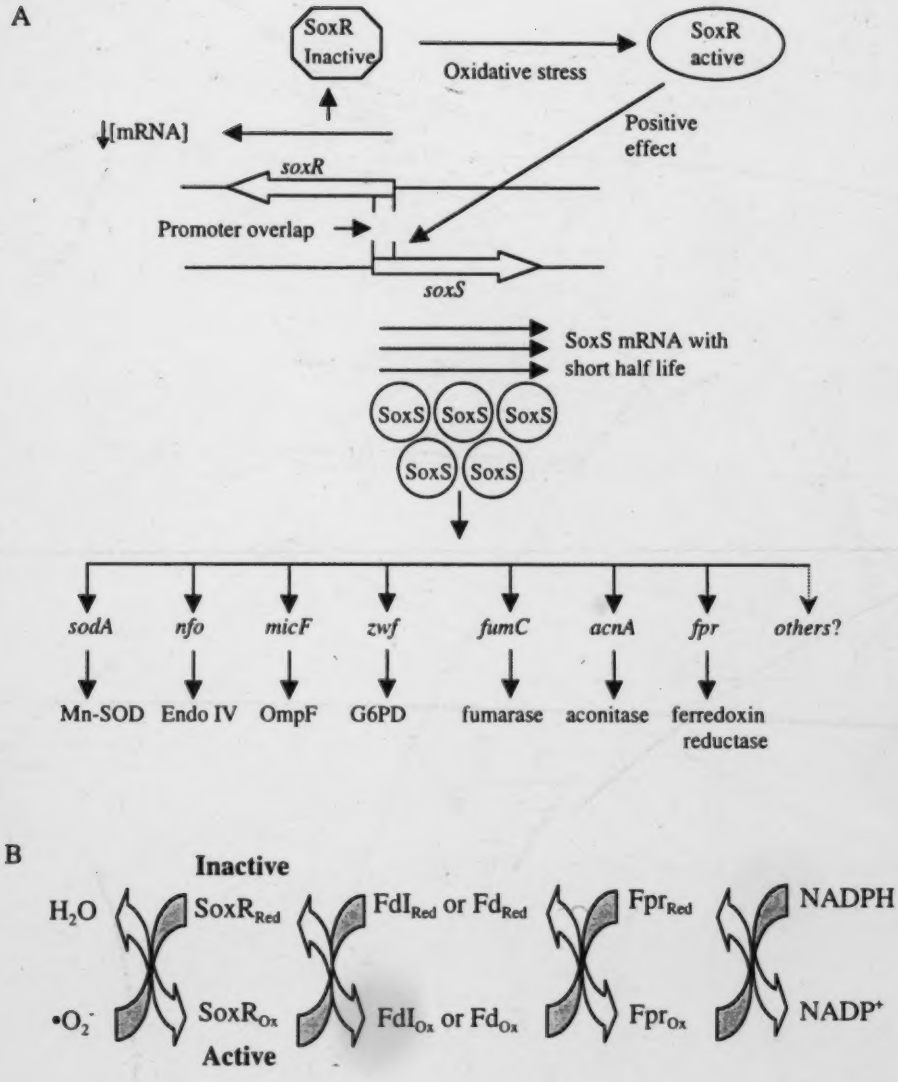

Figure 1.10 Model of the SoxRS oxidative stress sensing system in *E. coli*.

A) Model of SoxR interaction with SoxS and resulting expression of oxidative stress response proteins (modified from Demple, 1996).

B)

B) Model of SoxR activation and deactivation by the action of ferredoxin (Fd = *E. coli* ferredoxin, FdI = *A. vinelandii* ferredoxin I). Fpr = ferredoxin reductase. Model based on Liochev *et al.*, (1994) and Isas *et al.*, (1994).

polymerase leading to *soxS* mRNA formation (Hidalgo & Demple, 1997). Unlike SoxR, SoxS has a low affinity for its DNA targets (~ 10^{-9} M) thus, high concentrations of SoxS must be present to activate genes in the Sox regulon (Ding & Demple, 1997). The sequence bound by SoxS, known as a "sox box", is AN_2GCAYN_7CWA where N is any base, Y is a pyrimidine, and W is A or T (Li & Demple, 1996). As well, under conditions of oxidative stress, the half-life of *soxS* mRNA is reduced from 3.6 min to 1.3 min (Ding & Demple, 1997). This allows the cell to rapidly shut down the Sox system once oxidative stress has been removed as soxS mRNA degradation leads to a rapid decrease of intracellular SoxS concentrations and a cessation of regulon activation.

Recently, it has been shown that in addition to promoting *soxS* expression, SoxR also inhibits the expression of its own gene *soxR*. In this work by Hidalgo *et al.* (1998) the *soxR* and *soxS* genes have been shown to be located on opposite sides of the same strand of DNA with promoter elements that overlap. Thus, SoxR autorepresses its own formation keeping the cellular concentration of SoxR within fixed limits and at a constant level regardless of the oxidative state of the cell.

Superoxide dismutase (SOD) is one of the most important enzymes in the Sox regulon formed in response to oxygen stress. SOD promotes the dismutation of two superoxide molecules into one molecule of hydrogen peroxide. In doing so, it removes a potentially dangerous ROI and also provides a substrate for catalase (McCormick *et al.*, 1998). *E. coli* forms a Mn-SOD encoded by the *sodA* gene and a Fe-SOD encoded by the *sodB* gene (Fee, 1991). Both enzymes carry out the same function, but Mn-SOD appears to be better at preventing superoxide mediated damage to DNA, whereas Fe-SOD protects cytoplasmic enzymes to a greater degree (Nunoshiba, 1996).

In terms of regulation, *sodA* is positively regulated by the SoxS protein in response to oxygen stress. However, *sodA* is also regulated by the Fur protein which can repress the synthesis of *sodA* under iron sufficient conditions. Normally the Fe-SOD product of *sodB* is expressed in a constitutive manner and only under conditions of increased oxygen stress is the Mn-SOD produced.

1.6.5 SoxRS-like system in *A. vinelandii*

The SoxRS system has been extended to *A. vinelandii* by the work of Barbara Burgess and co-workers who have proposed a role for the ferredoxin I reductase protein of *A. vinelandii* such that it interacts with an as yet unidentified SoxR homologue to regulate a response to superoxide stress (Yannone & Burgess, 1998; Isas *et al.*, 1995; Isas & Burgess, 1994) (Fig. 1.10-B). Burgess and her co-workers base this suggestion on the fact that in *A. vinelandii* strain LM100 ferredoxin I has been insertionally inactivated and ferredoxin I reductase is seen to accumulate. Burgess and her group suggest that ferredoxin I is required to keep SoxR in its reduced, inactive form. As a result of the mutation in ferredoxin I, SoxR continues to promote the expression of oxidative stress management proteins, such as the ferredoxin I reductase, through a SoxS homologue, thus strain LM100 constitutively responds to a "perceived" oxidative stress. This model is based on what has been observed in *E. coli* and it should be noted that as of yet, SoxRS homologues have not been identified in *A. vinelandii*.

1.7 Scope of thesis

By the end of this project, the goals set out in Section 1.2.6 had been met. The new catecholate compound seen under high molybdate concentrations was determined to be the tricatecholate protochelin. Once identified, protochelin was characterized in terms of its chemical nature and its ability to function as a siderophore. This work also included the characterization of the nature of iron binding to azotochelin and aminochelin for

comparison to protochelin. The question as to the role of molybdate in protochelin accumulation was addressed and a number of proposed roles were discounted. The site of molybdate interaction with the cell to promote protochelin accumulation was determined to be ferric-siderophore uptake, likely by the inhibition of the action of a ferric reductase. Finally, an additional role for protochelin as a mediator of oxygen stress resistance was suggested, based on previous work in *P. aeruginosa* and the fact that protochelin is formed at high levels in *A. vinelandii* strain LM100. This necessitated some evaluation of the oxygen stress response, especially in iron-limited *A. vinelandii*.

Overall, this work has contributed to the understanding of how *A. vinelandii* responds to stress conditions in its environment to ensure its survival. A new siderophore has been characterized and it appears to be not only a mediator of iron acquisition, but also serves in defense of *A. vinelandii* to increased oxygen stress. As this project drew to a close, many questions had been answered, but more are posed to be answered later in further experimentation.

CHAPTER 2 - Materials and Methods

2.1 Analysis of cells and cell culture fluids

2.1.1 Growth conditions and bacterial strains

The capsule-negative *Azotobacter vinelandii* strain UW (OP, ATCC 13705) and siderophore-defective mutants derived from this strain were used in these studies. The mutants included the azotobactin-deficient strain UA1 (Page & Huyer, 1984), the catecholate-deficient strain F196 and the siderophore-deficient strain P100 (Sevinc & Page, 1992). In addition the isogenic *A. vinelandii* UW ferredoxin I (*fdx*A)-negative mutant strain LM100 (Morgan *et al.*, 1988) also was used.

The basic medium used in this study was Burk's medium which contained 1% (w/v) glucose, 15 mM CH_3COONH_4, 1 µM $Na_2MoO_4 \cdot 2H_2O$, 0.81 mM $MgSO_4$, and 0.58 mM $CaSO_4$ in a 6 mM potassium phosphate (pH 7.6) buffer (Sevinc & Page, 1992). This medium was modified such that it contained excess (1 mM) molybdate or was made N-free by the substitution of 15 mM sodium acetate for 15 mM ammonium acetate. In addition, iron-sufficient medium contained 20 to 75 µM ferric citrate, iron-limited medium contained only 1 µM ferric citrate, and when the repression of the siderophore azotobactin was required, 3 µM ferric citrate was used. In some cases, paraquat (1,1'-dimethyl-4,4'-bipyridinium dichloride) was added at 0.25 to 30 µM concentrations or progressively smaller volumes of medium were incubated with shaking (225 rpm) in 500 ml Erlenmeyer flasks, to increase oxidative stress on the cultures (Korbashi *et al.*, 1986). All glassware used in these studies was acid-washed with 4 M HCl then rinsed with 50 mM EDTA (pH 7.0) and Milli-Q deionized water (Millipore) to remove contaminating iron (Page, 1993).

The strains were maintained on slants of Burk's medium containing 1.8% (w/v) agar and incubated for 72 hr at 28°C. Cells were washed from slants with 2.5 ml of 6 mM potassium phosphate buffer (pH 7.6) and were used (2.5% v/v) to inoculate either 20 ml

of medium in a 50 ml Erlenmeyer flask or 100 ml of medium in a 500 ml Erlenmeyer flask. Cultures were incubated for 20 to 24 hr at 28°C with shaking at 225 rpm on a New Brunswick model G-76 gyrotory water bath shaker or a New Brunswick model G10 gyrotory platform shaker. This temperature and agitation speed were the standard conditions used through out this work. If larger quantities of cells and culture fluid were required, cells were grown in iron-limited medium in a 5.0-l Bioflo III fermentor (New Brunswick Scientific) at 30°C with agitation (air flow at 5.0-l min^{-1} with mixing at 500 rpm).

2.1.2 Spectrophotometric and colorimetric analyses

Siderophores were detected spectrophotometrically by scanning iron-limited culture supernatant fluid which had been acidified to pH 1.8 with 6 M HCl. Absorption peaks were measured using a Hitachi U-2000 recording spectrophotometer at A_{310} for catechols and A_{380} for azotobactin (Page & Huyer, 1984). Catecholate siderophore concentrations in stock solutions were quantified by using the extinction coefficient for 2,3-dihydroxy-benzoic acid (2,3-DHBA) in 80% methanol of $3.26*10^3$ A_{310} cm^{-1} M^{-1}, or in 6 mM potassium phosphate buffer (pH 7.6) of $3.25*10^3$ A_{310} cm^{-1} M^{-1}, corrected for the number of 2,3-DHBA moieties per siderophore.

Catechol was quantified by the colorimetric assay of Barnum (1977). Samples of up to 1.0 ml containing a maximum of 200 nmol of catechol were combined with 0.5 ml of a 3 M sodium acetate buffer (pH 5.2) and 0.5 ml of a solution of 2 M $NaNO_2$ and 0.1 M $Na_2MoO_4 \cdot 2H_2O$. This mixture was allowed to incubate at room temperature for 30 min before the addition of 0.5 ml of 6 M NaOH. The absorbance of the resulting solution was measured at 503 nm. Quantities of catechol present were determined by comparison to a calibration curve of 1 to 200 nmol catechol.

Total cellular protein was determined by the method of Lowry *et al.* (1951). Cell pellets were digested at 80°C for 60 min in 0.1 M NaOH. Samples of up to 500-µl containing a maximum of 100 µg of protein were mixed with 2.5 ml of "reagent A". "Reagent A" was made by combining 1.0 ml of 1% (w/v) sodium potassium tartrate and 1.0 ml of 0.5% (w/v) $CuSO_4$ in 50 ml of 2% (w/v) Na_2CO_3 in 0.1 M NaOH. This was incubated for 10 min at room temperature before the addition of 0.25 ml of "reagent B". "Reagent B" was made by combining 1 volume of distilled H_2O with 1 volume of Folin & Ciocalteu's Phenol Reagent (Sigma chemicals #F-9252). After 30 min incubation at room temperature, the absorbance of each sample was read at 620 nm and protein concentration was determined by comparison to a calibration curve of 1 to 100 µg of bovine serum albumin.

2.1.3 Extraction and identification of catecholate siderophores

Azotochelin and 2,3-DHBA present in acidified (pH 1.8) iron-limited *A. vinelandii* culture supernatant fluid were extracted into ethyl acetate leaving aminochelin in the acidic aqueous phase (Page & von Tigerstrom, 1988). The ethyl acetate fraction evaporated to dryness, then dissolved in 200-µl of ethyl acetate. Aminochelin was extracted from the acidic aqueous phase after neutralization to pH 7.0 with 12 M NaOH using *n*-butanol (Page & von Tigerstrom, 1988). The ethyl acetate soluble catecholate components of these extracts were resolved by thin layer chromatography (TLC) using silica gel G plates (Macherey-Nagel #805-012) with a benzene:acetic acid:water (125:72:3) solvent system (Sevinc & Page, 1992) whereas aminochelin was resolved in a similar manner using a *n*-butanol:acetic acid: water (150:30:30) solvent system (Page & von Tigerstrom, 1988). Standards used included 2,3-DHBA (Sigma chemicals #D-5395), azotochelin and aminochelin prepared from strain UA1 (Page & von Tigerstrom, 1988), and protochelin from the methylotrophic microorganism DSM #5746 (Taraz *et al.*, 1990). A sample of pure protochelin was a gift from Dr H. Budzikiewicz. TLC plates were

developed with ascending solvent to within 1 cm of the top of the plate. Catecholates were visualized by spraying the TLC plate with a solution of 0.1% (w/v) *N,N'*-dipyridyl and 0.1% (w/v) ferric chloride solution in 95% ethanol (Krebs *et al.*, 1969). Plate images were recorded photographically with either Polaroid 667 film (room lighting, 1/30 sec exposure, 5.6 F-stop) or 665 film (high intensity lighting, 1/30 sec exposure, 5.6 F-stop). Alternatively, plates were scanned using an AGFA Snapscan 310 flatbed scanner with Color It 3.0 (Microfrontier Inc) software.

2.1.4 Cell free extract preparation and membrane differentiation

Strains UW and LM100 were grown under standard conditions for 24 hr in 200 ml of iron-limited or iron-sufficient (25 to 75 μM ferric citrate) Burk's medium. Cells were harvested by centrifugation (4,000 ***g***, 10 min) in a Sorval RC-5 (Dupont Instruments) centrifuge and the cell pellet was washed twice with 50 mM potassium phosphate buffer (pH 7.6) containing 2 mM dithiothretol. Cells were re-suspended in buffer and lysed by passage through a French press at 20,000 lb in^{-2}. Cell lysis was confirmed by microscopic examination. RNAse 1 and DNAse were added to a final concentration of 0.05 mg ml^{-1} each. In some cases, when cells were resistant to lysis, lysozyme was added to a final concentration of 0.1 mg ml^{-1}. The cell extract was cleared by centrifugation (40,000 ***g***, 1 hr) and the resulting cell free extract (CFX) was aliquotted and stored at -20°C (Page & von Tigerstrom, 1982).

The pellet containing cell membranes was differentiated into inner and outer membrane fractions with sodium lauroyl sarcosine (sarcosyl) (Page & Huyer, 1984). The pellet was re-suspended in 5 ml of 50 mM phosphate buffer (pH 7.6) and centrifuged at 40,000 ***g*** for 1 hr. The supernatant was discarded and the pellet re-suspended in 1 ml of 50 mM potassium phosphate buffer (pH 7.6) and protein was determined by the method of Lowry *et al.*, (1951) (Section 2.1.2). Sarcosyl was added such that the final ratio of protein and

sarcosyl was 6:1 (w/w). The membrane suspension was shaken at 250 rpm at room temperature for 30 min followed by centrifugation at 40,000 ***g*** for 60 min to pellet the sarcosyl insoluble outer membrane fraction. The supernatant containing the inner membrane fraction and sarcosyl soluble proteins, was removed, quantified for protein content, and frozen at -20°C for later use.

The pellet from the sarcosyl differentiation step was re-suspended in 2 ml of 50 mM potassium phosphate buffer (pH 7.6) and centrifuged at 40,000 ***g*** for 1 hr. It was re-suspended in 1 ml of 50 mM potassium phosphate buffer (pH 7.6), quantified for protein content and frozen at -20°C for later use (Page & Huyer, 1984).

2.2 Characterization of protochelin

2.2.1 Purification of protochelin by silicic acid chromatography

The culture supernatant fluid from strain UA1 grown overnight in iron-limited medium containing 1 mM molybdate was acidified and extracted with ethyl acetate. The solvent fraction was evaporated to dryness, dissolved in ethyl acetate to give an $A_{310} = 67.5$, and 5 ml of this was applied to a silicic acid column. The column was formed in a 2.1 cm x 25 cm all glass Kontes column loaded with 9.0 g of silicic acid suspended in ethyl acetate:benzene (1:4) saturated with 0.5 M formic acid which had been equilibrated overnight. The column was eluted with ethyl acetate:benzene at a flow rate of approximately 0.5 ml min^{-1}, fractions (3 ml) were collected and A_{310} was used to determine the location of catechol-containing compounds. TLC was then used to identify catecholate compounds by comparison to authentic standards (Section 2.1.3).

2.2.2 Production and purification of catecholate siderophores

Strain LM100 culture supernatant fluid was used as a source of all catecholate siderophores since protochelin was formed without the addition of 1 mM molybdate.

Iron-limited medium (400 ml in a 2-l flask) was inoculated with iron-limited strain LM100 (4% v/v) and after 24 hr incubation cells were removed by tangential flow filtration using dual 0.22 µm pore size Pellicon (Millipore) filters. The culture fluid volume (9.6-l) was reduced to 400 ml under vacuum, in the dark at 37°C using a Buchi RE111 rotary evaporator. All volume reduction and solvent evaporation was done under either vacuum or nitrogen in the dark to reduce oxidation of the catecholate siderophores.

Siderophores were isolated according to the following protocol. The culture fluid was acidified to pH 1.8 with 12 M HCl and extracted twice with an equal volume of ethyl acetate to concentrate azotochelin, protochelin, and 2,3-DHBA in the ethyl acetate layer. The remaining acidic aqueous layer contained only aminochelin (Page & von Tigerstrom, 1988).

Aminochelin in the acidic aqueous layer and was neutralized to pH 7.0 with 12 M NaOH, reduced in volume to 50 ml and extracted five times with an equal volume of *n*-butanol. This extract was then evaporated to dryness under nitrogen. The resulting residue was dissolved in 5 mM ammonium acetate (pH 7.0) for application to a 2.5 cm x 30 cm CM-Sephadex (Pharmacia) column equilibrated in 5 mM ammonium acetate (pH 7.0). Fractions (5 ml) were eluted with a 400 ml gradient of 5 to 2,000 mM ammonium acetate (pH 7.0) and A_{310} was used to detect catecholates. Fractions containing aminochelin were confirmed with TLC by comparison to authentic aminochelin isolated by the methods of Page & von Tigerstrom (1988). Ammonium acetate concentration in fractions was determined by conductivity measurement and comparison to a calibration curve. Fractions containing aminochelin were pooled, reduced in volume to 25 ml or less and extracted five times into *n*-butanol. The *n*-butanol extract was then evaporated to dryness and the resulting residue was dissolved in 80% methanol and stored at –20°C.

The ethyl acetate layer was reduced in volume to 200 ml and was washed twice with an equal volume of 100 mM sodium phosphate buffer (pH 7.0), which removed azotochelin and 2,3-DHBA. Protochelin remained in the ethyl acetate layer and was concentrated by evaporation before being dissolved in 80% methanol. Purity was confirmed by TLC and the protochelin solution was stored at -20°C.

The aqueous phase containing azotochelin and 2,3-DHBA was reduced to 200 ml, acidified to pH 1.8 with 12 M HCl, and extracted twice with an equal volume of ethyl acetate. The resulting residue was dissolved in a minimum volume of 80% methanol for application to a 2.5 cm x 30 cm Sephadex LH-20 (Pharmacia) column equilibrated with 80% methanol, and eluted with 80% methanol to separate azotochelin and 2,3-DHBA. Catecholates in fractions were detected by A_{310} and identified by TLC. Azotochelin containing fractions were pooled, evaporated under nitrogen, dissolved in a minimal volume of 80% methanol, and stored at -20°C.

2.2.3 Total and partial hydrolysis of protochelin

Total acid hydrolysis of protochelin was performed by incubating protochelin (final A_{310} = 10) in 6 M HCl for 25 hr at 100°C. Amino acid standards including lysine and putrescine (0.5 µmol ml^{-1}) and products from the total hydrolysis of protochelin were resolved by TLC on silica gel G plates (Brinkman) using a *n*-propanol:ammonium hydroxide (63:33) solvent system. The plates were sprayed with 0.2% (w/v) ninhydrin in acetone to visualize the resolved amino-N compounds (Page & von Tigerstrom, 1988).

A partial acid hydrolysis time course was performed under similar conditions using 1 M HCl for 8 hr. Samples were then extracted twice with equal volumes of ethyl acetate. Catecholate hydrolysis products were resolved by TLC using the benzene:acetic acid:water (125:72:3) solvent system and visualized with 0.1% (w/v)

dipyridyl and 0.1% (w/v) ferric chloride (Sevinc & Page, 1992). Resolved components of protochelin hydrolysis were identified by comparison to authentic standards (Page and von Tigerstrom, 1988).

2.2.4 Fast atom bombardment (FAB) spectrometry

The mass of purified *A. vinelandii* protochelin and the protochelin standard was determined by FAB mass spectrometry (Department of Chemistry, University of Alberta) using methanol as a solvent on a dithiothreitol:dithioerythritol (6:1) matrix.

2.2.5 Chrome Azurol-S (CAS) siderophore assay

The CAS assay (Schwyn & Neilands, 1987) was used as a universal assay to detect siderophore activity by monitoring spectrophotometrically the deferration of the synthetic, chromogenic iron chelate of CAS. The CAS assay solution was prepared as follows: Solution 1, combine 15-µl of 0.1 M $FeCl_3$ in 10 mM HCl with 7.5 ml of 2 mM CAS. Solution 2, combine 4.30 g of piperazine dissolved in 20 ml of Milli-Q dH_2O with 6.35 ml of 12 M HCl. Then, in a 100 ml volumetric flask containing 20 ml of Milli-Q dH_2O, combine 6.0 ml of 10 mM hexadecyltrimethylammonium bromide (HDTMA), Solution 1 slowly, in a drop wise manner, and finally Solution 2. Milli-Q dH_2O was then added to bring the final volume to 100 ml. Caution was exercised to avoid the formation of foam when adding each reagent and mixing them together. The final solution was stored, protected from light, at 37°C.

The CAS assay solution did not include the sulfosalicylic acid which could be used to destabilize the CAS-iron complex as described in Schwyn & Neilands (1987) as all siderophores tested decolorized the CAS complex to some degree. Pure protochelin dissolved in a small volume of 95% ethanol or iron-limited culture supernatant fluid from strains UA1 or F196 diluted in Milli-Q dH_2O was used in the assay. The siderophore

sample was added to the assay to a final A_{310} of 0.31 for the catecholates (azotochelin and aminochelin), a final A_{380} of 0.25 for azotobactin, and a final A_{310} of 0.35 for protochelin. Equal (0.5 ml) volumes of siderophore and the CAS assay solution were mixed and decolorization was monitored at 630 nm for 20 min. One unit of siderophore activity was calculated as the amount of sample required to decrease the A_{630} of the CAS by 0.001 s^{-1}. Total siderophore specific activity was calculated as siderophore units (mg cell protein)$^{-1}$ in 1.0 ml of culture fluid.

2.2.6 Siderophore bioassay using strain P100

Plates of Burk's medium containing 50 µM ferric citrate and 50 µg ml^{-1} of the artificial iron chelator ethylenediamine di-(o-hydroxyphenylacetic acid) (EDDHA) were spread with a lawn of strain P100. Sterile, iron-limited supernatant fluid from strains UA1 (catecholates A_{310} = 0.50) and F196 (azotobactin A_{380} = 0.75) and purified protochelin (A_{310} = 0.50) were absorbed into 0.5-cm sterile paper disks and dried. These disks were placed aseptically onto the lawn and moistened with 15-µl of sterile 6 mM potassium phosphate buffer (pH 7.6), which also was added to a control disk. The plates were incubated for five days at 28°C and zones of strain P100 growth around each disk were measured.

2.2.7 ^{55}Fe-uptake assay

Three day old cultures of *A. vinelandii* UW grown on slants were suspended (2.5 ml) in 6 mM potassium phosphate buffer (pH 7.6) and were used to inoculate (2.5% v/v) 100 ml of iron-limited Burk's medium in a 500 ml Erlenmeyer flask. After 24 hr, under standard conditions, these cells were aseptically harvested by centrifugation (16,300 ***g***, 10 min) and the cell pellet was washed twice with 50 ml of chilled iron-limited uptake buffer composed of Burk's medium containing 0.5% (w/v) glucose and 10 mM sodium citrate. This uptake buffer was prepared 1 week in advance of experimental work and was

filtered through 0.45 µm Millipore HA filter disks (Millipore #HAWG047S3) just before use. The cells were re-suspended to a final OD_{600} of 7.0 in uptake buffer and kept on ice until needed. The total number of viable cells in the suspension was determined by plating on to Burk's medium plates, which were incubated for 3 days at 28°C.

When culture supernatant fluids were used as a source of siderophores, cells were removed by centrifugation (16,300 ***g*** 10 min) and the supernatant fluid was filtered through sterile 0.45 µm Millex HA filters (Millipore #SLHA025OS). Sterile glucose and sodium citrate were aseptically added to the culture supernatant fluid to a final concentration of 0.5% (v/v) and 10 mM, respectively. A protochelin solution was made by adding pure protochelin to uptake buffer. The catecholate-containing culture supernatant fluids and the protochelin solution were made to a final A_{310} of 0.30 and culture fluid containing azotobactin was made to a final A_{380} of 0.30 in uptake buffer. Prior to the start of the uptake assay, these solutions (16 ml) were incubated for 60 min at 28°C with 160-µl of a 7.0 µg ml^{-1} $^{55}FeCl_3$ solution (specific activity of 37.5 µCi ml^{-1}) in a sterile 50 ml Erlenmeyer flask and shaking at 225 rpm.

At the start of the assay, the above $^{55}Fe^{3+}$-siderophore solution was divided into two 50 ml Erlenmeyer flasks each containing 8 ml of uptake buffer. The test reaction mixture was warmed to 28°C with shaking at 225 rpm while the control reaction was placed on ice. At this time the cell suspension was also warmed to 28°C with shaking at 225 rpm. After 5 min, 2 ml of the cell suspension was added to the 8 ml test sample. Samples were taken in 3 min intervals for 12 min from the test solution which was kept at 28°C, with shaking at 225 rpm. Duplicate 0.5 ml samples were vacuum filtered through Millipore HA 0.45 µm filter disks (Millipore #HAWP02500) pre-wetted with 5 ml of uptake buffer. Each filter was then rinsed twice with 25 ml of uptake buffer. The filter disks were dried and placed in 20 ml scintillation vials with 8 ml of Aqueous Counting Scintillant

(Amersham International #NACS104) and counted in the ^{3}H window of a Beckman LS3801 scintillation counter. The $^{55}Fe^{3+}$ content of the cells was then expressed as $\mu g\ ^{55}Fe^{3+}\ ml^{-1}$ (10^{8} $cells^{-1}$) after correction for non-specific binding. When the $^{55}Fe^{3+}$-uptake rates for siderophore mixtures were compared, the iron-limited strain UW cells used in the assays were all from the same culture and hence were identical, thus the uptake rates do not reflect the number of cells present (Knosp *et al.*, 1984).

The cells in the control reactions were incubated on ice during the uptake assay, with shaking at 225 rpm and sampled at similar time intervals. This allowed for the quantification of non-specific binding of the ferric-siderophore complex to the cells.

2.2.8 Molar iron and molybdenum siderophore binding ratios

Molar binding ratios of the three catecholate siderophores and iron (III) were determined by the continuous variation method of Job (Chaberek & Martell, 1959). Each catecholate siderophore was mixed with iron (III) (as ferric nitrate) in 100 mM MOPS buffer (pH 7.0) at various ratios and the absorbance of these mixtures was measured at 300 nm to 700 nm until each solution reached equilibrium. Each solution was monitored for up to 376 hr to ensure that equilibrium was reached. The ratio of siderophore to iron (III) that gave the maximum absorbance represented the molar binding ratio. The wavelength of the maximum absorbance at the molar binding ratio was used in all further work. In addition, the same process was carried out with each siderophore and various concentrations of molybdate, such that the molar binding ratio of a molybdo-siderophore complex was determined. Using the absorbance values generated and the molar quantities of metal-siderophore complex present, the molar extinction coefficient for each complex was calculated.

2.2.9 Iron and molybdate siderophore affinity determination

The affinity of each siderophore for iron (III) and iron (II), expressed as the formation constant of the iron-siderophore complex was determined by competition with EDTA as described by Reid *et al.* (1993). The iron-siderophore complex (0.1 mM final concentration) was allowed to form and equilibrate for 72 hr before being mixed with 0.05 mM to 2.0 mM (final concentration) EDTA. Conversely, solutions containing 0.05 mM to 2.0 mM Fe-EDTA complex were incubated with 0.1 mM siderophore for 96 hr.

In a manner similar to that used for iron, the affinity of each siderophore for molybdate, expressed as the formation constant of the molybdo-siderophore complex, was determined by competition between molybdo- and ferric-siderophore complexes. The ferric-siderophore complex (0.1 mM final concentration) was allowed to form and equilibrate for 72 hr before being mixed with 0.05 mM to 2.0 mM (final concentration) molybdate with incubation for 96 hr. Alternatively, a molybdo-siderophore complex (0.1 mM final concentration) was allowed to form for 72 hr before mixing with 0.05 mM to 2.0 mM (final concentration) iron (III) with incubation for 96 hr.

In both ferric- and molybdo-siderophore formation constant determinations, the concentration of ferric-siderophore present in each equilibrium reaction was determined spectrophotometrically by comparison to a calibration curve formed when the initial competition reactions were begun. The concentration of each component present at equilibrium was based on this value and the stoichometric relationship between the ferric-siderophore and other species present in the reaction mixture as defined by Equation (1) in Section 1.4.4. The concentration value of each component of a competition test reaction was then substituted into Equation (4) of Section 1.4.4, this allowed the calculation of the pH-dependent formation constant of the siderophore complex being tested with iron or molybdate.

As the molar binding ratios of the different siderophores and iron or molybdate were different, it was not possible to directly compare the formation constants calculated for each complex to one another. Thus, the affinity of a siderophore for a particular metal was expressed by determining the amount of free metal present in a hypothetical system containing 10^{-5} M siderophore and 10^{-6} M metal at pH 7.4 (Section 1.4.4) and comparing these values.

Protochelin was added to these assays in 80% methanol because of the low solubility of the uncomplexed ligand in aqueous solution, as in (Harris *et al.*, 1979). Aminochelin and azotochelin stocks were dried under a nitrogen stream and dissolved in 100 mM MOPS buffer (pH 7.0) before use. The competition reaction was set up in plastic, disposable 96-well microtiter plate (Corning Costar #3594) and was incubated under nitrogen gas, in the dark, in an air-tight chromatography tank flushed with nitrogen under high humidity conditions. Humidity was maintained by the use of a wet paper towel in the bottom of the incubation chamber. In all reactions, the final reaction volume was 250-µl, absorbance was measured with a Biotek Instruments EL311 microtiter plate reader with a minimum of two duplicate series containing six replicates of each reaction mixture being used for the calculations with each siderophore.

2.3 Interaction of metals and protochelin

2.3.1 Molybdate-iron siderophore complex competition

The interaction of iron, molybdate and the catecholate siderophores was studied by observing the formation of ferric- or molybdo-siderophore complexes over time. This was accomplished by combining ferric nitrate, sodium molybdate and one of the three siderophores in the following molar ratios. Protochelin 1:1 with iron (III) and 1:1 or 2:3 with molybdate, azotochelin 3:2 with iron (III) and 1:1 with molybdate, and finally

aminochelin 3:1 with iron (III) and 2:1 with molybdate. The formation of a metal-siderophore complex was then monitored at A_{490} for ferric-protochelin and ferric-aminochelin, A_{570} for ferric-azotochelin. The reaction mixture for protochelin (1:1 protochelin to molybdate) contained 0.20 µmol siderophore, 0.20 µmol molybdate and 0.20 µmol iron (III) or 0.16 µmol siderophore, 0.23 µmol molybdate and 0.16 µmol iron (III) for the 2:3 protochelin to molybdate complex. The reaction mixture for azotochelin contained 0.20 µmol siderophore, 0.20 µmol molybdate, and 0.13 µmol iron (III). Finally, the reaction mixture of aminochelin contained 0.30 µmol siderophore, 0.15 µmol molybdate, and 0.10 µmol iron (III). In each case, the total volume of a reaction was brought to 2 ml with 6 mM potassium phosphate buffer (pH 7.6).

The formation of a molybdo-siderophore complex in the presence of a ferric-protochelin or ferric-azotochelin complex was also investigated. In this study, a solution containing 12.5 µM ferric-protochelin or ferric-azotochelin was challenged with either 12.5 µM or 1,000 µM molybdate and the formation of molybdo-protochelin or molybdo-azotochelin was monitored at 375 nm.

The reactions were set up in plastic, disposable cuvettes (Bio-Rad #223-9955) incubated under nitrogen gas, in the dark, in an air-tight chromatography tank flushed with nitrogen under high humidity conditions. Humidity was maintained by the use of a wet paper towel in the bottom of the incubation chamber. The formation of ferric- or molybdo-siderophore complexes was monitored for up to 338 hr.

The percent of maximum complex present at a given time point was then calculated as the ratio of metal-siderophore complex present and the maximum possible concentration of metal-siderophore complex present in a reaction mixture based on the amount of free metal and siderophore added. These concentrations values were calculated using the

following molar extinction coefficients: ferric-protochelin $5.45*10^3$ M Abs^{-1} cm^{-1}, ferric-azotochelin $1.01*10^4$ M Abs^{-1} cm^{-1}, ferric-aminochelin $4.76*10^3$ M Abs^{-1} cm^{-1}, molybdo-protochelin $7.26*10^3$ M Abs^{-1} cm^{-1} (1:1 protochelin: molybdate complex) or $1.57*10^4$ M Abs^{-1} cm^{-1} (2:3 protochelin: molybdate complex), molybdo-azotochelin $5.75*10^3$ M Abs^{-1} cm^{-1}, and molybdo-aminochelin $4.86*10^3$ M Abs^{-1} cm^{-1}.

2.3.2 Effect of metals on protochelin accumulation

The effect of metals other than molybdate on the accumulation of protochelin was examined by growing strain UW in iron-limited Burk's medium (20 ml in a 50 ml Erlenmeyer flask) under standard conditions, with the addition of metals at concentrations from 10 to 1,000 mM. The metals used were: $NiCl_2 \cdot 6H_2O$, $CoCl_2 \cdot 6H_2O$, $Al_2(SO_4)_3 \cdot 18H_2O$, $MgSO_4 \cdot 7H_2O$, $Cr_2(SO_4)_3$, $Na_2Cr_2O_7$, $NaVO_3 \cdot 2H_2O$, $CaCl_2 \cdot 2H_2O$, $CdSO_4$, $ZnSO_4 \cdot 7H_2O$, Na_2WO_3, $MnCl_2 \cdot 4H_2O$, and $SrCl_2 \cdot 6H_2O$. The catecholate siderophores produced were then extracted, resolved, and identified by TLC. Growth and catecholates produced were estimated as previously described in Section 2.1.2.

2.3.3 Effect of metals on $^{55}Fe^{3+}$-siderophore uptake

The uptake of $^{55}Fe^{3+}$-protochelin, $^{55}Fe^{3+}$-azotochelin, and $^{55}Fe^{3+}$-aminochelin was examined in the presence of 70 µM Na_2MoO_4, 100 µM $NaVO_3 \cdot 2H_2O$, 30 µM Na_2WO_3, 500 µM $ZnSO_4 \cdot 7H_2O$, and 70 µM $MnCl_2 \cdot 4H_2O$. The uptake assays were performed as described in Section 2.2.7 with the following modifications. The cell suspension used in the uptake assay was 20 hr old and was grown in the presence of 3 µM ferric citrate to repress the formation of azotobactin. Ferric-siderophore complexes (1.6 ml) containing 12.5 µM $^{55}Fe^{3+}$ had been allowed to form for 72 hr in the dark before they were added to 14.4 ml of sterile uptake buffer. This mixture was dispensed, 8 ml, into two 50 ml Erlenmeyer flasks so that 7.0 µg ml^{-1} of $^{55}Fe^{3+}$ (specific activity 37.5 µCi ml^{-1}) was present in each assay reaction. The uptake assay was begun with the addition of 2 ml of a

cell suspension with an OD_{600} of approximately 7. The uptake assay continued for 16 min with samples taken at four min intervals. The effect of other metal ions on uptake was determined by adding 70 µl of a 100X stock of the metal immediately after the 8 min sample was taken. Uptake rates for each siderophore were calculated from the first 8 min of the assay. The uptake rate after the addition of a metal was determined from the last 8 min of the assay. Inhibition of uptake was calculated as the ratio of (change in uptake rate with or without metal) to the (uptake rate without metal) and expressed as a percent.

2.3.4 SDS-PAGE examination of IROMPs

The iron-repressible outer membrane proteins (IROMPs) of strains UA1 and UW were examined to determine if growth in the presence of 1 mM molybdate affected the protein content of the cellular outer membrane. Membrane samples were prepared and fractionated with sarcosyl as described in Section 2.1.4 and were separated on a 10% SDS-PAGE mini gel (100 cm x 80 cm, Hoeffer). The 10% resolving gel was prepared as follows to a final volume of 10 ml:

40% (w/v) Acrylamide:bis-acrylamide (29:1)	2.50 ml
1.0 M Tris-HCl pH 8.0	3.75 ml
Milli-Q dH_2O	4.17 ml
20% (w/v) sodium dodecylsulphate (SDS)	0.025 ml
10% (w/v) ammonium persulphate	0.05 ml
TEMED	0.02 ml

The resolving gel was poured and overlaid with a 3 mm layer of *n*-butanol. Once set, the *n*-butanol was removed and the gel was rinsed with Milli-Q dH_2O. A 5% stacking

gel was made by combining the following to a final volume of 3 ml:

40% (w/v) Acrylamide:bis-acrylamide (29:1)	0.38 ml
1.0 M Tris-HCl pH 6.8	0.38 ml
Milli-Q dH_2O	2.22 ml
20% (w/v) SDS	0.008 ml
10% (w/v) ammonium persulphate	0.04 ml
TEMED	0.004 ml

Protein samples of 10 µg were mixed with a 5X sample loading buffer which contained 40% (v/v) glycerol, 5% (w/v) SDS, 0.3% (w/v) bromophenol blue, and 25% (v/v) β-mercaptoethanol in 50 mM Tris-HCl buffer (pH 8.0) and were incubated at 100°C for 5 min prior to loading on the gel. A solution of protein size markers containing 204-kDa, 116-kDa, 97.4-kDa, 66-kDa, 45-kDa, and 29-kDa protein standards (Sigma #SDS-6H) in a loading buffer of 10% (v/v) glycerol, 2% (w/v) SDS, 0.001% (w/v) bromophenol blue, and 5% (v/v) β-mercaptoethanol in 50 mM Tris-HCl buffer (pH 8.0) was heated at 100°C for 1 min just prior to loading on the gel. Proteins were separated using a constant current of 15 mA gel^{-1} through the stacking gel and 25 mA gel^{-1} through the resolving gel. The gel was run until the bromophenol blue tracking dye just ran off the bottom of the gel (approximately 1.5 hr).

The gel was then stained for 24 hr in a solution of Sypro Orange (Molecular Probes #S-6650) in accordance with the protocol provided (1:5,000 dilution of stock stain solution in 7.5% (v/v) acetic acid). The gel was photographed with Polaroid 667 film under UV illumination using a Sypro Orange protein gel photographic filter (Molecular Probes #S-6656) with an F-stop of 5.6 and a 3 sec exposure time. The resulting photograph was

scanned using an AGFA Snapscan 310 flatbed scanner with Color It 3.0 (Microfrontier Inc.) software.

SDS stock solutions were prepared fresh such that there was no precipitate present in the solution. The 10% (w/v) ammonium persulphate solution was made fresh prior to use and was good for up to 1 week when stored at –20°C.

2.3.5 Ferric reductase assay

The activity of ferric reductase in cell free extracts was measured by the method described in Page (1995). The following components were mixed into 50 mM Tris-HCl buffer (pH 7.6):

10.0 mM $MgCl_2$	100 µl
1.6 mM iron (III) source	100 µl
4 mM NADH	100 µl
500 µM FMN	40 µl
50 mM Tris-HCl pH 7.6	to 800 µl total

This reaction mixture was allowed to incubate in the dark at 37°C for at least 60 min before the addition of 100-µl ferrozine (3-(2-pyridyl)-5,6-bis(4-phenylsufonic acid)-1,2,4-triazine) (Sigma #P-9762) to a final concentration of 0.8 mM. The assay was started with the addition of up to 100-µl of CFX (described in Section 2.1.4). The reduction of iron (III) was detected as an iron(II)-ferrozine complex and was monitored by A_{562} for 5 min. When present, additional metals were added to the assay mixture just prior to the ferrozine and CFX and the volume of 50 mM Tris-HCl (pH 7.6) was reduced accordingly. Metals used were 70 µM Na_2MoO_4, 100 µM $NaVO_3 \cdot 2H_2O$, 30 µM Na_2WO_3, 500 µM $ZnSO_4 \cdot 7H_2O$, and 70 µM $MnCl_2 \cdot 4H_2O$. Iron (III) to iron (II) conversion rates were calculated using the molar extinction coefficient for the iron (II)-ferrozine complex of $2.79*10^4$ M Abs^{-1} cm^{-1} (Stookey, 1970). Ferric reductase activity

was expressed as nmol Fe^{2+} min^{-1} (mg protein)$^{-1}$. The effect of metal addition was determined by expressing the ratio of ferric reductase activity in the presence of a metal to the activity of ferric reductase alone as a percentage.

All stock solution used were made in 50 mM Tris buffer (pH 7.6). The stock solution of NADH was made fresh, just prior to its use, as it was unstable in solution. The stock solution of FMN was made and stored at –20°C until needed and the 10X stock solution of ferrozine used was also kept on ice, in the dark until needed. The 1.6 mM iron (III) source used was ferric-citrate, ferric-protochelin, ferric-azotochelin, or ferric-aminochelin.

2.3.6 Effect of high molybdate concentrations on *A. vinelandii* P100 growth

The manner in which *A. vinelandii* strain P100, which is unable to produce any siderophores, responds to high molybdate concentrations was examined by growing the microorganism for 24 hr in 100 ml iron-limited Burk's medium containing 3 µM ferric citrate (500 ml Erlenmeyer flask) under standard conditions. Cells in 10 ml samples were aseptically harvested by centrifugation (International Equipment clinical centrifuge, setting 5) and washed twice with sterile 6 mM potassium phosphate buffer (pH 7.6). Cell pellets were re-suspended in 20 ml iron-limited Burk's medium (50 ml Erlenmeyer flask) containing 1 µM ferric citrate and strain UA1 culture supernatant fluid containing approximately 1 A_{310} unit of azotochelin and aminochelin or purified protochelin with 1, 10, 100, or 1000 µM of molybdate and 50 µg EDDHA ml^{-1} to restrict iron availability. These cultures were incubated for 24 hr under standard conditions and growth in terms of total cellular protein was quantified by the method of Lowry *et al.* (1951) (Section 2.1.2).

2.4 Determination of the role of protochelin in O_2 stress management

2.4.1 Non-denaturing PAGE of CFX proteins

Proteins present in iron-sufficient (75 µM ferric citrate) and iron-limited (1 µM ferric citrate) CFX (Section 2.1.4) were separated in 7.5% acrylamide non-denaturing mini gels (100 cm x 80 cm, Hoeffer). The 7.5% resolving gel was prepared as follows to a final volume of 10 ml:

40% (w/v) Acrylamide: bis-acrylamide (29:1)	1.88 ml
1.0 M Tris-HCl pH 8.0	3.9 ml
Milli-Q dH_2O	4.17 ml
10% (w/v) ammonium persulphate (fresh)	0.05 ml
TEMED	0.004 ml

The resolving gel was poured and overlaid with a 3 mm layer of *n*-butanol. Once set, the *n*-butanol was removed and the gel was rinsed with Milli-Q dH_2O. A 5% stacking gel was made by combining the following to a final volume of 4 ml:

40% (w/v) Acrylamide: bis-acrylamide (29:1)	0.5 ml
1.0 M Tris-HCl pH 6.8	0.5 ml
Milli-Q dH_2O	2.96 ml
10% (w/v) ammonium persulphate (fresh)	0.04 ml
TEMED	0.004 ml

Protein samples (15 µg) were mixed with 0.1% (w/v) bromophenol blue tracking dye in 50 mM potassium phosphate buffer (pH 7.6) with 50% (v/v) glycerol. Electrophoresis was performed using a running buffer of 25 mM Tris-HCl and 192 mM glycine. Proteins were separated using a constant current of 15 mA gel^{-1} through the stacking gel and 25 mA gel^{-1} through the resolving gel until the bromophenol blue band ran off the bottom of the gel (approximately 1.5 hr). The gel was then stained as described in Section 2.4.2 or Section 2.4.3. The 10% (w/v) ammonium persulphate solution was made fresh prior to use and was good for up to 1 week when stored at –20°C.

2.4.2 Catalase assay

Catalase activity was determined by following the inhibition of H_2O_2-mediated reduction of dichromate Cr (VI) to chromic Cr (II) acetate (Sinha, 1972). This was done by combining 4 ml of 200 mM H_2O_2, 5 ml of 50 mM potassium phosphate buffer (pH 7.6) and 1 ml of CFX containing catalase to give an reaction mixture of 10 ml. The assay was started with the addition of the catalase-containing CFX. Once the assay was started, 1 ml samples were removed at 1, 3, and 5 min time points. Samples were taken in duplicate and mixed with 2 ml of a dichromate:acetic acid solution. This solution was made by combining 5% (w/v) $K_2Cr_2O_7$ in dH_2O with concentrated acetic acid in a 1:3 (v/v) ratio. The assay sample and dichromate:acetic acid solution were then heated at 100°C for 10 min followed by the measurement of A_{570}. The µmol of H_2O_2 present in each sample was calculated by comparison to a calibration curve of 1 to 160 µmol H_2O_2. The calibration curve was made by combining increasing amounts of H_2O_2 in 50 mM potassium phosphate buffer (pH 7.6) to a total volume of 1 ml and then adding 2 ml of the dichromate:acetic acid solution. Standards were then heated to 100°C for 10 min and A_{570} values were read. One unit of catalase activity was defined as the degradation of 1 µmol H_2O_2 min^{-1} $(ml)^{-1}$ enzyme and was calculated graphically by taking the slope of a plot of the µmol H_2O_2 present in a sample vs. time (min) and expressing this value per protein (ng) in the CFX used.

Catalase activity in non-denaturing PAGE gels was demonstrated as described in Clare *et al.* (1984) with the following exceptions. The gel was soaked in 100 ml of 10 U horse radish peroxidase ml^{-1} for 105 min. This solution was removed and replaced with 100 ml of 5.0 mM H_2O_2. After 45 min, the H_2O_2 solution was removed and the gel was soaked in 100 ml of 0.75 mg ml^{-1} diamidobenzidine (DMB) at which point, any catalase bands present were visible within 15 min. Catalase bands were recorded photographically with

Polaroid 667 film using an F-stop of 5.6, an exposure time of 1/30 sec and illumination from a light box beneath the gel. The resulting photograph was scanned using an AGFA Snapscan 310 flatbed scanner with Color It 3.0 (Microfrontier Inc.) software.

2.4.3 Superoxide dismutase (SOD) assay

SOD activity was measured by its ability to inhibit the reduction of nitroblue tetrazolium (NBT) by $\bullet O_2^-$ (Oberley & Spitz, 1985). This was done using a stock reaction mixture made from the following to a final volume of 16 ml:

50 mM potassium phosphate buffer (pH 7.6)	5.2 ml
1.8 mM xanthine	3.4 ml
2.23 mM NBT	5.0 ml
13.3 diethylenetriaminepentaacetic acid (DTPA)	1.6 ml
40 U ml^{-1} catalase	0.5 ml
330 mM NaCN (only to measure Mn-SOD) or buffer	0.3 ml

The assay was performed by combining 800-µl of the above solution with 100-µl of enzyme solution (CFX-Section 2.1.4) or buffer in the blank reaction. The assay solution was used to zero the spectrophotometer before the addition of 100-µl of 100 mU ml^{-1} xanthine oxidase to start the reaction.

Activity was calculated by first determining the rate of NBT decolorization in the absence of SOD. This value, as were all values, was corrected for spontaneous decolorization by using a blank reaction mixture that did not contain any xanthine oxidase. The percent inhibition generated by the SOD present in the enzyme solution was calculated as:

% Inhibition = ((Rate without SOD – Rate with SOD)/(Rate without SOD)) * 100

A minimum of three of these values were plotted against the protein (μg) content of the CFX used and the amount of protein required to give 50% inhibition was calculated from the graph. This value was divided by 1000 to give enzyme Units mg protein^{-1}. One Unit of SOD activity was defined as the amount of protein required to inhibit the maximal rate of NBT reduction by 50% (Oberley & Spitz, 1985). Values reported were means calculated from at least duplicate assays in which the standard deviation was not greater than 10%.

The NBT solution used was made fresh and stored in the dark. The 1.8 mM xanthine solution was made by boiling in buffer to dissolve the xanthine and then storing the solution at 37°C, for up to one week. All solutions were made in 50 mM potassium phosphate buffer (pH 7.6).

SOD activity was located on non-denaturing PAGE gels as described in Beauchamp & Fridovich (1971). The gel was soaked for 20 min in 100 ml of 2.45 mM NBT in 50 mM potassium phosphate buffer (pH 7.6). This solution was removed and the gel was soaked in 100 ml of 28 mM TEMED and 280 μM riboflavin in 50 mM potassium phosphate buffer (pH 7.6) for 15 min. This was removed and the gel was exposed to a 60 W incandescent lamp at a distance of 10 to 15 cm for 5 to 10 min. This caused the gel to turn blue while bands of SOD activity appeared as regions of white. The Fe-SOD was inhibited by soaking the gel in 5 mM H_2O_2 for 20 min before the above SOD activity stain was applied (Allgood & Perry, 1985). Visible bands were recorded electronically using "The Imager" (Appligene) and were either saved as TIFF files for later electronic use or were printed out using a Mitsubishi (#P68U) video copy processor. Alternatively, the resulting gel was scanned using an AGFA Snapscan 310 flatbed scanner with Color It 3.0 (Microfrontier Inc.) software.

2.4.4 Oxygen radical mediated iron (II) release

The ability of a siderophore to withhold iron from the Fenton reaction was tested by following iron (III) released from a ferric-siderophore complex after its reduction to iron (II) by $\bullet O_2^-$. This was done by monitoring the formation of a iron (II)-ferrozine complex at A_{562} (Coffman *et al.*,1990) using a reaction mixture containing the following, to a final volume of 900-µl:

600 mM potassium phosphate buffer (pH 7.6)	100 µl
100 mM ferrozine	100 µl
2 mM hypoxanthine	100 µl
3000 U ml^{-1} catalase (when added)	100 µl
50,000 U ml^{-1} SOD (when added)	100 µl
400 µM Fe^{3+}-siderophore complex	variable volume
Milli-Q dH_2O	to 900 µl

The reaction was started with the addition of 100-µl of 1.0 U ml^{-1} xanthine oxidase and the reaction was monitored for 15 min at A_{562}. Reaction mixtures with ferric-siderophore complexes containing a potential free iron (II) concentration of 15 to 45 µM were used. The molar extinction coefficient for the iron (II)-ferrozine complex of $2.79*10^4$ M Abs^{-1} cm^{-1} (Stookey, 1970) was used to calculate the amount of iron (II) released. These values were plotted against time and the rates of iron (II) release from 2 to 6 min were calculated.

A ferric-siderophore complex was formed by drying down siderophore from an 80% methanol stock by evaporation under N_2, and dissolving the siderophore in 60 mM potassium phosphate buffer (pH 7.6) at 37°C. Ferric nitrate (10 mM) was mixed with the siderophore in the appropriate molar ratio to obtain a complex that was 100% saturated with iron (III). These complexes were allowed to form for at least 72 hr before use. All stock solutions were made in Milli-Q dH_2O. Hypoxanthine was made in boiling 60 mM

potassium phosphate buffer (pH 7.6) until dissolved and the solution was good for 1 week when stored at 37°C. The xanthine oxidase solution was prepared immediately prior to use. Control reactions contained 500 U catalase ml^{-1} or 30 U SOD ml^{-1} to demonstrate the dependence of iron (II) release on $\bullet O_2^-$ or H_2O_2.

2.4.5 Inhibitory role of siderophores in •OH generation

The detection of •OH generation by the Fenton reaction was based on Coffman *et al.* (1990) and was done using a reaction mixture that contained the following, to a final volume of 950 µl:

90 mM deoxyribose	50 µl
2 mM hypoxanthine	100 µl
50,000 U ml^{-1} catalase (when added)	10 µl
3,000 U ml^{-1} SOD (when added)	10 µl
400 µM iron (III)-siderophore complex	variable volume
6 mM potassium phosphate buffer (pH 7.6)	to 950 µl

The reaction was started with the addition of 50-µl of 1 U ml^{-1} xanthine oxidase and was allowed to proceed for 15 min at room temperature. Reactions were stopped by the addition of 250-µl of 14.4% (w/v) trichloroacetic acid. Deoxyribose that had reacted with •OH formed a colored complex with the addition of 250-µl of 1% (w/v) thiobarbituric acid in 0.1 M NaOH. After heating for 15 min at 100°C, the resulting A_{532} value obtained was expressed as a percentage of the value obtained from the ferric-EDTA containing control.

Ferric-siderophore complexes were formed as in Section 2.4.4 and •OH generation reactions performed contained potential free iron (II) concentrations of 5 to 30 µM. Ferric-EDTA in the same concentration range was used as a positive control of •OH generation. Hypoxanthine was made in boiling 60 mM potassium phosphate buffer (pH

7.6) until dissolved and was stored for up to one week at 37°C. The xanthine oxidase solution was prepared immediately prior to use. Control reactions contained catalase (500 U ml^{-1}) and SOD (30 U ml^{-1}) to demonstrate the dependence of •OH generation on the presence of $•O_2^-$ or H_2O_2

CHAPTER 3 - Results and Discussion

3.1 Characterization of protochelin

3.1.1 Production of an unknown catecholate compound by *A. vinelandii*

In the course of studying the effect of molybdenum on the iron-limited growth of *A. vinelandii* UA1 (a spontaneous mutant only able to form catecholate siderophores), it was observed that 1 mM molybdate caused a brilliant orange color to form in the culture fluid. Although this was spectacular, it was not surprising as it is well documented that molybdenum will complex with catechol-containing compounds to give a yellow-orange color (Hider 1984). When the catechols from this iron-limited culture fluid were extracted into ethyl acetate and examined by TLC, it was observed that the pattern of catecholate spots normally produced by *A. vinelandii* UA1 had changed. The production of 2,3–DHBA (R_F= 0.85) was unaffected, but the azotochelin spot (R_F= 0.45) was not present and an unknown catecholate spot migrating at R_F= 0.27 was formed (Fig. 3.1). Spectrophotometric analysis of the acidified aqueous supernatant left after ethyl acetate extraction showed that aminochelin, another catecholate siderophore normally produced by *A. vinelandii* UA1, was also absent (data not shown).

This growth condition was repeated using the parent strain UW with identical results. However, a spot coinciding with the unknown catecholate was only faintly visible after ethyl acetate extraction of the culture fluid of cells grown in iron-limited medium containing 1 μM molybdate (Fig. 3.2). This suggested that the unknown catecholate was a natural product of wild-type *A. vinelandii*. It appeared to be formed in very small amounts in normal iron-limited Burk's medium, but its production was increased in medium containing higher concentrations of molybdate. Studies were carried out to define conditions under which this new compound was produced and showed that strain UA1 required a minimum of 70 μM molybdate for this new compound to appear (Fig. 3.3).

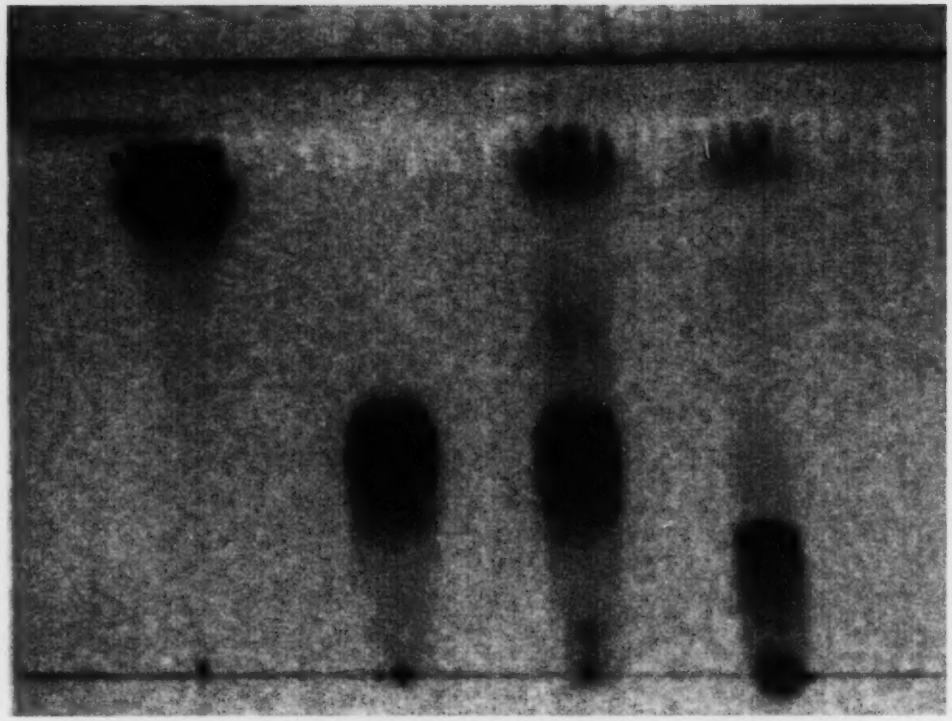

Figure 3.1 TLC analysis of the catecholates extracted from strain UA1 culture supernatant grown in molybdate-containing medium.

(1) 2,3-DHBA standard. (2) Azotochelin standard. (3) Ethyl acetate extract of 1 μM molybdate-containing culture supernatant. (4) Ethyl acetate extract 1 mM molybdate-containing culture supernatant.

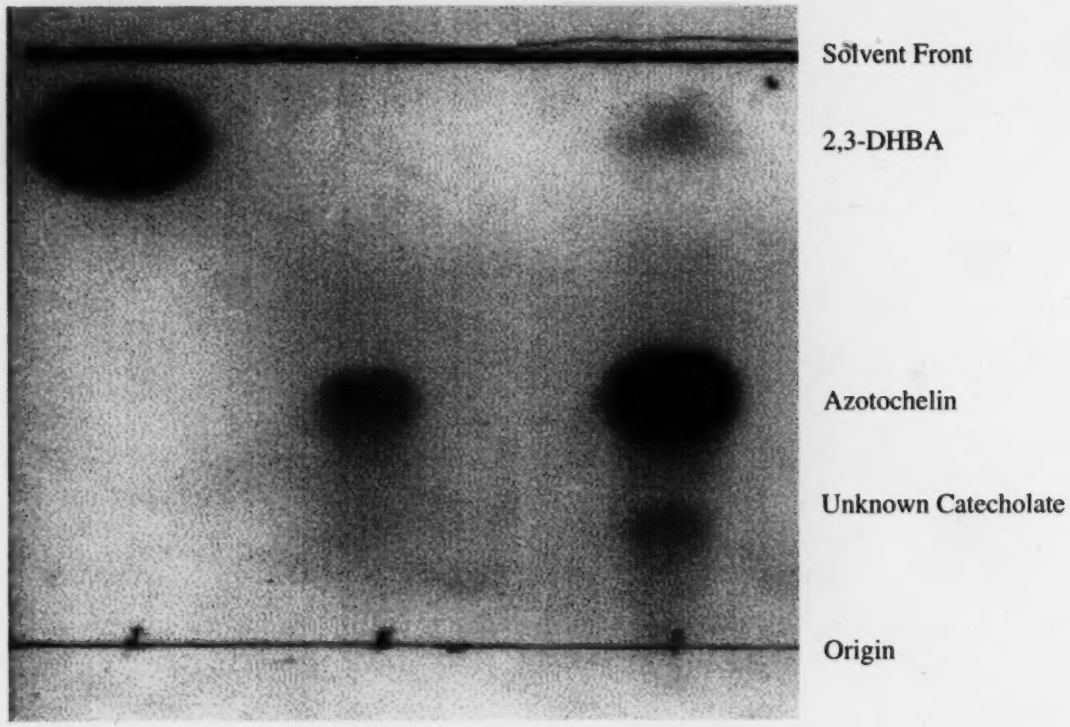

Figure 3.2 TLC analysis of the catecholates extracted from strain UW culture supernatant grown in 1 μM molybdate-containing medium.

(1) 2,3-DHBA standard. (2) Azotochelin standard. (3) Ethyl acetate extract 1 μM molybdate-containing culture supernatant.

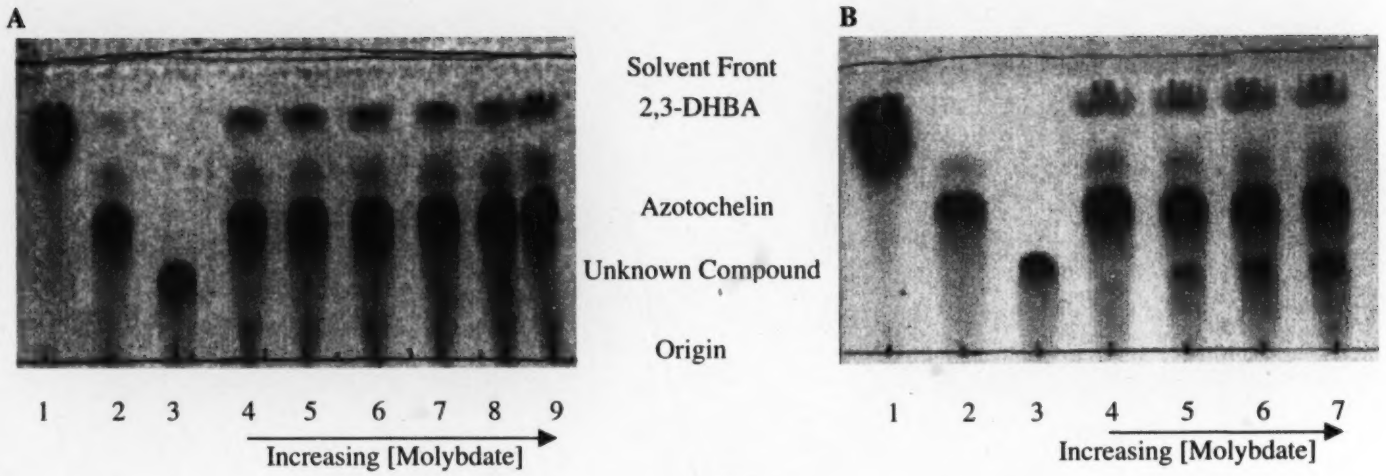

Figure 3.3 Effect of molybdate concentration on the accumulation of unknown catecholate.

In all figures: (1) 2,3-DHBA standard. (2) Azotochelin standard. (3) Ethyl acetate extract of culture supernatant from strain UA1 grown in 1 mM molybdate.
(A) Ethyl acetate extract of strain UA1 culture supernatant with added molybdate: (4) 10 μM, (5) 20 μM, (6) 30 μM, (7) 40 μM, (8) 50 μM, (9) 60 μM.

(B) Ethyl acetate extract of strain UA1 culture supernatant with added molybdate: (4) 30 μM, (5) 70 μM, (6) 80 μM, (7) 90 μM.

3.1.2 Purification of unknown catecholate by silicic acid chromatography

Strain UA1 was cultured under iron-limited conditions containing 1 mM molybdate and the unknown catecholate was purified by chromatography on a silicic acid column. Under these conditions, the majority of the ethyl acetate extractable catecholate was eluted as a single peak from the silicic acid column (data not shown).

3.1.3 Acid hydrolysis of unknown catecholate

The catecholate compound purified from strain UA1 was subjected to partial acid hydrolysis with 1 M HCl over 8 hr which resulted in a gradual decrease in the intensity of the R_f= 0.27 catecholate spot and an increase in intensity of azotochelin and 2,3-DHBA spots (Fig. 3.4A). Spectrophotometric scans of the acidified aqueous digestion mixture that remained after ethyl acetate extraction showed an increase in A_{310} during partial digestion suggesting the presence of aminochelin (data not shown). Extraction of the aqueous layer with *n*-butanol and subsequent TLC showed that aminochelin was being formed (TLC not shown). Total hydrolysis of the R_F= 0.27 catecholate in 6 M HCl and subsequent TLC showed the presence of compounds with the same R_F values as lysine and putrescine (Fig. 3.4B). The partial hydrolysis data suggested that the new catecholate compound was likely a condensation of azotochelin and aminochelin as these were the compounds which appeared when the new compound was hydrolyzed. This assertion was strengthen by the appearance of compounds with the same R_F values as lysine and putrescine from the total digestion of the new catecholate. Lysine and putrescine are the amino-nitrogen components of aminochelin and azotochelin, respectively (Fig. 1.2).

3.1.4 Molecular mass of unknown catecholate

If the new catecholate was a condensation product of aminochelin and azotochelin it would have a predicted molecular weight of 624 g mol^{-1}. This would be the sum of

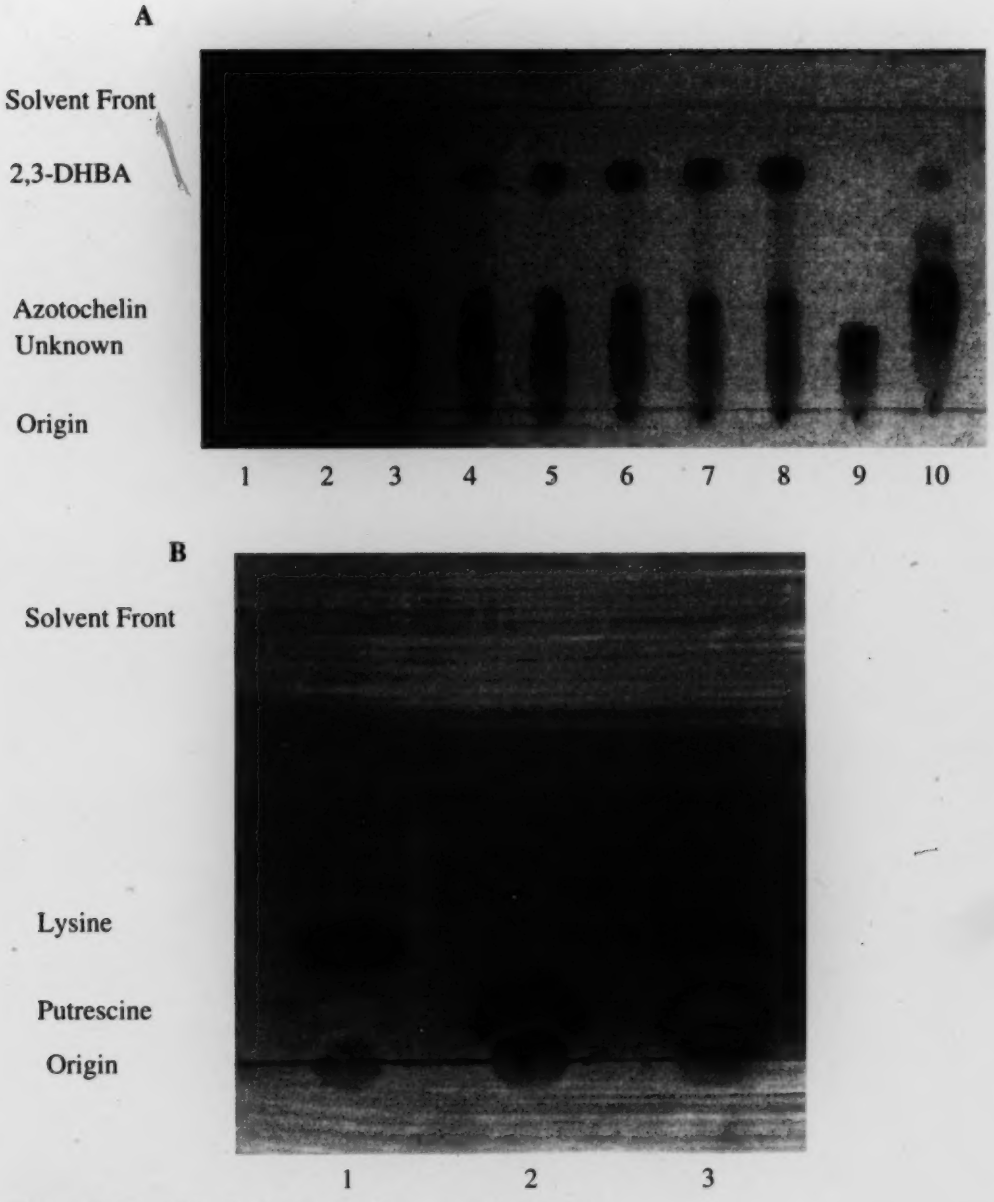

Figure 3.4 Acid hydrolysis of unknown catecholate.

(A) Ethyl acetate extract from hydrolysis time course. (1) 2,3-DHBA standard. (2) 0 hr, (3) 0.5 hr, (4) 2.0 hr, (5) 3.5 hr, (6) 5.0 hr, (7) 6.5 hr, (8) 8.0 hr after acid hydrolysis. (9) Unknown Catecholate from strain UA1 culture supernatant grown in 1 mM molybdate. (10) Azotochelin standard.

(B) Total Hydrolysis of (1) Lysine standard. (2) Putrescine standard. (3) Unknown compound after total hydrolysis. All stained with ninhydrin for amino nitrogen compounds.

azotochelin (418 g mol^{-1}) and aminochelin (224 g mol^{-1}) molecular weights minus 18 g mol^{-1} for the water lost during the condensation reaction. As can be seen in Figure 3.5 the mass obtained for the purified compound was 625 g mol^{-1} (624 + 1 hydrogen). Also indicated in the FAB mass spectra were peaks at 419, 225, and 155 g mol^{-1} representing the major breakdown products azotochelin + 1 hydrogen, aminochelin + 1 hydrogen, and 2,3-DHBA + 1 hydrogen, respectively.

A tricatecholate compound with this structure, containing both aminochelin and azotochelin residues had been isolated from an unrelated methylotrophic bacterium DSM 5746 (Taraz *et al.*, 1990) and was known as protochelin (Fig. 3.6-C). An authentic sample of protochelin was obtained and subjected to partial and full acid digestion (data not shown), FAB mass spectroscopy (Fig. 3.7), TLC analysis (Fig. 3.8) and was shown to have characteristics identical to the new catecholate. Thus, protochelin is also a natural product formed by iron-limited *A. vinelandii*.

3.1.5 Purification of *A. vinelandii* catecholate siderophores

For protochelin to be formed by strain UA1, a minimum 70 μM molybdate had to be present in the culture medium. However, it was found that *A. vinelandii* strain LM100 (which has a mutational insertion in the *fdx*A gene and is unable to sense oxidative stress-Section 1.6.5) did not require any extra molybdate beyond the 1 μM molybdate found in Burk's medium to accumulate protochelin. In addition, strain LM100 was found to produce not only protochelin under these conditions, but also aminochelin, azotochelin, and 2,3-DHBA as well. As a result of this, culture supernatant from strain LM100 was used as a source for all three catecholate siderophores using the protocol described (Section 2.2.2).

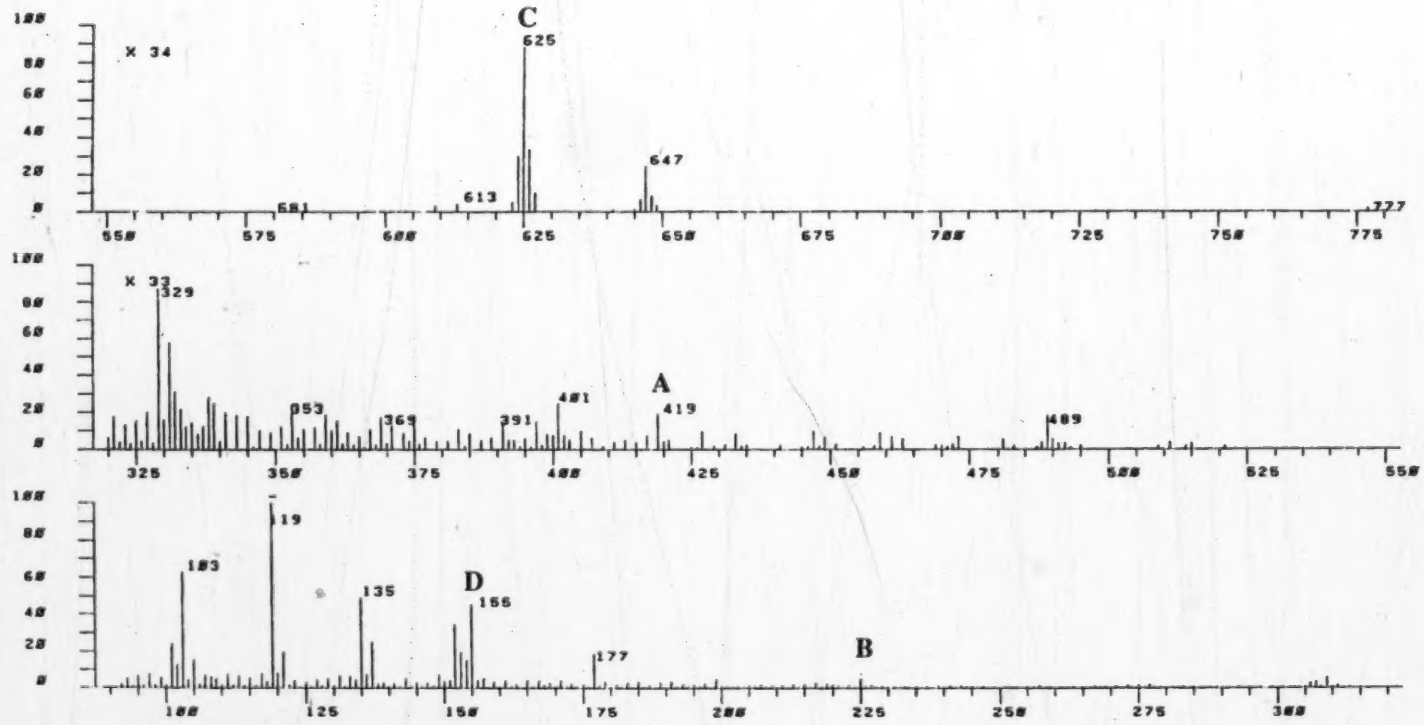

Figure 3.5 FAB mass spectrum of unknown catecholate.

(A) Azotochelin + hydrogen. (B) Aminochelin + hydrogen. (C) Unknown + hydrogen. (D) 2,3-DHBA + hydrogen.

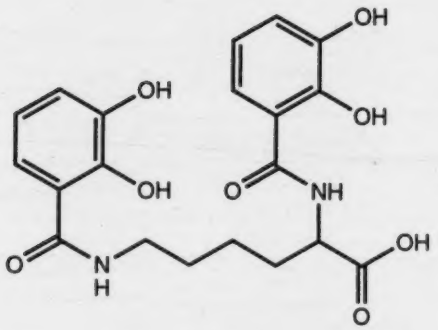

(A) Azotochelin
Molecular Weight: 418 Da

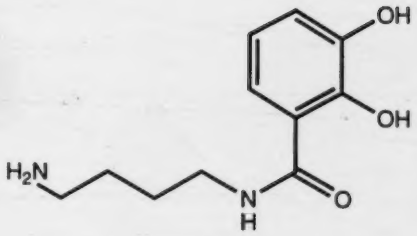

(B) Aminochelin
Molecular Weight: 224 Da

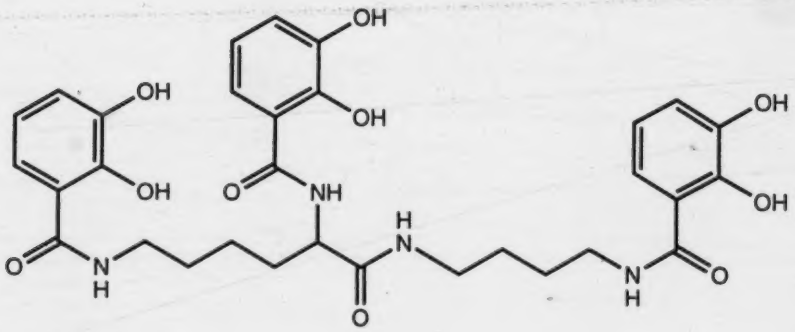

(C) Protochelin
Molecular Weight: 624 Da

Figure 3.6 Structures of the siderophores of *A. vinelandii*.

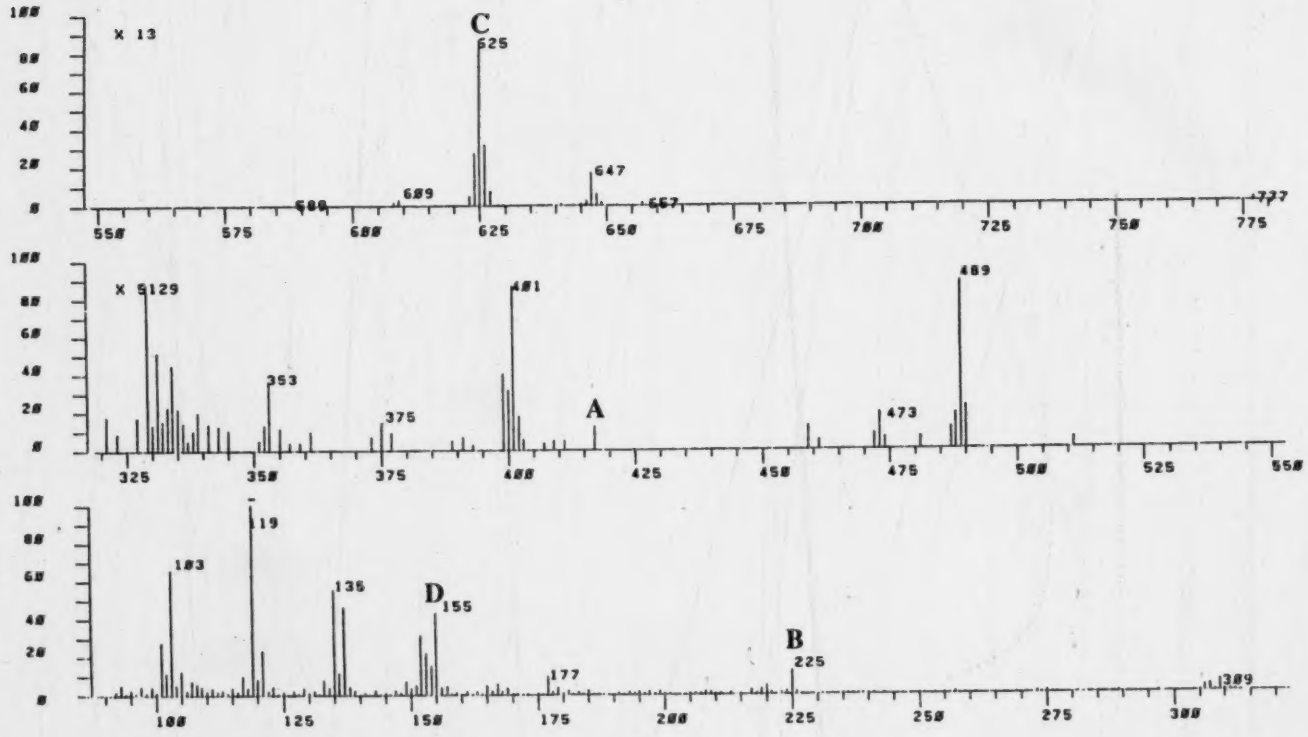

Figure 3.7 FAB mass spectrum of protochelin standard.

(A) Azotochelin + hydrogen. (B) Aminochelin + hydrogen. (C) Protochelin + hydrogen. (D) 2,3-DHBA + hydrogen.

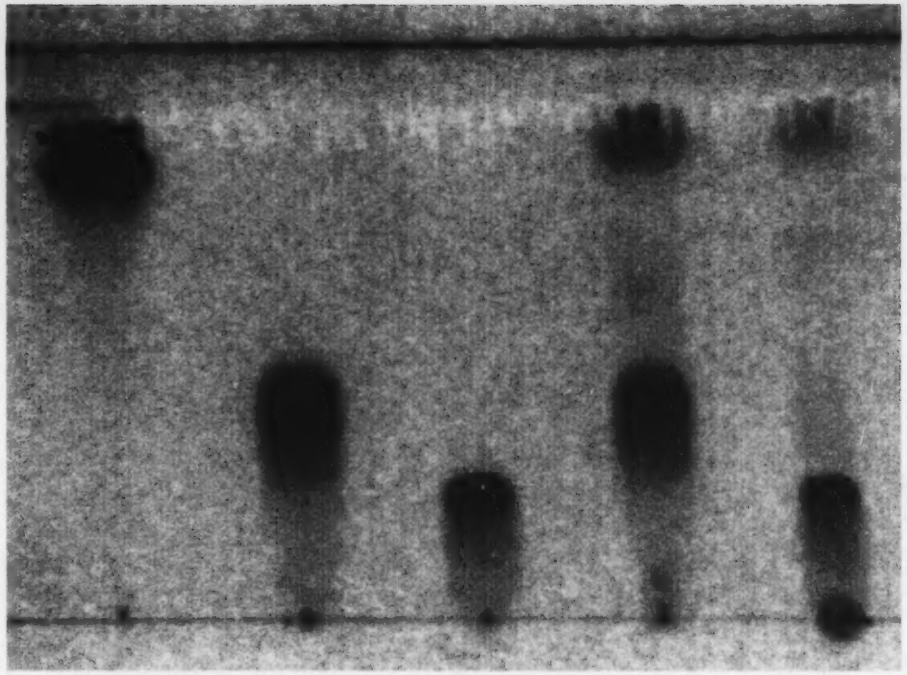

Figure 3.8 TLC analysis of unknown catecholate compound extracted from strain UA1 grown in 1 mM molybdate culture supernatant and protochelin standard.

(1) 2,3-DHBA standard. (2) Azotochelin standard. (3) Protochelin standard (4) Ethyl acetate extract of 1 μM molybdate culture supernatant. (5) Ethyl acetate extract of 1 mM molybdate UA1 culture supernatant.

Culture supernatant (9.6 L) was pooled and had a total A_{310} of $8.90*10^3$. The culture fluid was concentrated, acidified and extracted with ethyl acetate, after which it had a total A_{310} of $2.52*10^3$, which represented aminochelin. After washing the ethyl acetate pool with sodium phosphate buffer (pH 7.0) it had a total A_{310} of $1.45*10^3$, which represented protochelin. The pooled sodium phosphate washes had a total A_{310} of $3.22*10^3$ as azotochelin. Among these three pools 80% of the material absorbing radiation at A_{310} originally present in culture fluid was recovered.

The acidified culture supernatant fluid was neutralized to pH 7.0, reduced in volume to 50 ml and extracted with *n*-butanol. The *n*-butanol was evaporated to dryness and the residue dissolved in 5 mM ammonium acetate and applied to a CM-Sephadex column and eluted as described in Section 2.2.2. Fig. 3.9 shows the elution profile obtained from the 5 ml samples collected. Fraction 101 was extracted with *n*-butanol and analyzed by TLC using a butanol:acetic acid:water (150:30:30) solvent system; catecholates present were developed as before. The major spot that appeared on the TLC had an R_F of 0.38 which was close to the literature value of 0.42 for aminochelin and reacted strongly with ninhydrin indicating the presence of a primary amine (TLC not shown) (Page & von Tigerstrom, 1988). This fraction was subjected to FAB mass spectrometry which indicated the presence of a compound with an *m/e* of 221 g mol^{-1} which would correspond to aminochelin which had lost 3 hydrogen atoms. Also present on the mass spectrum were peaks at *m/e* = 241 and 269 g mol^{-1} which corresponded to aminochelin + OH or aminochelin + COOH (data not shown). The hydroxyl and carboxyl counter ions were most likely present due to the use of the ammonium acetate gradient to elute aminochelin from the column. This evidence taken together indicated that aminochelin was the catecholate present in the major peak seen on the CM-Sephadex elution profile. Fraction 101 was then used as an aminochelin standard for the TLC analysis of fractions 95 to 105 (Fig. 3.9 inset).

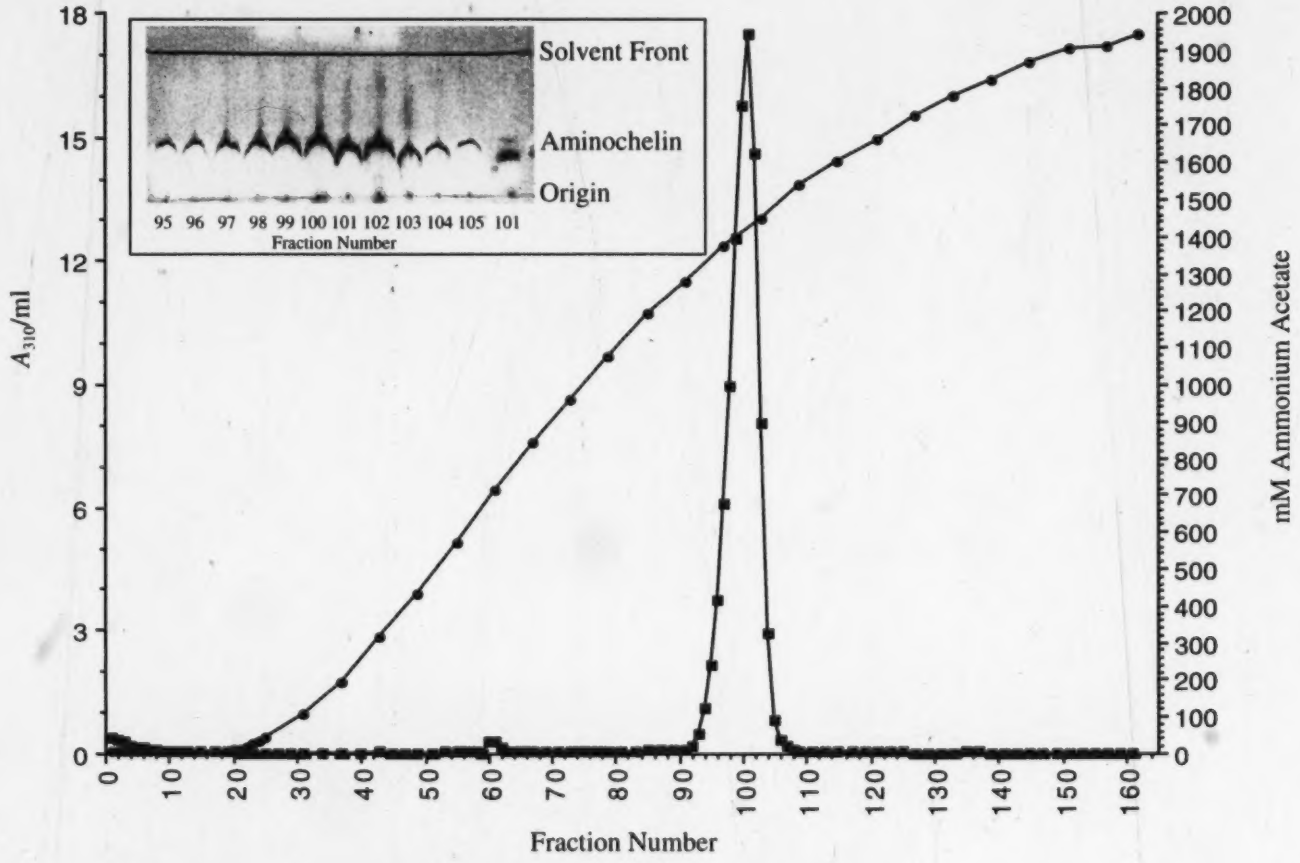

Figure 3.9 Elution profile of aminochelin from CM Sephadex column.

(■) Column fraction A_{310}/ml. (●) Ammonium acetate concentration (mM).
Inset: TLC of column fractions and peak fraction (101) aminochelin used for FAB mass spectrometry analysis.

A 250 µl sample of the sodium phosphate-washed ethyl acetate layer was dried under nitrogen gas and analyzed by standard TLC methods and indicated that the sodium phosphate-washed ethyl acetate layer contained only protochelin, based on comparison to an authentic standard (Fig. 3.10) (Taraz *et al.*, 1990). As a result of this, the sodium phosphate-washed ethyl acetate pool was dried under nitrogen, dissolved in 80% methanol and stored at -20°C for later use.

The azotochelin present in the sodium phosphate buffer was extracted into ethyl acetate and found to be contaminated with other, unknown catecholate compounds (Fig. 3.10 lane 5). The ethyl acetate was then dried under nitrogen and the residue was dissolved in 3.2 ml of 80% methanol for application to a Pharmacia LH-20 column. The resulting elution profile is shown in Fig. 3.11. Analysis of the major peak on the elution profile by TLC identified azotochelin as the sole catecholate present in those fractions (Fig. 3.11 inset). These fractions were pooled and stored at -20°C for later use.

3.1.6 Molar binding ratios of iron-siderophore complexes

To determine how iron and the catecholate siderophores interacted, the molar binding ratio of each siderophore and Fe^{3+} or Fe^{2+} was determined. An assay of the molar iron-binding ratio showed that each purified siderophore bound either Fe^{3+} or Fe^{2+} in a ratio consistent with siderophore structure (Fig. 3.6). Protochelin was found to bind Fe^{3+} and Fe^{2+} 1:1 from 18 hr to 219 hr (Fig. 3.12). Azotochelin initially bound Fe^{3+} and Fe^{2+} 1:1, but beginning at 68.5 hr the 3:2 azotochelin:iron complex is present (Fig. 3.13). The longer time taken to form the 3:2 azotochelin:iron complex compared to the 1:1 protochelin:iron complex is consistent with the formation of a siderophore-iron "bridge" required for this type of complex. Finally, aminochelin bound Fe^{3+} and Fe^{2+} in a 3:1 aminochein:iron ratio beginning at 18 hr, this complex was stable until at least 40 hr, after which point other ratios of aminochelin and iron dominate (Fig. 3.14). In all cases,

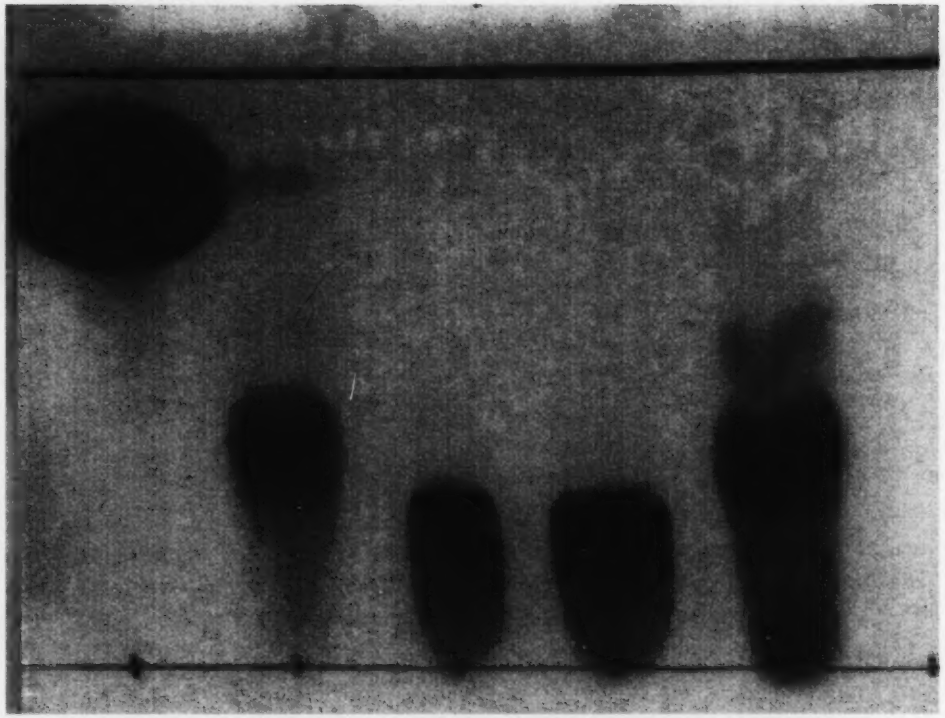

Figure 3.10 TLC analysis of catecholate siderophores present in ethyl acetate and sodium phosphate buffer pool fractions.

(1) 2,3-DHBA standard. (2) Azotochelin standard. (3) Protochelin standard. (4) 100 mM sodium phosphate buffer (pH 7.0) washed ethyl acetate layer. (5) Ethyl acetate extract of 100 mM sodium phosphate buffer (pH 7.0) layer.

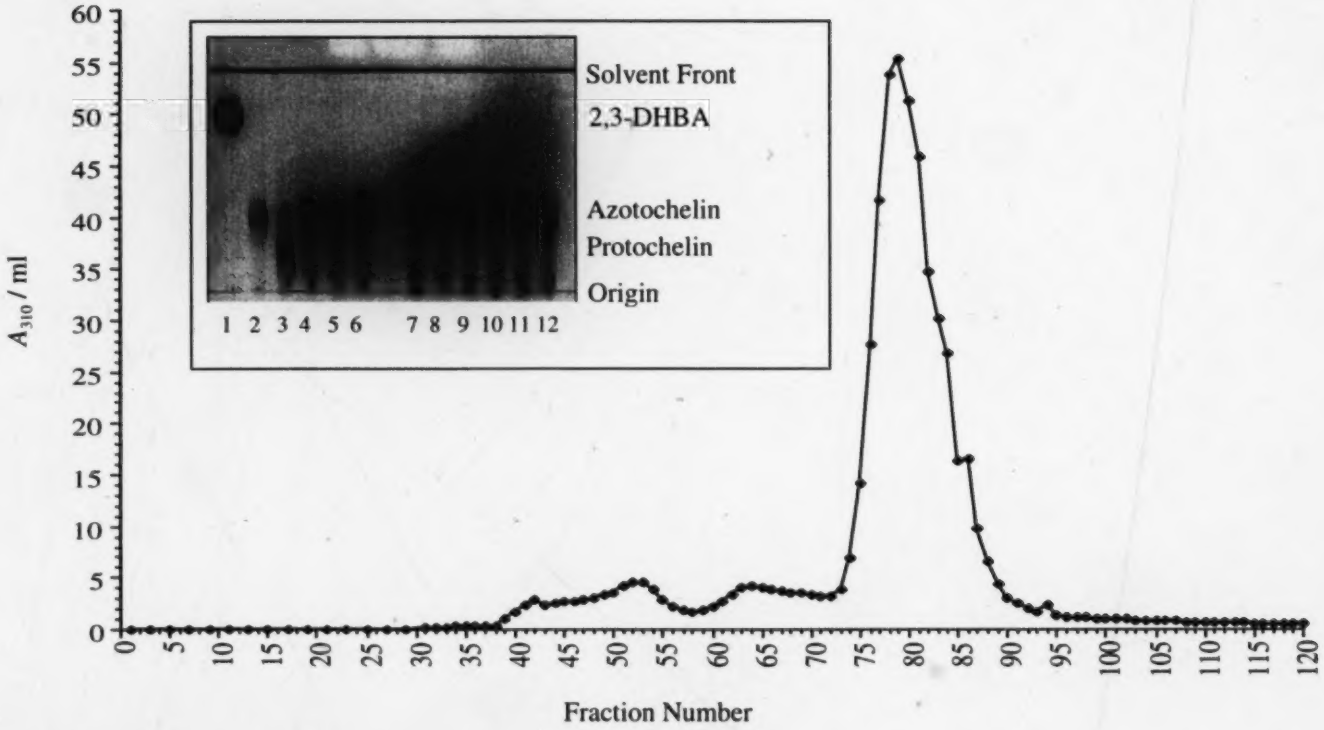

Figure 3.11 Elution profile of azotochelin from Sephadex LH-20 column.

(◆) Column fraction A_{310}/ml.
Inset: TLC of (1) 2,3-DHBA standard. (2) Azotochelin standard. (3) Protochelin standard. Column fractions: (4) #80. (5) #81. (6) #82. (7) #83 and #84. (8) #85. (9) #86. (10) #87. (11) #88. (12) #89.

A

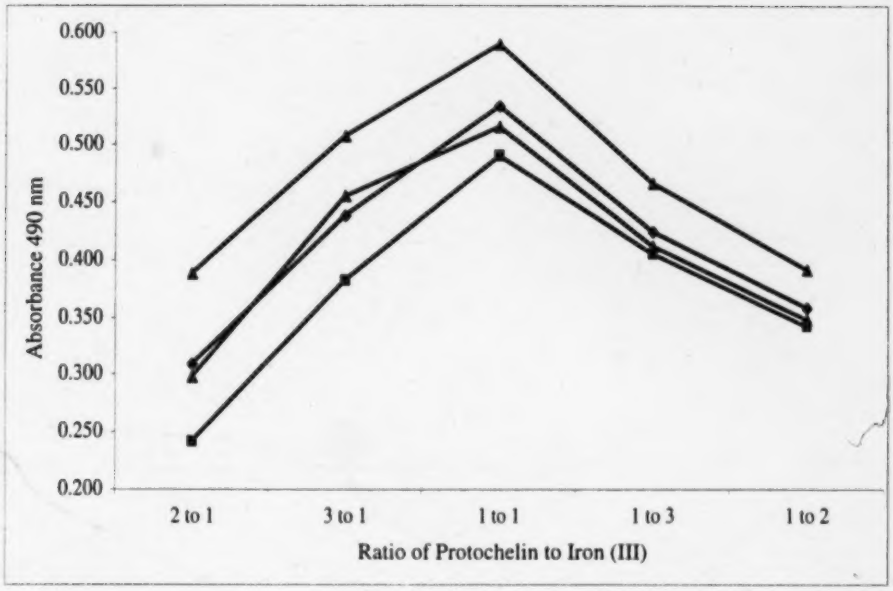

B

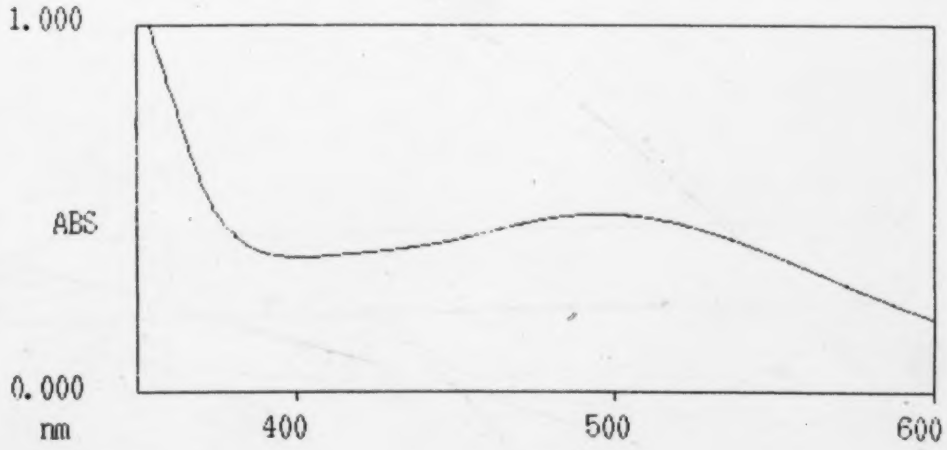

Figure 3.12 Spectrophotometric characteristics of ferric-protochelin.

(A) Molar binding ratio of ferric-protochelin complex. (■) 18 hr. (▲) 40 hr. (◆) 68.5 hr. (▲) 219 hr.
(B) Absorbance spectrum of ferric-protochelin complex.

A

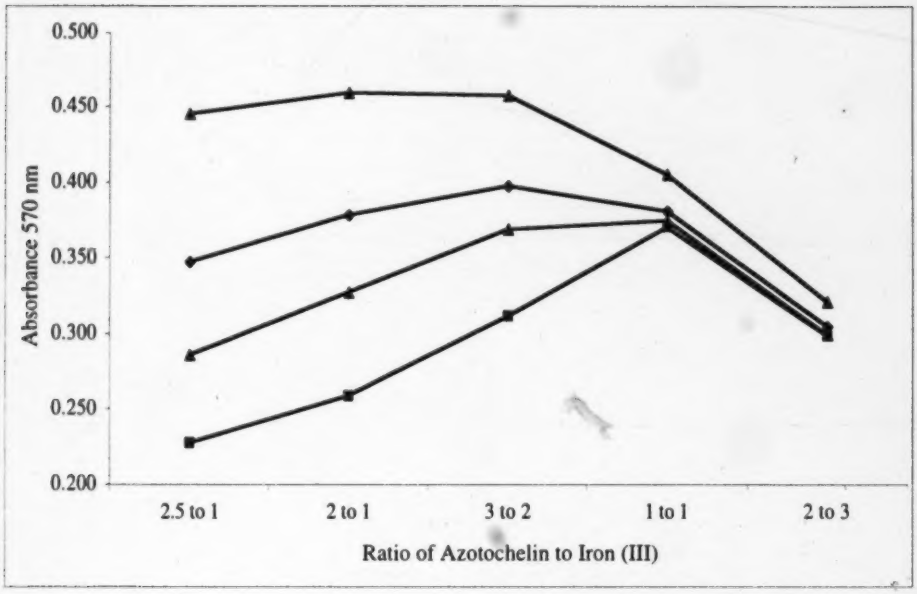

B

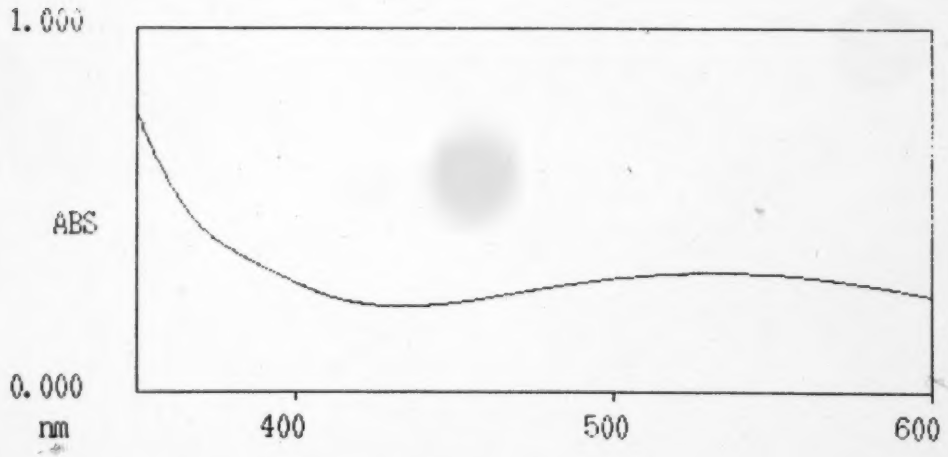

Figure 3.13 Spectrophotometric characteristics of ferric-azotochelin.

(A) Molar binding ratio of ferric-azotochelin complex. (■) 18 hr. (▲) 40 hr. (◆) 68.5 hr. (▲) 219 hr.
(B) Absorbance spectrum of ferric-azotochelin complex.

A

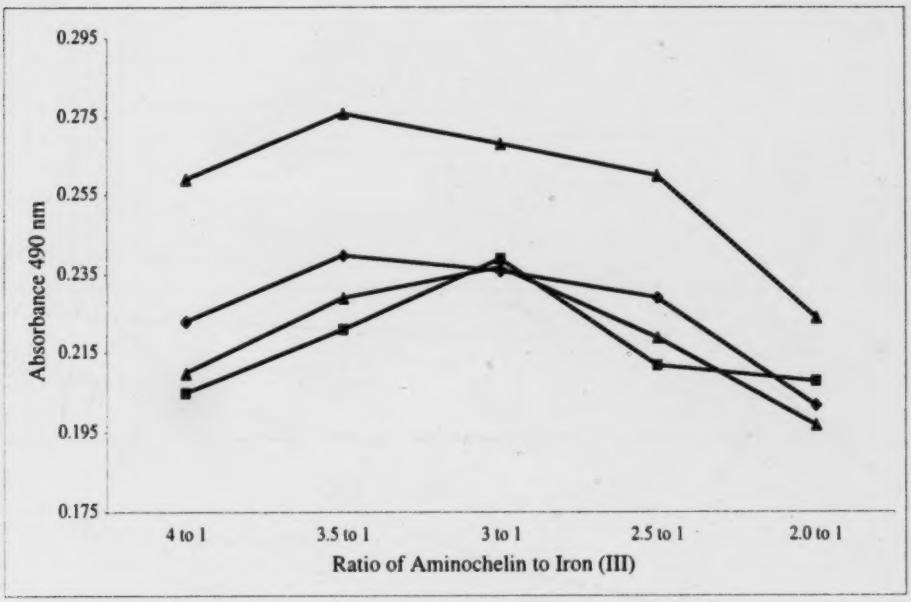

B

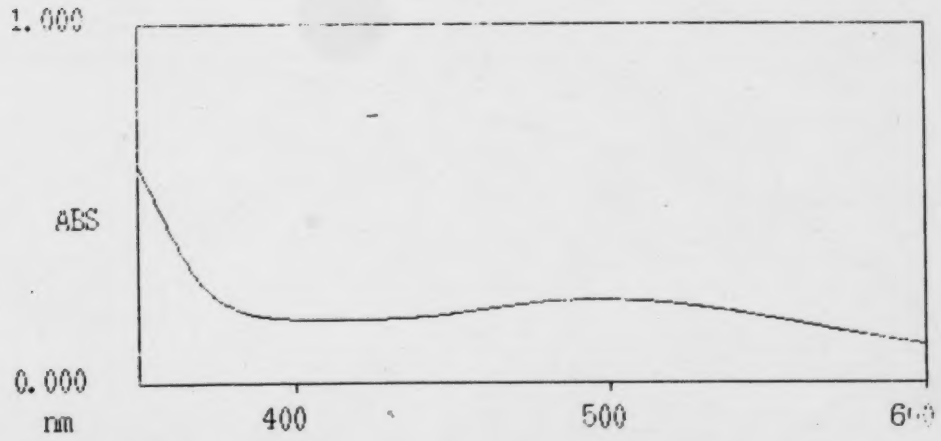

Figure 3.14 Spectrophotometric characteristics of ferric-aminochelin.

(A) Molar binding ratio of ferric-aminochelin complex. (■) 18 hr. (▲) 40 hr. (◆) 68.5 hr. (▲) 219 hr.
(B) Absorbance spectrum of ferric-aminochelin complex.

the Fe^{3+}- and Fe^{2+}-siderophore complexes exhibited broad spectral peaks, with the A_{max} at equilibrium obtained at 490 nm for protochelin (Fig. 3.12, Fe^{3+} data only) and 570 nm for azotochelin (Fig. 3.13, Fe^{3+} data only). Only aminochelin demonstrated different A_{max} wavelengths with Fe^{3+} at 490 nm (Fig. 3.14) or Fe^{2+} at 540 nm (data not shown). A stable complex with iron was formed most rapidly by protochelin (18 hr), followed by aminochelin (40 hr) and by azotochelin (68 hr) which correlated with increasing iron-siderophore coordination complexity.

3.1.7 Affinity of catecholate siderophores for Fe^{3+} and Fe^{2+}

Using the determined molar binding ratios, the proton-dependent formation constant for each siderophore with Fe^{3+} and Fe^{2+} was determined by competition with EDTA. Data were collected from nine different reactions each done at least six times and ferric-siderophore formation constants were calculated. In a similar manner, data for the determination of the formation constants of Fe^{2+}-siderophore complexes were also gathered (Appendix 1-sample calculation). Equilibrium was approached from either direction as the Fe-siderophore complex was challenged with EDTA or the Fe-EDTA complex was challenged with siderophore. The values of K_{Form} generated were very close to each other and are summarized in Table 3.1. This indicated that equilibrium could be approached from either direction.

However, because of the different stoichometry of each of the iron-binding reactions it was impossible to directly compare the formation constants generated for each siderophore, since each value had different units. For example, the formation constant found for the ferric-protochelin complex had units of M^{-1}, whereas the formation constant of the ferric-aminochelin complex had units of M^{-3} (Appendix 1-sample calculation). Thus, it was only possible to directly compare the formation constants that each siderophore had for Fe^{3+} or Fe^{2+} (Table 3.1). From this comparison it was clear that each

Reaction tested[A]	Log_{10} K_{Form}	Ave Log_{10} K_{Form}[B]	Reaction tested[A]	Log_{10} K_{Form}	Ave Log_{10} K_{Form}[B]
Pc Fe^{3+} + EDTA	24.3±0.84	24.1±0.86	Pc Fe^{2+} + EDTA	13.4±0.08	13.4±0.17
Pc + Fe^{3+}EDTA	23.5±0.51		Pc + Fe^{2+}EDTA	13.9±0.0	
AzC Fe^{3+} + EDTA	53.6±0.42	53.5±0.85	AzC Fe^{2+} + EDTA	31.6±0.33	31.7±0.33
AzC + Fe^{3+}EDTA	53.4±0.90		AzC + Fe^{2+}EDTA	31.8±0.04	
AmCFe^{3+} + EDTA	30.1±0.90	30.6±1.1	AmCFe^{2+} + EDTA	19.2±.027	19.3±0.46
AmC + Fe^{3+}EDTA	31.3±1.0		AmC + Fe^{2+}EDTA	19.5±.073	

A. Ligands: Pc = protochelin, AzC = azotochelin, and AmC = aminochelin were used at appropriate molar binding ratios.

B. Weighted average of multiple determinations ± standard deviation.

Table 3.1 Catecholate siderophore formation constants with Fe^{3+} and Fe^{2+}.

siderophore had a higher affinity for Fe^{3+} than for Fe^{2+}, which is one of the defining characteristics of a siderophore (Hider, 1984).

To directly compare the ability of different siderophores to bind Fe^{3+}, the amount of free Fe^{3+} in a theoretical Fe^{3+}-siderophore system at pH 7.4 was calculated, as described by Harris *et al.* (1979). Comparison of the free Fe^{3+} concentration was thus representative of the affinity that each siderophore had for Fe^{3+}. This required the calculation of the proton-independent solubility coefficients for each siderophore using the proton-dependent solubility constants (pH 7.0) for each siderophore and Ka values from the model compound *N,N*-dimethyl-2,3-dihydroybenzamide (Loomis & Raymond, 1991) as shown in Section 1.4.4 Equations 5 and 6 (Reid *et al.*, 1993). From this value a proton-dependent solubility constant at pH 7.4 for each siderophore was calculated. This value was used to determine the free Fe^{3+} concentration in the hypothetical system (Appendix 1-sample calculation). This value was expressed as pFe^{3+} ($-\log_{10}[Fe^{3+}]$). Thus the larger the pFe^{3+} value, the lower the concentration of free Fe^{3+} in solution, and the higher affinity a siderophore has for iron. Protochelin was found to have a pFe^{3+} value of 27.5, which was approximately the same as ferrioxamine E (27.7) and about 8 orders of magnitude smaller than enterobactin (35.6). The pFe^{3+} value for azotochelin was calculated to be 23.3, which was the same as the value of aerobactin (23.3) and 1 order of magnitude larger than aminochelin (22.0) (Table 3.2). Therefore, of the catecholate siderophores produced by *A. vinelandii*, protochelin had the highest affinity for iron followed by azotochelin and aminochelin.

3.1.8 Iron repressibility of protochelin production

Growth of *A. vinelandii* under standard conditions in Burk's medium with increasing iron concentrations from 1 to 50 μM of ferric citrate was performed to investigate how the formation of protochelin was affected by iron concentrations. As the ferric citrate content

Ligand	pFe^{3+A}
Enterobactin[B]	35.6
MECAM[B]	29.1
Ferrioxamine E[B]	27.7
Protochelin	**27.5**
Ferroxamine B[B]	26.6
N-acetylferrioxamine[B]	26.5
Ferrichrysin[B]	25.8
Ferrichrome[B]	25.2
Diethylenetriaminepentaacetic acid[B]	24.7
Transferrin[B]	23.6
Azotochelin	**23.3**
Aerobactin[B]	23.3
Aminochelin	**22.0**
Rhodotorulic acid[B]	21.9
2,3-Dihydroxy-N,N-dimethylbenzamide[B]	≈15[C]

A. Iron concentration expressed as $pM=-\log[Fe^{3+}]$ for pH 7.4 solutions containing 10^{-6} M total iron and 10^{-5} M total ligand.

B. Taken from Harris *et al.* (1979).

C. Exceeds solubility product of ferric hydroxide indicating precipitation under prescribed conditions (Harris *et al.*, 1979).

Table 3.2. Free iron concentrations in ferric-siderophore systems.

of the Fe-limited medium (containing 1 mM molybdate) increased, the intensity of the protochelin spot seen on a TLC plate decreased (Fig. 3.15). Although a spot is seen at an iron (III) concentration of 50 μM with an R_F similar to that of protochelin, catecholate quantification indicated that the catecholate concentration in the 50 μM ferric citrate culture supernatant was 0.003 mM, thus this spot was not considered to represent protochelin and was artifactual. In addition to the decrease in intensity of protochelin, catechol (mg cell protein)$^{-1}$ values were also seen to decrease with increasing ferric citrate (Fig. 3.16 -■-). Parallel results were seen in medium containing 1 μM molybdate (Fig. 3.16 -♦-). TLC showed that protochelin in the 1 mM molybdate-containing medium and azotochelin and aminochelin in the 1 μM molybdate-containing medium were all repressed at about 9 μM ferric citrate. In addition to affecting the form of catecholate released from the cell, 1 mM molybdate also promoted at least a two-fold greater catecholate production than 1 μM molybdate, at all iron concentrations of 4 to 8 μM (Fig. 3.16). These results indicated that although molybdate appeared to affect the yield of protochelin, protochelin formation in *A. vinelandii* was iron repressible, a defining characteristics of all siderophores.

3.1.9 Protochelin reaction in the CAS assay

To test the ability of protochelin to act as a competitive iron chelator, it was mixed with the synthetic, chromogenic iron chelator chrome azurol S in the CAS universal assay for siderophores (Schwyn & Neilands, 1987). Iron-limited culture supernatant from strains F196 (only azotobactin present) and UA1 (azotochelin, aminochelin and 2,3-DHBA present) decolorized the CAS assay solution within 2 min, but purified protochelin decolorized the solution in less than 5 sec (Table 3.3). Dilution of the protochelin solution prior to CAS assay did not slow the progress of decolorization, but only limited the amount of CAS decolorized. This indicated that protochelin, like the other siderophore solutions tested, had the ability to remove iron from the CAS complex. This

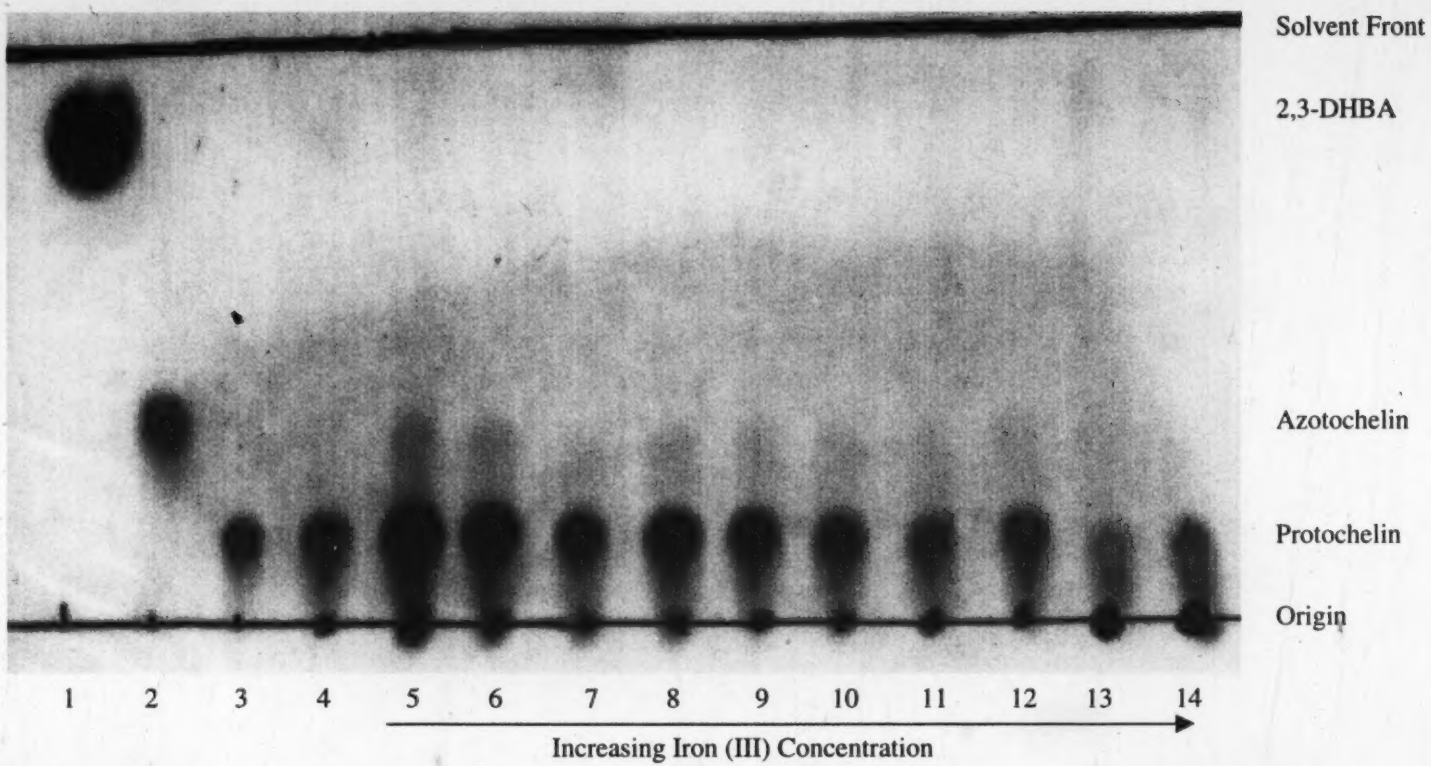

Figure 3.15 TLC of catechol siderophores under increasing iron (III) concentrations in Burk's medium containing 1 mM molybdate.

(1) 2,3-DHBA standard. (2) Azotochelin standard. (3) Protochelin standard. Ethyl acetate extract of strain UA1 culture supernatant containing: (4) 1 µM, (5) 2 µM, (6) 3 µM, (7) 4 µM, (8) 5 µM, (9) 6 µM (10) 7 µM, (11) 8 µM, (12) 9 µM, (13) 10 µM,

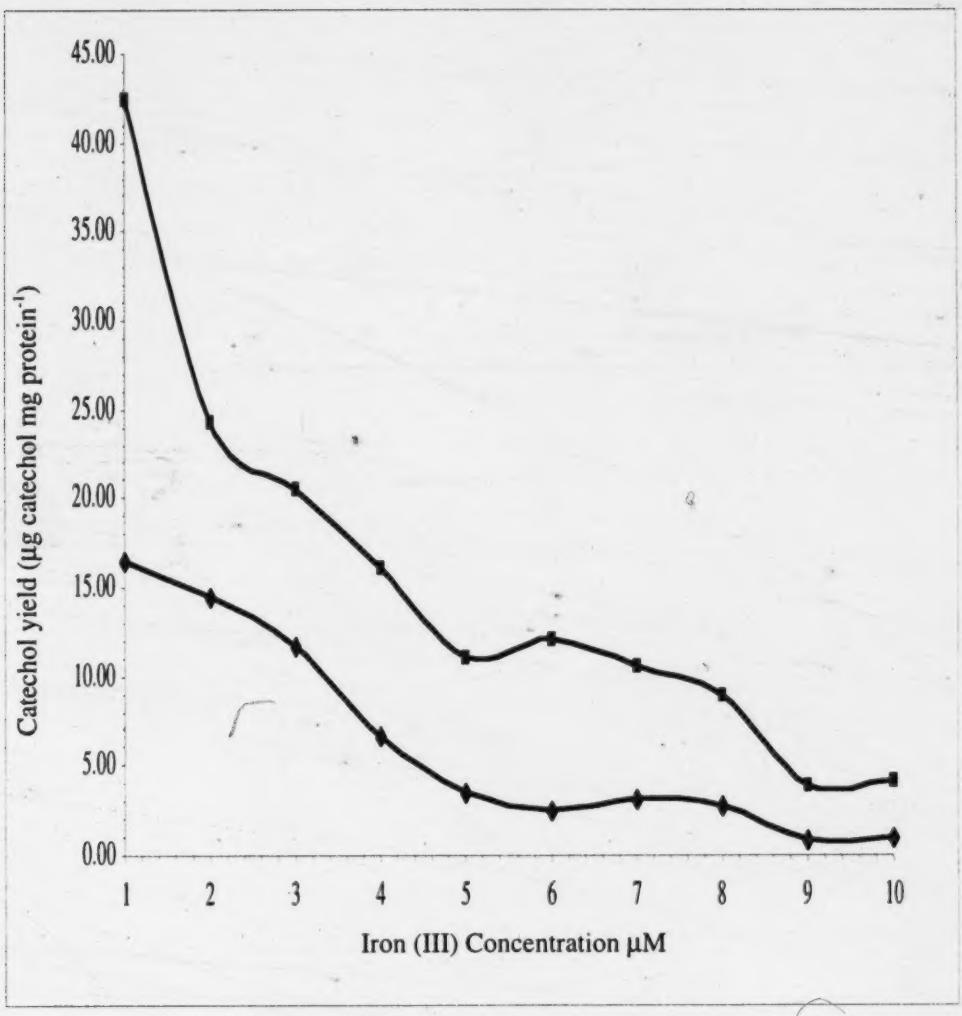

Figure 3.16 Effect of increasing iron (III) on catecholates produced by *A. vinelandii* strain UA1.

Burk's medium containing various iron (III) conditions and (■) 1 mM molybdate or (◆) 1 µM molybdate.

Siderophore preparation[A]	Siderophore Units[B]	Total siderophore activity[C]	CAS reaction end point (sec)
Catecholates	82	470	60-120
Azotobactin	37	220	60-120
Protochelin	64	120	<5

A. As iron-limited culture supernatant from strain UA1 grown in the presence of 1 μM molybdate (catecholates, $A_{310} = 0.310$), strain F196 (azotobactin, $A_{380} = 0.246$) grown in shake flasks, or as protochelin ($A_{310} = 0.350$) purified from strain UA1 grown with 1 mM molybdate.

B. One Unit is a change in A_{630} of 0.001 sec^{-1}.

C. Total siderophore activity, as Units (mg cell protein)$^{-1}$ present in 1.0 ml of culture.

Table 3.3 Activity of siderophore preparations in the CAS assay.

suggested that protochelin has the ability to remove iron from a stable complex, much as a siderophore must do to supply iron to the cell.

If protochelin was mixed with 1 mM molybdate immediately prior to its addition to the CAS solution, decolorization did not occur. Thus, the binding of molybdate to the hydroxyl-groups of protochelin (Hider, 1984) appears to have effectively prevented its iron-binding activity under the conditions of the CAS assay. This observation may also explain the increased yield of catechol (mg cell protein)$^{-1}$ observed in the presence of 1 mM molybdate in Fig. 3.16. The presence of 1 mM molybdate in the medium must hinder the binding of iron to protochelin, such that the cell presumably fails to correctly detect the concentration of exogenous iron in the medium, which results in continued production of the chelator. At higher iron concentrations (≥9 μM, Fig. 3.16) the affinity of the ligand for iron (III) may promote ligand saturation in the presence of molybdate and ensuing iron-transport results in the repression of ligand production. Alternatively, iron may enter the cell through the constitutive low-affinity uptake route, leading to repression of ligand formation.

3.1.10 Protochelin promotes iron-restricted growth of *A. vinelandii*

The function of protochelin as an iron-carrier was tested in a bioassay using the siderophore-deficient strain P100. When this strain is placed in medium in which the available iron is complexed in a non-useable form, in this case as Fe^{3+}-EDDHA, growth will be dependent on added siderophores (Sevinc & Page, 1992). The promotion of strain P100 growth in the plate bioassay was only observed around disks containing protochelin or strain F196 culture fluid containing azotobactin (halo diameters 10 and 12 mm, respectively). Growth promotion was not observed around the disk containing UA1 grown in 1 μM molybdate culture supernatant or the control disk impregnated with phosphate buffer. This result was unexpected since these siderophores formed by strain

UA1 growing on an EDDHA plate appeared previously to promote the growth of strain P100 (Sevinc & Page, 1992). The results may be reconciled if the growth promotion previously observed was caused by small amounts of protochelin formed during the 8 day incubation of strain UA1 on EDDHA plates, while growth promotion was not observed in the current study using the culture fluid from strain UA1 pre-grown 24 hr in iron-limited medium, where no detectable protochelin was formed.

When strain P100 was incubated in iron-restricted liquid medium containing 50 μg EDDHA ml^{-1} and 1 μM molybdate, growth was approximately doubled from 0.20 mg ml^{-1} protein to 0.42 mg ml^{-1} protein by the addition of protochelin to a final A_{310} of 0.40. After the 24 hr incubation, these culture fluids were acidified and extracted with ethyl acetate. In all cases only protochelin was detectable by TLC analysis (TLC not shown).

3.1.11 Uptake of ^{55}Fe-siderophore complexes

Uptake of the ^{55}Fe-protochelin complex by wild-type strain UW was tested using experimental techniques described in Section 2.2.7. The wild-type strain UW was used in uptake assays to establish that protochelin use was a normal process in *A. vinelandii*. $^{55}Fe^{3+}$-protochelin was taken up by iron-limited cells in this single assay at a rate of 1.3 ng $^{55}Fe^{3+}$ ml^{-1} $(min)^{-1}$, compared to 0.73 ng $^{55}Fe^{3+}$ ml^{-1} $(min)^{-1}$ for the Fe^{3+}-azotobactin complex (from strain F196), 0.50 ng $^{55}Fe^{3+}$ ml^{-1} $(min)^{-1}$ for a mixture of ferricatecholates (azotochelin, aminochelin and 2,3-DHBA from strain UA1) and 0.091 ng $^{55}Fe^{3+}$ ml^{-1} $(min)^{-1}$ seen with $^{55}Fe^{3+}$-citrate in uptake buffer alone (Fig. 3.17). In all cases the uptake of $^{55}Fe^{3+}$ have been corrected for non-specific binding of $^{55}Fe^{3+}$ to the cell by subtraction of control values obtained for each mixture incubated on ice.

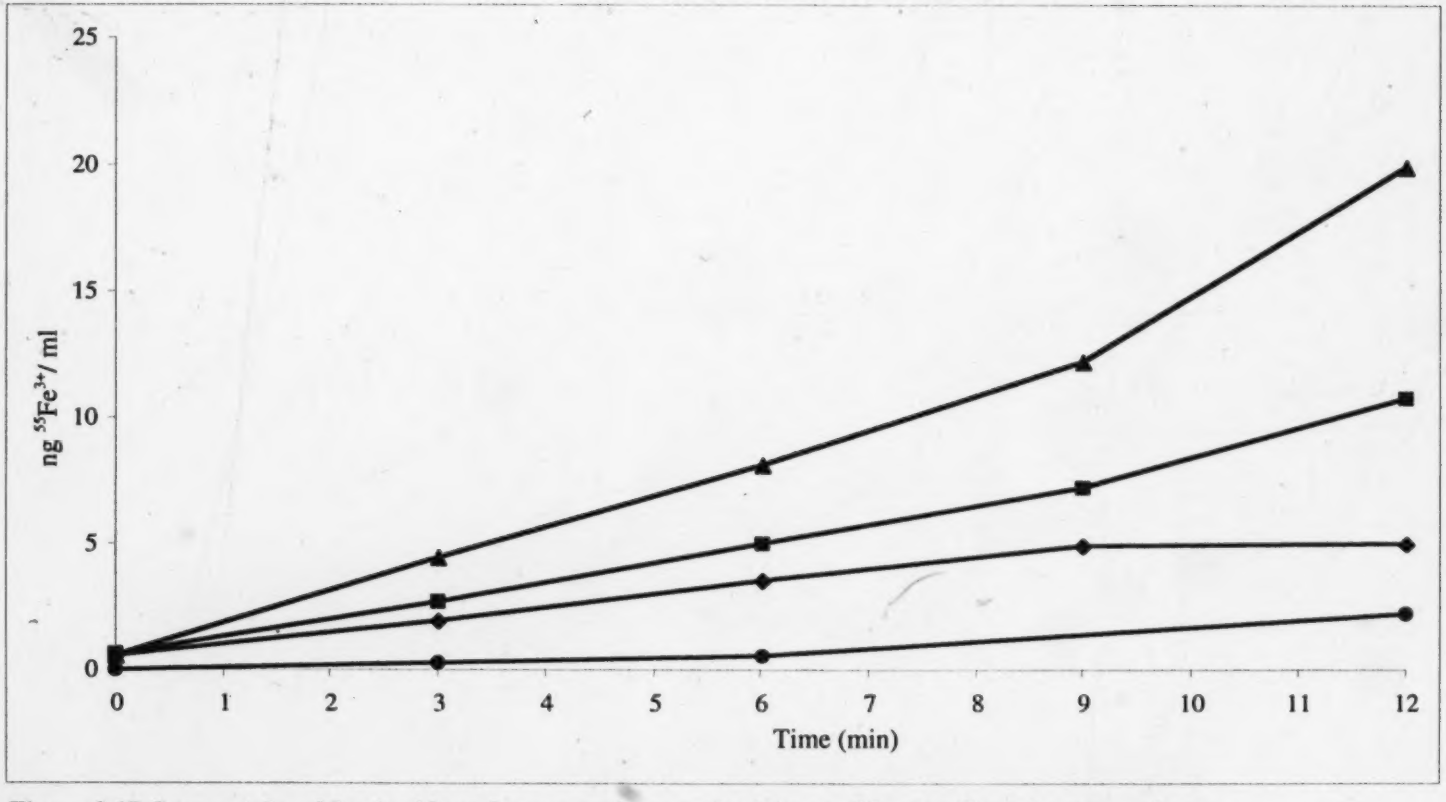

Figure 3.17 Iron uptake of ferric-siderophore complexes and mixtures of ferric-siderophore complexes.

$^{55}Fe^{3+}$ uptake into strain UW using; (◆) Ferric-azotochelin and ferric-aminochelin, (■) Ferric-azotobactin, (▲) Ferric-protochelin, or a (●) Buffer Control from a single assay.

The uptake of ferric-siderophore complexes was also examined using siderophores purified by the scheme in 2.2.2. Ferric-siderophore complexes were made as described in Section 2.3.3 in the correct molar binding ratio determined for each (Section 3.1.6). Strain UW was grown under standard conditions in the presence of 3 μM ferric citrate to repress the synthesis of azotobactin and the outer membrane proteins associated with its uptake. Results of this work indicated that protochelin was taken up by the cell even when the cell was grown in 1 μM molybdate at a corrected rate of 6.0 ng $^{55}Fe^{3+}$ ml^{-1} 10^8 $cell^{-1}$ $(min)^{-1}$. In addition, the $^{55}Fe^{3+}$-azotochelin complex was also rapidly taken up by the cell at a corrected rate of 7.0 ng $^{55}Fe^{3+}$ ml^{-1} 10^8 $cell^{-1}$ $(min)^{-1}$ (Fig. 3.18). Surprisingly, $^{55}Fe^{3+}$-aminochelin complexes were not actively taken up by the cell and any uptake seen was equivalent to the non-specific binding seen in control reactions incubated on ice (data not shown).

In the initial iron uptake studies performed the rates of $^{55}Fe^{3+}$-protochelin and $^{55}Fe^{3+}$-azotochelin uptake appear to be quite different (Fig. 3.17). However, in the work done with purified siderophores, the two rates are much closer in value (Fig.3.18). This can be explained by the fact that $^{55}Fe^{3+}$-aminochelin is not taken up by the cell and in the study where a mixture of $^{55}Fe^{3+}$-aminochelin and $^{55}Fe^{3+}$-azotochelin, from strain UA1 were used, the lack of $^{55}Fe^{3+}$-aminochelin uptake would presumably lower the observed uptake rate of $^{55}Fe^{3+}$-azotochelin by dilution. Furthermore, these results indicate that the production of the receptor for $^{55}Fe^{3+}$-protochelin binding and $^{55}Fe^{3+}$-uptake into the cell does not require the presence of high molybdate concentration, as the UW cells used in these assays were grown in medium containing only 1 μM molybdate.

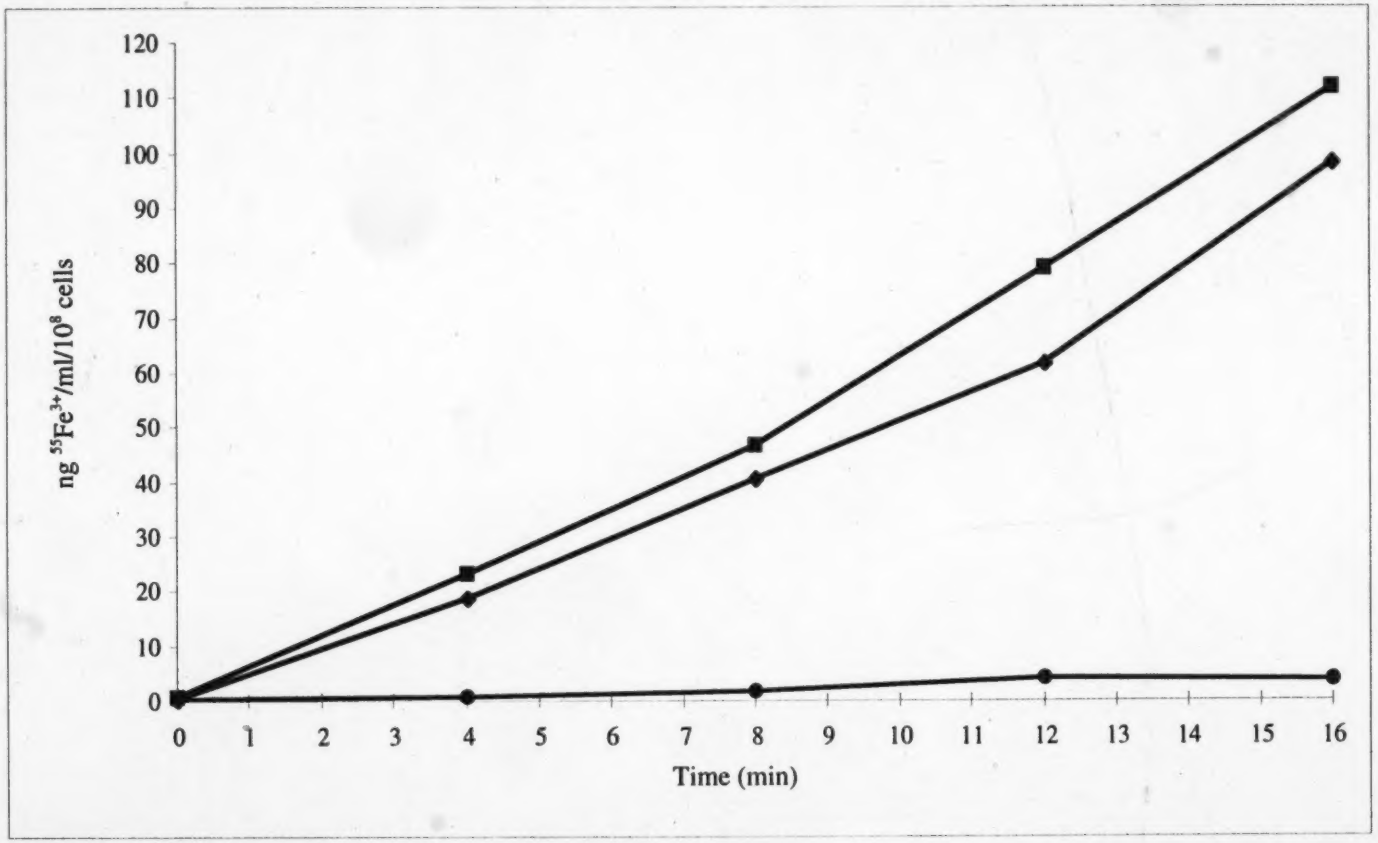

Figure 3.18 Iron uptake of individual ferric-siderophore complexes.

$^{55}Fe^{3+}$ uptake into strain UW using; (◆) Ferric-protochelin, (■) Ferric-azotochelin, or a (●) Buffer control. Assay done twice with similar results in both.

3.2 Role of molybdate and other metals in the accumulation of protochelin

3.2.1 Effect of molybdate on protochelin stability and production

To begin to understand the role that 1 mM molybdate played in the accumulation of protochelin, a study was undertaken to discover at what point in the growth of *A. vinelandii* or in the extraction of siderophores, that molybdate exerted its effect. Since the formation of protochelin by the unknown methylotrophic organism DSM 5746 (Taraz *et al.*, 1990) did not require the presence of high concentrations of molybdate, it was possible that the formation of protochelin by *A. vinelandii* UA1 was promoted by molybdate in the culture fluid or that molybdate acted to stabilize protochelin in the ethyl acetate extraction process. Finally, the possibility remained that unlike strain DSM 5746, *A. vinelandii* required the presence of molybdate during growth to form protochelin.

The stability of protochelin in water or growth media in the presence or absence of 1 mM molybdate was examined. It was found that purified protochelin dissolved in growth medium or water was extracted intact into ethyl acetate at pH 1 to 2 without molybdate present (Fig. 3.19-A lanes 4 and 5) . In addition, protochelin was stable in ethyl acetate, ethanol or distilled water without molybdate present and survived repeated freeze-thaw cycles (data not shown). Thus, molybdate was not required for protochelin stability or for its extraction into ethyl acetate. When 1 mM molybdate was added to iron-limited culture supernatant from strain UA1 grown in 1 μM molybdate (containing aminochelin and azotochelin) the supernatant turned bright yellow-orange. When this colored fluid was extracted with ethyl acetate and examined by TLC, only 2,3-DHBA and azotochelin were present (Fig. 3.19-B lanes 4 and 5). Therefore, protochelin did not form chemically because 1 mM molybdate was present during ethyl acetate extraction of iron-limited culture fluid. Rather, it appeared that molybdate was required during *A. vinelandii* growth for protochelin to be produced. Also seen in Fig. 3.19-B is a spot with an R_F intermediate to azotochelin and 2,3-DHBA. Although this spot had been observed on

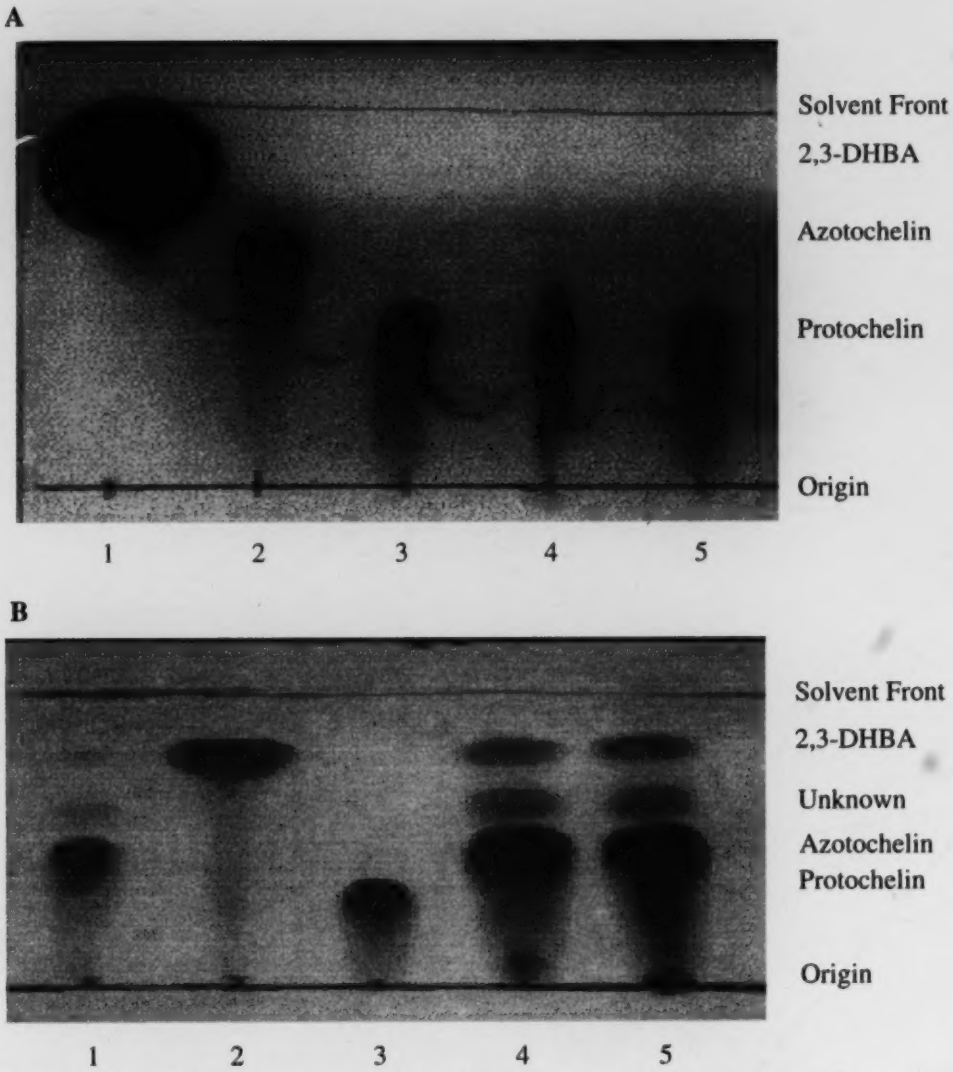

Figure 3.19 Stability of protochelin and formation in 1 mM molybdate.

(A) Stability of protochelin in water. (1) 2,3-DHBA standard. (2) Azotochelin standard. (3) Protochelin standard. (4) Ethyl acetate extract of protochelin before dissolution into water. (5) Ethyl acetate extract of protochelin after water treatment.

(B) Formation of protochelin from aminochelin and azotochelin.
(1) Azotochelin standard. (2) 2,3-DHBA standard. (3) Protochelin standard. (4) Ethyl acetate extract of azotochelin and aminochelin mixture before 1 mM molybdate addition. (5) Ethyl acetate extract of azotochelin and aminochelin mixture after 1 mM molybdate addition.

TLC plates its identity is unknown and as it did not affect either the protochelin or azotochelin spot on the TLC plate its identity was not pursued.

3.2.2 Molar binding ratio of molybdo-siderophore complexes

To determine how molybdate interacted with the catecholate siderophores, the molar binding ratios of each siderophore with molybdate was determined. This assay showed that azotochelin and aminochelin both interacted with molybdate as expected based on the fact that molybdate has four free coordinate sites at pH 7.0 (Duhme, 1996). Thus, azotochelin chelated molybdate in a 1:1 ratio for up to 191 hr (Fig. 3.20). The formation of the 2:1 aminochelin:molybdate complex took longer to form as it was not seen until 28 hr and was only stable until 98 hr, after which point it was replaced by other molybdo-aminochelin complexes (Fig. 3.21).

The interaction of protochelin and molybdate was less obvious. The predicted stoichometry of a molybdo-protochelin complex is 2:3 based on the fact that molybdate at pH 7.0 has four free coordination sites and protochelin can form six coordinate bonds with a metal. This type of complex was observed in continuous variation studies done at pH 6.0 in MES buffer (Fig. 3.22). However, data collected using "Job's method of continuous variation" (Section 1.4.4) at pH 7.0 in MOPS buffer indicated that a complex with a 1:1 ratio of protochelin to molybdate was being formed (Fig. 3.23). This would imply that at equilibrium protochelin would have two empty coordination sites, a condition that would not be expected considering the amount of free molybdate in the test solution. Although the number of coordination bonds formed by molybdate is pH sensitive (Section 1.3.1) the pH range of 6.0 to 7.0 should not affect the manner in which molybdate coordinates ligands (Pope *et al.*, 1980). As a result of this, both 1:1 and 2:3 complexes were considered in further calculations of protochelin and molybdate affinity.

A

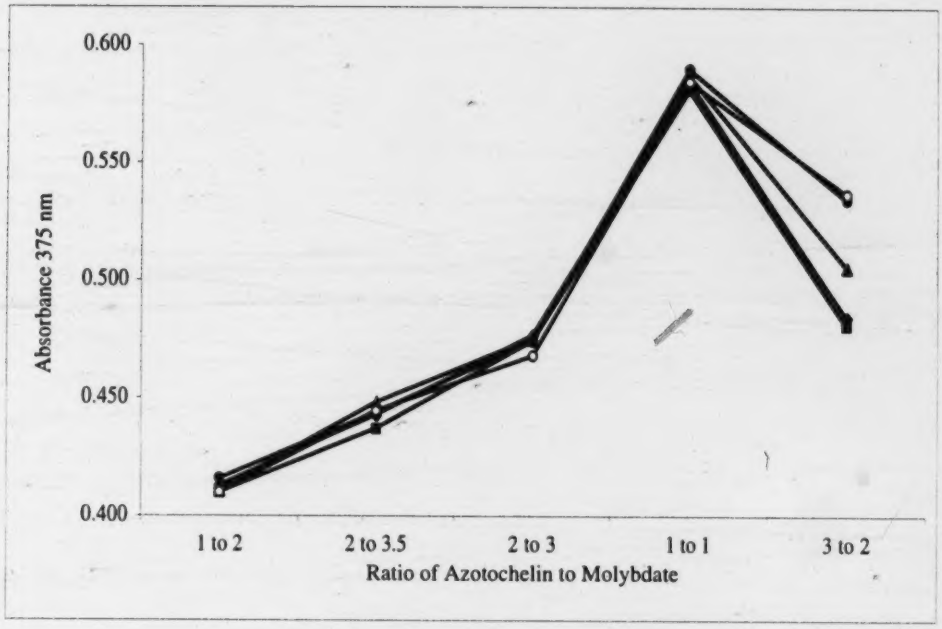

B

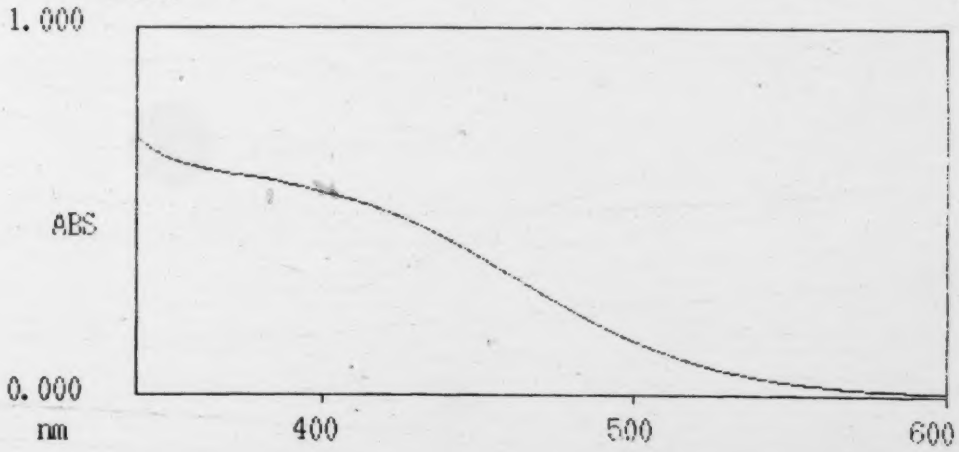

Figure 3.20 Spectrophotometric characteristics of molybdo-azotochelin complex.

(A) Molar binding ratio of molybdo-azotochelin complex. (■) 0 hr, (◆) 28 hr, (▲) 98 hr, (●) 167 hr, (○) 191 hr.
(B) Absorbance spectrum of molybdo-azotochelin complex.

A

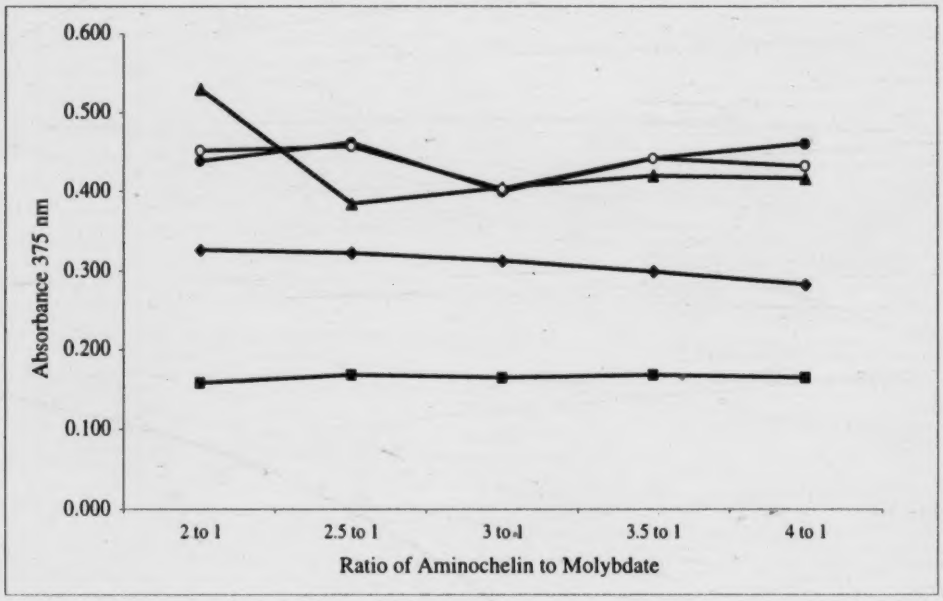

B

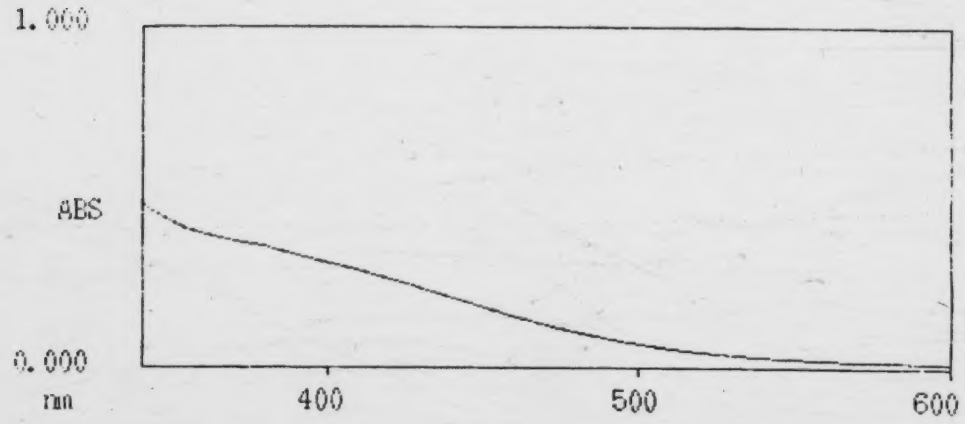

Figure 3.21 Spectrophotometric characteristics of molybdo-aminochelin complex.

(A) Molar binding ratio of molybdo-aminochelin complex. (■) 0 hr, (◆) 28 hr, (▲) 98 hr, (●) 167 hr, (○) 191 hr.
(B) Absorbance spectrum of molybdo-aminochelin complex.

A

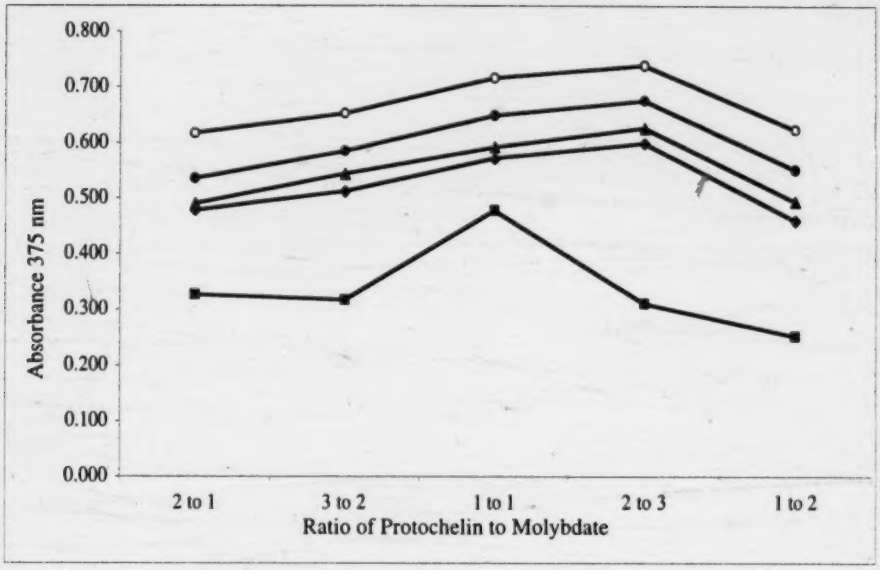

B

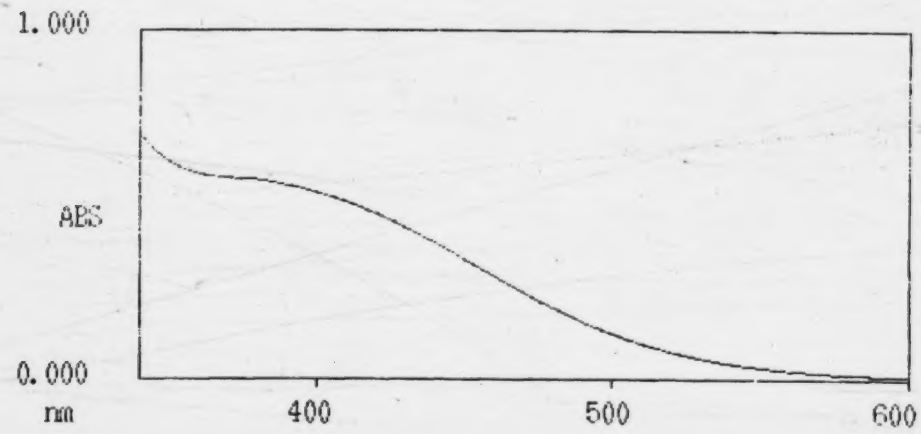

Figure 3.22 Spectrophotometric characteristics of molybdo-protochelin in MES Buffer pH 6.0.

(A) Molar binding ratio of molybdo-protochelin complex. (■) 0.2 hr, (◆) 22.5 hr, (▲) 44 hr, (●) 174 hr, (○) 372 hr.
(B) Absorbance spectrum of molybdo-protochelin complex.

A

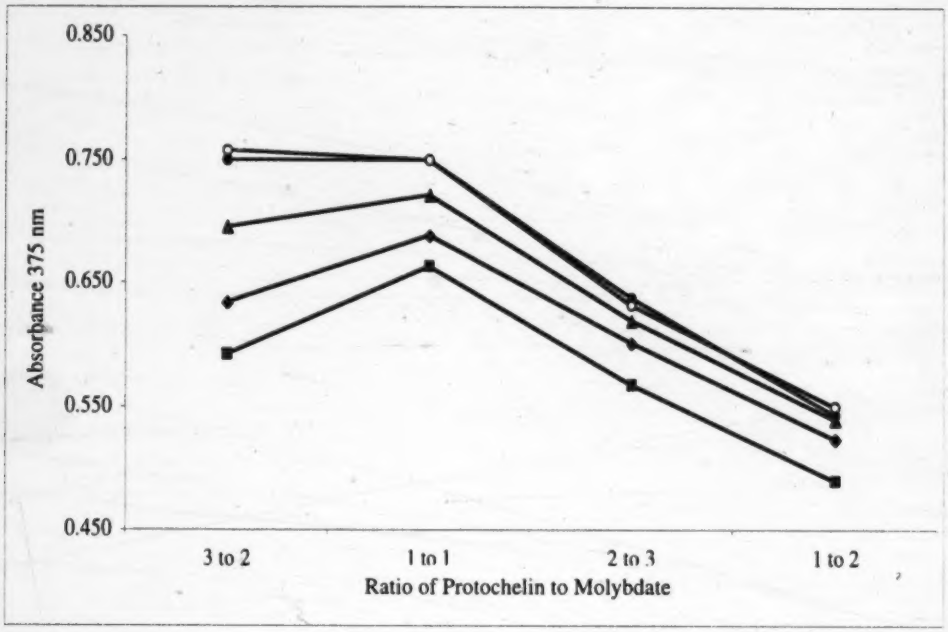

B

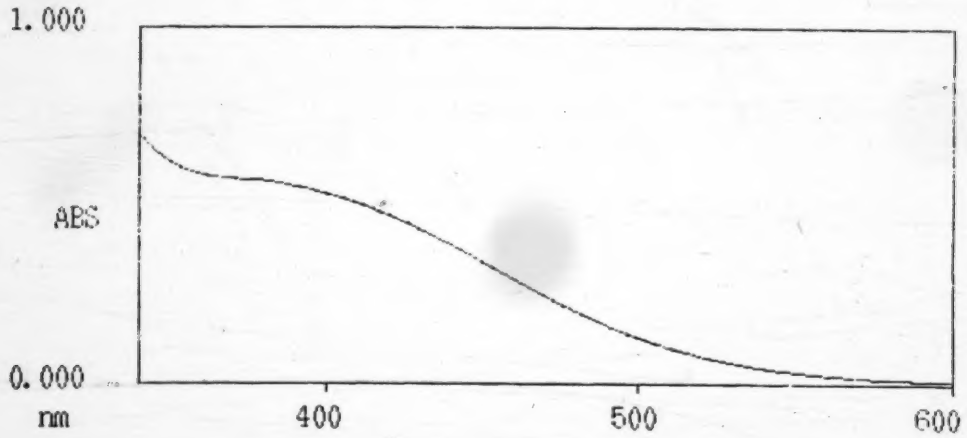

Figure 3.23 Spectrophotometric characteristics of molybdo-protochelin in MOPS buffer pH 7.0.

(A) Molar binding ratio of molybdo-protochelin complex. (■) 0 hr, (◆) 28 hr, (▲) 98 hr, (●) 167 hr, (○) 191 hr.
(B) Absorbance spectrum of molybdo-protochelin complex.

The 1:1 molybdo-protochelin complex was found to be stable for 167 hr, while the 2:3 complex was stable for 376 hr.

In all cases the molybdo-siderophore complex had a broad absorbance spectrum from approximately 500 to 300 nm (Fig. 3.20, 3.21, 3.22, 3.23), thus the absorbance of the molybdo-siderophore complexes was always read at 375 nm. These molybdo-siderophore complexes were found to behave in a similar manner in either MOPS buffer (pH 7.0) or potassium phosphate buffer (pH 7.0).

3.2.3 Affinity of siderophores for molybdate

Using a 2:3 protochelin:molybdate ratio, a 1:1 protochelin:molybdate ratio, a 1:1 azotochelin:molybdate ratio, and a 2:1 aminochelin:molybdate ratio the proton-dependent formation constants for each siderophore with molybdate was determined by competition with ferric-siderophore complexes. Data were collected from up to nine different reactions each done at least six times, and molybdo-siderophore formation constants were calculated (Appendix 1-sample calculation for ferric-siderophore value). Equilibrium was approached from either direction as the ferric-siderophore complex was challenged with molybdate and the molybdo-siderophore complex was challenged with iron (III). The K_{Form} values for each equilibrium tested for each siderophore were similar (Table 3.4) and this indicated that equilibrium can in fact be approached from either direction. The formation constant for molybdo-aminochelin was only approached by competition between the ferric-siderophore complex and molybdate due to a lack of pure aminochelin. As a result, the formation constant value given in Table 3.4 for molybdo-aminochelin cannot be considered as confidently as the values given for protochelin and azotochelin.

Reaction Tested[A]	Log_{10} K_{Form}[B]	Average Log_{10} K_{Form}[B]
PC : MoO_4^{2-} 1:1 Complex		
$PCMoO_4 + Fe^{3+}$	24.2±0.24	22.7±1.7
$PCFe^{3+} + MoO_4^{2-}$	21.1±0.49	
PC : MoO_4^{2-} 2:3 Complex		
$PC_2(MoO_4)_3 + Fe^{3+}$	48.0±0.62	49.1±1.3
$PCFe^{3+} + MoO_4^{2-}$	50.2±1.2	
$AzCMoO_4 + Fe^{3+}$	3.6±0.05	3.6±0.06
$AzC_3(Fe^{3+})_2 + MoO_4^{2-}$	3.5±0.02	
$AmC_2MoO_4 + Fe^{3+}$	3.9±0.01	3.9±0.01
$AmC_3Fe^{3+} + MoO_4^{2-}$	ND[C]	

A. Ligands : PC = protochelin, AzC = azotochelin, AmC = aminochelin

B. Average of multiple determinations ± standard deviation of value

C. ND = Not determined.

Table 3.4 Log_{10} K_{Form} of molybdo-siderophore complexes in 100 mM MOPS buffer (pH 7.0).

As a result of the ambiguity of the molar binding ratio data generated for molybdo-protochelin both the 1:1 and the 2:3 complexes were considered in the affinity calculations. The differences in how molybdate and protochelin interacted had a significant effect on the outcome of this analysis. The reason for this lies in the manner in which the differences in molar binding ratio effect the chemical equations which form the basis for the affinity calculation. For a 1:1 complex of protochelin and molybdate the three equations that make up the affinity calculation were as follows:

$$Pc + Fe \leftrightarrows PcFe \qquad K_{Form} = [PcFe] / [Pc]\,[Fe] \qquad (9)$$

$$PcFe + MoO_4^{2-} \leftrightarrows PcMoO_4 + Fe \qquad K_{Form} = [PcMoO_4]\,[Fe] / [PcFe]\,[MoO_4^{2-}] \qquad (10)$$

$$Pc + MoO_4^{2-} \leftrightarrows PcMoO_4 \qquad K_{Form} = [PcMoO_4] / [Pc]\,[MoO_4^{2-}] \qquad (11)$$

Based on this, Equation 10 is the experimental equation and is actually measured. The only value in Equation 10 that is measurable is [PcFe], as the rest of the components of the reaction are colorless or have absorbance maxima near 310 nm, which is also the wavelength of maximum absorbance of the uncomplexed ligand. As a result the concentrations of all components of Equation 10 are based on [PcFe] and the stoichometric relationship between it and the other components in the reaction. The K_{Form} of the reaction of interest, Equation 11, is the product of the K_{Form} values of Equations 9 and 10, or it is the sum of the Log_{10} of the K_{Form} values for Equations 9 and 10 (Section 1.4.4). If, however, the protochelin and molybdate complex exists in a 2:3 ratio then the above equations dramatically change as follows:

$$2Pc + 2Fe \leftrightarrows 2PcFe \qquad K_{Form} = [PcFe]^2 / [Pc]^2\,[Fe]^2 \qquad (12)$$

$$2PcFe + 3MoO_4^{2-} \leftrightarrows Pc_2(MoO_4)_3 + 2Fe \qquad K_{Form} = [PcMoO_4]\,[Fe]^2 / [PcFe]^2\,[MoO_4^{2-}]^3 \qquad (13)$$

$$2Pc + 3MoO_4^{2-} \leftrightarrows Pc_2(MoO_4)_3 \qquad K_{Form} = [Pc_2(MoO_4)_3] / [Pc]^2\,[MoO_4^{2-}]^3 \qquad (14)$$

Equation 13 is the equation which is experimentally tested and all values in the equation are stoichometrically based on [PcFe]. The K_{Form} of interest is that of Equation 14; however, its value has now changed considerably from Equation 11. The units on the formation constant are now M^{-4}, as opposed to M^{-1} in Equation 11 and its numerical value is also very different (Table 3.4). The overall result of this is that the manner in which protochelin and molybdate interact dramatically effects the affinity protochelin has for molybdate.

This is obvious when the affinity values are interpreted in terms of the amount of free molybdate present in a hypothetical system, as was done for iron (III) in Section 3.1.7. Using Equations 5 and 6 from Section 1.4.4 and making appropriate modifications, allowed the substitution of variables from the molybdo-siderophore equilibrium into these equations to calculate the amount of free molybdate present. Free molybdate concentration, expressed as $pMoO_4^{2-} = -\log_{10} [MoO_4^{2-}]$, is 26.0 if protochelin interacts with molybdate in a 1:1 ratio and is 16.0 if the interaction is 2:3 (Appendix 1-sample calculation for ferric-siderophore value). This would imply, that if the 1:1 ratio forms, then the affinity of protochelin for molybdate is similar to its affinity for iron (III) in terms of free metal remaining in the hypothetical system. If the interaction is 2:3 however, the affinity of protochelin for molybdate is approximately 10^{-11} times smaller for molybdate compared to iron (III). By comparison, the $pMoO_4^{2-}$ values for molybdo-azotochelin and molybdo-aminochelin are 6.1 and 5.6 respectively.

As a result of this great difference in affinity of protochelin for molybdate, based on the type of complex formed, it was important to determine which complex was being formed. These results should provide a better understanding of the interaction of protochelin and molybdate in terms of how molybdate acts to promote the accumulation of protochelin.

3.2.4 Molybdate-iron siderophore complex competition

In order to clarify the interaction of molybdate and protochelin, the influence of molybdate on the formation of the Fe^{3+}-protochelin complex was examined, as were the effects of molybdate on the formation of all the ferric-siderophore complexes. This was done by observing the formation of ferric-siderophore complexes in the presence of molybdate either at the correct molar binding ratio(s) or in excess with respect to iron concentration. The concentration of ferric-siderophore complex in a given reaction was calculated using molar extinction coefficients given in Section 2.3.1. This value was expressed as a percentage of the theoretical maximum concentration of ferric-siderophore complex present based on the amount of iron, molybdate and siderophore added to a reaction. The results for the formation of ferric-protochelin, ferric-azotochelin, and ferric-aminochelin in the presence of molybdate are shown in Figures 3.24, 3.25, and 3.26, respectively. As can be seen protochelin is not affected by the presence of molybdate (Fig. 3.24) while aminochelin and azotochelin were affected to a greater degree (Fig. 3.25 and 3.26). Each of these assays were done three times with similar results being generated in each. When molybdate was added in excess to already formed ferric-siderophore complexes, no decrease in ferric-siderophore complex was seen and no molybdo-siderophore complex was formed (data not shown).

In terms of the interaction of molybdate and protochelin, these data suggest that protochelin and molybdate exist in a 2:3 complex. If protochelin and molybdate formed a 1:1 complex, then the affinity of protochelin for molybdate would be approximately equal to the affinity protochelin had for iron. If this were the case, then molybdate should affect the formation of the ferric-siderophore complex by effectively competing with iron for protochelin binding. This was not the case however, as inhibition of the formation of the ferric-protochelin complex was not seen over a period of 230 hr (Fig. 3.24). Given this time frame, if molybdate was able to form a stable complex with protochelin, there

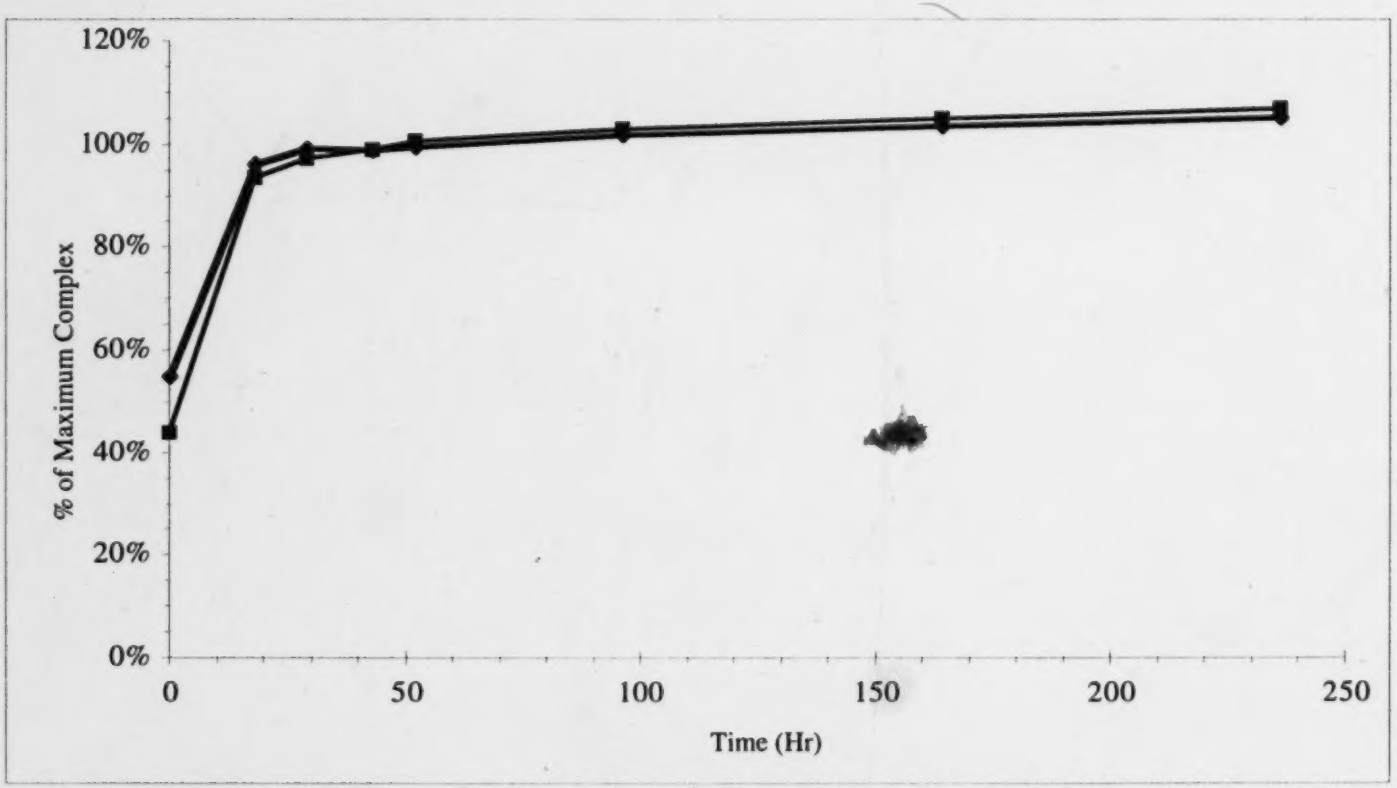

Figure 3.24 Effect of molybdate competition of the formation of a ferric-protochelin complex.

(◆) Formation of ferric-protochelin only. (■) Formation of ferric-protochelin in the presence of 0.2 mM molybdate. Assay done twice with similar results.

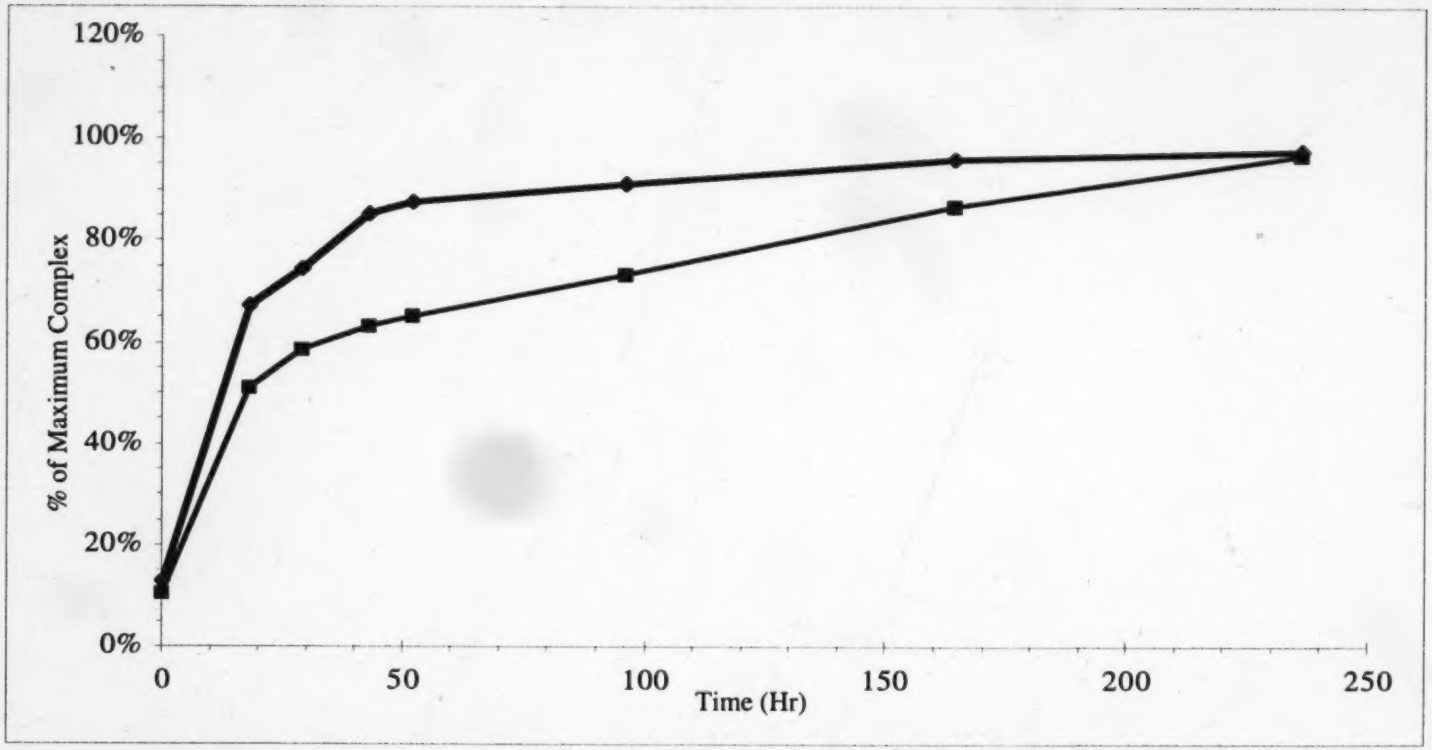

Figure 3.25 Effect of molybdate competition of the formation of a ferric-azotochelin complex.

(◆) Formation of ferric-azotochelin only. (■) Formation of ferric-azotochelin in the presence of 0.2 mM molybdate. Assay done twice with similar results.

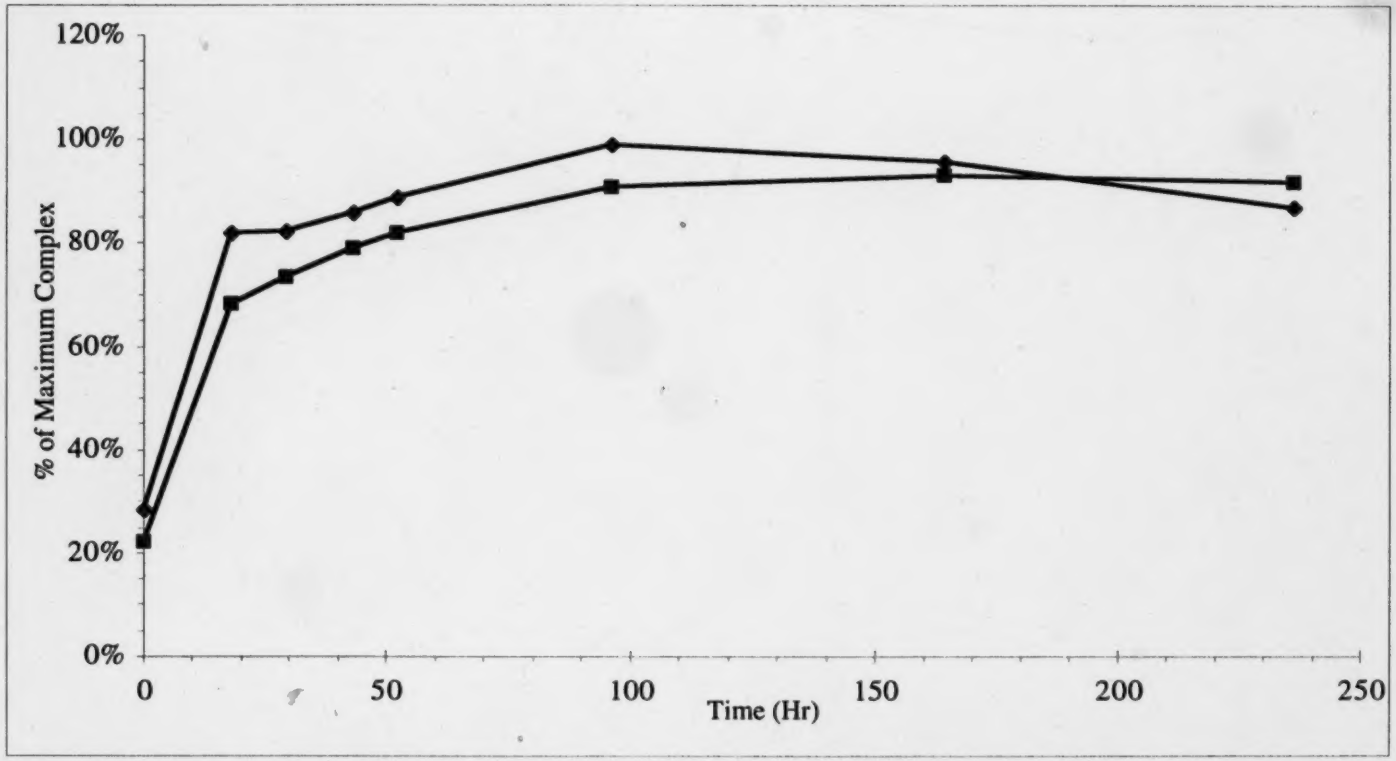

Figure 3.26 Effect of molybdate competition of the formation of a ferric-aminochelin complex.

(◆) Formation of ferric-aminochelin only. (■) Formation of ferric-aminochelin in the presence of 0.2 mM molybdate. Assay done twice with similar results.

should have been some evidence of this occurring. Although this is indirect evidence for the formation of a 2:3 molybdo-protochelin complex it is the best explanation of the current data, other more direct evidence could be collected by studying the formation of the molybdo-protochelin complex potentiometrically, but this was beyond the scope of this work.

3.2.5 Effect of metals on protochelin accumulation

Other metals were tested for their ability to increase protochelin accumulation, these metals included a number of transitions metals that form ionic compounds that are chemically similar to molybdate. Of the 13 metals tested only vanadate, tungstate, Mn^{2+}, and Zn^{2+} promoted protochelin accumulation (Fig. 3.27). The minimum concentrations of the above metals required for the promotion of protochelin accumulation was determined to be: 60 μM vanadate, 30 μM tungstate, 70 μM Mn^{2+}, and 500 μM Zn^{2+}. In terms of tungstate addition, small amounts of protochelin were seen at 10 μM (Fig. 3.27-B lane 4) but definite protochelin accumulation was not seen until 30 μM (Fig. 3.27-B lane 5). At these concentrations the metals which promoted protochelin accumulation were not detrimental to the growth of *A. vinelandii* in terms of total cellular protein (data not shown).

3.2.6 Effect of metals on ^{55}Fe-siderophore uptake

The effect of molybdate and the other metals that promoted protochelin accumulation on the uptake of the individual $^{55}Fe^{3+}$-siderophore complexes by *A. vinelandii* was studied as described in Section 2.3.3. The effect of molybdate was studied the most intensely, whereas the other metals were just tested for their ability to affect uptake. The effect of molybdate on $^{55}Fe^{3+}$-protochelin and $^{55}Fe^{3+}$-azotochelin was studied by preincubating cells used in the uptake assay for 5 min in 1 mM molybdate. Excess molybdate was removed by centrifugation and was absent from the assay. In addition, some cells were

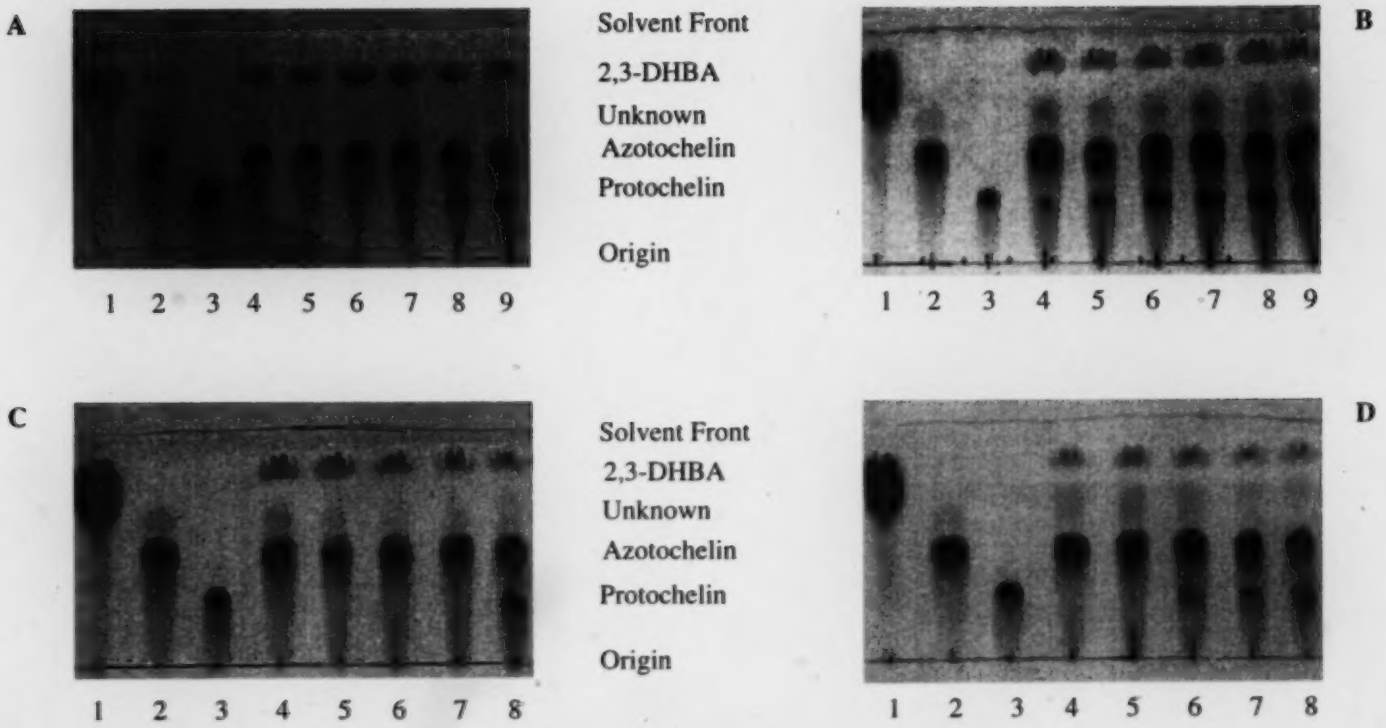

Figure 3.27 The effect of metals other than molybdate on protochelin accumulation.

In all figures: (1) 2,3-DHBA standard. (2) Azotochelin standard. (3) Protochelin standard. Ethyl acetate extracts of culture supernatant from strain UA1 grown in the presence of: (A) Vanadate addition at: (4) 10 μM, (5) 20 μM, (6) 30 μM, (7) 40 μM, (8) 50 μM, (9) 60 μM. (B) Tungstate addition at: (4) 10 μM, (5) 30 μM, (6) 50 μM, (7) 60 μM, (8) 70 μM, (9) 90 μM.
(C) Mn^{2+} addition at: (4) 10 μM, (5) 30 μM, (6) 50 μM, (7) 60 μM, (8) 70 μM.
(D) Zn^{2+} addition at: (4) 100 μM, (5) 300 μM, (6) 500 μM, (7) 600 μM, (8) 700 μM.

also incubated in 1 mM molybdate for 5 min prior to assay, but the excess molybdate was not removed. This allowed for the investigation of the possibility that molybdate affected the ability of the cell to bind a $^{55}Fe^{3+}$-siderophore complex. The possibility that molybdate displaced iron in a $^{55}Fe^{3+}$-siderophore complex was studied by allowing $^{55}Fe^{3+}$, molybdate and siderophore to incubate together for 72 hr prior to the uptake assay. Finally, molybdate was added to the uptake assay in a final concentration of 50 μM and 1000 μM at 6 min, to study the effect it had on $^{55}Fe^{3+}$-siderophore uptake once uptake was initiated. The effects of molybdate addition, under the conditions described, on $^{55}Fe^{3+}$-protochelin and $^{55}Fe^{3+}$-azotochelin uptake are summarized in Table 3.5.

The pretreating of cells with molybdate before the addition of a $^{55}Fe^{3+}$-siderophore complex appears to have the greatest effect on uptake (Table 3.5). Removing excess molybdate before ^{55}Fe-siderophore addition lessened the effect, but uptake of $^{55}Fe^{3+}$-protochelin and $^{55}Fe^{3+}$-azotochelin is still reduced by 78% and 58% of uninhibited rates respectively. This would suggest that the effect of molybdate can be reduced by washing the cells indicating that the effect of molybdate is transient. Molybdate did affect uptake when included in solution with $^{55}Fe^{3+}$ and siderophore during complex formation. This was likely due to the interaction of molybdate with the cell when the uptake assay began as molybdate does not affect the formation of $^{55}Fe^{3+}$-siderophore complexes (Fig. 3.24). Finally, it would appear that the higher the final concentration of molybdate in the uptake assay, the greater the effect on $^{55}Fe^{3+}$ uptake rates. A twenty-fold increase in molybdate concentration resulted in an approximately two-fold decrease in both $^{55}Fe^{3+}$-protochelin and $^{55}Fe^{3+}$-azotochelin uptake (Table 3.5).

A sample uptake curve for $^{55}Fe^{3+}$-protochelin demonstrated that the addition of molybdate, vanadate, or tungstate decreased the rate at which $^{55}Fe^{3+}$-protochelin was taken up by the cell (Fig. 3.28-A). A similar effect was also seen with the addition of

Assay Conditions [A]	% Decrease $^{55}Fe^{3+}$PC Uptake[B]	% Decrease $^{55}Fe^{3+}$AzC Uptake[B]
Control	0	0
Cells pre-incubated with 1000 µM MoO_4^{2-} (5 min)excess MoO_4^{2-} **not** removed.	78	58
Cells pre-incubated with 1000 µM MoO_4^{2-} (5 min)excess MoO_4^{2-} removed.	89	68
Fe^{3+} + MoO_4^{2-} + siderophore competition 72 hr prior to assay.	85	43
50 µM MoO_4^{2-} added to assay at 6-min time point.	38	47
1000 µM MoO_4^{2-} added to assay at 6-min time point.	80	78

A. Results from single assays.

B. Ligands are PC = protochelin, AzC = azotochelin.

Table 3.5 The effects of various molybdate treatments on the uptake of $^{55}Fe^{3+}$ by *A. vinelandii*.

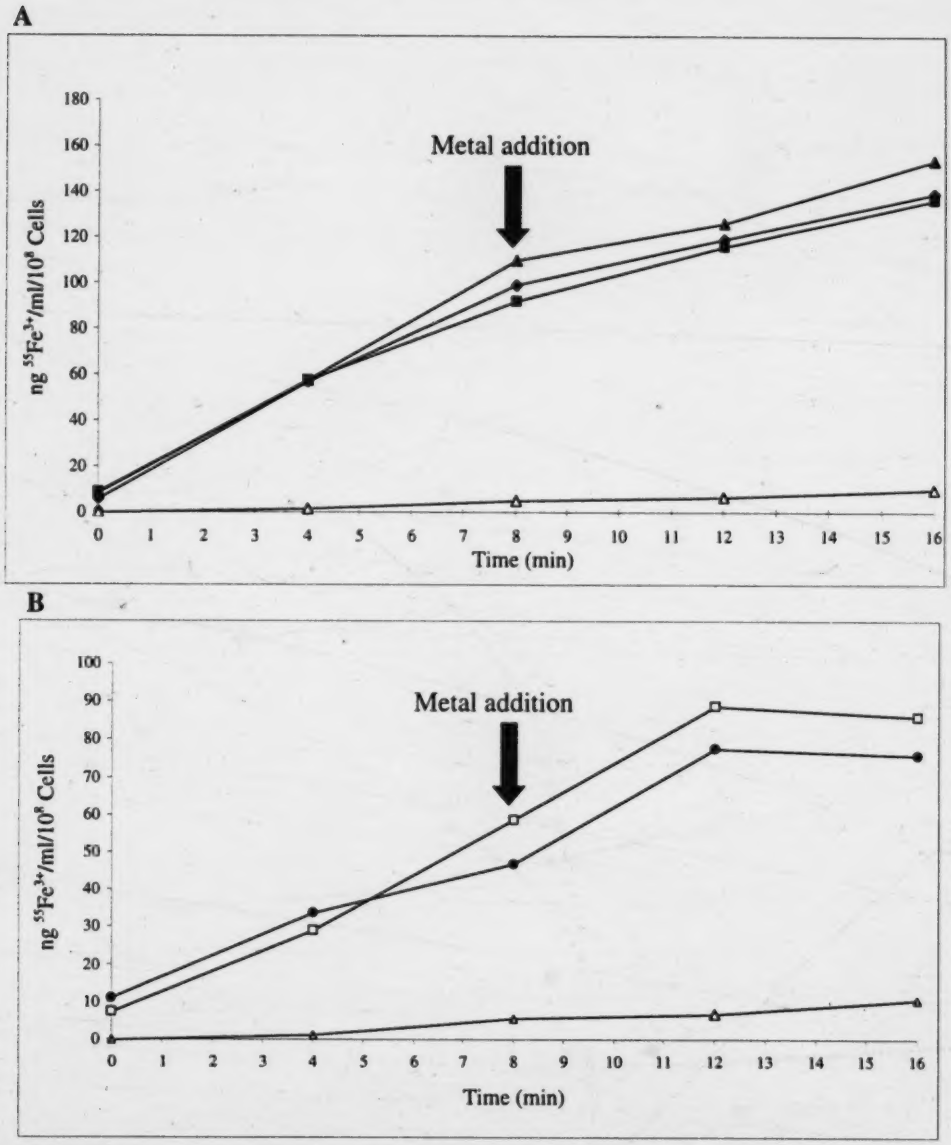

Figure 3.28 The effect of metals on the uptake of the $^{55}Fe^{3+}$-protochelin complex.

$^{55}Fe^{3+}$ uptake into strain UW in the presence of:
(A) (■) 70 µM molybdate, (▲) 30 µM tungstate, (◆) 100 µM vanadate.
(B) (●) 500 µM Zn^{2+}, (□) 70 µM Mn^{2+}.
In both cases metals added after 8 min of uptake of ^{55}Fe-siderophore alone, or a (△) siderophore-free control. Assay done twice with similar results. Uptake in the absence of metal Fig. 3.18 p. 118.

Zn^{2+} or Mn^{2+}, although a dramatic decrease in uptake was not seen until after 12 min (Fig. 3.28-B). Similar data for $^{55}Fe^{3+}$-azotochelin are presented in Figure 3.29. The uptake of the ferric-siderophore complexes, using the same pure siderophore stock solutions, normally shows an slight increase in rate from 8 to 16 min (Fig. 3.16). The effect of the metals on $^{55}Fe^{3+}$-protochelin and $^{55}Fe^{3+}$-azotochelin uptake is summarized in Table 3.6 where is can be seen that, although all of the metals decreased ferric-siderophore uptake, the effect of Zn^{2+} was somewhat variable. The effect of 70 μM molybdate on the uptake of $^{55}Fe^{3+}$-protochelin and $^{55}Fe^{3+}$-azotochelin was also examined by pre-incubating the cells in 70 μM molybdate for 10 min and then examining the uptake of the $^{55}Fe^{3+}$-siderophore complexes. The uptake rates determined were compared to uptake rates in the absence of molybdate and the effect molybdate had on the uptake of $^{55}Fe^{3+}$-siderophores was expressed as a percent as before. Under these conditions 70 μM molybdate decreased the uptake of $^{55}Fe^{3+}$-protochelin by 33% and the uptake of $^{55}Fe^{3+}$-azotochelin by 35% (Appendix 2). This is consistent with the effect molybdate reported in Table 3.5 on the uptake of $^{55}Fe^{3+}$-protochelin and $^{55}Fe^{3+}$-azotochelin.

3.2.7. Effect of molybdate on IROMP profiles of *A. vinelandii*

The effect of molybdate on the expression of iron-repressible outer membrane proteins (IROMPs) by *A. vinelandii* UW and UA1 was examined after fractionation of the cell envelope with sarcosyl (Section 2.1.4). IROMPs are high molecular weight outer membrane proteins in the 73-kDa to 93-kDa range that are iron-repressible (Page & von Tigerstrom, 1982). Although there were some differences in protein profiles between strains, there was no difference in the IROMPs produced at 1 μM and 1 mM molybdate (Fig. 3.30).

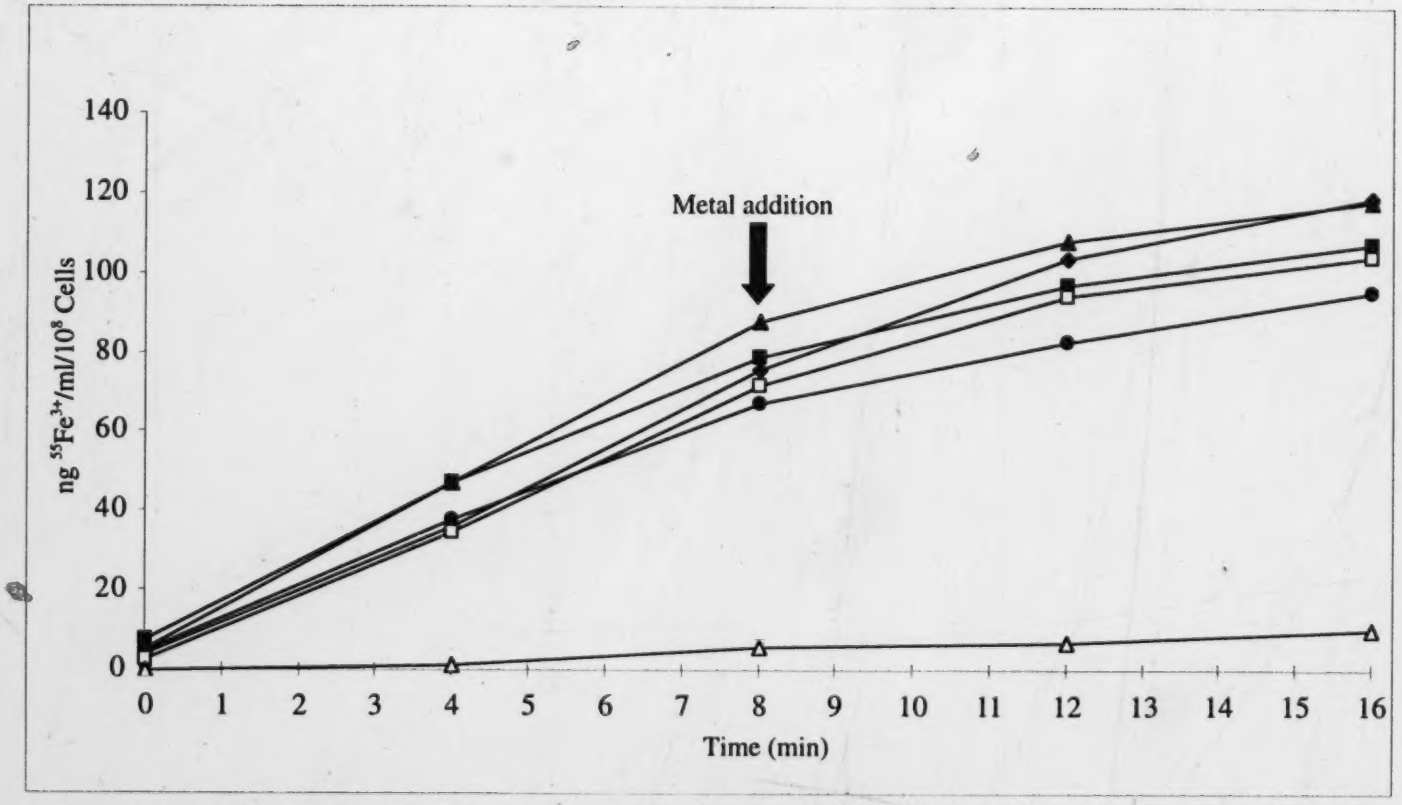

Figure 3.29 The effect of metals on the uptake of the $^{55}Fe^{3+}$-azotochelin complex.

$^{55}Fe^{3+}$ uptake into strain UW in the presence of: (■) 70 µM molybdate, (▲) 30 µM tungstate, (◆) 100 µM vanadate, (●) 500 µM Zn^{2+}, (□) 70 µM Mn^{2+} added after 8 min of uptake of ^{55}Fe-siderophore alone, or a (△) Siderophore-free control. Assay done twice with similar results. Uptake in the absence of metal Fig. 3.18 p. 118.

Metal	Concentration of Metal (μM)	^{55}Fe-Pc Uptake [A] (Average % Decrease)[B]	^{55}Fe -AzC Uptake [A] (Average % Decrease)[B]
No metal[C]	N/A	No decrease	No decrease
Molybdate	70	40±7	75±8
Vanadate	100	55±2	27±15
Tungstate	30	51±6	74±6
Mn^{2+}	70	29±17	71±15
Zn^{2+}	500	56±37	90±31

A. Ligands PC = protochelin, AzC = azotochelin.

B. ±Range of values.

C. From Fig. 3.18, p. 118

Table 3.6 The effect of metals that promote protochelin accumulation on the uptake of ferric-protochelin and ferric-azotochelin.

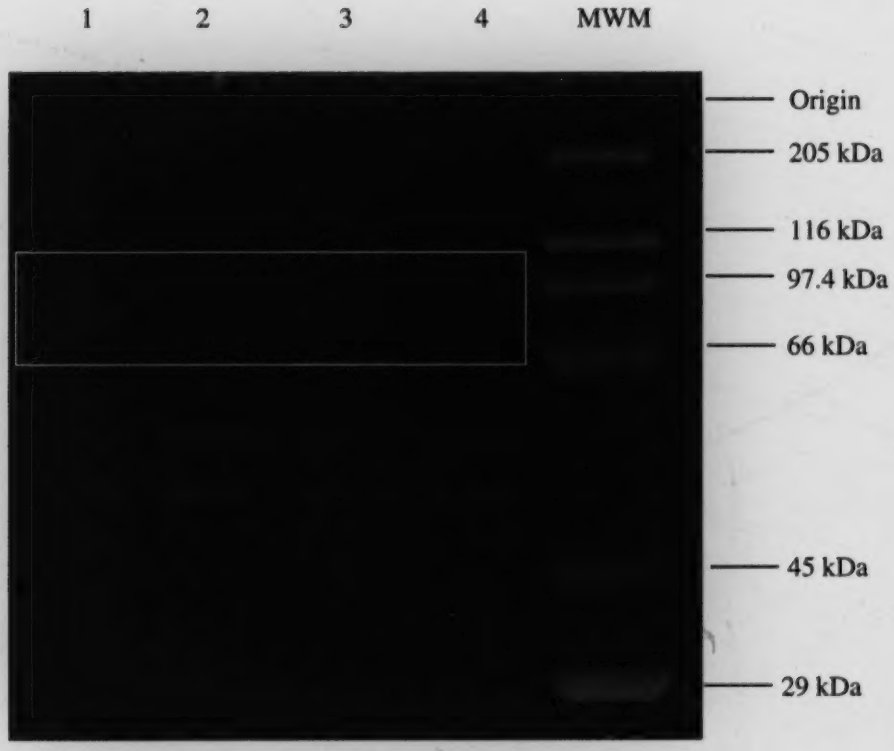

Figure 3.30 SDS-PAGE of IROMPs from strains UW and UA1 grown in Burk's medium with 1 mM or 1 μM molybdate.

(MWM) Molecular weight markers. Iron-limited: (1) Strain UW grown in the presence of 1 μM molybdate. (2) Strain UW grown in the presence of 1 mM molybdate. (3) Strain UA1 grown in the presence of 1 μM molybdate. (4) Strain UA1 grown in the presence of 1 mM molybdate. White box indicates protein bands of interest (IROMPs). Gel stained with Sypro-Orange and photographed on a UV box.

3.2.8 Ferric reductase assay

The effect of the metals, determined to promote protochelin accumulation, on the activity of ferric reductase was studied. As the ferric reductase enzyme is able play a role in iron-uptake in some microorganisms, how it reacted to these metals was of interest. CFX was prepared from strain UW grown in the presence of 1 μM molybdate and 3 μM ferric citrate. Ferric reductase activity was examined using the CFX and various iron (III) sources as substrates including ferric citrate and iron (III) complexes of each of the three catecholate siderophores (Section 2.3.5). As summarized in Table 3.7, each metal decreased the activity of the ferric reductase to some degree with each of the four sources of iron (III) used. This indicated that each metal was able to inhibit the ability of ferric reductase to convert iron (III) to iron (II) and as a result may reduce the amount of iron (II) available to the cell.

3.2.9 Effect of high molybdate concentrations on *A. vinelandii* P100 growth in iron-restricted medium

The ability of increasing concentrations of molybdate from 1 μM to 1000 μM to affect the growth of the siderophore non-producing strain P100 was examined under iron-restricted growth conditions using 50 μg EDDHA ml^{-1}, as in Section 3.1.10, supplimented with protochelin to a final A_{310} of 1.0 or a mixture of azotochelin and aminochelin to a final A_{310} of 1.5. The results indicated that as the concentration of molybdate increased, the growth of P100 decreased in the presence of protochelin. The addition of 10 μM molybdate decreased growth, in terms of total cell protein, by 33% of a control grown in the presence of 1 μM molybdate. Addition of 100 μM molybdate decreased growth by 28% and 1000 μM molybdate decreased growth by 44%. Similar effects were seen with cultures supplemented with a mixture of azotochelin and aminochelin where increasing molybdate decreased growth by up to 14% of the control. Thus, the ability of molybdate to inhibit the uptake of ferric-siderophore complexes has the effect of reducing the ability

Iron (III) Source in assay	Percent of control ferric reductase activity[A]				
	Molybdate 1000 μM	Vanadate 100 μM	Tungstate 30 μM	Mn^{2+} 70 μM	Zn^{2+} 500 μM
Ferric-protochelin	86±6	42±ND	64±8	77±7	32±3
Ferric-azotochelin	71±4	66±3	75±6	87±5	61±1
Ferric-aminochelin	60±1	44±5	83±5	46±4	94±1
Ferric-citrate	53±5	36±6	51±3	36±2	78±5

A. ± Standard deviation of values from a minimum of two replicates.

Table 3.7 Effect of metals that promote protochelin accumulation on ferric reductase activity.

of strain P100 to grown under conditions were it is solely dependent on exogenous siderophores for iron acquisition.

3.3 Role of protochelin in O_2 stress management

3.3.1 Strain LM100 and protochelin accumulation

As described in Section 3.1.5, *A. vinelandii* strain LM100 did not require the addition of 1 mM molybdate to accumulate large amounts of protochelin. Strain LM100 is an isogenic ferredoxin I (*fdxA*)-negative strain of *A. vinelandii* UW and as such is thought to be unable to properly respond to oxidative stress, based on the model described in Section 1.6.4. Growth of this strain under standard conditions in Burk's medium containing 5 μM ferric citrate resulted in the formation of protochelin and the other catecholate siderophores after 15 hr of growth. These siderophores were resolved and identified by TLC (Fig. 3.31). The fact that in strain LM100 protochelin formation appeared less sensitive to iron-repression and did not require 1 mM molybdate for accumulation suggested that in some way the formation of protochelin may be related to oxygen stress management.

3.3.2 Oxidative stress and catecholate siderophore production

3.3.2.1 Increased aeration effects

To investigate how *A. vinelandii* responded to increased oxygen stress, the wild-type strain UW and strain LM100 were grown under conditions of increasing oxygen stress to observe how they reacted to such conditions. This was accomplished by (1) limiting the growth medium in iron to reduce the synthesis of protective enzymes such as superoxide dismutase, (2) removing a fixed nitrogen source so that the microorganism must fix nitrogen, thereby increasing respiration and oxygen stress to protect the nitrogenase, and finally by (3) increasing aeration by decreasing the amount of medium added to each growth flask as this has been demonstrated to increase the rate of oxygen absorption by

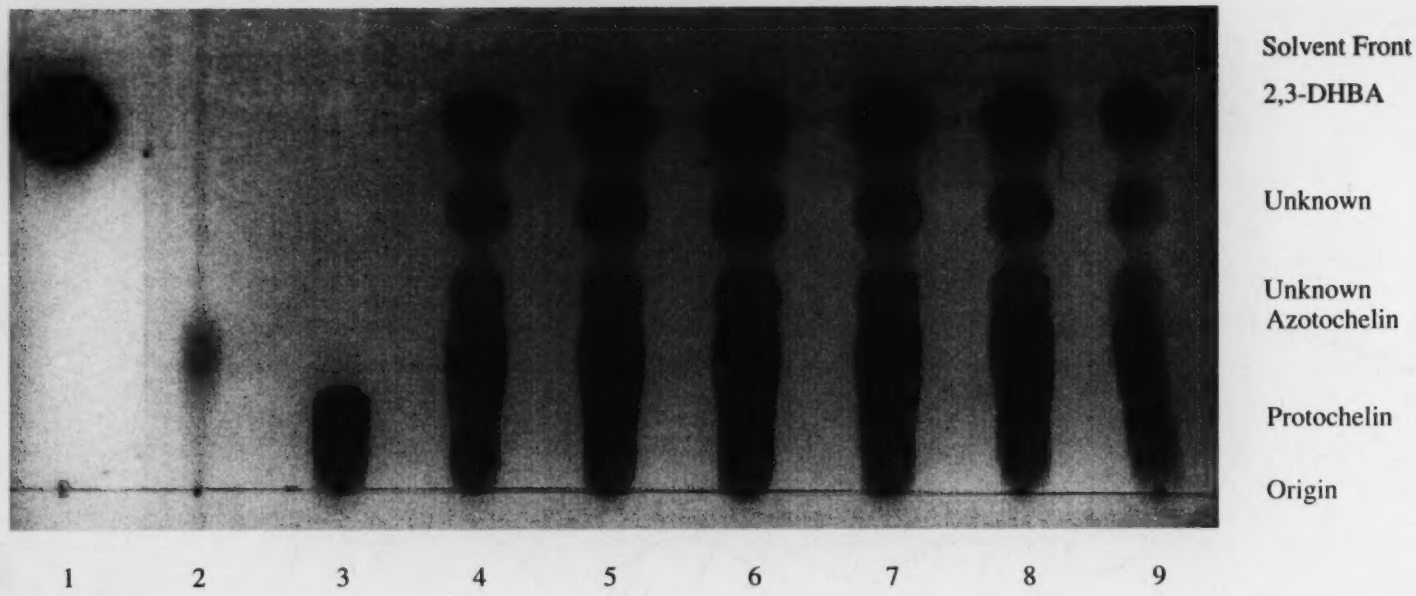

Figure 3.31 TLC analysis of the time course for the production of siderophores by *A. vinelandii* strain LM100.

(1) 2,3-DHBA standard. (2) Azotochelin standard. (3) Protochelin standard. Ethyl acetate extracts of culture supernatants after growth for; (4) 13 hr, (5) 14 hr, (6) 15 hr, (7) 16 hr, (8) 17 hr, and (9) 18 hr.

the medium (Page, 1982). Under these conditions, after 22 hr of incubation, growth of strain UW was largely unchanged in iron-limited, nitrogen-sufficient medium at volumes of 250 ml to 150 ml. As aeration increased in the 100 ml to 25 ml cultures, protein values were observed to decrease (Fig. 3.32-A -●-). Strain LM100 demonstrated a similar growth pattern, although it was adversely affect by aeration to a greater degree than strain UW at the two highest aeration conditions. (Fig. 3.32-A -■-). Growth of both strain LM100 and UW under nitrogen-limited conditions was not dramatically affected by aeration until the highest aerations conditions where a decrease in protein values was seen (Fig. 3.32-A -□- and -○-). This lack of sensitivity to increased oxygenation is consistent with the "oxygen wasting" mechanism used by *A. vinelandii* to maintain an oxygen free environment for the nitrogenase enzyme (Section 1.2.3).

Under iron-limited, nitrogen-sufficient conditions, strains UW and LM100 both demonstrated increased production of catecholate siderophores per mg cell protein as the ratio of medium volume to flask volume decreased, coincident with increased protein production, until the highest aeration levels (Fig. 3.32-B -●- and -■-). There was no apparent response of azotobactin production to increased aeration (data not shown), so this siderophore was not examined further. Catecholate siderophore overproduction was most evident in nitrogen-fixing cultures, where both strains formed more catecholate per mg protein than the corresponding cells grown with ammonium, even at low aeration (Fig. 3.32-B -□- and -○-). This was the case even as total cellular protein concentrations dropped at increased aeration levels. This suggested that the catechols being produced were not being formed to acquire iron for growth, as protein concentrations decreased at higher aeration levels.

Culture supernatants from strains UW and LM100 were fractionated with ethyl acetate and sodium phosphate and the catecholates present in each fraction were identified by

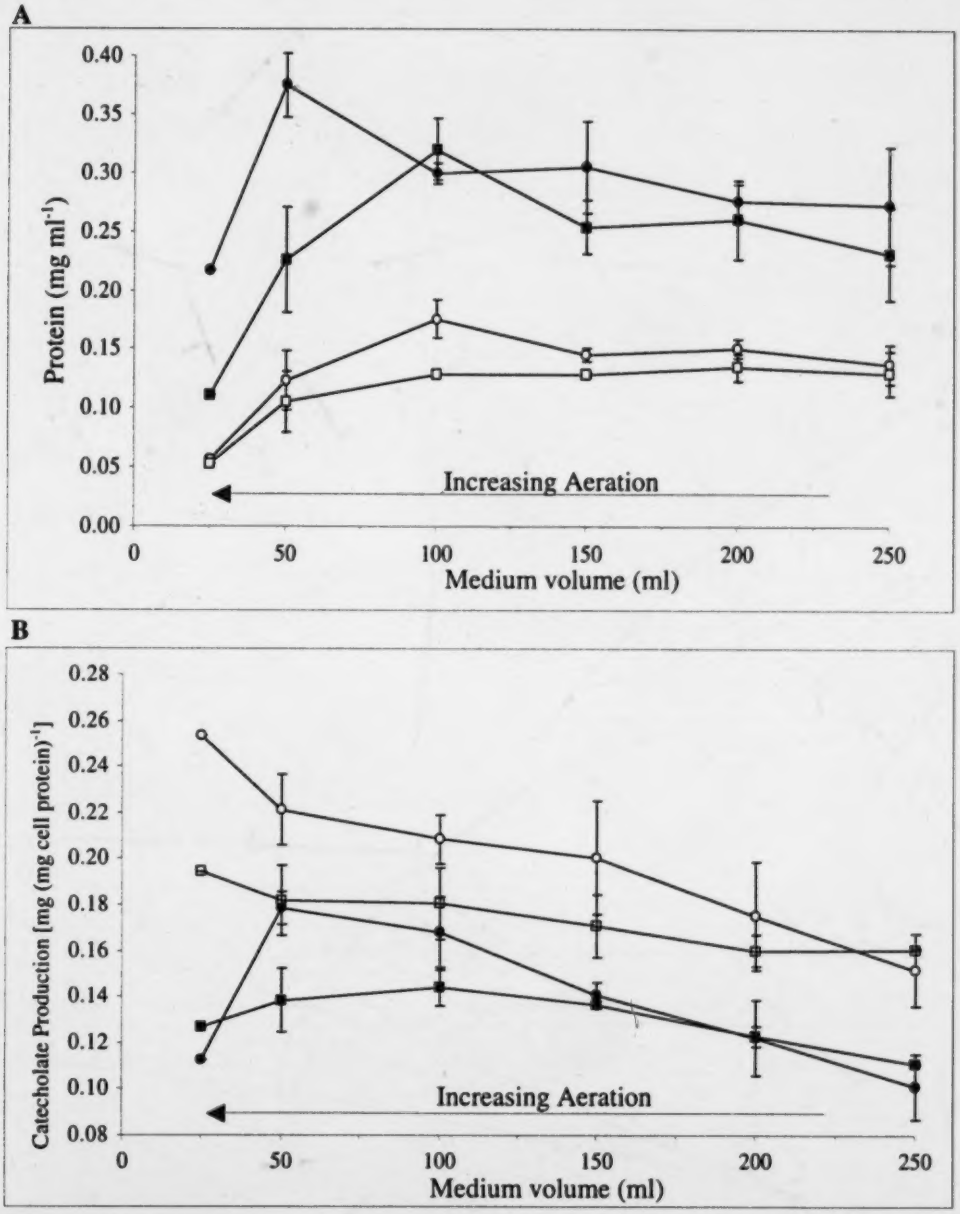

Figure 3.32 Effect of increasing aeration on *A. vinelandii* strains UW and LM100 after 22 hr of growth.

(A) Growth in iron-limited, nitrogen-sufficient medium (●) UW, (■) LM100 and growth in iron-limited, nitrogen-free media (○) UW, (□) LM100.
(B) Catecholate production by strains UW and LM100. Conditions and symbols are the same as in (A). Error bars indicate range of values obtained in duplicate experiments.

TLC (Fig. 3.33) and quantified by A_{310} (data not shown). In strain UW nitrogen-sufficient and nitrogen-free culture, aminochelin and azotochelin were present in a 1:0.9 ratio and accounted for about 95 to 97% of the catecholates present, regardless of aeration rate. Protochelin was barely detectable on TLC and accounted for only about 4 to 5% of total catecholates or 3 to 4 μM in culture fluid (Fig. 3.33-A). Similarly, in strain LM100 nitrogen-free culture, aminochelin and azotochelin were present in a 1:0.8 ratio and accounted for about 92% of the catecholates present. Protochelin was also barely visible on TLC (Fig. 3.33-B lanes 5 to 8 -NH_4^+) and accounted for about 6% of total catecholates, regardless of aeration rate. Similar abundance of the three catecholates were found in nitrogen-sufficient strain LM100 culture at low aeration, but protochelin became very definite on TLC and accounted for 17% of total catecholates (17 μM in culture fluid) as aeration was increased (150 ml per flask in Fig. 3.33-B lane 6 -NH_4^+). At the next two higher aeration rates which were growth inhibitory (Fig. 3.33-B lanes 5 and 4 -NH_4^+), protochelin declined to 13% and 6% of total catecholates.

3.3.2.2 Effect of paraquat on the growth of *A. vinelandii* strains LM100 and UW

Sensitivity to oxygen stress was also studied by the addition of increasing concentrations of the redox cycling compound paraquat to culture medium to generate superoxide ($\bullet O_2^-$). After 24 hr of growth, strain UW was much more resistant to paraquat and the generation of $\bullet O_2^-$ than was strain LM100. In iron-sufficient, nitrogen-sufficient medium strain UW growth was inhibited completely by 40 μM paraquat while the growth of iron-sufficient, nitrogen-fixing cells was inhibited by 30 μM paraquat. In parallel iron-limited cultures, strain UW in the presence of fixed nitrogen was more sensitive to paraquat (20 μM and 10 μM paraquat respectively) (Table 3.8). Strain LM100, however, was much more sensitive to growth inhibition by paraquat, consistent with an inability to deal effectively with $\bullet O_2^-$. Growth inhibition of strain LM100 growth was complete at 5 μM paraquat

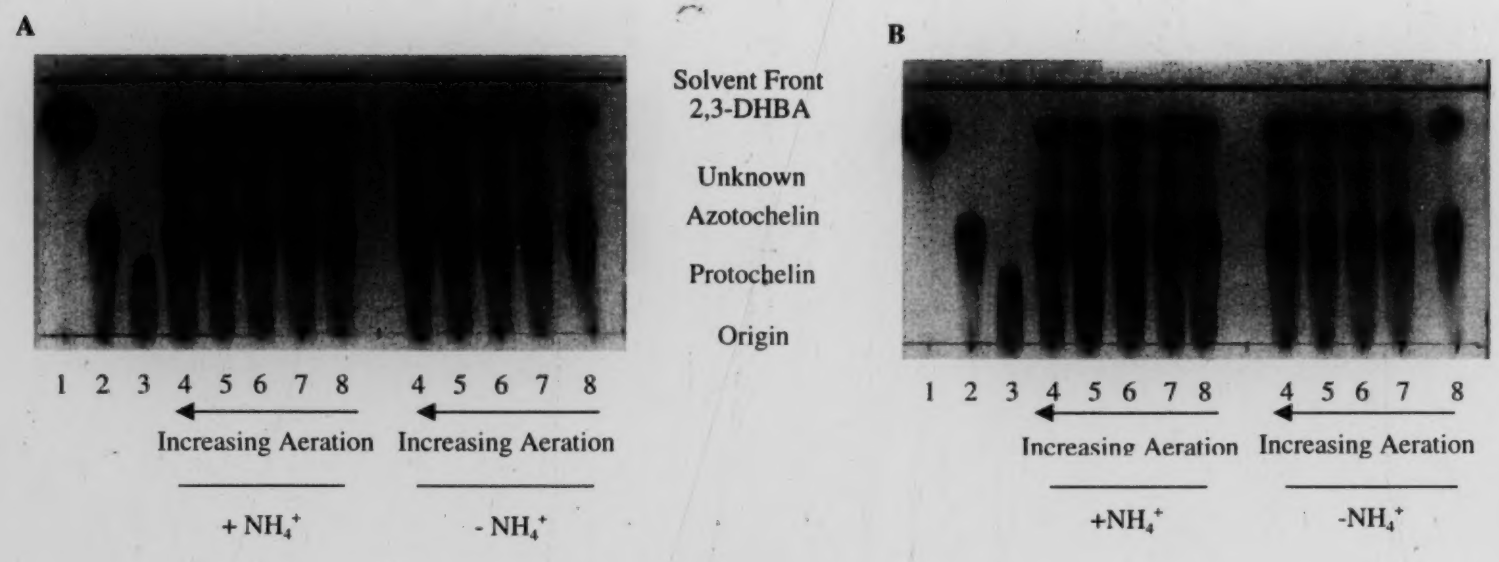

Figure 3.33 The effects of increasing aeration on the siderophores produced by *A. vinelandii* strains UW and LM100.

In all figures: (1) 2,3-DHBA standard. (2) Azotochelin standard. (3) Protochelin standard.
Culture volumes in all figures: (4) 50 ml, (5) 100 ml, (6) 150 ml, (7) 200 ml, (8) 250 ml.
TLC (A) Ethyl acetate extracts of strain UW culture supernatant.
TLC (B) Ethyl acetate extracts of strain LM100 culture supernatant.

Strain	NH_4 Prsent	[Iron] µM	Control [Protein]^A mg ml^{-1}	[Paraquat] µM to inhibit growth	[Protein]^A mg ml^{-1} at inhibitory [Paraquat]
UW	+	20	1.5	40	0.04
UW	-	20	1.0	30	0.02
UW	+	1	0.63	20	0.03
UW	-	1	0.35	10	0.09
LM100	+	20	1.1	5	0.04
LM100	-	20	0.80	5	0.07
LM100	+	1	0.31	3	0.07
LM100	-	1	0.14	3	0.05

A. Determined by the method of Lowry *et al.* (1951). Each value is the average of duplicate determinations.

Table 3.8 Effect of paraquat on the growth of nitrogen-sufficient and -limited and iron-sufficient and -limited cultures of *A. vinelandii* strains UW and LM100 after 24 hr.

iron-sufficient cells and 3 μM paraquat in iron-limited cells, regardless of nitrogen source (Table 3.8).

3.3.3 Activity of enzymes in oxygen stress management

To better understand how strains UW and LM100 manage oxygen stress, the activity and presence of the enzyme superoxide dismutase (SOD) was examined. As SOD is the enzyme responsible for the removal of $\bullet O_2^-$ from the cell, its activity is an estimation of how well the cell may cope with oxygen stress. The enzyme was studied in two ways, either by measuring the activity of the enzyme in a CFX, or by looking for the presence of the enzyme on a non-denaturing PAGE gel. The CFX used was generated from cells grown under standard conditions in the presence of 1 μM or 75 μM ferric citrate (Section 2.1.4). The activity of SOD was notably decreased by iron-limitation in strain UW and in strain LM100 cultures (Table 3.9). However, even in iron-sufficient medium, strain LM100 had only 39% of the SOD activity of strain UW. Examination of the species of SOD produced indicated that both strains had an identical single species of SOD with an R_F of 0.9, which was inactivated by 5% H_2O_2, indicating that it was an iron-SOD (data not shown). The fact that the SOD present in LM100 had only 39% of the activity of the same enzyme in the wild type would suggest that strain LM100 is not able to effectively deal with $\bullet O_2^-$.

The activity and presence of catalase was also examined in strains UW and LM100 using the CFXs described above. Catalase activity in strain LM100 was only 45-50% of that found in strain UW and in both strains the overall activity of catalase activity appeared unaffected by iron-limitation (Table 3.9). The examination of the species of catalase produced indicated that both strains produced two electromorphs with similar R_F values of 0.5 and 0.6, but that a third electromorph with an R_F of 0.2 present in strain UW was

Strain	Iron content of medium (μM)	SOD activity (Units mg protein^{-1})	Catalase activity (Units mg protein^{-1})
UW	1	1.2	38.4
	75	47.0	38.6
LM100	1	1.9	20.2
	75	18.4	18.5

Table 3.9. Enzyme activities and electromorph relative mobilities from cells grown under iron-sufficient and iron-limited conditions.

barely present in strain LM100 grown in 1 μM ferric citrate (Fig. 3.34 lane 5). The catalase band produced by strain LM100 grown in 75 μM ferric citrate was fainter than the equivalent band seen in strain UW grown cultured in the same concentration of ferric citrate (Fig 3.34 compare lanes 4 and 2). This reduced or missing activity in strain LM100 may account for the difference in overall enzyme activity observed between the two strains. These results indicate that in addition to reduced SOD activity, LM100 is also limited in the manner with which it can deal with H_2O_2, the toxic oxygen product formed by the activity of SOD. The overall effect of this would be to decrease the ability of strain LM100 to effectively deal with oxidative stress.

3.3.4 Oxygen radical mediated iron (II) release

The ability of each catecholate siderophore to retain iron (II) in the presence of $\bullet O_2^-$ was examined by allowing each Fe^{3+}-siderophore complex to incubate in the presence of $\bullet O_2^-$. If a siderophore was able to retain iron (II) then this indicated that it would not promote the Fenton reactions (Section 1.6.2) and would not contribute to oxidative stress. The presence of Fe^{2+} was detected by monitoring the formation of the Fe^{2+}-ferrozine complex at 562 nm. The results indicated that both Fe^{3+}-protochelin and Fe^{3+}-azotochelin were stable in the presence of $\bullet O_2^-$, but ferric aminochelin released a significant amount of Fe^{2+}. As the amount of potential free Fe^{2+} in the assay was increased from 5 to 50 μM, ferric-aminochelin continued to be the only siderophore that released Fe^{2+}. When ferric-aminochelin was present at 15 μM Fe^{2+} it was released at a rate of 1.24 μM Fe^{2+} min^{-1} while Fe^{3+}-protochelin and Fe^{3+}-azotochelin released Fe^{2+} at rates of 0.07 and 0.13 μM Fe^{2+} min^{-1}, respectively when they were also present at 15 μM. Addition of SOD to the Fe^{3+}-aminochelin reaction decreased the rate of Fe^{2+} release by 30% to 0.95 μM Fe^{2+} min^{-1} indicating that Fe^{2+} release was $\bullet O_2^-$ mediated. Preventing the formation $\bullet O_2^-$ by the omission of hypoxanthine and xanthine oxidase (the source of $\bullet O_2^-$ in the assay) prevented the release of Fe^{2+} altogether.

Figure 3.34 Non-denaturing PAGE gel of catalase activity from *A. vinelandii* strains UW and LM100 under high and low iron (III) concentrations.

(1) Catalase standard. Strain UW grown in Burk's medium with; (2) 75 μM Fe^{3+} or (3) 1 μM Fe^{3+}. Strain LM100 grown in Burk's medium with; (4) 75 μM Fe^{3+} or (5) 1 μM Fe^{3+}.

A. Bands very faint.

3.3.5 Inhibitory role of siderophores in •OH generation

The ability of each siderophore to participate in the formation of •OH via the Fenton reaction was also studied. This was done by incubating a Fe^{3+}-siderophore complex in the presence of $•O_2^-$ and deoxyribose which served as a hydroxyl radical trap. When deoxyribose was allowed to react with thiobarbituric acid a colored complex formed if the deoxyribose had reacted with hydroxyl radicals. The Fe^{3+}-aminochelin complex was equal to a Fe^{3+}-EDTA positive control in its ability to catalyze the formation of •OH, whereas Fe^{3+}-protochelin and Fe^{3+}-azotochelin generated 70% less •OH under identical conditions compared to the positive Fe^{3+}-EDTA control. Addition of catalase and or SOD blocked •OH formation and indicated that the formation of colored complexes with thiobarbituric acid was depended on the presence of reactive oxygen intermediates.

CHAPTER 4 – General Discussion

4.1 Characterization of unknown compound as protochelin, a tricatecholate siderophore

All microorganisms must respond to different forms of environmental stress in order to survive. In the course of studying the response of *A. vinelandii* to increased molybdate concentration, the formation of a new catecholate compound was observed. Based on the reaction of this compound to the 2,2'-dipyridyl spray reagent used to visualize catecholates on TLC plates and its reaction in the Barnum assay it was determined that it was catecholate in nature. Further analysis by acid hydrolysis showed that it contained both azotochelin and aminochelin molecules, and total acid hydrolysis indicated the presence of lysine and putresine, the amine compounds that form the backbones of azotochelin and aminochelin respectively. This suggested that the new catecholate compound may be protochelin (Taraz *et al.*, 1990), a molecule formed from one molecule of azotochelin and one molecule of aminochelin. FAB mass spectrometry indicated that the new compound had a molar mass of 624 g mol^{-1}; consistent with the prediction of 1 azotochelin and 1 aminochelin molecule being condensed. Similar analysis of an authentic sample of protochelin gave identical results as those observed for the new compound, confirming its identity as protochelin.

The realization of the existence of protochelin immediately posed the question, was protochelin the primary siderophore produced by *A. vinelandii*? If this was the case, it would imply that azotochelin and aminochelin were really breakdown products of protochelin cleavage. Conversely, protochelin may only be formed from azotochelin and aminochelin precursors in the presence of high molybdate. Answering this question and understanding the role of molybdate in the accumulation of protochelin became one of the goals of this work.

It was important to establish if protochelin could function as a siderophore. Chemical analysis of the binding of protochelin with iron demonstrated that protochelin formed a 1:1 ferric-siderophore complex as predicted by its structure. At the same time, both aminochelin and azotochelin were also shown to form the complexes with iron that were predicted by their structures. Thus, azotochelin bound iron in a 3:2 siderophore:iron ratio, similar to that seen with rhodotorulic acid (Carrano & Raymond, 1978) whereas aminochelin formed a 3:1 siderophore:iron complex. The time taken to form a ferric-siderophore complex also corresponded to the intricacy of the complex formed, thus, ferric-protochelin formed most quickly, followed by ferric-aminochelin and ferric-azotochelin. Protochelin had the greatest affinity for iron (III) of the three siderophores. In terms of the free iron (III) in an equilibrium system, as defined by Harris *et al.* (1979), protochelin had an affinity for iron (III) 6 orders of magnitude larger than azotochelin and 7 orders of magnitude greater than aminochelin. This was consistent with the ability of protochelin to form a complex with iron (III) using 6 coordinate bonds. In all cases, the affinity that each siderophore had for iron (II) was less than its affinity for iron (III).

For comparison to other tricatecholate siderophores, the proton independent formation constant of protochelin was found to be $10^{43.9}$. This was close to the value of $10^{44.6}$ predicted by Duhme *et al.* (1997), working with chemically synthesized protochelin, and about 5 orders of magnitude smaller than the value of 10^{49} reported for enterobactin. Enterobactin is often used as a standard for siderophore affinity comparison as it is considered to be the most effective of all siderophores for binding iron (III). The reason for the difference in iron binding between these two tricatecholates is the fact that in enterobactin, the catechol groups that coordinate iron are attached to a tri-serine ester ring that pre-organizes the catechol groups to bind iron (III) (Crumbliss, 1991). Protochelin, on the other hand, is a linear molecule that lacks such pre-organization. A similar difference in formation constants is seen between enterobactin and its linearized form

which has a proton independent formation constant of 10^{43} (Scarrow *et al.*, 1991). However, protochelin binds iron (III) with a higher affinity than ferrioxamine B (10^{39}), pyoverdin PaA ($10^{30.8}$), ferrichrome ($10^{29.1}$), and aerobactin ($10^{22.5}$) (Reid *et al.*, 1993).

Thus, from a chemical standpoint, and by comparison to compounds already identified as siderophores, protochelin appeared to have the ability to function in iron acquisition. However, the question remained, could it acquire iron in a biological system?

This was addressed by looking at biological characteristics of siderophores and determining if they applied to protochelin. To this end, protochelin was found to be repressed by an iron (III) concentrations of 9 μM, similar to the other catechol siderophore produced by *A. vinelandii* (Page & von Tigerstrom, 1988). This is in agreement with recent data that demonstrates that the expression of the first gene in catecholate synthesis in *A. vinelandii*, *csbC* (catecholate siderophore biosynthesis C), is repressed at iron (III) concentrations between 7 to 10 μM (Sharpe, 1999). Protochelin, and similarly a mixture of aminochelin and azotochelin, were found to deferrate the chromogenic iron chelator Chrome Azurol A in the CAS assay. Protochelin was also shown to promote the growth of the siderophore-negative strain P100 when the microorganism was grown under conditions made iron-limited by the addition of EDDHA.

Finally, in ^{55}Fe-uptake assays, ferric-protochelin was rapidly taken up by *A. vinelandii* in the same manner as reported for ferric-aminochelin and ferric-azotochelin (Page & von Tigerstrom, 1988; Knosp *et al.*, 1984). Ferric-protochelin was taken up at a faster rate than a mixture of ferric-aminochelin and ferric-azotochelin, but the rate of uptake of pure ferric-protochelin was very similar to that of pure ferric-azotochelin. Surprisingly, in pure siderophore studies, ferric-aminochelin was not taken up by the cells. This

contradicts previous results where aminochelin was shown to be readily taken up by *A. vinelandii* (Page & von Tigerstrom, 1988). It was not clear what was responsible for this discrepancy, although it is possible that the aminochelin stock solution may have contained some contaminating butanol from the purification process. As butanol has a solubility in water of 10 ml per 100 ml of water (Merck Index, 1989) it is conceivable that a small amount of butanol could have adversely affected the cells in the iron-uptake assay, but would not be a factor in the chemical characterization of aminochelin. However, as aminochelin was not the focus of this study, this discrepancy was not pursued further.

From these data, it can be confidently stated that protochelin is one of the siderophores formed by *A. vinelandii* under iron-limited conditions. It meets all of the criteria of a siderophore and has been shown to be better at iron-chelation and transport than the siderophores previously characterized for *A. vinelandii*. These data however, do not indicate whether protochelin is the primary siderophore of *A. vinelandii*. The high affinity of protochelin for iron (III) does suggest that, like enterobactin (Brickman & McIntosh, 1992), cleavage of protochelin may be necessary to release iron for use by the cell. As a result, azotochelin and aminochelin could very well be breakdown products formed during iron release. To determine if this is the case, and to determine the role molybdate plays in protochelin accumulation, the interaction of molybdate and protochelin was examined.

4.2 Interaction of molybdate and protochelin

The presence of molybdate negatively affected the function of protochelin as a siderophore. Molybdate prevented protochelin from deferrating CAS, and prevented protochelin from promoting the growth of strain P100 under iron-limited conditions in

the presence of EDDHA. As well, the presence of molybdate dramatically reduced the uptake of ferric-protochelin and ferric-azotochelin complexes by the cell.

To understand the manner in which protochelin and molybdate interacted, it was first determined that molybdate did not cause the spontaneous formation of protochelin from azotochelin and aminochelin in solution. Thus, protochelin only accumulated in culture fluid when molybdate was present during growth. It was also noted that the addition of tungstate, vanadate, Zn^{2+}, and Mn^{2+} also promoted the accumulation of protochelin in culture fluid. The manner in which vanadate and tungstate affected protochelin accumulation was thought to be the same as molybdate since these three metals are chemically very similar (Section 1.3.4). It was, however, unclear as to the manner in which Zn^{2+} and Mn^{2+} also lead to protochelin accumulation.

Both iron and molybdate are Lewis acids and both can both form stable complexes with catecholates. Molybdate is known to interact with catecholate siderophores through the hydroxyl groups of the catechol moieties in a manner similar to that of iron (Hider, 1984). Azotochelin and aminochelin were found to chelate molybdate in a manner consistent with their chemical structure and the fact that molybdate has a total of four empty coordinate bonds sites at neutral pH. In the case of azotochelin, this was consistent with the results of Duhme *et al.* (1998) who demonstrated that azotochelin and molybdate could form a 1:1 complex. The manner in which protochelin coordinated molybdate was less obvious, although based on a combination of data from affinity studies of protochelin and molybdate, and the results of competition experiments between iron and molybdate for binding to protochelin, it would appear that protochelin also bound molybdate in a manner predicted by its structure. This was a 3:2 molybdate:protochelin complex that is likely similar in form to the 3:2 siderophore:iron complex described for rhodotorulic acid and iron (III) (Carrano & Raymond, 1978).

Unlike the formation of ferric-siderophore complexes, molybdo-siderophore complexes formed very quickly regardless of the ratio in which molybdate interacted with the siderophore. This was explained by the higher solubility of molybdate in water compared to that of iron (III) (Section 1.3.1 & 1.4.1) even though molybdate may form polymolybdate compounds. Iron (III) tends not to go into solution, even thought it may dissolve in buffer. Instead, it forms a colloidal water-iron gel that limits it solubility (Cotton & Wilkinson, 1980). As a result, molybdate can bind to catecholates faster than iron (III) which must first be solublized by the siderophore. The ease with which molybdate goes into solution, coupled with the fact that molybdate can act like iron to bind catecholates, would support the hypothesis that the reason molybdate affected the biological characteristics of protochelin was by binding to it such that it could no longer interact with iron. This is consistent with data of Duhme *et al.* (1996) which demonstrated the ability of molybdate to slow the formation of a ferric-azotochelin complex, which was also demonstrated in this study. As well, the formation of the ferric-aminochelin complex was mildly affected by the presence molybdate, which is consistent with its relatively low affinity for both iron (III) and molybdate. However, competition studies done with iron (III), molybdate and protochelin demonstrated that the presence of molybdate has little effect on the formation of ferric-protochelin. This would indicate that, unlike azotochelin or aminochelin, the affinity of protochelin for iron (III) was great enough to negate the competitive effects of molybdate.

This was confirmed when the affinity of protochelin for molybdate was determined by competition with iron (III). Using the free metal concept of Harris *et al.* (1979), the pFe value for protochelin was 28, whereas the $pMoO_4^{2-}$ value for protochelin was 16, 10^{12} times smaller. Thus, the affinity that protochelin has for iron (III) is much greater than its affinity for molybdate. In terms of the CAS assay, this would explain how molybdate

affects the ability of protochelin to remove iron from the CAS complex over a 5 min period. In this short period of time, the competition between molybdate, iron (III) for protochelin is significant. However, over a 20 hr growth period, the affinity of protochelin for iron would be high enough to overcome the presence of molybdate. If this was the only effect, the presence of molybdate would not affect the ability of protochelin to promote the growth of strain P100, but it does. Thus, there must be another mechanism, other than direct interaction, by which molybdate affects the siderophores of *A. vinelandii*.

Initial studies of the uptake of ferric-protochelin demonstrated that cells which were not grown in the presence of high molybdate concentrations could take up ferric-protochelin. Based on this, the ferric-protochelin receptor was likely one of the *A. vinelandii* iron-repressible outer membrane proteins that have already been described (Page & von Tigerstrom, 1982) and was not an outer membrane protein formed in response to high molybdate concentrations. In fact, SDS-PAGE analysis of cells grown in the presence of 1 mM molybdate demonstrated that they had the same outer membrane profile as cells grown in 1 μM molybdate. In addition, work done on protochelin accumulation in high molybdate concentrations using *A. vinelandii* strain RP40 (Mouncey *et al.*, 1995), which lacks both high and low affinity molybdate uptake systems, demonstrated that protochelin still accumulates (Dzwiniel, 1996). Thus, the accumulation of protochelin was not a result of molybdate causing changes in cell surface proteins, or even entering the cell itself.

When molybdate was added to iron-uptake assays with ferric-protochelin or ferric-azotochelin it caused a dramatic inhibition of ferric-siderophore uptake. This effect, however, was reversible and inhibition was overcome by washing the molybdate-treated cells with buffer prior to the assay. Since competition assays indicated that there was no

formation of molybdo-siderophore complexes once the ferric-siderophore complexes had formed, the short time that the molybdate interacted with the ferric-siderophore in the uptake assay would not displace iron from the ferric-siderophore complex. Finally, the addition of molybdate, and the other heavy metals shown to cause protochelin accumulation, to iron-uptake assays that were in progress caused a rapid decrease in the rate at which ferric-siderophore complexes were taken up by the cell. Although it did not explain how, this confirmed that the metals which caused protochelin accumulation did so by inhibiting the uptake of a ferric-siderophore complex, not by affecting the actual ferric-siderophore complex itself.

The results of the uptake assays and the fact that protochelin accumulated in RP40 culture fluid indicated that the accumulation of protochelin was the result of an event at the cell surface, as opposed to being the result of the incorporation of a large amount of molybdate by the cell.

4.3 Effect of metals on ferric reductase activity

A deeper understanding of the role that Zn^{2+}, Mn^{2+}, vanadate, molybdate, and tungstate played in the inhibition of iron-uptake came when the activity of ferric reductase was examined in the presence of these metals. Previously, ferric reductase activity had been shown to be inhibited by Zn^{2+} and Mn^{2+} and this was coincident with an increase in azotobactin and catecholate siderophore production by *A. vinelandii* (Page, 1995; Huyer & Page, 1989). Ferric reductases have been shown to play a role in iron acquisition (Section 1.5.4), and it is reasonable to suspect that ferric reductase inhibition could effect the uptake of the ferric-siderophore complexes in *A. vinelandii*. In some microorganisms, ferric reductase enzymes have been shown to be cell surface associated (Gaines *et al.*, 1981: Fischer *et al.*, 1990). Although the two isoenzymes of *A. vinelandii* ferric reductase appear to be localized in the cytoplasm (Huyer & Page, 1989); the membrane

fraction of the cell has not been examined for ferric reductase activity. Thus, it is possible that one of the two ferric reductases may be surface associated while the other is located in the periplasm or the cytoplasm. A surface ferric reductase could be rapidly inactivated by molybdate and the other metals observed, thus preventing the ferric-siderophore complex from entering the cell. This would account for the decrease in iron uptake seen in the iron-uptake assays, thereby causing siderophore to accumulate in the culture fluid. The cell would continue to "sense" iron-limitation and form more siderophore which would still not be taken up by the cell and would continue to accumulate in the culture fluid.

When ferric reductase activity was examined in the presence of Zn^{2+}, Mn^{2+}, molybdate, vanadate, and tungstate at the same concentrations that promoted protochelin accumulation, ferric reductase activity was shown to be reduced by up to 70% of uninhibited activity. This was the case regardless of the source of iron (III) used, whether it was ferric-siderophore or ferric citrate. In the studies, performed it was not possible to inhibit ferric reductase activity completely, as shown previously with Zn^{2+} (Page, 1995; Huyer & Page, 1989). This lack of complete inhibition is the result of the type of inhibition exerted on ferric reductase by Zn^{2+} (Huyer & Page, 1989) which was characteristic of a mixed or partial type inhibitor where Zn^{2+} is both a competitive and non-competitive inhibitor. As a result, Zn^{2+} is not able to completely inhibit the activity of the enzyme. Based on this pattern of inhibition, Mn^{2+} also appears to be a partial inhibitor of ferric reductase (Page, 1995). This may also be the case for molybdate, vanadate, and tungstate, although the type of inhibition caused by these metals was not determined. The fact that none of the added metals completely inhibited the enzyme may explain why the presence of the metals did not prevent growth. Iron continued to reach the cells either by residual ferric-siderophore transport, or by an as yet undefined mechanism, such as the one thought to allow the minimal growth of strain P100 under

iron-limited conditions (Sevinc & Page, 1992), or perhaps a low affinity iron shuttle between 2,3-DHBA and the S-layer (Page & Huyer, 1984).

This mechanism for molybdate action also provides indirect evidence as to whether protochelin is a condensation product or if azotochelin and aminochelin are hydrolysis products of protochelin. When strain UA1 was grown in the presence of 1 mM molybdate, only protochelin and 2,3-DHBA were shown to accumulate. Since molybdate inhibits azotochelin uptake as well as protochelin uptake, if azotochelin were formed before, or coincident with protochelin it would also be expected to accumulate in the culture fluid, but this was not the case. Thus, protochelin is the catecholate siderophore formed first by *A. vinelandii* in response to iron-limitation and azotochelin and aminochelin are breakdown products. This explains why, under normal iron-limited growth conditions protochelin is not seen to accumulate, while azotochelin and aminochelin do. The cleavage of ferric-protochelin has been demonstrated *in vitro* in preliminary studies using cell free extracts (data not shown), but has not been pursued further. It appears that *A. vinelandii* also uses these breakdown products as siderophores once they are formed, since azotochelin has a reasonable affinity for iron (III). This is analogous to the manner in which *E. coli* has the ability to take up ferric-2,3-dihyroxylbenzoylserine molecules when they are formed by the cleavage of enterobactin (Guerinot, 1994).

4.4 Alternative explanation of role of MoO_4^{2-} in protochelin accumulation

It has been suggested by Duhme *et al.* (1998) that protochelin is the primary compound used for high affinity iron uptake and that azotochelin is the compound used for high affinity molybdate uptake by the cell. The authors base this on the fact that azotochelin and molybdate form a 1:1 complex and that azotochelin has some affinity for molybdate. The authors report a conditional formation constant for molybdo-azotochelin as $10^{4\pm1}$,

which is in agreement with the value of $10^{3.6}$ determined in this study. However, my results show that azotochelin still has an affinity for iron (III) that is $10^{16.3}$ times larger than its affinity for molybdate, based on the analysis of Harris *et al.* (1979). In competition assays done in this study and in Duhme *et al.* (1996), it has been shown that although molybdate slows the formation of ferric-azotochelin, it still forms with time. As a result, the only way in which azotochelin could effectively bind and transport molybdate would be if it could be quickly bound and rapidly incorporated into the cell by an as yet unidentified component of the high affinity molybdate uptake system (Mod proteins-Fig. 1.4). The hypothesis Duhme *et al.* (1998) have put forth would be strengthened by demonstrating azotochelin-mediated molybdate uptake using ^{99}Mo labeled molybdate in a manner analogous to ^{55}Fe-uptake studies. In addition, if azotochelin were the mediator of high affinity molybdate uptake, its formation should be evident under low molybdate, high iron conditions, which is not the case, since all of the catecholate compounds formed by *A. vinelandii* are under the control of iron concentration and are repressed by 6 to 7 μM iron (This study; Sharpe, 1999; Page & von Tigerstrom, 1988; Knosp *et al.*, 1984). This control mechanism in *A. vinelandii* has been reinforced recently with the discovery of a Fur homologue (Mehrotra, 1997) and the identification of a "iron box" in front of the *A. vinelandii entC* homologue *csbC* (Sharpe, 1999).

In addition to the above problems with the use of azotochelin as a "molybdophore", Duhme *et al.* (1998) also state that protochelin is only formed in the absence of functional azotochelin. Their rationale for this is that protochelin is formed as an iron carrier only when azotochelin is completely bound to molybdate. However, this is not the case! Protochelin has been shown to be formed coincident with azotochelin in the wild type *A. vinelandii* UW (This study). Strain UW is the same strain as strain CA used by Duhme *et al.* (1998). Although protochelin was formed in small amounts, it was definitely formed

in the presence of azotochelin at 1 μM molybdate. Protochelin was also formed in large amounts in the presence of azotochelin by *A. vinelandii* strain LM100, without dependence on molybdate, the significance of which will be addressed on its own (Section 4.5). Secondly, Duhme *et al.* (1998) refer to the "toxicity of high molybdate levels in the growth media" as being a result of an iron deficiency due to Fe-MoO_4^{2-} antagonism. This is also not the case, as high levels of molybdate (1 mM) do not adversely affect the growth of the microorganism (This study). Finally, this study has shown that under the conditions which Duhme *et al.* (1998) state would promote the formation and function of protochelin as an iron-specific chelator ferric-protochelin uptake is reduced by 40%, while at the same time the uptake of ferric-azotochelin is reduced by 75% at 70 μM molybdate, this decrease in uptake increases to 80% and 78% respectively for ferric-protochelin and ferric-azotochelin at 1,000 μM molybdate (Table 3.6 and 3.5) . It would not be advantageous for the cell to replace azotochelin with protochelin under conditions where both are inhibited in their ability to transport iron.

Based on these points, the hypothesis of Duhme *et al.* (1998) that protochelin acts as an iron carrier only in the presence of high molybdate concentrations does not explain the results observed in this work. That said, azotochelin may play a secondary role in the high affinity molybdate transport system induced at molybdate concentrations below 10 μM (Mouncey *et al.*, 1995), but the molybdate concentrations (> 70 μM) described by Duhme *et al.* (1998) will inhibit this transport system. This hypothesis requires further study and refinement.

4.5 Effect of oxygen stress on iron-limited *A. vinelandii*

As was mentioned in Section 2.2.2, strain LM100 forms large amounts of protochelin without the addition of high concentrations of molybdate. Strain LM100, as described in Section 1.6.5, is believed to constitutively respond to oxygen stress due to a mutation in

the FdI protein which is part of a SoxRS-like system in *A. vinelandii* (Section 1.6.4) (Yannone & Burgess, 1998; Isas *et al.*, 1995). This indicated a possible connection between oxygen stress management and the formation of protochelin.

In order to bring about oxygen-stress, *A. vinelandii* cells were grown under increasingly aerobic conditions in iron-limited medium. These cells had greatly decreased Fe-SOD activity compared to iron-sufficient cells and as a result $\bullet O_2^-$ was expected to be the main effector of oxidative stress. Decreased SOD activity observed under iron-limited conditions could arise from the production of an iron-deficient apoenzyme (Beyer & Fridovich, 1991) or could indicate that SOD transcription is activated by the presence of iron, as reported for *E. coli* and *P. aeruginosa* (Niederhoffer *et al.*, 1990; Hassett *et al.*, 1996). However, unlike the latter cells (Demple, 1996), *A. vinelandii* has no alternative Mn-SOD to replace the missing Fe-SOD (This study; Jurtshuk *et al.*, 1984). Unchecked, $\bullet O_2^-$ can promote the Fenton reaction, but the formation of •OH may be limited by iron and H_2O_2 availability. Thus, the presence of undiminished catalase activity in iron-limited *A. vinelandii* strain UW may substantially decrease the impact of decreased SOD activity. Such was not the case in LM100, which had decreased activity of both SOD and catalase even under iron-sufficient growth conditions. LM100 also was extremely sensitivity to paraquat as compared to strain UW. This would suggests that strain LM100 was unable to respond to oxygen stress, in contradiction of the hypothesis put forth by Burgess and her coworkers (Yannone & Burgess, 1998; Isas *et al.*, 1995).

However, an alternative explanation is that the extreme paraquat sensitivity of LM100 may be a result of how the cell copes with paraquat as opposed to how it reacts to oxygen stress. With the electron flow from NADPH via FdI to SoxR interrupted in LM100, SoxR is never reduced back to its inactive form and as a result continues to promote the expression of *soxS* and ultimately all of the genes associated with the response of the cell

to oxygen stress, including the *fpr* gene. Fpr, in addition to passing electrons to FdI for use in SoxR reduction, has also been identified as a NADPH:paraquat diaphorase involved in the reduction of paraquat (II) to paraquat (I) (Fig 1.9). It is this consumption of reducing power, in addition to the subsequent generation of $\bullet O_2^-$, that allows paraquat to impose oxidative stress on the cell (Liochev *et al.*, 1994).

LM100 overproduces Fpr (ferredoxin I reductase) as would be expected by the above model. This means that there is a greater "pool" of Fpr available to convert paraquat (II) present in the growth medium to paraquat (I). The result of this is that a greater proportion of the paraquat (II) added to the medium can be cycled between redox states to generate $\bullet O_2^-$, hence leading to higher levels of $\bullet O_2^-$ in LM100 compared to wild type cells where the levels of Fpr are lower. In strain UW, lower, "normal" levels of Fpr result in a smaller proportion of paraquat (II) being active in the Fpr-mediated generation of $\bullet O_2^-$ and as a result the cells could grow in the presence of higher concentrations of paraquat.

Normally the $\bullet O_2^-$ generated by paraquat (I) would be converted to H_2O_2 by the action of SOD, but as was demonstrated in LM100 and the wild type, SOD formation is reduced under iron-limited conditions. Thus, instead of suggesting that LM100 is unable to respond to oxidative stress, increased sensitivity to paraquat indicates that the overproduction of the NADPH:paraquat diaphorase results in this otherwise protective response being counter-productive to cell survival. The low activity of SOD may force the cell to use alternative methods to reduce $\bullet O_2^-$. It should be noted that although the SoxRS system has been extended to *A. vinelandii*(Section 1.6.5), there is no direct biochemical evidence that such a system exists in *A. vinelandii*.

An alternative method in which *A. vinelandii* can deal non-enzymatically with oxidative stress was suggested when strain LM100 and UW were grown under nitrogen-limited conditions of increasing aeration. Under these conditions, increased electron flow and electron leakage would be expected to increase oxidative stress. When these conditions were coupled with iron-limitation, *A. vinelandii* overproduced catecholate siderophores compared to low aeration, nitrogen-sufficient, iron-limited conditions. In this case, catecholates were not sequestering iron for growth, as total cell protein decreased at higher aeration levels. This response was not as pronounced in nitrogen-sufficient cultures, but there still was a trend towards greater catecholate production at higher aeration. Nitrogen fixing cells may be more sensitive to oxidative stress since $\bullet O_2^-$ can directly oxidize metal-containing enzymes or uncouple redox reactions, as well as participate in the Fenton reaction (Fridovich, 1986). Thus, it was questioned whether catecholate siderophores could play a role in limiting Fenton-mediated oxidative damage by sequestering iron in a manner similar to that seen in *P. aeruginosa* (Coffman, 1990).

Azotobacter spp. have previously demonstrated the ability to use chemical methods to deal with oxidative stress. *A. salinestris* has been shown to produce catechol melanin to bind iron and minimize Fenton-mediated oxidative stress (Page & Shivprasad, 1995; Shivprasad & Page, 1989). In light of this example, it would not be unreasonable for catecholate siderophores to play a role in oxidative stress management.

Of particular interest was protochelin, as it was overproduced by strain LM100 and has a high affinity for iron (III). It was shown that iron chelated by protochelin or azotochelin was not reduced by $\bullet O_2^-$ and limited •OH formation in the Fenton reaction. The affinity of protochelin for iron (III) was higher than that of pyoverdin PaA, a siderophore shown to prevent Fenton-mediated •OH formation (Coffman *et al.*, 1990), thus protochelin was expected not to promote •OH formation. Only iron chelated by aminochelin was unable

to limit the Fenton reaction; it was readily reduced by $\bullet O_2^-$ and generated as much •OH as a ferric-EDTA control. These results were consistent with the calculated affinity that each siderophore had for iron (III).

In a mixture of all three catecholates, as formed in iron-limited *A. vinelandii* culture, protochelin probably has the greatest effect in limiting the Fenton reaction. Protochelin is likely to form a stable iron complex first owing to its higher affinity for iron (III) and faster reaction time. However, one of the questions that surrounds protochelin is why is such a superior iron chelator produced in such small amounts? It may be that a small amount (about 4 to 5 μM) of protochelin is sufficient, if one of its major functions is to prevent iron-catalyzed oxidative damage under the low iron (III) growth conditions (6 μM or less), where catecholates siderophores are formed (Page & von Tigerstrom, 1988) and SOD is not (Page & Galibois, unpublished data), as opposed to being formed solely for iron acquisition. Thus, the overproduction of protochelin by strain LM100 may well be compensating for the decrease in SOD activity observed in iron-limited cells in addition to being a consequence of the mutation in ferredoxin 1.

These collective results suggest that catecholate biosynthesis in *A. vinelandii* may be under the dual control of iron-repression and oxidative stress-induction. It has already been shown that *A. vinelandii* has a homologue of the Fur repressor (Mehrotra, 1997), so negative regulation by iron may follow the classic regulatory mechanism described by de Lorenzo *et al.* (1987). Consistent with this, is the identification of a Fur box in front of *csbC* (Sharpe, 1999), the gene in *A. vinelandii* homologous to the *entC* gene in *E. coli* which encodes isochorismate synthesase, the first enzyme in the enterobactin synthesis pathway (Section 1.5.1). In addition, analysis of the nucleotide sequence upstream of *csbC* shows the presence of two sox boxes, one located upstream of the *csbC* promoter and another which overlays the -10 region of the gene (Sharpe, 1999). Thus, dual control

of siderophore synthesis in *A. vinelandii* by iron-limitation and oxygen stress is possible, the proof of which awaits further investigation.

4.6 Model for the synthesis of protochelin

The notion that protochelin results from the intracellular condensation of azotochelin and aminochelin is not likely to be an accurate interpretation of how protochelin is formed *in vivo*. Modeled on the EntF protein of *E. coli* (Section 1.5.1) it is conceivable that *A. vinelandii* could synthesize protochelin from the precursors lysine and ornithine in response to iron-limitation or oxidative stress (Fig. 4.1). The formation of 2,3-DHBA moieties would be carried out in *A. vinelandii* in a manner similar to that of *E. coli* using the products of genes homologous to *entC*, *entB*, and *entA*, but, the formation of protochelin would begin with the addition of an ornithine molecule to the PCP domain of an EntF type molecule. Addition of 2,3-DHBA would then occur to the free amine closest to the PCP domain, but not to the terminal amine of ornithine, in a manner similar to the nucleophilic attack that occurs between the amine of serine-holo-EntF and holo-EntB-DHB in *E. coli* (Fig. 1.7). The addition of only one 2,3-DHBA group could be controlled by the number of holo-EntB-DHB molecules present or some other mechanism. The 2,3-DHB-ornithine group could then be transferred to the TE domain of an EntF homologue by the action of a nucleophilic attack of the hydroxyl group within the TE domain on the carbonyl oxygen within ornithine. This would free the PCP domain for the incorporation of a lysine group. Lysine would also have 2,3-DHB moieties added in a manner similar to above, only in this case both amine groups would have 2,3-DHB groups added. This again could be controlled by the number of holo-EntB-DHB molecules present, or by some characteristic of the EntF homologue complex. The lysine and ornithine residues would be joined by the attack of the underivatised amine of ornithine on the carbonyl group of the lysine attached to the PCP domain of EntF. This would lead to the formation of the amide bond found in protochelin. Release

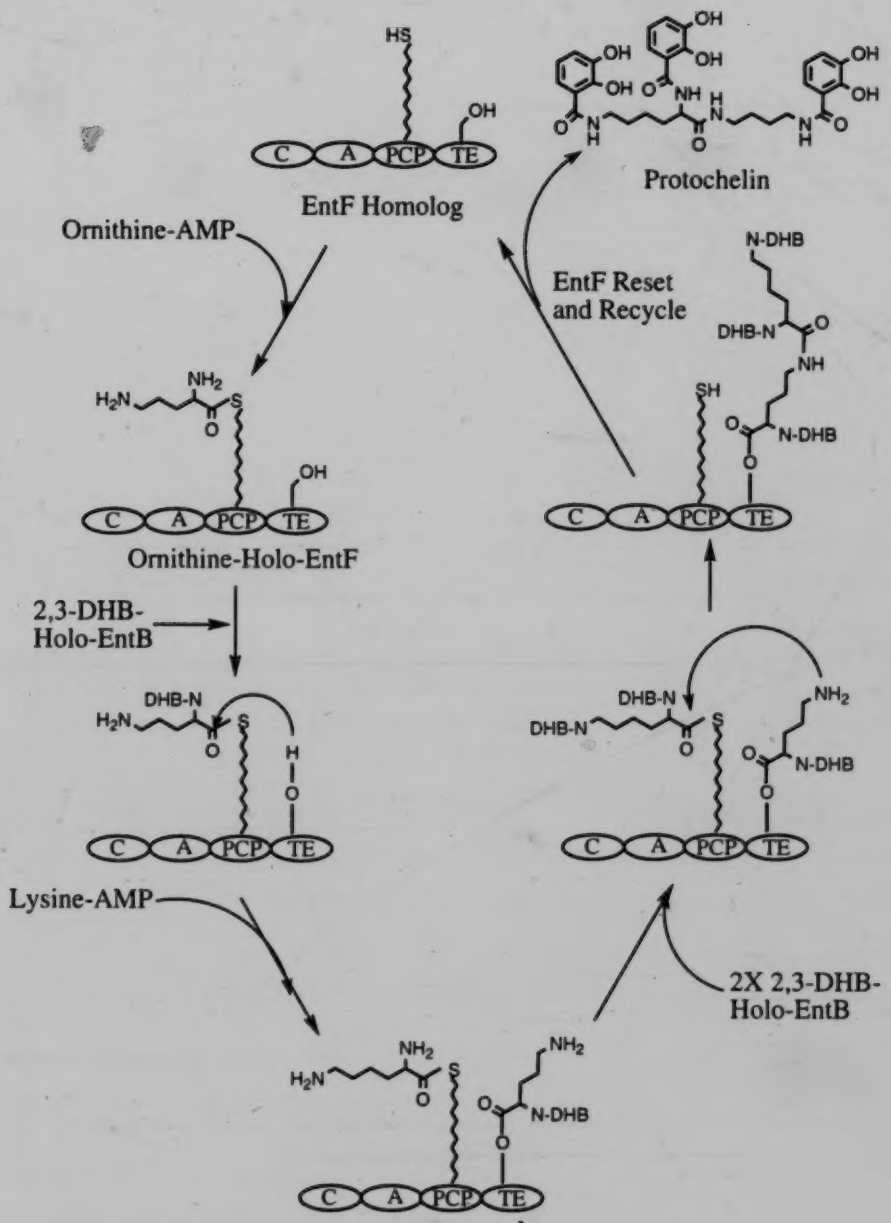

Figure 4.1 Proposed protochelin synthesis by EntF homolog.

C=condensation domain, A=adenylation domain, PCP=peptidyl carrier protien domain TE=thioesterase domain of EntF. DHB=2,3-dihydroxylbenzoic acid.

~~~~SH= phosphopantetheine group.
~~~~

of protochelin could then occur through the carbonyl group which attaches protochelin to the EntF homologue. Loss of CO_2 at this point by a decarboxylase type reaction would recycle the EntF homologue to form more protochelin (Fig. 4.1). All of the precursors in this mechanism; 2,3-DHB-holo-EntB, ornithine-AMP, and lysine-AMP could be formed via reactions described in Section 1.5.1, Figs. 1.5, and 1.6, but free aminochelin or azotochelin are not reactants in the biosynthesis, and cannot be released as products. In support of this hypothesis, preliminary work on *in vitro* synthesis of protochelin indicates that protochelin is not assembled from lysine and putrescine as would be suggested by its structure (data not shown). As a result another precursor, like ornithine could be involved. Based on this proposed mechanism, it is possible that a siderophore other than protochelin could be formed if the terminal amine of ornithine were derivatized as opposed to being left open for attachment to lysine. If this were the case, then some other type of catecholate should be formed with protochelin in the presence of 1 mM molybdate or in the *in vitro* assays as both compounds would be formed by the cell. This is not the case, as only protochelin and 2,3-DHBA are seen to be formed at 1 mM molybdate. This would indicate that protochelin is the sole siderophore formed and that this synthesis is controlled enzymatically. It is therefore most likely, that azotochelin and aminochelin, found in a 1:1 ratio in culture fluids (Page & von Tigerstrom, 1988) are the result of the hydrolysis of protochelin that occurs during uptake and deferration.

In addition to the enzymatic and non-enzymatic systems described for oxidative stress management, many microorganisms including: *E. coli, Saccharomyces cerevisiae, Physarum polycehpalum, Neurospora crassa, Aspergillus nidulans* (Tabor & Tabor, 1985), produce compounds called polyamines which have been shown to protect DNA from $\bullet O_2^-$ (Khan *et al.*, 1992). This includes the polyamine spermine, which has been shown to be present in *A. vinelandii* (Auling *et al.*, 1991). In *E. coli*, these compounds are synthesized from the precursors ornithine and arginine by the action of the products

of the *speA*, *speB*, and *speC* genes. Presumably, if *A. vinelandii* can produce spermine, it must also have similar genes and use a pathway similar to that seen in *E. coli*. If increased oxidative stress increases the synthesis of polyamines, such as spermine, to protect DNA, this would require a larger cellular pool of precursors such as ornithine, which in turn could be used to form protochelin to aid in the reduction of oxidative stress. If this were the case, then the increased production of protochelin would necessitate the formation of more 2,3-DHBA to be used in siderophore synthesis. This would explain the presence of oxidative regulatory elements in front of the *csbC* gene of *A. vinelandii*.

Initial studies into the validity of this proposed mechanism could be undertaken a in number of ways. The *in vitro* formation of protochelin could be examined using a CFX from iron-limited cultures and all of the required precursors to form protochelin including ATP, ornithine and lysine. The resulting reaction mixtures could then be analyzed by TLC as described in Section 2.1.3. Alternatively, analysis could be undertaken using HPLC techniques under conditions described in Duhme *et al.* (1998) to resolve protochelin and the other catecholates produced by *A. vinelandii*.

If the formation of protochelin is dependent on the precursor ornithine, then the proposed pathway could be tested by growing *A. vinelandii* in the presence of compounds which inhibit the formation of ornithine by the cell. As *A. vinelandii* is grown on Burk's medium, a very minimal medium, amino compounds such as ornithine must be synthesized for use. As a result, difluoromethylornithine (DMFO), which inhibits ornithine decarboxylase, should have a profound effect on the formation of protochelin by *A. vinelandii* if ornithine is a precursor in the synthesis of protochelin. The first step in such a study would be to determine if DMFO has an inhibitory effect on the cell under iron-sufficient conditions. In addition, DMFO must be dissolved in dimethlysulfoxide (DMSO) the presence of DMSO would have to be examined to insure that it was not

inhibitory to the cell. If both DMSO and DMFO were found not to be inhibitory to the growth of *A. vinelandii* under iron-sufficient conditions then the microorganism could be grown under iron-limited conditions in the presence of DMFO and the catecholate siderophores examined as described in Section 2.1.3 or by HPLC (Duhme *et al.*, 1998).

4.7 Overview of study and perspective on results

The data presented in this study indicated that in addition to azotobactin, azotochelin and aminochelin, *A. vinelandii* produces a fourth siderophore, protochelin, with an exceptionally high affinity for iron (III). In addition, the manner in which molybdate affects the production of protochelin would suggest that, protochelin is the primary catecholate siderophore produced by *A. vinelandii* and that azotochelin and aminochelin are actually cleavage products of protochelin that can also function as siderophores. Evidence has also been presented that shows that molybdate promotes the accumulation of protochelin by inhibiting its uptake by the cell. Finally, a second role for protochelin in the reduction of oxidative stress has been described and is supported by both chemical data and the overproduction of protochelin in *A. vinelandii* LM100, which constitutively responds to oxidative stress.

It might be questioned why the study of the siderophores of *A. vinelandii* is valuable? *A. vinelandii* is not a human pathogen and the elucidation of how it adapts to its environment will likely not have any direct socio-economic benefit . However, like *A. vinelandii* there are a number of microorganisms that produce small siderophores, some of which appear to be ineffective in iron chelation, but at the same time have been shown to be virulence factors. These include: Chrysobactin (Fig 4.2), produced by *Erwinia chrysanthemi* (Enard *et al.*, 1991), Anguibactin (Fig. 4.2) produced by *Vibrio anguillarum*, (Jalal *et al.*, 1989), Myxochelin A (Fig. 4.2) isolated from *Angiococcus disciformis* strain An d30 (Kunze *et al.*, 1989), Serratiochelin produced by *Serratia*

marcescens (Ehlert *et al.*, 1994), and finally pyochelin (Fig 4.2) from *Pseudomonas aeruginosa* (Cox *et al.*, 1981). Based on the precedent set by the small siderophores of *A. vinelandii*, this poses the question, are these the primary siderophores produced by these microorganisms, or is there a larger, more effective siderophore that does not accumulate in culture fluid and is not detected? Using metal ions like molybdate to "trap" these larger siderophores could reveal the parent compound and explain more about their role in iron acquisition.

The second area where a deeper understanding of siderophores could be useful comes in the area of antibiotic development. The emergence of multiple antibiotic resistance systems in microorganisms such as *Pseudomonas* spp. has lead to the search for new classes of antibiotics and new ways to control bacteria (Miller *et al.*, 1991). A class of compounds exists that is taken up by bacteria via siderophore-mediated transport mechanisms but also has the ability to kill bacteria. Natural examples of these compounds are albomycin and ferrimycin A1 which are related to hydroxamate siderophores and ß-lactam antibiotics. Beginning in the early 1990's, attempts were made to form siderophore-drug conjugates in the hopes of utilizing siderophore-mediated uptake to transport antibiotics into bacteria, circumventing antibiotic resistance based on drug exclusion (Minnick, 1992). Once in the periplasm, the antibiotic would be free to inactivate its target after being "smuggled" into the cell as a source of iron. Diarra *et al.* (1996) tested 21 drug conjugates against 11 different types of bacteria with somewhat negative results. A similar study by Mollmann *et al.* (1998) tested 17 different siderophore-antibiotic conjugates with mixed results. In the two studies, many of the conjugates promoted the growth of the test microorganisms under iron-limited conditions, but only a few were inhibitory. In both cases the authors suggest that part of the problem with the lack of inhibitory action was the poor uptake of the conjugate into the targeted bacterium. Although the use of siderophore-antibiotic conjugates suggests a

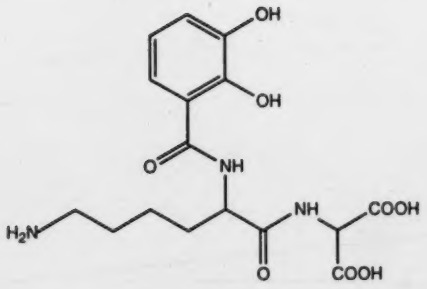

Chrysobactin

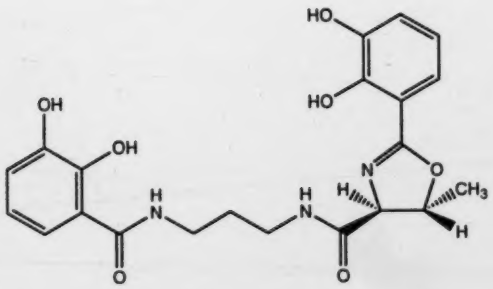

Serratiochelin

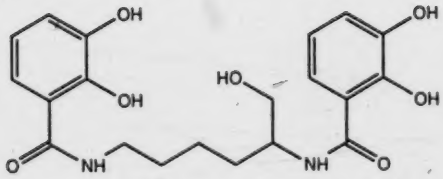

Myxochelin A

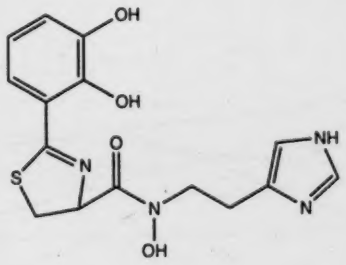

Anguibactin

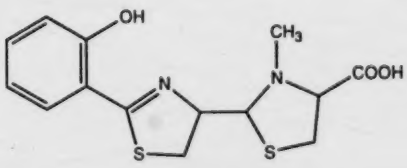

Pyochelin

Figure 4.2 Small siderophores produced by different microorganisms.

Taken from: Enard *et al.*, (1991); Jalal *et al.*, (1989); Kunze *et al.*, (1989); Ehlert *et al.*, (1994); Cox *et al.*, (1981).

promising new approach to antimicrobial therapy, it is obvious from the above studies that much work is left to be done before clinical applications for these compounds could be considered. It is only by understanding how bacteria use siderophores to acquire iron that the use of compounds such as siderophore-antibiotics conjugates will be possible.

Finally, that *A. vinelandii* appears to also use its siderophore protochelin for oxygen stress management is an example of how an microorganism can use components of one stress response system to deal with another form of environmental stress. The fact that molybdate, vanadate, tungstate, Zn^{2+}, and Mn^{2+} all inhibit ferric reductase to promote the accumulation of protochelin only leads to more questions and more experiments to be carried out in the future.

REFERENCES

Abdallah, M. A. (1991). Pyoverdins and pseudobactins. In *CRC Handbook of Microbial Iron Chelates*, pp. 139-153. Edited by G. Winkelmann. Boca Raton FL: CRC Press.

Achenbach, L. A. & Yang, W. (1997). The *fur* gene from *Klebsiella pneumoniae*: characterization, genomic organization and phylogenetic analysis. *Gene* **185**, 201-207.

Allgood, G. S. & Perry, J. J. (1985). Oxygen defense systems in obligately thermophilic bacteria. *Can J Microbiol* **31**, 1006-1010.

Altuvia, S., Almiron, M., Huisman, G., Kolter, R. & Storz, G. (1994). The *dps* promoter is activated by OxyR during growth and by IHF and σ^S in stationary phase. *Mol Microbiol* **13**, 265-272.

Armstrong, S. K., Pettis, G. S., Forrester, L. J. & McIntosh, M. A. (1989). The *Escherichia coli* enterobactin biosynthesis gene, *entD*: Nucleotide sequence and membrane localization of its product. *Mol Microbiol* **3**, 757-766.

Auling, G., Busse, H., Filz, F., Webb., Kneifel, H. & Claus, D. (1991). Rapid differentiation, by polyamine analysis, of *Xanthomonas* strains from phytopathogenic pseudomonads and other member of the class *Proteobacteria* interacting with plants. *Int J Syst Bacteriol* **41**, 223-228.

Barghouthi, S., Payne, S. M., Arceneaux, J. E. L. & Byers, B. R. (1991). Cloning, mutagenesis, and nucleotide sequence of a siderophore biosynthetic gene (*amoA*) from *Aeromonas hydrophila*. *J Bacteriol* **173**, 5121-5128.

Barnum, D. W. (1977). Spectrophotometric determination of catechol, epinephrine, DOPA, dopamine and other aromatic vic-dols. *Anal Chim Acta* **89**, 157-166.

Beauchamp, C. & Fridovich, I. (1971). Superoxide dismutase: Improved assays and an assay applicable to acrylamide gels. *Anal Biochem* **44**, 276-287.

Beyer, W. F. & Fridovich, I. (1991). *In vivo* competition between iron and manganese for occupancy of the active site region of the manganese-superoxide dismutase of *Escherichia coli*. *J Biol Chem* **266**, 303-308.

Bingle, W. H., Doran, J. L. & Page, W. J. (1984). Regular surface layer of *Azotobacter vinelandii*. *J Bacteriol* **159**, 251-259.

Bishop, P. (1993). Three genetically distinct nitrogenase systems in *Azotobacter vinelandii*. In *Iron Chelation in Plants and Soil Microorganisms*, pp. 310-324. Edited by L. Barton & B. C. Hemming. San Diego: Academic Press.

Braun, V., Gaisser, S., Herrmann, C., Kampfenkel, K., Killmann, H. & Traub, I. (1996). Energy-coupled transport across the outer membrane of *Escherichia coli:* ExbB binds ExbD and TonB *in vitro*, and leucine 132 in the periplasmic region and aspartate 25 in the transmembrane region are important for ExbD activity. *J Bacteriol* **178**, 2836-2845.

Brickman, T. J. & McIntosh, M. A. (1992). Overexpression and purification of ferric enterobactin esterase from *Escherichia coli*: Demonstration of enzymatic hydrolysis of enterobactin and its iron complex. *J Biol Chem* **267**, 12350-12355.

Briskot, G., Taraz, K. & Budzikiewicz, H. (1989). Pyoverdin-type siderophores from *Pseudomonas aeruginosa*. *Liebigs Ann Chem* 375-384.

Budwill, K., Fedorak, P. M. & Page, W. J. (1996). Anaerobic microbial degradation of poly(3-hydroxyalkanoates) with various terminal electron acceptors. *J Environ Polym Degrad* **4**, 91-102.

Carlsson, J., Nyberg, G. & Wrethen, J. (1978). Hydrogen peroxide and superoxide radical formation in anaerobic broth media exposed to atmospheric oxygen. *Appl Environ Microbiol* **36**, 223-229.

Carrano, C. J. & Raymond, K. N. (1978). Coordination chemistry of microbial iron transport compounds. 10. Characterization of the complexes of rhodotorulic acid, a dihydroxamate siderophore. *J Am Chem Soc* **100**, 5371-5374.

Chaberek, S & Martell, A. E. (1959). Organic Sequestering Agents, New York, NY:John Wiley and Sons, Inc.

Chenault, S. S. & Earhart. C. F. (1991). Organization of genes encoding membrane proteins of the *Escherichia coli* ferrienterobactin permease. *Mol Microbiol* **5**, 1405-1413.

Chenault, S. S. & Earhart. C. F. (1992). Identification of hydrophobic proteins FepD and FepG of the *Escherichia coli* ferrienterobactin permease. *J Gen Micrbiol* **138**, 2167-2171.

Christman, M. F., Morgan, R. W., Jacobson, F. S. & Ames, B. N. (1985). Positive control of a regulon for defenses against oxidative stress and some heat shock proteins in *Salmonella typhimurium*. *Cell* **41**, 753-762.

Clare, D. A., Duong, M. N., Darr, D., Archibald, F. & Fridovich, I. (1984). Effects of molecular oxygen on detection of superoxide radical with nitroblue tetrazolium and on activity stains for catalase. *Anal Biochem* **140**, 532-537.

Coffman, T. J., Cox, C. D., Edeker, B. L & Britigan, B. E. (1990). Possible role of bacterial siderophores in inflammation. Iron bound to the *Pseudomonas* siderophore pyochelin can function as a hydroxyl radical catalyst. *J Clin Invest* **86**, 1030-1037.

Cohen, G. (1994). Enzymatic/Nonenzymatic sources of oxyradicals and regulation of antioxidant defenses. *Ann New York Acad Sci* **738**, 8-14.

Corbin, J. L. & Bulen, W. A. (1969). The isolation and identification of 2,3-dihydroxybenzioc acid and 2-N,6-N-di(2,3-dihydroxybenzoyl)-L-lysine formed by iron-deficient *Azotobacter vinelandii*. *Biochemistry* **8**, 757-762.

Cornelissen, C. N. & Sparling, P. F. (1994). Iron piracy: acquisition of transferrin-bound iron by bacterial pathogens. *Mol Microbiol* **14**, 843-850.

Cotton, F. A. & Wilkinson, G. (1980). Advanced Inorganic Chemistry. A Comprehensive Text. New York: John Wiley & Sons, Inc.

Cox, C. D. (1980). Iron reductase in *Pseudomonas aeruginosa*. *J Bacteriol* **141**, 199-204.

Cox, C. D., Rinehart Jr, K. L., Moore, M. & Carter Cook Jr, J. (1981). Pyochelin: Novel structure of an iron-chelating growth promoter for *Pseudomonas aeruginosa*. *Proc Natl Acad Sci USA* **78**, 4256-4260.

Crosa, J. H. (1989). Genetics and molecular biology of siderophore-mediated iron transport in bacteria. *Microbiol Rev* **53**, 517-530.

Crumbliss, A. L. (1991). Aqueous solution equilibrium and kinetic studies of siderophore and model siderophore complexes. In *CRC Handbook of Microbial Iron Chelates*. Edited by G. Winkelmann. pp.177-233. Boca Raton FL: CRC Press.

da Silva F. & J. J. R. & Williams, R. J. P. (1991). The Biological Chemistry of the Elements. The Inorganic Chemistry of Life. Oxford: Clarendon Press.

Davies, K. J. A. & Lin, S. W. (1988). Degradation of oxidatively denatured proteins in *Escherichia coli*. *J Free Radic Biol Med* **5**, 215-223.

Deisseroth, A. & Dounce, A. L. (1970). Catalase: Physical and chemical properties, mechanism of catalysis, and physiological role. *Physiol Rev* **50**, 319-375.

de Lorenzo, V., Herrero, M., Giovannini, F. & Neilands, J. B. (1988). Fur (ferric uptake regulation) protein and CAP (catabolite-activator protein) modulate transcription of *fur* gene in *Escherichia coli*. *Eur J Biochem* **173**, 537-546.

Demple, B. (1996). Redox signaling and gene control in *Escherichia coli soxRS* oxidative stress regulon - a review. *Gene* **179**, 53-57.

de Vos, P., van Landschoot, A., Segers, P., Tytgat, R., Gillis, M., Bauwens, M., Rossau, R., Goor, M., Pot, B., Kersters, K., Lizzaraga, P. & de Ley, J. (1989). Genotypic relationships and taxonomic localization of unclassified *Pseudomonas* and *Pseudomonas*-like strains by deoxyribonucleic acid:ribosomal ribonucleic acid hybridizations. *Int J Syst Bacteriol* **39**, 35-49.

Diarra, M. S., Lavoie, M. C., Jacques, M., Darwich, I., Dolence, E. K., Dolence, J. A., Ghosh, A., Ghosh, M., Miller, M. J. & Malouin, F. (1996). Species selectivity of new siderophore-drug conjugates that use specific iron uptake for entry into bacteria. *Antimicrob Agents Chemother* **40**, 2610-2617.

DiGuiseppi, J. & Fridovich, I. (1984). The toxicity of molecular oxygen. *CRC Crit Rev Toxicol* **12**, 315-343.

Ding, H. & Demple, B. (1997). *In vivo* kinetics of a redox-regulated transcriptional switch. *Proc Natl Acad Sci USA* **94**, 8445-8449.

Doran, J. L., Bingle, W. H., & Page, W. J. (1987). Role of calcium in assembly of the *Azotobacter vinelandii* surface array. *J Gen Microbiol* **133**, 399-413.

Duhme, A. K., Hider, R. C. & Khodr, H. H. (1996). Spectrophotometric competition study between molybdate and Fe(III) hydroxide on *N,N'*-bis(2,3-dihydroxylbenzoyl)-L-lysine, a naturally occurring siderophore synthesized by *Azotobacter vinelandii*. *Biometals* **9**, 245-248.

Duhme, A. K., Hider, R. C. & Khodr, H. H. (1997). Synthesis and iron-binding properties of protochelin the tris(catecholamide) siderophore of *Azotobacter vinelandii*. *Chem Ber/Recueil* **130**, 969-973.

Duhme, A. K., Hider, R. C., Naldrett, M. J. & Pau, R. N. (1998). The stability of the molybdenum-azotochelin complex and its effect on siderophore production in *Azotobacter vinlandii*. *J Biol Inorg Chem* **3**, 520-526.

Dzwiniel, T. (1996). *Iron-limitation and oxygen stress reponse in Azotobacter vinelandii.* A.F.H.M.R. Summer Student Project, University of Alberta.

Ehlert, G., Taraz, K. & Budzikiewicz, H. (1994). Serratiochelin, a new catecholate siderophore from *Serratia marcescens. Z Naturforsch* **49**, 11-17.

Enard, C., Franza, T., Neema, C., Gill, P. R., Persmark, M., Neilands, J. B. & Expert, D. (1991). The requirement of chrysobactin dependent iron transport for virulence incited by *Erwinia chrysanthemi* on *Saintpaulia ionantha. Plant Soil* **130**, 263-271.

Escolar, L., Perez-Martin, J. & de Lorenzo, V. (1998). Coordinated repression *in vitro* of the divergent *fepA-fes* promoters of *Escherichia coli* by the iron uptake regulation (Fur) protein. *J Bacteriol* **180**, 2579-2582.

Fath, M. J. & Kolter, R. (1993). ABC transporter: bacterial exporters. *Microbiol Rev* **57**, 995-1017.

Fee, J. A. (1991). Regulation of *sod* genes in *Escherichia coli:* Relevance to superoxide dismutase function. *Mol Microbiol* **5**, 2599-2610.

Fischer, E., Strehlow, B., Harts, D. & Braun, V. (1990). Soluble and membrane-bound ferrisiderophore reductases of *Escherichia coli* K-12. *Arch Microbiol* **153**, 329-336.

Flahaut, S., Hartke, A., Giard, J., Benachour, A., Boutibonnes, P. & Auffray, Y. (1996). Relationship between stress response towards bile salts, acid and heat treatment in *Enterococcus faecalis. FEMS Microbiol Lett* **138**, 49-54.

Foster, J. W. & Hall, H. K. (1992). Effect of *Salmonella typhimurium* ferric uptake regulator (*fur*) mutations on iron- and pH-regulated protein synthesis. *J Bacteriol* **174**, 4317-4323.

Franz, T. & Expert, D. (1991). The virulence-associated chrysobactin iron uptake system of *Erwinia chrysanthemi* 3937 involved an operon encoding transport and biosynthetic functions. *J Bacteriol* **173**, 6874-6881.

Fridovich, I. (1986). Biological effects of the superoxide radical. *Arch Biochem Biophys* **247**, 1-11.

Gaines, C. G., Lodge, J. S., Arceneaux, J. E. L. & Byers, B. R. (1981). Ferrisiderophore reductase activity associated with an aromatic biosynthetic enzyme complex in *Bacillus subtilis. J Bacteriol* **148**, 527-533.

Gauda, P., Moon, N. & Weiss, B. (1997). Regulation of the *soxRS* oxidative stress regulon; Reversible oxidation of the Fe-S centers of SoxR *in vivo*. *J Biol Chem* **272**, 5082-5086.

Gauthier, M. J. & Clement, R. L. (1994). Effect of a short period of starvation in oligotrophic waters on the resistance of enteric bacterial pathogens to gastric pH conditions. *FEMS Microbiol Ecol* **14**, 275-284.

Gehring, A. M., Bradley, K. A. & Walsh, C. T. (1997). Enterobactin biosynthesis in *Escherichia coli*: Isochorismate lyase (EntB) is a bifunctional enzyme that is phosphopantetheinylated by EntD and then acylated by EntE using ATP and 2,3-dihydroxybenzoate. *Biochemistry* **36**, 8495-8503.

Gehring, A. M., Mori, I. & Walsh, C. T. (1998). Reconstitution and characterization of the *Escherichia coli* enterobactin synthetase from EntB, EntE, and EntF. *Biochemistry* **37**, 2648-2659.

George, S. E., Costenbader, C. J. & Melton, T. (1985). Diauxic growth in *Azotobacter vinelandii*. *J Bacteriol* **164**, 866-871.

Ghassemain, M. & Straus, N. A. (1996). Fur regulates the expression of iron-stress genes in the cyanobacterium *Synechococcus* sp. strain PCC 7942. *Micrbiology* **142**, 1469-1476.

Grossman, T. H., Tuckman, M., Ellestad, S. & Osburne, M. S. (1993). Isolation and characterization of *Bacillus subtilis* genes involved in siderophore biosynthesis: Relationship between *B. subtilis* spf[0] and *Escherichia coli entD* genes. *J Bacteriol* **175**, 6203-6211.

Grunden, A. M., Ray, R. M., Resentel, J. K., Healy, F. G. & Shammugam, K. T. (1996). Repression of the *Escherichia coli modABCD* (molybdate transport) operon by modE. *J Bacteriol* **178**, 735-744.

Guerinot, M. L. (1994). Microbial iron transport. *Annu Rev Microbiol* **48**, 743-772.

Gutteridge, J. M. C. (1987). Ferrous-salt-promoted damage to deoxyribose and benzoate. *Biochem J* **243**, 709-714.

Halle, F. & Meyer, J. (1992a). Ferrisiderophore reductases of *Pseudomonas*: Purification, properties and cellular location of the *Pseudomonas aeruginosa* ferripyoverdine reductase. *Eur J Biochem* **209**, 611-620.

Halle, F. & Meyer, J. (1992b). Iron release from ferrisiderophores: A multi-step mechanism involving a NADH/FMN oxidoreductase and a chemical reduction by $FMNH_2$. *Eur J Biochem* **209**, 621-627.

Hantash, F. M., Ammerlaan, M. & Earhart, C. F. (1997). Enterobactin synthase polypeptides of *Escherichia coli* are present in an osmotic shock-sensitive cytoplasmic locality. *Microbiology* **143**, 147-156.

Harris, D. C. (1982). Quantitative Chemical Analysis. San Francisco, CA: W. H. Freeman and Company.

Harris, W. R., Carrani, C. J., Cooper, S. R., Sofen, S. R., Avdeef, A. E., McArdle, J. V. & Raymond, K. N. (1979). Coordination chemistry of microbial iron transport compounds. 19. Stability constants and electrochemical behavior of ferric enterobactin and model complexes. *J Am Chem Soc* **101**, 6097-6104.

Harris, W. E. and Kratochvil, B. (1981). An Introduction to Chemical Analysis. Philadelphia, PA: Sanders College Publishing.

Hasset, D. J., Howell, M. L., Sokol, P. A., Vasil, M. L. & Dean, G. E. (1997). Fumarase C activity is elevated in response to iron deprivation and in mucoid, alginate-producing *Pseudomonas aeruginosa*: cloning and characterization of *fumC* and purification of native FumC. *J Bacteriol* **179**, 1442-1451.

Hasset, D. J., Sokol, P. A., Howell, M. L., Ma, J., Schweizer, H. T., Ochsner, U. & Vasil, M. L. (1996). Ferric uptake regulator (Fur) mutants of *Pseudomonas aeruginosa* demonstrate defective siderophore-mediated iron uptake, altered aerobic growth and decreased superoxide dismutase and catalase activities. *J Bacteriol* **178**, 3996-4003.

Hausinger, R. P. & Howard, J. B. (1983). Thiol reactivity of the nitrogenase Fe-protein from *Azotobacter vinelandii*. *J Biol Chem.* **258**, 13486-13492.

Heidinger, S., Braun, V., Pecoraro, V. L. & Raymond, K. N. (1983). Iron supply to *Escherichia coli* by synthetic analogs of enterochelin. *J Bacteriol* **153**, 109-115.

Heipieper, H. J., Meulenbeld, G., Oirschot, Q. & De Bont, J. A. M. (1996). Effect of environmental factors on the *trans/cis* ratio of unsaturated fatty acids in *Pseudomonas putida* S12. *Appl Environ Microbiol* **62**, 2773-2777.

Henikoff, S., Haughn, G. W., Calvo, J. M. & Wallace, J. C. (1988). A large family of bacterial activator proteins. *Proc Natl Acad Sci USA* **85**, 6602-6606.

Hidalgo, E. & Demple, B. (1997). Spacing of promoter elements regulates the basal expression of the *soxS* gene and converts SoxR from a transcriptional activator into a repressor. *EMBO J* **16**, 1056-1065.

Hidalgo, E., Leautaud, V. & Demple, B. (1998). The redox-regulated SoxR protein acts from a single DNA site as a repressor and an allosteric activator. *EMBO J* **17**, 2629-2936.

Hider, R. C. (1984). Siderophore mediated absorption of iron. In *Structure and Bonding: Siderophores from Microorganisms and Plants*, vol. 58., pp. 26-87. Edited by M. J. Clarke, J. A. Ibers, D. M. P. Mingos, G. A. Palmer, P. J. Sadler, & R. J. P. Williams. Berlin, Germany: Springer-Verlag.

Higgs, P. I., Myers, P. S. & Postle, K. (1998). Interactions in the TonB-dependent energy transduction complex: ExbB and ExbD form homomultimers. *J Bacteriol* **180**, 6031-6038.

Hille, R. (1996). Structrue and function of mononuclear molybdenum enzymes. *J Biol Inorg Chem* **1**, 397-404.

Hofte, M., Buysens, S., Koedam, N. & Cornelis, P. (1993). Zinc affects siderophore-mediated high affinity iron uptake systems in the rhizosphere *Pseudomonas aeruginosa* 7NSK2. *Biometals* **6**, 85-91.

Hollifield, W. C. & Neilands, J. B. (1978). Ferric enterobactin transport system in *Escherichia coli* K-12. Extraction, assay, and specificity of the outer membrane receptor. *Biochemistry* **17**, 1922-1928.

Huyer, M. & Page, W. J. (1989). Ferric reductase activity in *Azotobacter vinelandii* and its inhibition by Zn^{2+}. *J Bacteriol* **171**, 4031-4037.

Isas, J. M. & Burgess, B. K. (1994). Purification and characterization of a $NADP^+$/NADPH-specific flavoprotein that is overexpressed in FdI^- strains of *Azotobacter vinelandii*. *J Biol Chem* **269**, 19404-19409.

Isas, J. M., Yannone, S. M. & Burgess, B. K. (1995). *Azotobacter vinelandii* NADPH:ferredoxin reductase cloning, sequencing, and overexpression. *J Biol Chem* **36**, 21258-21263.

Iuchi, S. & Lin, E. C. C. (1991). Adaptation of *Escherichia coli* to respiratory conditions: regulation of gene expression. *Cell* **66**, 5-7.

Jalal, M. A. F., Hossain, M. B., van der Helm, S., Sanders-Lochr, J., Actis, L. A. & Crosa, J. H. (1989). Structure of anguibactin, a unique plasmid-related bacterial siderophore from the fish pathogen *Vibrio anguillarum*. *J Am Chem Soc* **111**, 292-296.

Ji, G. & Silver, S. (1995). Bacterial resistance mechanisms for heavy metals of environmental concern. *J Indust Microbiol* **14**, 61-75.

Jurtshuk , P., Jong-Kang, L., & Moore, E. R. B. (1984). Comparative cytochrome oxidase and superoxide dismutase analyses on strains of *Azotobacter vinelandii* and other related free-living nitrogen-fixing bacteria. *Appl Environ Microbiol* **47**, 1185-1187.

Jurtshuk, P. & Yang, T. (1980). Oxygen reactive hemoprotein components in bacterial respiratory systems. In *Diversity of Bacterial Respiratory Systems*, pp. 138-159. Edited by C. J. Knowles. Boca Raton, FL: CRC Press.

Kampfenkel, K. & Braun, V. (1992). Membrane topology of the *Escherichia coli* ExbD protein. *J Bacteriol* **174**, 5485-5487.

Kampfenkel, K. & Braun, V. (1993). Topology of the ExbB protein in the cytoplasmic membrane of *Escherichia coli*. *J Biol Chem* **8**, 6050-6057.

Ketchum, P. A. & Owens, M. S. (1975). Production of a molybdenum-coordinating compound by *Bacillus thuringiensis*. *J Bacteriol* **122**, 412-417.

Khan, A. U., di Mascio, P., Medeiros, M. H. G. & Wilson, T. (1992). Spermine and spermidine protection of plasmid DNA against single-strand breaks induced by singlet oxygen. *Proc Natl Acad Sci USA* **89**, 11428-11430.

Knosp, O., von Tigerstrom, M. & Page, W. J. (1984). Siderophore-mediated uptake of iron in *Azotobacter vinelandii*. *J Bacteriol* **159**, 341-347.

Korbashi, P., Kohen, R., Katzhendler, J. & Chevion, M. (1986). Iron mediates paraquat toxicity in *Escherichia coli*. *J Biol Chem* **261**, 12472-12476.

Koval, S. F. (1988). Paracrystalline protein surface arrays on bacteria. *Can J Microbiol* **34**, 407-414.

Kow, Y. W. & Burris, R. H. (1984). Purification and properties of membrane-bound hydrogenase from *Azotobacter vinelandii*. *J Bacteriol* **159**, 564-569.

Krebs, K. G., Heusser, D. & Wimmer, H. (1969). Spray reagents. In *Thin Layer Chromatography: A Laboratory Handbook*, pp. 854-909. Edited by E. Stahl. New York: Springer Verlag

Kunze, B., Bedorf, N., Kohl, W., Hofle, G. & Reichenbach, H. (1989). Myxochelin A, a new iron-chelating compound from *Angiococcus disciformis* (Myxobacterales). Production, isolation, physio-chemical and biological properties. *J Antibiotics* **42**, 14-17.

Lambalot, R. H., Gehring, A. M., Flugel, R. S., Zuber, P., LaCelle, M., Marahiel, M. A., Reid, R., Khosla, C. & Walsh, C. T. (1996). A new enzyme superfamily - the phosphopantetheinyl transferases. *Chem Biol* **3**, 923-936.

Larsen, R. A., Foster-Hartnett, D., McIntosh, M. A. & Postle, K. (1997). Regions of *Escherichia coli* TonB and FepA proteins essential for *in vivo* physical interactions. *J Bacteriol* **179**, 3213-3221.

Larsen, R. A., Myers, P. S., Skare, J. T. Seachord, C. L., Darveau, R. P. & Postle K. (1996). Identification of TonB homologs in the family *Enterobacteriaceae* and evidence for conservation of TonB-dependent energy transduction complexes. *J Bacteriol* **178**, 1363-1373.

Lee, S. Y. (1995). Bacterial polyhydroxyalkanoates. *Biotechnol Bioeng* **49**, 2-14.

Letain, T. E. & Postle, K. (1997). TonB protein appears to transduce energy by shuttling between the cytoplasmic membrane and the outer membrane in *Escherichia coli*. *Mol Microbiol* **24**, 271-283.

Li, Z. & Demple, B. (1996). Sequence specificity for DNA binding by *Escherichia coli* SoxS and Rob proteins. *Mol Microbiol* **20**, 937-945.

Liochev, S. I., Hausladen, A., Beyer Jr., W. F. & Fridovich, I. (1994). NADPH:ferredoxin oxidoreductase acts as a paraquot diaphorase and is a member of the *soxRS* regulon. *Proc Natl Acad Sci USA* **91**, 1328-1331.

Liu, J. K., Lee, F. T., Lin, C. S., Yao, X. T., Davenport, J. W. & Wong, T. Y. (1995). Alternative function of the electron transport system in *Azotobacter vinelandii*: removal of excess reductant by the cytochrome *d* pathway. *Appl Environ Microbiol* **61**, 3998-4003.

Liu, J., Quinn, N., Berchtold, G. A. & Walsh, C. T. (1990). Overexpression, purification, and characterization of isochorismate synthase (EntC), the first enzyme involved in the biosynthesis of enterobactin from chorismate. *Biochem* **29**, 1417-1425.

Lodge, J. S., Gaines, C. G., Arceneaux, J. E. L. & Byers, B. R. (1980). Non-hydrolytic release of iron from ferrienterobactin analogs by extracts of *Bacillus subtilis*. *Biochem Biophys Res Commun* **97**, 1291-1295.

Lodge, J. S., Gaines, C. G., Arceneaux, J. E. L. & Byers, B. R. (1982). Ferrisiderophore reductase activity in *Agrobacterium tumefaciens*. *J Bacteriol* **149**, 771-774.

Loomis, D. L. & Raymond, K. N. (1991). Solution equilibria of enterobactin and metal-enterobactin complexes. *Inorg Chem* **30**, 906-911.

Lowry, O. H., Rosebrough, N. J., Farr, A. L. & Randall, R. J. (1951). Protein measurement with the folin phenol reagent. *J Biol Chem* **193**, 265-275.

Ma, D., Cook, D. N., Alberti, M., Pon, N. P., Nikaido, H. & Hearst, J. E. (1995). Genes *arcA* and *acrB* encode a stress-induced efflux system of *Escherichia coli*. *Mol Micrbiol* **16**, 45-55.

Maldonado, R., Jimenez, J. & Casadesus, J. (1994). Changes in ploidy during the *Azotobacter vinelandii* growth cycle. *J Bacteriol* **176**, 3911-3919.

Manna, A. C. & Das, H. K. (1993). Determination of the size of the *Azotobacter vinelandii* chromosome. *Mol Gen Genet* **241**, 719-722.

McCormick, M. L., Buettner, G. R. & Britigan, B. E. (1998). Endogenous superoxide dismutase levels regulate iron-dependent hydroxyl radical formation in *Escherichia coli* exposed to hydrogen peroxide. *J Bacteriol* **181**, 622-625.

Mehrotra, M. (1997). *Role of iron in the regulation of phenylalanyl-tRNA synthetase activity in* Azotobacter vinelandii. PhD Thesis, University of Alberta.

Menon, A. L. & Robson, R. L. (1994). *In vivo* and *in vitro* nickel-dependent processing of the [NiFe] hydrogenase in *Azotobacter vinelandii*. *J Bacteriol* **176**, 291-295.

Merck Index. An Encyclopedia of Chemicals, Drugs, and Biologicals. Eleventh Edition, (1989). Edited by S. Budavari, M. J. O'Neil, A. Smith & P. E. Heckeman. Rahway, NJ: Merck and Co.

Miller, M. J., Mckee, J. A., Minnick, A. A. & Dolence, K. (1991). The design, synthesis and study of siderophore-antibiotic conjugates. *Biometals* **4**, 62-69.

Minnick, A. A., Mckee, J. A., Dolence, K. & Miller, M. J. (1992). Iron transport-mediated antibacterial activity of and development of resistance to hydroxamate and catechol siderophore-carbacephalosporin conjugates. *Antimicrob Agents Chemother* **36**, 840-850.

Miyamoto, K., Kanaya, S., Morikawa, K. E. & Inokuchi, H. (1994). Overproduction, purification, and characterization of ferrochelatase from *Escherichia coli*. *J Biochem* **115**, 545-551.

Moeck, G. S. & Coulton, J. W. (1998). TonB-dependent iron acquisition: mechanisms of siderophore-mediated active transport. *Mol Micrbiol* **28**, 675-681.

Mollmann, U., Ghosh, A., Dolence, E. K., Dolence, J. A., Ghosh, M., Miller, M. J. & Reissbrodt, R. (1998). Selective growth promotion and growth inhibition of gram-negative and gram-positive bacteria by synthetic siderophore-ß-lactam conjugates. *Biometals* **11**, 1-12.

Moreno, J., Gonzalez-Lopez, J. & Vela, G. R. (1986). Survival of *Azotobacter* spp. in dry soils. *Appl Environ Microbiol* **51**, 123-125.

Morgan, T. V., Lundell, D. J. & Burgess, B. K. (1988). *Azotobacter vinelandii* ferredoxin I: cloning, sequencing, and mutant analysis. *J Biol Chem* **263**, 1370-1375.

Moshiri, F., Kim, J. W., Fu, C. & Maier, R. J. (1994). The FeSII protein of *Azotobacter vinelandii* is not essential for aerobic nitrogen fixation, but confers significant protection to oxygen-mediated inactivation of nitrogenase *in vitro* and *in vivo*. *Mol Microbiol* **14**, 101-114.

Mouncey, N. J., Mitchenall, L. A. & Pau, R. N. (1995). Mutational analysis of genes of the *mod* locus involved in molybdenum transport, homeostasis, and processing in *Azotobacter vinelandii*. *J Bacteriol* **177**, 5294-5302.

Mukhopadhyay, S. & Schellhorn, H. E. (1997). Identification and characterization of hydrogen peroxide-sensitive mutants of *Escherichia coli*: Genes that require OxyR for expression. *J Bacteriol* **179**, 330-338.

Neilands, J. B. (1992). Mechanism and regulation of synthesis of aerobactin in *Escherichia coli* K12 (pColV-K30). *Can J Microbiol* **38**, 728-733.

Neilands, J. B. (1994). Effects of iron deprivation on outer membrane protein expression. In *Methods of Enzymology: Bacterial pathogenesis. Part A; Identification and regulation of virulence factors*, vol. 235., pp. 344-352. Edited by V. L. Clark & P. M. Bavoil. New York: Academic Press.

Niederoffer, E. C., Naranjo, C. M., Bradley, K. L. & Fee, J. A. (1990). Control of *Escherichia coli* superoxide dismutase (*sodA* and *sodB*) genes by ferric uptake regulation (*fur*) locus. *J Bacteriol* **172**, 1930-1938.

Nunoshiba, T. (1996). Two-stage gene regulation of the superoxide stress response *soxRS* system in *Escherichia coli*. *Crit Rev Euk Gene Express* **4**, 377-389.

Oberley, L. W. & Spitz, D. R. (1985). Nitroblue tetrazolium. In *CRC Handbook of Methods for Oxygen Radical Research*, pp. 217-220. Edited by R. A. Greenwald. Boca Raton, FL: CRC Press.

O'Sullivan, D. J., Morris, J. & O'Gara, F. (1990). Identification of an additional ferric-siderophore uptake gene clustered with receptor, biosynthesis, and *fur*-like regulatory genes in fluorescent *Pseudomonas* sp. strain M114. *Appl Environ Microbiol* **56**, 2056-2064.

Ozenberger, B. A., Brickman, T. L. & McIntosh, M. A. (1989). Nucleotide sequence of *Escherichia coli* isochorismate synthetase gene *entC* and evolutionary relationship or isochorismate synthetase and other chorismate-utilizing enzymes. *J Bacteriol* **171**, 775-783.

Ozenberger, B. A., Nahlik, M. S. & McIntosh, M. A. (1987). Genetic organization of multiple *fep* genes encoding ferric enterobactin transport functions in *Escherichia coli*. *J Bacteriol* **169**, 3639-3646.

Page, W. J. (1982). Optimal conditions for induction of competence in nitrogen-fixing *Azotobacter vinelandii*. *Can J Microbiol* **28**, 389-397.

Page, W. J. (1983). Formation of cystlike structures by iron-limited *Azotobacter vinelandii* strain UW during prolonged storage. *Can J Microbiol* **29**, 1111-1118.

Page, W. J. (1985). Genetic transformation of molybdenum-starved *Azotobacter vinelandii*: increased transformation frequency and recipient range. *Can J Microbiol* **31**, 659-662.

Page, W. J. (1992). Production of poly-ß-hydroxybutyrate by *Azotobacter vinelandii* UWD in media containing sugars and complex nitrogen sources. *Appl Microbiol Biotechnol* **38**, 117-121.

Page, W. J. (1993). Growth conditions for the demonstration of siderophores and iron-repressible outer membrane proteins in soil bacteria, with an emphasis on free-living diazotrophs. In *Iron Chelation in Plants and Soil Microorganisms*, pp. 75-110. Edited by L. L. Barton & B. C. Hemmings. New York: Academic Press.

Page, W. J. (1995). The effect of manganese oxides and manganese ion on growth and siderophore production by *Azotobacter vinelandii*. *Biometals* **8**, 30-36.

Page, W. J. & Collinson, K. (1982). Molybdenum enhancement of nitrogen fixation in Mo-starved *Azotobacter vinelandii* Nif⁻ mutant. *Can J Microbiol* **28**, 1173-1180.

Page, W. J., Collinson, K., Demange, P., Dell, A. & Abdallah, M. A. (1991). *Azotobacter vinelandii* strains of disparate origin produce azotobactin siderophores with identical structures. *Biometals* **4**, 217-222.

Page, W. J. & Doran, J. L. (1981). Recovery of competence in calcium-limited *Azotobacter vinelandii*. *J Bacteriol* **146**, 33-40.

Page, W. J. & Huyer, M. (1984). Derepression of the *Azotobacter vinelandii* siderophore system using iron-containing minerals to limit iron repletion. *J Bacteriol* **158**, 496-502.

Page, W. J. & Knosp, O. (1989). Hyperproduction of poly-ß-hydroxybutyrate during exponential growth of *Azotobacter vinelandii* UWD. *J Bacteriol* **55**, 1334-1339.

Page, W. J. & Shivprasad, S. (1995). Iron binding to *Azotobacter salinestris* melanin, iron mobilization and uptake mediated by siderophores. *Biometals* **8**, 59-64.

Page, W. J. & von Tigerstrom, M. (1982). Iron- and molybdenum-repressible outer membrane proteins in competent *Azotobacter vinelandii*. *J Bacteriol* **151**, 237-242.

Page, W. J. & von Tigerstrom, M. (1988). Aminochelin, a catecholamine siderophore produced by *Azotobacter vinelandii*. *J Gen Microbiol* **134**, 453-460.

Pannekoek, Y., Van Putten, J. & Dankert, J. (1992). Identification and molecular analysis of a 63-kilodalton stress protein from *Neisseria gonorrhoeae*. *J Bacteriol* **174**, 6928-6937.

Patel, U., Baxi, M. D. & Modi, V. V. (1988). Evidence for the involvement of iron siderophore in the transport of molybdenum in cowpea *Rhizobium*. *Curr Microbiol* **17**, 179-182.

Pau, R. N., Mitchenall, L. A. & Robson, R. L. (1989). Genetic evidence for an *Azotobacter vinelandii* nitrogenase lacking molybdenum and vanadium. *J Bacteriol* **171**, 124-129.

Pienkos, P. T. & Brill, W. J. (1981). Molybdenum accumulation and storage in *Klebsiella pneumoniae* and *Azotobacter vinelandii*. *J Bacteriol* **145**, 743-751.

Pierce, J. R. & Earhart, C. F. (1986). *Escherichia coli* K-12 envelope proteins specifically required for ferrienterobactin uptake. *J Bacteriol* **166**, 930-936.

Poole, K., Heinrichs, D. E. & Neshat, S. (1993a). Cloning and sequence analysis of an EnvCD homologue in *Pseudomonas aeruginosa*: regulation by iron and possible involvement in the secretion of the siderophore pyoverdine. *Mol Micrbiol* **10**, 529-544.

Poole, K., Krebes, K., McNally, C. & Neshat, S. (1993b). Multiple antibiotic resistance in *Pseudomonas aeruginosa*: evidence for involvement of an efflux operon. *J Bacteriol* **175**, 7363-7372.

Poole, K., Zhao, Q., Neshat, S., Heinrichs, D. E. & Dean, C. R. (1996). The *Pseudomonas aeruginosa tonB* gene encodes a novel TonB protein. *Microbiol* **142**, 149-1458.

Pope, M. T., Still, E. R. & Williams, R. J. P. (1980). A comparison between the chemistry and biochemistry of molybdenum and related elements. In *Molybdenum and molybdenum-containig enzymes*, pp. 3-40. Edited by M. P. Coughlan. New York: Pergamon Press.

Postle, K. (1993). TonB protein and energy transduction between membranes. *J Bioenerg Biomembr* **25**, 591-601.

Premakumar, R., Jacoitz, S., Ricke, S. C. & Bishop, P. E. (1996). Phenotypic characterization of a tungsten-tolerant mutant of *Azotobacter vinelandii*. *J Bacteriol* **178**, 691-696.

Reid, R. T., Live, D. H., Faulkner D. J. & Butler, A. (1993). A siderophore from a marine bacterium with an exceptional ferric ion affinity constant. *Nature* **336**, 455-458.

Robson, R. L. & Postgate, J. R. (1980). Oxygen and hydrogen in biological nitrogen fixation. *Annu Rev Microbiol* **34**, 183-207.

Rosentel, J. K., Healy, F., Maupin-Furlow, J. A., Lee, J. H. & Shanmugam, K. T. (1995). Molybdate and regulation of *mod* (molybdate transport), *fdhF*, and *hyc* (formate dehydrogenlyase) operons in *Escherichia coli*. *J Bacteriol* **177**, 4857-4864.

Rowland, B. M. & Taber, H. W. (1996). Duplicate isochorismate synthase genes of *Bacillus subtilis*: regulation and involvement in the biosyntheses of menaquinone and 2,3-dihydroxybenzoate. *J Bacteriol* **178**, 854-861.

Rusnak, F., Faraci, W. S. & Walsh, C. T. (1989). Subcloning, expression, and purification of the enterobactin biosynthetic enzyme 2,3-dihydroxybenzoate-AMP ligase: demonstration of enzyme-bound (2,3-dihydroxybenzoyl)adenylate product. *Biochemistry* **28**, 6827-6835.

Rusnak, F., Liu, J., Quinn, N., Berchold, G. A. & Walsh, C. T. (1990). Subcloning of the enterobactin biosynthetic gene *entB*: expression, purification, characterization, and substrate specificity of isochorismatase. *Biochemistry* **29**, 1425-1435.

Rusnak, F., Sakaitani, M., Drueckhammer, D., Reichert, J. & Walsh, C. T. (1991). Biosynthesis of the *Escherichia coli* siderophore enterobactin: sequence of the *entF* gene, expression and purification of EntF, and analysis of covalent phosphopantetheine. *Biochemistry* **30**, 2916-2927.

Sadoff, H. L. (1975). Encystment and germination in *Azotobacter vinelandii*. *Bacteriol Rev* **39**, 516-539.

Sadoff, H. L., Shimel, B. & Ellis, S. (1979). Characterization of *Azotobacter vinelandii* deoxyribonucleic acid and folded chromosomes. *J Bacteriol* **138**, 871-877.

Saxena, B., Vithlani, L. & Modi, V. V. (1989). Siderophore-mediated transport of molybdenum in *Azospirillum lipoferum* strain D-2. *Curr Microbiol* **19**, 291-295.

Scarrow, R. C., Ecker, D. J., Ng, C., Liu, S. & Raymond, K. N. (1991). Iron (III) coordination chemistry of linear dihydroxyserine compounds derived from enterobactin. *Inorg Chem* **30**, 900-906.

Schramm, E., Mende, J., Braun, V. & Kamp, R. M. (1987). Nucleotide sequence of the colicin B activity gene *cba*: Consensus pentapeptide among TonB-dependent colicins and receptors. *J Bacteriol* **169**, 3350-3357.

Schwyn, B. & Neilands, J. B. (1997). Universal chemical assay for detection and determination of siderophores. *Anal Biochem* **160**, 47-56.

Sevinc, M. S. & Page, W. J. (1992). Generation of *Azotobacter vinelandii* strains defective in sideophore production and characterization of a strain unable to produce known siderophores. *J Gen Microbiol* **138**, 587-596.

Shah, W. K., Ugalde, R. A., Imperial, J. & Brill, W. (1984). Molybdenum in nitrogenase. *Annu Rev Biochem* **53**, 231-257.

Sharpe, A. (1999). *Characterization of a gene required for catecholate siderophore biosynthesis in* Azotobacter vinelandii. MSc Thesis, University of Alberta.

Shea, C. M. & McIntosh, M. A. (1991). Nucleotide sequence and genetic organization of the ferric enterobactin transport system: homology to other periplasmic binding protein-dependent systems in *Escherichia coli*. *Mol Microbiol* **6**, 1415-1428.

Shivprasad, S. & Page, W. J. (1989). Catechol formation and melanization by Na^+-dependent *Azotobacter chroococcum*: a protective mechanism for aeroadaptation? *Appl Environ Microbiol* **55**, 1811-1817.

Silva, M. J. & Wong, J. L. (1995). Electrochemical bioassay system. Redox responses of *Escherichia coli* cultures to environmental stresses. *Bioelectrochem Bioenerg* **37**, 141-148.

Silver, S. & Walderhaug, M. (1992). Gene regulation of plasmid- and chromosome-determined inorganic ion transport in bacteria. *Microbiol Rev* **56**, 195-228.

Sinha, A. K. (1972). Colormetric assay of catalase. *Anal Biochem* **47**, 389-394.

Skare, J. T., Ahmer, B. M. M., Seachord, C. L., Darveau, R. P. & Postle, K. (1993). Energry transduction between membranes: TonB, a cytoplasmic membrane protein, can be chemically cross-linked *in vivo* to the outer membrane receptor FepA. *J Biol Chem* **22**, 16302-16308.

Sleytr, U. B. & Messner, P. (1988). Crystalline surface layers in prokaryotes. *J Bacteriol* **170**, 2891-2897.

Staab, J. F. & Earhart, C. F. (1990). EntG activity of *Escherichia coli* enterobactin synthetase. *J Bacteriol* **172**, 6403-6410.

Stephens, D. L., Choe, M. D., & Earhart, C. F. (1995). *Escherichia coli* periplasmic protein FepB binds ferrienterobactin. *Microbiology* **141**, 1647-1654.

Stevenson, L. H. & Socolosky, M. D. (1966). Cyst formation and poly-ß-hydroxybutyric acid accumulation in *Azotobacter*. *J Bacteriol* **91**, 304-310.

Stookey, L. L. (1970). Ferrozine-a new spectrophotometric reagent for iron. *Anal Chem* **42**, 779-781.

Swenson, G. R., Patino, M. M., Beck, M. M., Gaffield, L. & Walden, W. E. (1991). Characterstics of the interaction of the ferritin repressor protein with the iron-responsive element. *Biometals* **4**, 48-55.

Tabor, C. W. & Tabor, H. (1985). Polyamines in microorganisms. *Microbiol Rev* **49**, 81-99.

Taraz, K., Ehlert, G., Geisen, K., Budzikiewicz, H., Korth, H. & Pulverer, G. (1990). Protochelin, ein catecholat-siderophor aus einem bakterium (DMS Nr. 5746). *Z. Naturforsch* **45b**, 1327-1332.

Tchan, Y. (1984). Family II. *Azotobacteraceae* pribram 1933. In *Bergey's Manual of Systematic Bacteriology*, vol 1., pp. 219-220. Edited by N. R. Krieg & J. G. Holt. Baltimore:Williams & Wilkins.

Tchan, Y. & New, P. B. (1984). Genus I. Azotobacter Beijerinck 1901, 567. In *Bergey's Manual of Systematic Bacteriology*, vol 1., pp. 220-229. Edited by N. R. Krieg & J. G. Holt. Baltimore:Williams & Wilkins.

Terzaghi, B. E. (1980). Ultraviolet sensitivity and mutagenesis of *Azotobacter*. *J Gen Microbiol* **118**, 271-273.

Thomas, C. E. & Sparling, P. F. (1996). Isolation and analysis of a *fur* mutant of *Neisseria gonorrhoeae*. *J Bacteriol* **178**, 4224-4232.

Torsvik, V., Sorheim, R. & Goksoyr, J. (1996). Total bacterial diversity in soil and sediment communities-a review. *J Indust Micriobiol* **17**, 170-178.

Tufano, T. P. & Raymond, K. N. (1981). Coordination chemistry of microbial iron transport compounds. 21. Kinetics and mechanism of iron exchange in hydroxamate siderophore complexes. *J Am Chem Soc* **103**, 6617-6624.

Walmsley, J. & Kennedy, C. (1991). Temperature-dependent regulation by molybdenum and vanadium of expression of the structural genes encoding three nitrogenases in *Azotobacter vinelandii*. *J Bacteriol* **57**, 622-624.

Wiggerich, H., Klauke, B., Koplin, R., Priefer, U. B. & Puhler, A. (1997). Unusual structure of the *tonb-exb* DNA region of *Xanthomonas campestris* pv. campestris: *tonB*, *exbB*, and *exbD1* are essential for ferric iron uptake, but *exbD2* is not. *J Bacteriol* **179**, 7103-7110.

Woolridge, K. G., Williams, P. H. & Ketley, J. M. (1994). Iron-responsive genetic regulation in *Campylobacter jejuni*: cloning and characterization of a *fur* homolog. *J Bacteriol* **176**, 5852-5856.

Wrigley-Jones, C. A., Richards, H., Thomas, C. & Ward, J. (1993). Stability of plasmid vector pIJ303 in *Streptomyces lividans* TK24 during laboratory-scale fermentations. *Biotechnol Bioeng* **41**, 148-155.

Wyckoff, E. E., Stoebner, J. A., Reed, K. E. & Payne, S. M. (1997). Cloning of a *Vibrio cholerae* vibriobactin gene cluster: identification of genes required for early steps in siderophore biosynthesis. *J Bacteriol* **179**, 7055-7062.

Yannone, S. M. & Burgess, B. K. (1998). The seven-iron FdI from *Azotobacter vinelandii* regulates the expression of NADPH:ferredoxin reductase via an oxidative stress response. *J Biol Inorg Chem* **3**, 253-258.

Yamashita, Y., Takehara, T. & Kuramitsu, H. K. (1993). Molecular characterization of a *Streptococcus mutans* mutant altered in environmental stress responses. *J Bacteriol* **175**, 6220-6228.

APPENDIX 1 - Sample Calculations

1. Sample calculation of conditional formation constants (K_{Form}). These calculations were done with an individual datum value to show how derived values were found. Values reported in this thesis were calculated with averages of multiple determinations. Similar calculations done for the determination of the affinity of a siderophore for molybdate.

A) Ferric-protochelin in competition with EDTA (4 to 1 $Fe^{3+}PC^{A}$ to EDTA).

Ferric-Protochelin formation reaction: $PC + Fe^{3+} \leftrightarrows Fe3^{+}PC$

Reaction Tested:	PC +	Fe^{3+}EDTA $\leftrightarrows$	Fe^{3+}PC +	EDTA
[Initial] (M)			$1.00*10^{-4}$	$4.00*10^{-4}$
[Equilibrium] (M)	$(5.06*10^{-6})^{B}$	$(5.06*10^{-6})^{B}$	$(9.49*10^{-5})^{C}$	$(3.94*10^{-4})^{B}$

$K_{Form} = ([Fe^{3+}PC] * [EDTA] / [PC] * [Fe^{3+}EDTA])$

$K_{Form} = 1.45*10^{3}$ $\quad Log_{10}K_{Form} = 3.16$

$K_{Fe\text{-}Sid} = K_{Fe\text{-}EDTA} * K_{Form}$ (Equation 3, Section 1.4.4)

$K_{Fe\text{-}Sid} = (10^{21.80})^{D} * 10^{3.16}$

$K_{Fe\text{-}Sid} = 10^{24.97}$ $\quad Log_{10}K_{Fe\text{-}Sid} = 24.97$

A. PC = protochelin

B. Detected $[Fe^{3+}PC]_{Equil}$ in assay, the difference between $[Fe^{3+}PC]_{Init}$ and $[Fe^{3+}PC]_{Equil}$ represents the amount of $Fe^{3+}PC$ lost in competition with EDTA. This is also the amount of EDTA consumed in the formation of Fe^{3+}EDTA and the [PC] that is unbound at equilibrium.

C. A_{500} of reaction mixture at 96 hr: 0.298, gives a concentration of $9.49*10^{-5}$ M from a calibration curve of ferric-protochelin.

D. Formation constant of Fe-EDTA from Harris (1982).

B) Ferric-azotochelin in competition with EDTA (4 to 1 $(Fe^{3+})_2AzC_3$[A] to EDTA).

Ferric-azotochelin formation reaction: $3AzC + 2Fe^{3+} + \leftrightarrows (Fe^{3+})_2AzC_3$

Reaction Tested:	$3AzC$ +	$2Fe^{3+}EDTA$ $\leftrightarrows$	$(Fe^{3+})_2AzC_3$	$+2EDTA$
[Initial] (M)			$5.00*10^{-5}$	$2.00*10^{-4}$
[Equilibrium] (M)	$(6.33*10^{-5})^B$	$(4.22*10^{-5})^B$	$(2.89*10^{-5})^C$	$(1.58*10^{-4})^B$

$K_{Form} = ([(Fe^{3+})_2AzC_3] * [EDTA]^2 / [AzC]^3 * [Fe^{3+}EDTA]^2)$

$K_{Form} = 1.58*10^9$ $\quad Log_{10}K_{Form} = 9.20$

$K_{Fe\text{-}Sid} = K_{Fe\text{-}EDTA} * K_{Form}$ (Equation 3, Section 1.4.4)

$K_{Fe\text{-}Sid} = (10^{43.60})^D * 10^{9.20}$

$K_{Fe\text{-}Sid} = 10^{52.80}$ $\quad Log_{10}K_{Fe\text{-}Sid} = 52.80$

A. AzC = azotochelin

B. Detected $[(Fe^{3+})_2AzC_3]_{Equil}$ in assay, the difference between $[(Fe^{3+})_2AzC_3]_{Init}$ and $[(Fe^{3+})_2AzC_3]_{Equil}$ represents the amount of $(Fe^{3+})_2AzC_3$ lost in competition with EDTA when stoichiometric equivalents are considered. This is also the amount of EDTA consumed in the formation of $Fe^{3+}EDTA$ and the [AzC] that is unbound at equilibrium when stoichiometric equivalents are considered.

C. A_{570} of reaction mixture at 96 hr: 0.209, gives a concentration of $2.89*10^{-5}$ M from a calibration curve of ferric-azotochelin.

D. Formation constant of Fe-EDTA from Harris (1982) is squared because 2 $Fe^{3+}EDTA$ are required to balance equation.

C) Ferric-aminochelin in competition with EDTA (4 to 1 $Fe^{3+}AmC_3$[A] to EDTA).

Ferric-aminochelin formation reaction: $3AmC + Fe^{3+} \leftrightharpoons Fe^{3+}AmC_3$

Reaction Tested:	$3AmC +$	$Fe^{3+}EDTA$	$\leftrightharpoons$	$Fe^{3+}AmC_3 +$	EDTA
[Initial] (M)				$1.00*10^{-4}$	$4.00*10^{-4}$
[Equilibrium] (M)	$(1.58*10^{-4})^B$	$(5.26*10^{-5})^B$		$(4.74*10^{-5})^C$	$(3.47*10^{-4})^B$

$K_{Form} = ([Fe^{3+}AmC_3] * [EDTA] / [AmC]^3 * [Fe^{3+}EDTA])$

$K_{Form} = 7.94*10^7$ $\quad Log_{10}K_{Form} = 7.90$

$K_{Fe\text{-}Sid} = K_{Fe\text{-}EDTA} * K_{Form}$ (Equation 3, Section 1.4.4)

$K_{Fe\text{-}Sid} = (10^{21.80})^D * 10^{7.90}$

$K_{Fe\text{-}Sid} = 10^{29.70}$ $\quad Log_{10}K_{Fe\text{-}Sid} = 29.70$

A. AmC = aminochelin.

B. Detected $[Fe^{3+}AmC_3]_{Equil}$ in assay, the difference between $[Fe^{3+}AmC_3]_{Init}$ and $[Fe^{3+}AmC_3]_{Equil}$ represents the amount of $Fe^{3+}AmC_3$ lost in competition with EDTA when stoichiometric equivalents are considered. This is also the amount of EDTA consumed in the formation of $Fe^{3+}EDTA$ and the [AmC] that is unbound at equilibrium when stoichiometric equivalents are considered.

C. A_{500} of reaction mixture at 96 hr: 0.146, gives a concentration of $4.47*10^{-5}$ M from a calibration curve of ferric-aminochelin.

D. Formation constant of Fe-EDTA from Harris (1982).

2. Sample calculation of free iron in the system of Harris *et al.*(1979). Calculations were done with an individual datum value to show how derived values were found. Values reported in this thesis were calculated using averages of multiple determinations. Similar calculations were done for the determination of free molybdate in the system of Harris *et al.* (1979).

A) Free iron in ferric-aminochelin equilibrium.

Ferric-aminochelin $K_{Form\ pH\ 7.0} = 10^{29.70}$

Calculate fraction of aminochelin fully deprotonated at pH 7.0 (Harris, 1982):

$\alpha_{AmC} = ((K_1K_2) / (\Sigma([H^+]^2 + K_1[H^+]^1 + K_1K_2)))^A$

$\alpha_{AmC} = (10^{-20.5}) / (10^{-14} + 10^{-15.4} + 10^{-20.5})$

$\alpha_{AmC} = 3.02*10^{-7}$

$K_{Form\ Independent} = K_{Form\ pH\ 7.0} / \alpha_{AmC}$ (Equation 5, Section 1.4.4)

$K_{Form\ Independent} = 10^{29.70} / 3.02*10^{-7}$ $K_{Form\ Independent} = 1.566*10^{36}$ $Log_{10} K_{Form} = 36.22$

The free metal system in Harris *et al.* (1979) is defined as $[Fe^{3+}]_{Init} = 1*10^{-6}$ M and $[siderophore]_{Init} = 1*10^{-5}$ M at pH 7.4, thus, needed to calculate conditional formation constant for ferric-aminochelin at pH 7.4. This was done using Equation 5 above and α_{AmC} at pH 7.4 of $2.00*10^{-6}$. From this the $K_{Form\ pH\ 7.4}$ of ferric aminochelin was found to be $3.17*10^{30}$.

Reaction tested:	3AmC	+	Fe^{3+}	⇆	$Fe^{3+}AmC_3$
[Initial]	$1*10^{-5}$ M		$1*10^{-6}$ M		
[Equilibrium]	$(1*10^{-5} - 3*10^{-6})^B$ M		X		$(1*10^{-6})^B$ M

$K_{Form} = [Fe^{3+}AmC_3] / ([AmC]^3 * [Fe^{3+}])$ Solve for $[Fe^{3+}] = X$

$[Fe^{3+}] = [Fe^{3+}AmC_3] / ([AmC]^3 * K_{Form})$ $[Fe^{3+}] = 1.0*10^{-6} / ((7.0*10^{-6})^3 * 3.17*10^{30})$

$[Fe^{3+}] = 9.19*10^{-22}$ $-(Log_{10}[Fe^{3+}]) = 21.0$

A. Where K_1 and K_2 are the dissociation constants of the protons of the catechol moieties of aminochelin. $K_1 = 10^{-12.1}$ and $K_2 = 10^{-8.4}$ (Loomis and Raymond, 1991), pH = 7, $[H^+] = 10^{-7}$

B. Due to high affinity of siderophore for iron (III), assume all of iron (III) consumed.

B) Free iron in ferric-azotochelin equilibrium.

Ferric-azotochelin $K_{Form\ pH\ 7.0} = 10^{52.80}$

Calculate fraction of azotochelin fully deprotonated at pH 7.0 (Harris, 1982):

$\alpha_{AzC} = ((K_1K_2K_3K_4K_5) / (\Sigma([H^+]^5 + K_1[H^+]^4 + K_1K_2[H^+]^3 ..... K_1K_2K_3K_4K_5)))^A$

$\alpha_{AzC} = 2.24*10^{-10}$

$K_{Form\ Independent} = K_{Form\ pH\ 7.0} / \alpha_{AzC}$ (Equation 5, Section 1.4.4)

$K_{Form\ Independent} = 10^{52.80} / 2.24*10^{-10}$ $K_{Form\ Independent} = 2.82*10^{62}$ $Log_{10} K_{Form} = 62.45$

The free metal system in Harris *et al.* (1979) is defined as $[Fe^{3+}]_{Init} = 1*10^{-6}$ M and $[siderophore]_{Init} = 1*10^{-5}$ M at pH 7.4, thus, needed to calculate conditional formation constant for ferric-azotochelin at pH 7.4. This was done using Equation 5 above and α_{AzC} at pH 7.4 of $2.28*10^{-8}$. From this the $K_{Form\ pH\ 7.4}$ of ferric-azotochelin was found to be $6.43*10^{54}$.

Reaction tested:	$3AzC$	+	$2Fe^{3+}$ ⇆	$(Fe^{3+})_2AzC_3$
[Initial]	$1*10^{-5}$ M		$1*10^{-6}$ M	
[Equilibrium]	$(1*10^{-5} - 6.67*10^{-7})^B$ M		X	$(5*10^{-7})^B$ M

$K_{Form} = [(Fe^{3+})_2AzC_3] / ([AzC]^3 * [Fe^{3+}]^2)$ Solve for $[Fe^{3+}] = X$

$[Fe^{3+}]^2 = [(Fe^{3+})_2AzC_3] / ([AzC]^3 * K_{Form})$ $[Fe^{3+}]^2 = 5*10^{-7} / ((9.33*10^{-6})^3 * 6.43*10^{54})$

$[Fe^{3+}]^2 = 9.57*10^{-47}$ $[Fe^{3+}] = 9.78*10^{-24}$ $-(Log_{10}[Fe^{3+}]) = 23.0$

A. Where K_1, K_2, K_3, K_4, and K_5 are the dissociation constants of the protons of the catechol moieties and carboxyl group of azotochelin. K_1, $K_2 = 10^{-12.1}$ and K_3, $K_4 = 10^{-8.4}$ (Loomis and Raymond, 1991) and K_5 is $10^{-3.6}$ (Duhme *et al.*, 1998), pH = 7 , $[H^+] = 10^{-7}$.

B. Due to high affinity of siderophore for iron (III), assume all of iron (III) consumed.

C) Free iron in ferric-protochelin equilibrium.

Ferric-protochelin $K_{Form\ pH\ 7.0} = 10^{24.97}$

Calculate fraction of protochelin fully deprotonated at pH 7.0 (Harris, 1982):

$\alpha_{PC} = ((K_1K_2K_3K_4K_5K_6) / (\Sigma([H^+]^6 + K_1[H^+]^5 + K_1K_2[H^+]^4 ..... K_1K_2K_3K_4K_5K_6)))^A$

$\alpha_{PC} = 3.16*10^{-20}$

$K_{Form\ Independent} = K_{Form\ pH\ 7.0} / \alpha_{PC}$ (Equation 5, Section 1.4.4)

$K_{Form\ Independent} = 10^{24.97} / 3.16*10^{-20}$ $K_{Form\ Independent} = 1.48*10^{44}$ $Log_{10} K_{Form} = 44.17$

The free metal system in Harris *et al.* (1979) is defined as $[Fe^{3+}]_{Init} = 1*10^{-6}$ M and $[siderophore]_{Init} = 1*10^{-5}$ M at pH 7.4, thus, needed to calculate conditional formation constant for ferric-protochelin at pH 7.4. This was done using Equation 5 above and α_{PC} at pH 7.4 of $7.94*10^{-18}$. From this the $K_{Form\ pH\ 7.4}$ of ferric protochelin was found to be $1.18*10^{27}$.

Reaction tested:	PC	+	Fe^{3+}	⇆	$Fe^{3+}PC$
[Initial]	$1*10^{-5}$ M		$1*10^{-6}$ M		
[Equilibrium]	$(1*10^{-5} - 1*10^{-6})^B$ M		X		$(1*10^{-6})^B$ M

$K_{Form} = [Fe^{3+}PC] / ([PC] * [Fe^{3+}])$ Solve for $[Fe^{3+}] = X$

$[Fe^{3+}] = [Fe^{3+}PC] / ([PC] * K_{Form})$ $[Fe^{3+}] = 1.0*10^{-6} / (9*10^{-6} * 1.18*10^{27})$

$[Fe^{3+}] = 9.41*10^{-29}$ $-(Log_{10}[Fe^{3+}]) = 28.0$

A. Where K_1, K_2, K_3, K_4, K_5, and K_6 are the dissociation constants of the protons of the catechol moieties of protochelin. K_1, K_2, $K_3 = 10^{-12.1}$ and K_4, K_5, K_6, $= 10^{-8.4}$ (Loomis and Raymond, 1991), pH = 7, $[H^+] = 10^{-7}$.

B. Due to high affinity of siderophore for iron (III), assume all of iron (III) consumed.

APPENDIX 2 - Additional $^{55}Fe^{3+}$ Uptake Assays

As described in Section 3.2.6, $^{55}Fe^{3+}$ uptake was examined in strain UW using $^{55}Fe^{3+}$-protochelin and $^{55}Fe^{3+}$-azotochelin with cells which had been pre-incubated with 70 μM molybdate for 10 min and control cells that were not exposed to 70 μM molybdate. Assays were done as described in Section 2.3.3, with the exception that $^{55}Fe^{3+}$ uptake was monitored for 12 min not 16 min. The uptake curves generated are shown in Figs A2.1 and A2.2. Uptake rates were determined by linear regression over the 12 min of the assay. In addition, data points from the molybdate exposed cells and the control cells were compared with paired T-test analysis (Harris and Kratovil, 1981) at 90% confidence limits.

This analysis indicated that in the uptake of $^{55}Fe^{3+}$protochelin values generated at 3 and 12 min were statistically different while values at 0, 6, and 9 min were the same. Values at 6 and 9 min would have been statistically different if there had been less variation in the duplicate samples taken. Identical analysis for the uptake of $^{55}Fe^{3+}$azotochelin indicated that the values generated at 3, 9, and 12 min were statistically different while values at 0 and 6 min were the same. Once again, the values at 6 min would have been statistically different if there had been less variation in the duplicate samples taken.

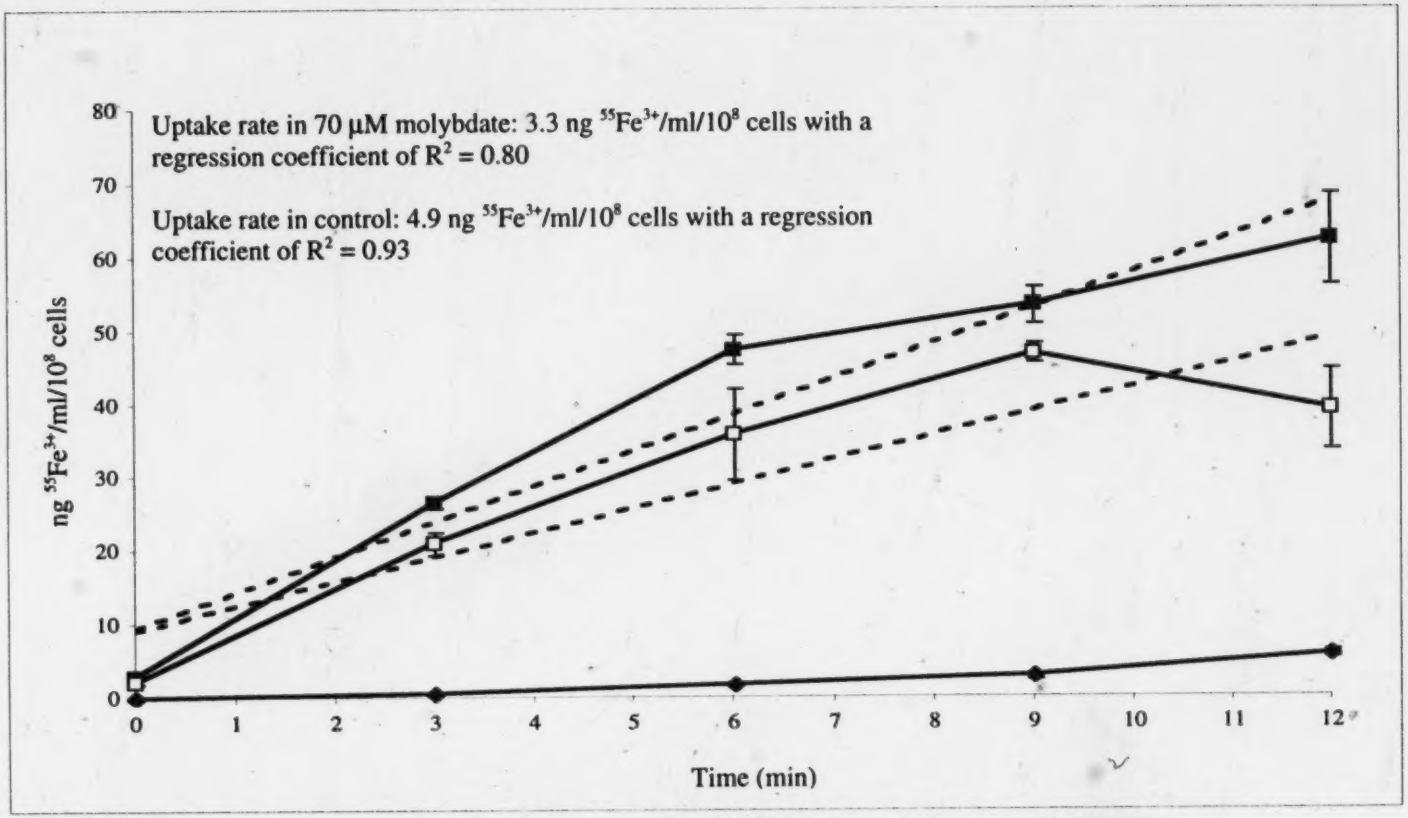

Figure A2.1 The effect of 70 µM molybdate on the uptake of $^{55}Fe^{3+}$-protochelin by *A. vinelandii* UW.

$^{55}Fe^{3+}$ uptake in the presence of: (□) 70 µM molybdate, (■) No added molybdate, or (◆) Siderophore-free control. (--------) denotes lines of linear regression. Error bars indicate variation between duplicate assay samples taken.

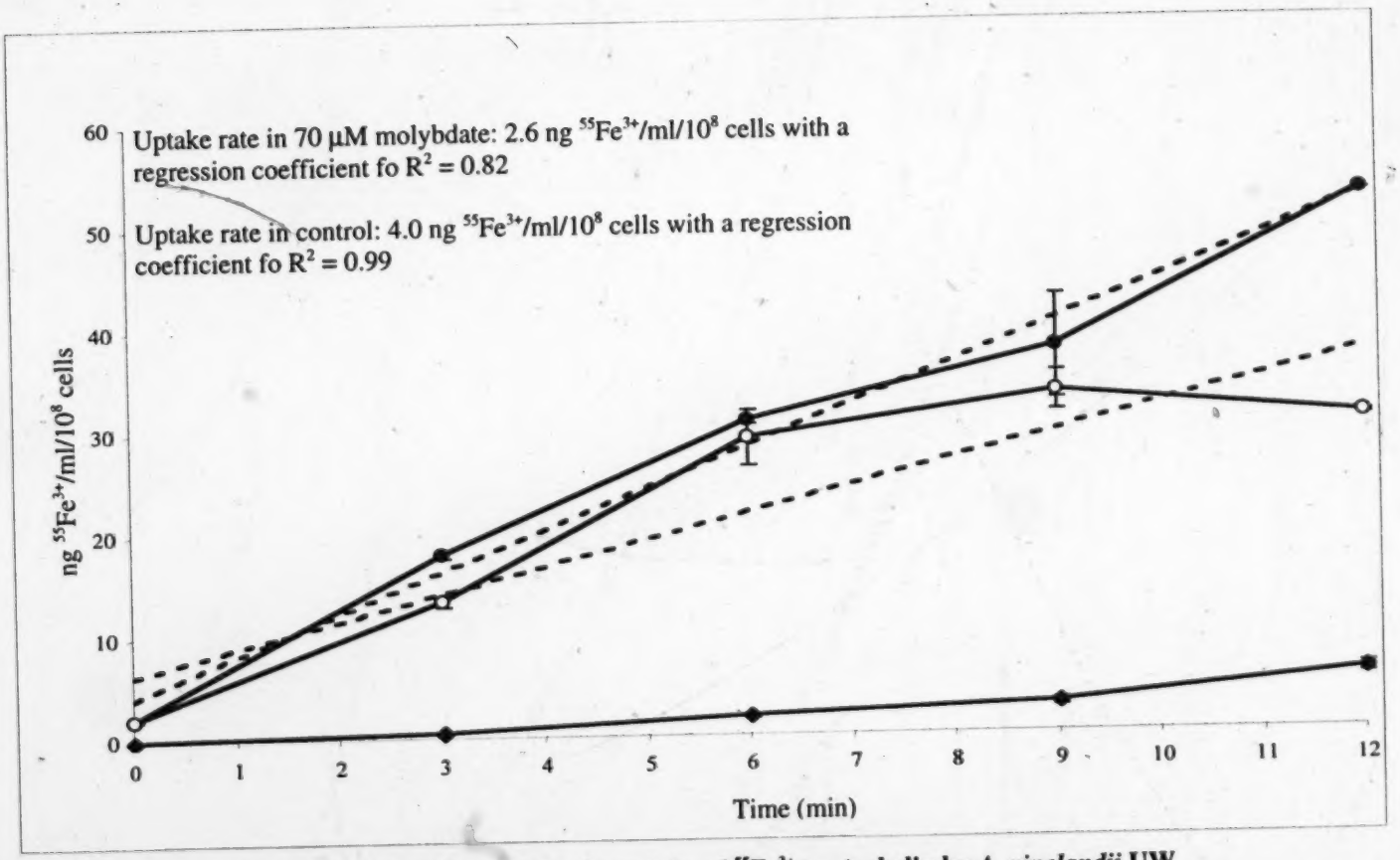

Figure A2.2 The effect of 70 µM molybdate on the uptake of $^{55}Fe^{3+}$-azotochelin by *A. vinelandii* UW.

$^{55}Fe^{3+}$ uptake in the presence of: (○) 70 µM molybdate, (●) No added molybdate, or (◆) Siderophore-free control. (--------) denotes lines of linear regression. Error bars indicate variation between duplicate assay samples taken.